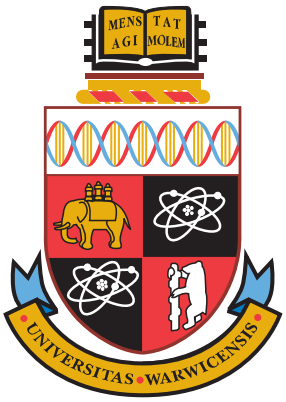

A Systems Pharmacology Approach to the Adenosine A_1 Receptor

by

Anthony Knight

A thesis submitted to the University of Warwick
for the degree of Doctor of Philosophy

Systems Biology Doctoral Training Centre

October 2015

Supervisors: Dr. Graham Ladds and Prof. Krasimira Tsaneva-Atanasova

"Don't Panic."

The Hitchhiker's Guide to the Galaxy

Contents

List of Figures

List of Tables

Abbreviations and acronyms

2CCPA	**2**-**C**hloro-N^6-**C**yclo**P**entyl**A**denosine
7TM	7 **T**rans-**M**embrane
A_1R	**A**denosine **A_1** **R**eceptor
A_2R	**A**denosine **A_2** **R**eceptor
A_{2A}R	**A**denosine **A_{2A}** **R**eceptor
A_{2B}R	**A**denosine **A_{2B}** **R**eceptor
A_3R	**A**denosine **A_3** **R**eceptor
AA	**A**mino **A**cid
AC	**A**denylate **C**yclase
ADP	**A**denosine **D**i**P**hosphate
ADR	**A**dverse **D**rug **R**eaction
ATP	**A**denosine **T**ri**P**hosphate
bp	**b**ase **p**air
BRET	**B**ioluminescence **R**esonance **E**nergy **T**ransfer
cAMP	**c**yclic **A**denosine **M**ono**P**hosphate
CAM	**C**onstitutively **A**ctive **R**eceptor
CFP	**C**yan **F**luorescent **P**rotein
cGMP	**c**yclic **G**uanine **M**ono**P**hosphate
CNS	**C**entral **N**ervous **S**ystem
CRF	**C**orticotrophin **R**eleasing **F**actor
DNA	**D**eoxy**Ribose** **N**ucleic **A**cid
DMSO	**Dim**ethyl **s**ulph**o**xide
DPCPX	**D**i-**p**ropyl**c**yclo**p**entyl**x**anthine
DR	**D**ose **R**atio
ECL	**E**xtra**C**ellular **L**oop

E. coli	***E**scherichia **coli***
E_{max}	**M**aximum Level of Signal
ERK	**E**xtracellular Signal-**R**egulated **K**inase
FDGlu	**F**luorescein di-β-**D**-**Glu**copyranoside
FOA	5-**F**luoro-**O**rotic **A**cid
FRET	**F**luorescence **R**esonance **E**nergy **T**ransfer
GAP	**G**TPase **A**ccelerating **P**rotein
GAPDH	**G**lycer**a**ldehyde **P**hosphate **D**e**h**ydrogenase
GDP	**G**uanosine **DiP**hosphate
GEF	**G**uanosine Nucleotide **E**xchange **F**actor
GFP	**G**reen **F**luorescent **P**rotein
GIRK	**G** Protein-Regulated **I**nward **R**ectifier $\mathbf{K}^+$ Channels
GLP-1	**G**lucagon-**l**ike **p**eptide-1
GLP-1R	**G**lucagon-**l**ike **p**eptide-1 **R**eceptor
GPCR	**G** **P**rotein-**C**oupled **R**eceptor
GRK	**G** Protein-Coupled **R**eceptor **K**inase
GTP	**G**uanosine **T**ri**P**hosphate
ICL	**I**ntra**c**ellular **L**oop
$\mathbf{IP_3}$	**I**nositol **T**ris**p**hosphate
JNK	**J**a**n**us **K**inase
MAPK	**M**itogen **A**ctivated **P**rotein **K**inase
MAPKK	**M**itogen **A**ctivated **P**rotein **K**inase **K**inase
MAPKKK	**M**itogen **A**ctivated **P**rotein **K**inase **K**inase **K**inase
mGluR	**m**etabotropic **Glu**tamate **R**eceptor
MOR	μ **O**piod **R**eceptor
NAM	**N**egative **A**llosteric **M**odulator
NECA	5'-**N**-**E**thyl**c**arboxyamido**a**denosine
OD	**O**ptical **D**ensity
ODE	**O**rdinary **D**ifferential **E**quation
ONPG	**O**-**N**itro**p**henyl-D-**G**alactoside
P	**P**robability
PAM	**P**ositive **A**llosteric **M**odulator
PDB	**P**rotein **D**ata**b**ase

PDE	**P**hospho**die**sterase
pEC$_{50}$	Negative Natural Logarithm of Median **E**ffective **C**oncentration
PIP$_2$	**P**hospha**i**nositol 4,5-bis**p**hosphate
PK/PD	**P**harmaco**k**inetic/**P**harmaco**d**ynamic
PKA	**P**rotein **K**inase **A**
PKC	**P**rotein **K**inase **C**
PLC	**P**hospho**l**ipase **C**
PM	**P**lasma **M**embrane
PAR-1	**P**rotease **A**ctivated **Receptor-1**
R	Inactive **R**eceptor
R*	Active **R**eceptor
RGS	**R**egulator of **G** Protein **S**ignalling
RTK	**R**eceptor **T**yrosine **K**inase
Sc. cerevisiae	*Saccharomyces cerevisiae*
Sz. pombe	*Schizosaccharomyces pombe*
TM	**T**rans-**M**embrane
YCK	**Y**east **C**asein **K**inase
YE	**Y**east **E**xtract
YFP	**Y**ellow **F**luorescent **P**rotein
YPD	**Y**east **P**eptone **D**extrose

Acknowledgements

Firstly, I would like to thank Dr. Graham Ladds and Prof. Krasimira Tsaneva-Atanasova for invaluable guidance throughout this PhD. Particular thanks to Graham, without whose support this work would not have been possible. Krasimira's patience as I learned new mathematical techniques is also greatly appreciated.

I am grateful to members of Ladds group past and present for their contributions to this work. I would particularly like to thank Dr. Wayne Croft, Alejandro Esparza-Franco, Robert Lockley, Dr. Magdalena Mos, Ingrid Tigges and Dr. Kathryn Richardson for providing a warm and friendly environment. Particular note goes to Dr. Juergan Zech and Dr. Pete Williams whose advice and perspectives were invaluable to my career ambitions. Thank you.

I would also like to thank the University of Bristol whose journal access, courtesy of Krasimira, was essential to this thesis. I would like to thank the Systems Biology Doctoral Training Centre and EPSRC for funding. I am grateful to Prof. Vicky Buchanan-Wollaston for her support throughout the MSc and PhD. I am particularly thankful to Anne Maynard for her guidance and administrative knowhow. Finally, I would like to thank Dr. Isolda Romero-Canelon and Prof. Peter Sadler for the flexible employment that allowed me to complete this work.

I would like to thank Dr. Simon Dowell, Prof. Arthur Christopoulos and Dr Lauren May for yeast strains and plasmids essential to this thesis. Special thanks go to Prof. Bruno Frenguelli, Martin Lochner and especially Dr Jennifer Hemmings for a productive and rewarding collaboration.

I am grateful to my friends and family for providing a safe harbour from work to rest and recharge. I am particularly grateful to my parents and sister who kept me grounded throughout my undergraduate and postgraduate studies. Thanks also go to Grancha whose eccentricity continues to provide new perspectives.

Most importantly, I am forever indebted to my new wife, Sarah Knight, for unwavering support and dedication throughout this PhD. Without her, I would not be who I am or where I am today and for that I am eternally grateful. This thesis is as much hers as mine.

Declaration of authorship

I, Anthony Knight, declare that this thesis titled, 'A Systems Pharmacology Approach to the Adenosine A_1 Receptor' and the work presented in it are my own. I confirm that:

- This work was done wholly or mainly while in candidature for a research degree at this University.
- Where any part of this thesis has previously been submitted for a degree or any other qualification at this University or any other institution, this has been clearly stated.
- Where I have consulted the published work of others, this is always clearly attributed.
- Where I have quoted from the work of others, the source is always given. With the exception of such quotations, this thesis is entirely my own work.
- I have acknowledged all main sources of help.
- Where the thesis is based on work done by myself jointly with others, I have made clear exactly what was done by others and what I have contributed myself.

Signed:

Date:

UNIVERSITY OF WARWICK

Abstract

Systems Biology Doctoral Training Centre

Doctor of Philosophy

by

Anthony Knight

The majority of drugs are prescribed on the premise that their desired and undesired effects are well characterised. However, the mechanisms underlying these effects can be elusive and are of interest to the pharmaceutical industry in terms of rational drug design. G protein-coupled receptors are a significant class of drug target that are capable of influencing multiple signalling processes, and downstream effects, simultaneously through a variety of effectors, such as G proteins or β-arrestins. The effector activated by a given receptor is often a function of the ligand. This is termed functional selectivity and can contribute to adverse drug effects. Understanding functional selectivity in a mammalian setting is hindered by cross-talk between many competing signalling components. The *Sc. cerevisiae* pheromone response can be modified to isolate individual mammalian receptor-G protein interactions. Therefore, this simple organism represents an excellent tool to study functional selectivity. Further, the simplicity of this organism allows this pathway to be mathematically modelled. By applying mathematical models to mammalian GPCR signalling in yeast it is possible to extract experimentally inaccessible quantitative parameters underlying functional selectivity. This interdisciplinary approach to pharmacological mechanisms is an example of systems pharmacology. Here a systems pharmacology approach is applied to adenosine receptor signalling in yeast with a view to understanding the contribution of the ligand, receptor and G protein to functional selectivity.

The first stage of this process was expression and characterisation of adenosine A_1R, $A_{2A}R$, $A_{2B}R$ and A_3R subtypes in yeast. Here, the A_1R and A_2R subtypes were shown to be functional in yeast, but the A_3R response was limited. The A_1R signals through G proteins representing the inhibitory $G\alpha_i$ family in yeast, while the $A_{2A}R$ and $A_{2B}R$ signal through both inhibitory and stimulatory G protein equivalents. Here ligand bias is quantified but further extended to describe adenosine receptor selectivity. Further, the yeast system was used to inform novel fluorescent compound development. Fluorescent ligand-binding rates would ultimately inform modelling studies.

A minimal mathematical framework was developed to described A_1R signalling in yeast. Ordinary differential equation models recreate dynamic cellular processes. Here an ODE model was applied to experimental time course data to predict rate constants throughout the yeast G protein cycle in the presence of the mammalian A_1R. This model predicts that G protein subtype influences the ligand-receptor-G protein interactions of the A_1R in yeast. Further modification of the system and fluorescent technologies may help validate these predictions.

Chapter 1

Introduction

1.1 Systems Pharmacology Approaches

Systems pharmacology applies systems biology approaches to understand the precise mechanisms through which drugs bring about their desired and adverse effects. Cellular and multicellular behaviour is governed by many complicated and interconnected signalling networks. The intricate workings of these networks, and the effects of drugs throughout these systems is difficult to assess experimentally. However, knowledge of the full range of effects of a given drug, and the underlying mechanisms, would be invaluable to rational drug design and development (Agoram and Demin, 2011; Sorger et al., 2011).

Systems biology integrates mathematical modelling and experimental techniques to gain insight into data that could not be achieved through either approach alone. However, this is a very broad field and systems biology can be divided into two approaches. - "top-down" and "bottom-up". "Top-down" approaches tease a plethora of patterns from large datasets to elucidate whole networks and their interactions on an organism or tissue level. In contrast, "bottom-up" approaches consider individual mechanisms in a pathway and how they contribute to a system-level response on molecular or cellular level. Basically, "top-down" approaches are used to generate hypotheses while "bottom-up" approaches are used to test mechanistic frameworks (Zou et al., 2013). While systems biology is "bottom-up", or "top-down", systems pharmacology is considered "middle-out" in that it combines traditional systems biology methods for a single purpose; to understand drug action on a molecular, cellular, organism and population level (Figure 1.1) (Berger and Iyengar, 2011; Vicini and van der Graaf, 2013).

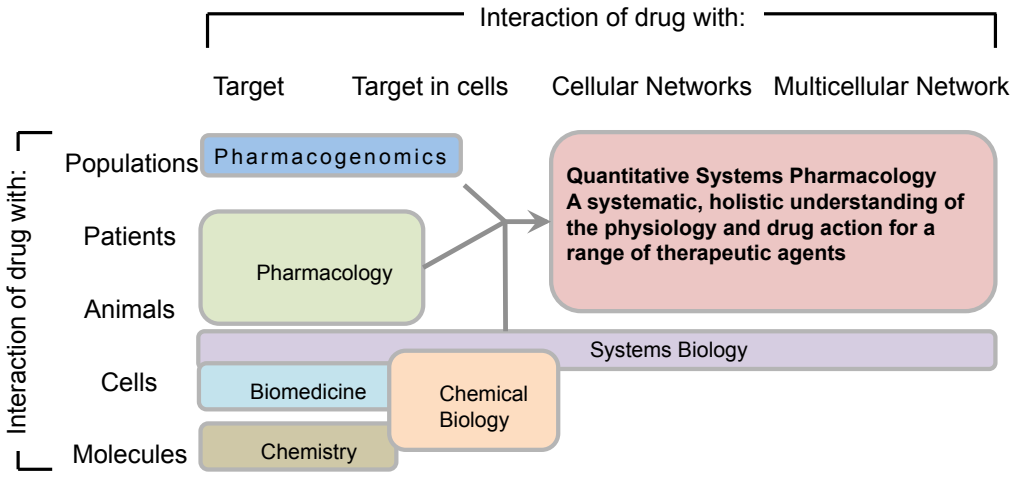

FIGURE 1.1: Systems Pharmacology is an emerging interdisciplinary approach that combines and integrates mathematical modelling and experimental methods to elucidate drug action on a system level. Unlike Systems Biology, which can be classed as "top-down" or "bottom up" Systems Pharmacology combines multiple data sources to predict drug mechanisms at molecular, cellular, organism and population levels. Figure adapted from (Sorger et al., 2011)

The explosion in "-omics" technologies have greatly influenced drug development. Transcriptomics, proteomics and metabolomics have been used to elucidate the full range of drug effects and hint at potential mechanisms of action throughout a cell, tissue or organism. Systems pharmacology also embraces pharmacodynamic/pharmacokinetic (PK/PD) approaches. These use mathematical models to describe the interactions between a drug and various tissues throughout an organism (Gabrielsson et al., 2010).

However, the emphasis of systems pharmacology still remains the direct effect of a drug on the plethora of cell signalling networks and how these accumulate to a system level response (Schrattenholz and Soskić, 2008; Bai et al., 2014). This thesis uses an interdisciplinary approach to understand the effect of a drug on multiple cell signalling processes through a single drug target.

1.1.1 Cell signalling and pharmacology

Cell signalling cascades are highly complex systems in which a signalling molecule binds a primary messenger or receptor. This, in turn, activates effectors that produce second messengers, small molecules that transmit and amplify a signal in specific cellular and subcelular locations, regulating various cellular processes. Pharmacological agents elicit their effects through influencing cellular behaviour. For instance, nitric oxide (NO) activates the effector guanylate cyclase. This converts guanine triphosphate (GTP) to the second messenger cyclic guanine monophosophate (cGMP). The increase in cytosolic cGMP affects various proteins, including kinases and ion channels that cause vasodilation and a decrease in blood pressure (Kukovetz et al., 1987). Historically, this pathway has been the target of nitroglycerine, which is converted to NO *in vivo*. More specific activation of this pathway has been achieved by targeting the negative regulator of cGMP signalling, phosphodiesterase (PDE). This prevents the metabolism of cGMP to GMP and has vasodilatory effects throughout the body. Indeed, the PDE5 inhibitor sidenafil, better known as Viagra, was designed for cardiovascular and blood pressure disorders but is noted for its effects on arousal (reviewed by Thatcher et al. (2004)).

Transcription is also a key process that can be influenced by cell signalling processes and a prominent drug target. Steroid hormones such as testosterone, cortisol and thyroxine bind to intracellular receptors. These receptors consist of a ligand-binding domain, a DNA-binding domain and multiple activation sites distributed throughout the molecule. Steroid receptors are ligand-dependent transcription factors that translocate to the nucleus and bind DNA directly to activate hormone-responsive genes (reviewed by Falkenstein et al. (2000))

Steroid hormones and small molecules, such as cortisol and NO, can directly influence intracellular processes. However, many ligands cannot permeate the cell membrane and must rely on their interaction with cell-surface receptors to mediate their effects. Ligand-gated ion channels regulate the flow of ions across the cell membrane. A notable example of this class of receptor is the nicotinic acetylcholine receptor. This receptor is essential for transmission of signal across synapses in both the central and peripheral nervous systems and has also been implicated in addiction (Dajas-Bailador and Wonnacott, 2004; Leslie et al., 2013). This pentameric receptor undergoes conformational changes in response to the endogenous ligand acetylcholine. This results in an influx of Na^+ and hyper polarisation of the cell membrane. Once this polarisation exceeds a threshold an action potential is created that propagates down the nerve cell to the next synapse (Leonard and Bertrand, 2001).

Transmembrane proteins are a common way to access cell-signalling machinery from the cell surface. Conformational changes in response to ligand binding affect their interactions with cytosolic proteins, transducing signal from the extracellular to the intracellular domains. Receptor-tyrosine kinases (RTKs) are a major drug target for a number of diseases (Robinson et al., 2000). A notable example of an RTK is the insulin receptor. Insulin is a protein hormone that cannot cross the cell surface but has key roles in glucose homeostasis and has been implicated in type-II diabetes. The insulin receptor has an extracellular α-domain linked to a transmembrane β-domain. Insulin binding promotes dimerisation of the α-subunits, bringing two β-subunits together. These transmembrane domains are tyrosine kinases that also contain multiple phosphorylation sites. The newly-associated β-subunits cross-phosphorylate each other inducing conformational changes that recruit a plethora of effector molecules. Downstream effects include activation of glycogen-synthase and membrane trafficking of glucose transporters (Avruch, 1998). Other notable examples of RTKs include the inteferon and interleukin receptors that are targets for immunological and inflammatory disorders (Robinson et al., 2000).

This thesis focuses on a particular class of cell surface receptor, the G protein-coupled receptor (GPCR), and its interactions with various cellular effectors as a function of ligand. By applying simple mathematical models to experimental data the aim is to better understand the kinetics of the drug-GPCR-effector interaction.

1.2 G protein-coupled receptors

GPCRs represent the largest class of cell-surface receptors. There are predicted to be around 800 human GPCRs alone, capable of binding a wide range of extracellular ligands; including photons, ions, amines, small molecules, peptides and pheromones (Fredriksson et al., 2003). GPCRs influence a myriad of intracellular effectors, influencing cellular behaviour in response to the bound ligand. The ubiquitous nature of GPCRs underlies their therapeutic importance as defects in GPCR signalling have been implicated in metabolic, degenerative and sensory disorders. Additionally, this class of receptor represents a key point of access through which to manipulate the intracellular processes of the cell. Currently, it is estimated that 30% of prescription drugs target this class of receptor (Correll and McKittrick, 2014).

1.2.1 GPCR structure

Rhodopsin was the first crystallised GPCR and has served as an excellent model for this receptor family (Palczewski et al., 2000). GPCR structures are highly conserved, consisting of 7-transmembrane (TM) α-helical domains connected by alternating intracellular and extracellular loops (ECL and ICL respectively) (Figure 1.2). The N-terminus projects into the extracellular space, the roles and length of which can vary between receptors. Typically, this region contains lipid modification sites and signalling sequences essential for membrane localisation. The ECL regions are also highly variable between receptors but have a prominent role in ligand recognition and binding, particularly ECL2 (Olah et al., 1994; Avlani et al., 2007).

The 7-TM domain consists of 7 membrane-spanning amphipathic α helices and is highly structurally conserved between GPCRs. The extracellular portion of these regions also serve in ligand binding. However, ligand binding significantly alters the conformation of these α-helices. In many GPCRs, the conformation of the TM region is maintained by an ionic lock between a E/DRY motif of TM3 and a glutamate residue within TM6. Ligand binding to the extracellular surface induces a 30° rotation of TM3 away from TM6. This, in turn, alters the positioning of the IC loops, particularly IC3 thus affecting the interactions of the receptor with cell signalling components (Bockaert and Pin, 1999; Ballesteros et al., 2001).

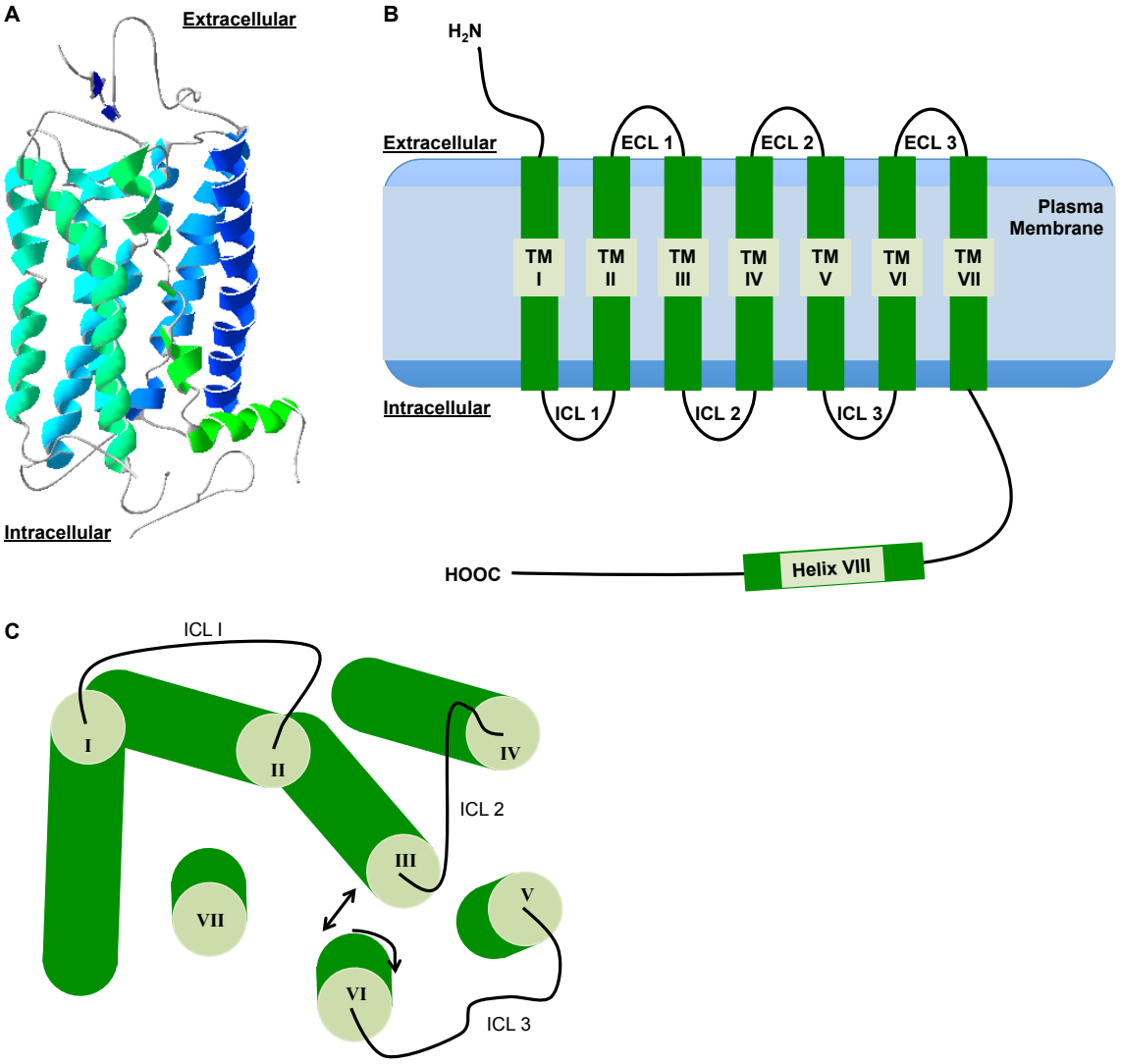

Figure 1.2: **GPCR structure and activation A.** The crystal structure of rhodopsin, the model GPCR. PDB ID 1F88 (Palczewski et al., 2000). **B.** The secondary structure of GPCRs. GPCRs consistent of 7-TM α-helices consisting of 20-28 hydrophobic residues, flanked by alternative intracellular and extracellular loops. The C-terminus has roles in GPCR trafficking while the extracellular loops and upper transmembrane domains have roles in ligand binding. The intracellular loops and N-terminus interact with cell-signalling machinery with roles in signal transduction and receptor internalisation. **C.** Helix arrangements of GPCR activation. The activation of rhodopsin viewed from the cytosolic face. Shown are TM1 - TM7 and the intracellular (IC) loops. An ionic lock between TM3 and TM6 holds the GPCR in an inactive conformation. During receptor activation TM3 rotates approximately 30° away from TM6 affecting the the positioning of the ICL regions. Figure adapted from (Bockaert and Pin, 1999).

1.2.2 GPCR families

Traditionally, GPCRs have been classified into six broad families (A-F) based on N-terminal sequence homology (Attwood and Findlay, 1994). Family A receptors are the largest family of GPCRs with 701 members (Kroeze et al., 2003). These receptors are also known as rhodopsin-like receptors due to their similarity to rhodopsin, the prototypical GPCR (Palczewski et al., 2000). This family is quite diverse and includes receptors that bind small molecules including nucleotides and biogenic amines such as dopamine and serotonin. Typically, the ligand-binding site is located between the TM domains of these receptors (Lebon et al., 2011; Chien et al., 2010). However, it has also been shown that the ECL regions have significant roles in ligand binding this class of receptor (Peeters et al., 2011, 2012).

Family B receptors, also known as secretin-like receptors, are characterised by their enlarged N-termini, consisting of 60-80 amino acids, that contribute to the binding of peptide hormones. Members of this family include the glucagon-like peptide-1 (GLP-1), glucagon and corticotrophin-releasing factor (CRF) receptors that have roles in paracrine signalling throughout the body (Laburthe et al., 2006).

Family C receptors include the metabotropic gluatamate receptors (mGluRs). Similar to family B GPCRs, a large N-terminus is a defining feature of this family. The N-terminus of family C GPCRs consists of two lobes connected by a hinge region. This "Venus fly-trap" domain binds ligands such as Ca^{2+} and glutamate and shares structural similarities with the periplasmic binding proteins of bacteria (O'Hara et al., 1993).

Family D and E receptors are not present in mammalian cells. Family D receptors include the fungal mating pheromone receptors discussed in further detail later in this thesis. Family E receptors represent cAMP receptors in organisms such as *Dictystelium discoidem* that are crucial in nutrient sensing and chemotaxis.

Class F GPCRs include the frizzled/ smoothened receptors. This family responds to secreted glycoproteins known as Wnts to influence cell fate, proliferation and differentiation. Thus these receptors have been heavily implicated in embryonic growth and development (Dirnberger and Seuwen, 2007).

A group of Class B receptors have been reclassified as new GPCR subtype, the adhesion receptors (Fredriksson et al., 2003). These receptors are noted for the N-terminal adhesin-like motifs that are rich in proline residues and glycosylation sites. These extremely large N-termini can be 200-2800 amino acids in length and are known as "mucin-like" stalks. Receptors from this family, such as the CD97 antigen receptor, have been noted their roles in cell-to-cell adhesion (Bjarnadóttir et al., 2007).

1.3 GPCR signalling

1.3.1 G protein-mediated signalling

A GPCR is defined by two features: their structure and their interaction with G proteins. G proteins are highly conserved binary switches that regulate a variety of cellular processes (Figure 1.3). Their state is dependent on the bound guanine nucleotide. Inactive G proteins are bound to a molecule of guanine diphosphate (GDP). G protein activation requires nucleotide exchange such that GDP is lost and GTP is bound. This process is driven by the differences in cellular abundance between GDP and GTP but can be accelerated by guanine exchange factors (GEFs). G protein inactivation is driven by GTP hydrolysis. This can be achieved through the intrinsic GTPase activity of the G protein or accelerated by GTPase activating proteins (GAPs) (Randazzo and Kahn, 1994; Bos et al., 2007).

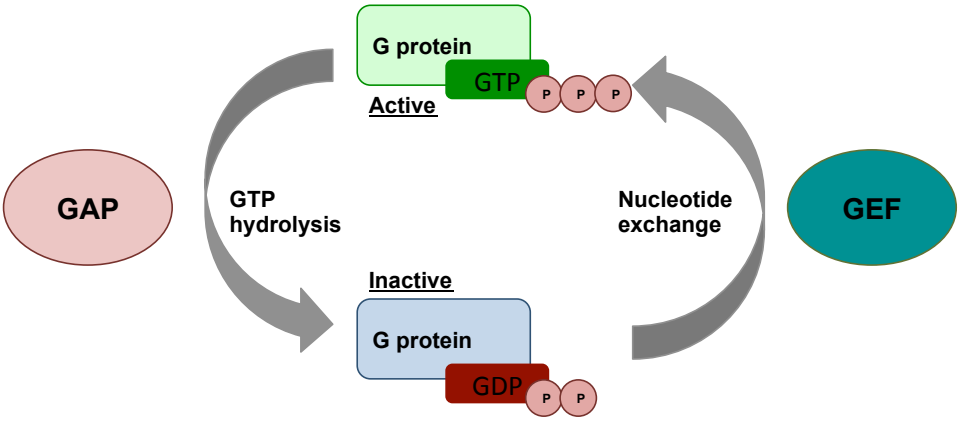

Figure 1.3: **Schematic of the G protein cycle.** Inactive G protein is bound to a molecule of GDP. G protein activation occurs through nucleotide exchange of GDP for GTP. This can happen spontaneously or be accelerated by GEFs. The active G protein reverts to its inactive state through GTP hydrolysis. This occurs through the GTPase activity of the G protein but can be accelerated by GAPs.

G proteins exist as both monomeric and multi-subunit complexes. Monomeric G proteins include the Ras superfamily. Defects in Ras signalling have been implicated in a range of human cancers. The Ras superfamily can be further subdivided into the Rab, Ras, Ran, Rho and Arg subfamilies (Papadaki et al., 2002). Each of these act as molecular switches in signal transduction pathways. While Ras proteins can act to transduce signal in response to GPCRs, this is usually via a number of effectors and second messengers. However, GPCRs directly couple to and signal through heterotrimeric G proteins consisting of a Gα subunit and a G$\beta\gamma$ dimer (Figure 1.4).

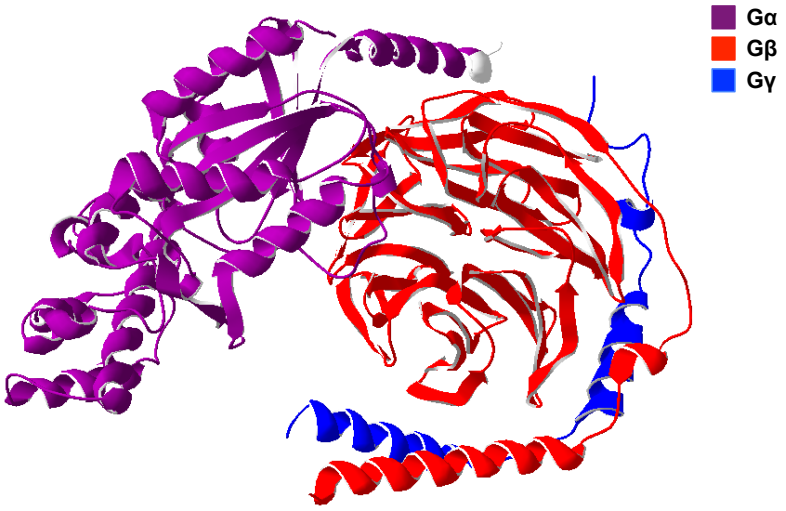

Figure 1.4: **The crystal structure of a G$\alpha\beta\gamma$ complex.** The Gα_t subunit (purple) was crystallised with its cognate G$\beta\gamma$ dimer (red and blue respectively). Gα binds guanine nucleotide and also couples to the GPCR. The Gα and Gγ also contain lipid modification sites essential to membrane tethering and localisation. PDB ID 1GOT (Lambright et al., 1996).

The Gα defines both the state and functional role of the G$\alpha\beta\gamma$ complex. When inactive the Gα is bound to a molecule of GDP. Activation of a GPCR results in changes in the conformation of the IC loops. This in turn alters the conformation of the Switch I, II and III regions of the Gα, exposing the nucleotide binding site to the cytosol (Sprang, 1997). The bound GDP is lost and replaced by GTP, which is around 30-100-fold more abundant in the cell. The now active Gα dissociates from the G$\beta\gamma$. Depending on the organism and pathway either the Gα or the G$\beta\gamma$ can propagate downstream signalling (Figure 1.5).

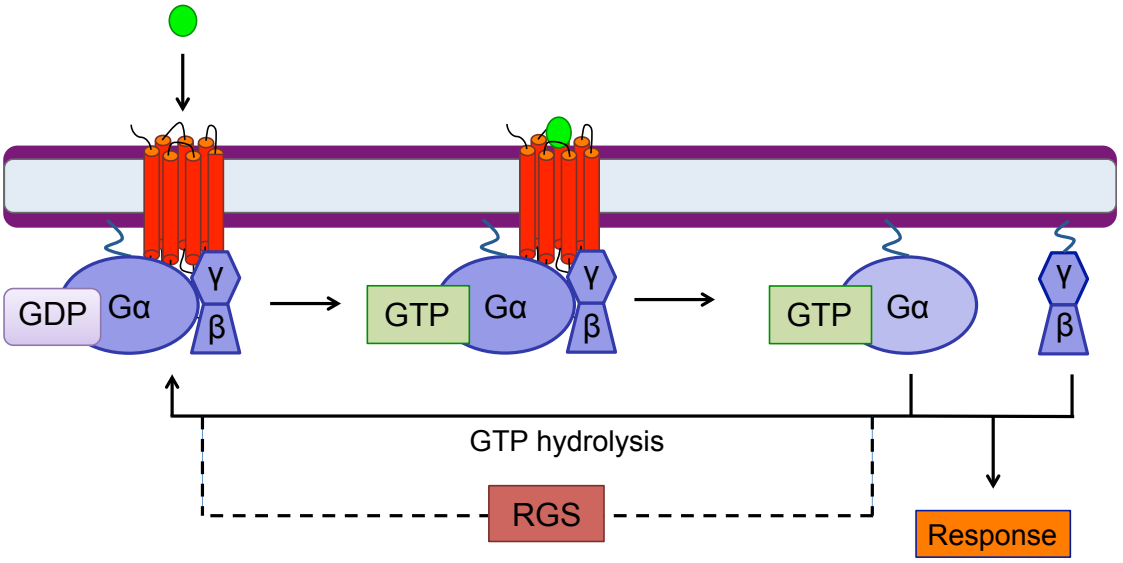

FIGURE 1.5: **The G protein cycle.** An inactive GPCR is coupled to a GDP bound G protein consisting of a Gα and a G$\beta\gamma$ dimer. Receptor activation, for example from ligand binding, promotes nucleotide exchange on the Gα such that GDP is lost and GTP is bound. The active G protein can dissociate and either the Gα or G$\beta\gamma$ can propagate downstream signalling depending on the organism and pathway. GTP hydrolysis by the intrinsic GTPase activity of the Gα, or greatly accelerated by RGS proteins, promote G protein deactivation and reassociation.

Negative regulation of signalling is essential to proper cellular function. This is achieved at the G protein level through hydrolysis of the GTP to GDP due to the intrinsic GTPase activity of the Gα subunit. The GDP-bound Gα reassociates with the G$\beta\gamma$, reforming the heterotrimeric G protein complex.

The GTPase activity of the Gα is relatively slow but can be greatly accelerated by regulator of G protein signalling (RGS) proteins (Dohlman et al., 1995). Despite a great deal of structural complexity RGS proteins are centred around the RGS-fold. Through this fold they interact directly with the active Gα state and carry out two functions; they accelerate the rate of GTP hydrolysis by the Gα and expedite GDP dissociation. RGS proteins have proven to be an effective negative regulator of signalling. In cases where the Gα propagates signalling the RGS can compete with effectors for the Gα-GTP, reducing downstream signalling (reviewed by Ross and Wilkie (2000); Willars (2006)).

1.3.2 Gα propagated signalling

The Gα subunit defines the G protein and largely determines the downstream signalling pathways activated. This G protein couples to a GPCR via its C-terminus (Figure 1.6). There are thought to be 16 Gα subunits in mammalian cells that can be broadly classified into four main families based on sequence homology, $G\alpha_s$, $G\alpha_i$, $G\alpha_q$ and $G\alpha_{12}$. Examples of these families and their common roles are shown in (Table 1.1).

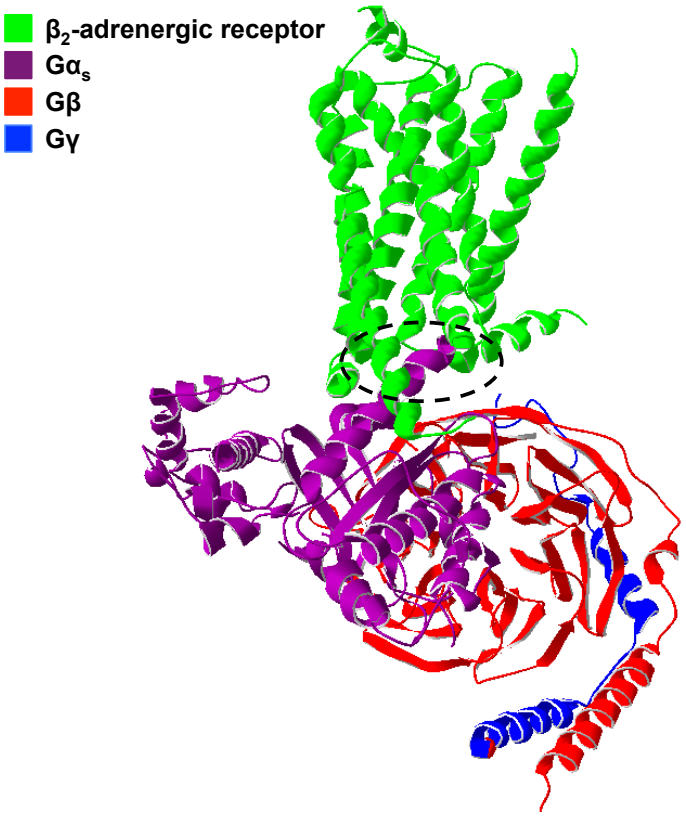

FIGURE 1.6: **Crystal structure of a GPCR-G protein complex.** The crystal structure of the active β_2-adrenergic receptor coupled to its native G protein containing $G\alpha_s$. The specificity of GPCR G protein interaction is largely determined by the C-terminus of the Gα. This interaction has been highlighted with a dotted line. PDB ID 3SN3 (Rasmussen et al., 2011).

TABLE 1.1: **A summary of Gα families and their common roles.**

Gα family	**Family members**	**Common role**
$G\alpha_s$	$G\alpha_s$ and $G\alpha_{olf}$	Stimulate adenylate cyclase
$G\alpha_i$	$G\alpha_{i1}$, $G\alpha_{i2}$, $G\alpha_{i3}$, $G\alpha_o$, $G\alpha_z$, $G\alpha_t$, $G\alpha_{gust}$	Inhibit adenylate cyclase
$G\alpha_q$	$G\alpha_q$, $G\alpha_{11}$, $G\alpha_{14}$, $G\alpha_{15}$ and $G\alpha_{16}$	Stimulate Phospholipase C-β activity
$G\alpha_{12}$	$G\alpha_{12}$ and $G\alpha_{13}$	Rho family GTPase signalling

The stimulatory G protein $G\alpha_s$ largely interacts with, and activates, the effector adenylate cyclase. This enzyme is responsible for the conversion of adenosine triphosphate (ATP) to cyclic adenosine monophosphate (cAMP). cAMP is a versatile secondary messenger within the cell capable of interacting with multiple signalling molecules to regulate processes in the majority of cell types (Edwards et al., 2012). For instance, cAMP activates protein kinase A (PKA), which phosphorylates a range of proteins to influence glycogen synthesis or the activation of Ca^{2+} channels and modulation of muscle contraction (Taussig and Zimmermann, 1998; Gancedo, 2013).

In direct contrast to $G\alpha_s$, the inhibitory $G\alpha_i$ proteins inhibit adenylate cyclase reducing the intracellular concentration of cAMP. However, it must be noted that $G\alpha_t$ subtype mediates phototransduction through activation of phosphodiesterases (PDEs) (Sokal et al., 2003). $G\alpha_i$ has also been implicated in the activation of inwardly-rectifying K^+ channels and can influence the activity of phospholipase C (PLC) (Peleg et al., 2002; Lei et al., 2003; Lüscher and Slesinger, 2010).

PLC produces inositol trisphosphate (IP_3) and diacylglycerol from phospholipid phosphatidylinositol 4,5-bisphosphate (PIP_2). DAG and IP_3 bind and activate protein kinase C and Ca^{2+} channels of the sarcoplasmic reticulum respectively. PLC exists in several isoforms and the $G\alpha_q$ family stimulate PLCβ to increase cytoplasmic Ca^{2+} concentrations (Berridge, 1993; Wettschureck, 2005; Berridge, 2009).

Finally, the $G\alpha_{12}$ family of G proteins are known to interact with Rho GTPases. Rho GTPases are small monomeric G proteins that are highly conserved throughout *Eukaryota*. Like $G\alpha$, Rho GTPases are binary switches whose state is determined by the bound nucleotide. When GTP bound, Rho GTPases are noted for their effects in cytoskeletal organisation, morphology and polarity in a range of cell types (Perez and Rincón, 2010).

1.3.3 G$\beta\gamma$ propagated signalling

There are estimated to be 5 Gβ and 12 human Gγ subunits in mammalian cells (Gautam et al., 1998; McCudden et al., 2005). While encoded by separate genes these proteins are synthesised and trafficked together and seldom found separately . The Gβ subunit contains a WD-40 (tryptophan-aspartic acid) tandem repeat region that folds into a propellor-like tertiary structure. This region is a defining feature of the Gβ subunit and a benchmark through which potential Gβ subunits can be identified (Mos et al., 2013). The Gγ subunit contains C-terminal lipid modification sites key to membrane localisation. It has also been suggested that this subunit plays a significant role in GPCR coupling (Chinault and Blumer, 2003).

The G$\beta\gamma$ dimer can act as negative regulator of G protein signalling. Indeed, by blocking the nucleotide binding site of the Gα subunit, G$\beta\gamma$ prevents spontaneous nucleotide exchange and G protein activation. However, G$\beta\gamma$ is also a signal propagator in its own right. It has long been known that G$\beta\gamma$ activates G protein-regulated inward rectifier K^+ (GIRK) channels to trigger cell hyperpolarisation *in vivo* (Logothetis et al., 1987). This subunit has been shown to regulate a variety of kinases including extracellular signal-regulated kinases (ERK), janus kinases (JNK) and MAPK such as p38 (reviewed by McCudden et al. (2005)). It has also been reported that the specific G$\beta\gamma$ combinations can selectively activate various signalling pathways (Logothetis et al., 1987; Wolfe et al., 2003).

1.4 GPCR Pharmacology

1.4.1 Receptor activation and GPCR ligands

The two-state receptor model predicts that the receptor population exists in an equilibrium between the R and R* state (Kenakin, 2004). Ligands are capable of selectively binding, altering and stabilising different receptor states, thus shifting this equilibrium (Figure 1.7). Agonists interact with the receptor to induce and stabilise the R* state. This in turn recruits and activates signalling molecules such as G proteins. The extent of downstream signalling following receptor activation defines the nature of the agonist. Full agonists interact with a receptor's orthosteric site to stimulate the maximal level of signal for a given system. Partial agonists only induce a fraction of this response. The two-state model predicts that this is likely to be due to the the differences in the R:R* equilibrium induced by agonists and partial agonists.

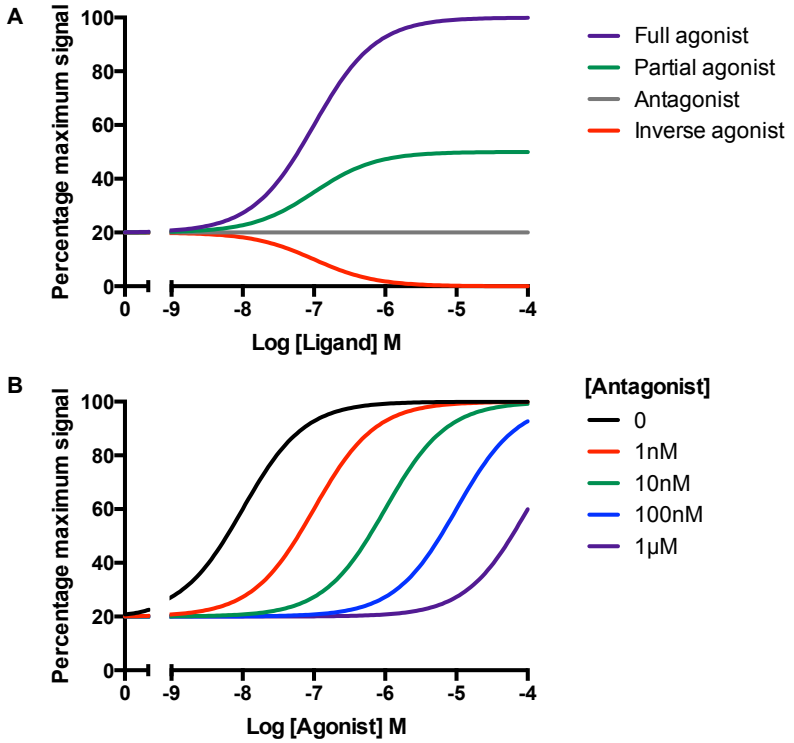

Figure 1.7: **The effect of ligands on concentration-response curves.** The two-state receptor model assumes a dynamic equilibrium between active (R) and inactive receptors (R*). Different ligands influence this equilibrium. **A.** Agonists and partial agonists push the equilibrium towards the R* state. Antagonists and inverse agonists stabilise the R state. **B.** Competitive antagonists shift agonist concentration-response curves rightwards.

In contrast, antagonists shift the equilibrium closer to the R state. Antagonists can be classified as competitive or non-competitive. Competitive antagonists bind the orthosteric site, preventing agonist binding. However, this interaction is transient and can be overcome by increasing agonist concentration (Figure 1.7). Non-competitive antagonists typically bind a site distinct from the orthosteric site, or covalently modify and permanently alter the orthosteric site, thus preventing generation of of the R* state.

Receptors can exist in the R* state in the absence of ligand. This spontaneous activation, and consequent downstream signalling, is termed constitutive activity and has been a useful tool in the targetting and study of GPCRs. Constitutively active mutant (CAM) variants of GPCRs can be generated that mimic the active receptor state (Ladds et al., 2005a). Most CAMs contain modifications that disrupt the ionic lock, particularly on TM6 and its interface with ICL3. This has provided an excellent experimental system to study the active state of a range of GPCRs, their structure and their implications for downstream signalling (Kobilka and Deupi, 2007).

Constitutive receptors are also of significant therapeutic interest. A number of pathologies, such as retinitis pigmentosa and hyperthyroidism have been linked to spontaneous generation of CAMs *in vivo* (Hwa et al., 1997). In these cases inverse agonists have great therapeutic potential. These ligands selectively bind and stabilise the R state. This manifests itself as a reduction in downstream signalling and therefore basal response. This has the potential to correct elevated signalling for undesirable CAMs. Inverse agonists also provide an avenue to reduce downstream signalling and second messenger concentrations through endogenous constitutively active GPCRs (Chalmers and Behan, 2002).

1.4.1.1 Allosterism

Secondary ligand binding sites known as allosteric sites exist across many receptor families, including GPCRs (De Smet et al., 2014). This allows a given receptor to simultaneously bind multiple ligands, the interactions of which can profoundly alter both receptor state and interactions with downstream signalling pathways (Wootten et al., 2013). There are multiple classes of allosteric ligand. One such class is the positive allosteric regulator (PAM). PAMs do not elicit any response through a receptor on their own but have cooperative effects when combined with agonists. Through binding the allosteric site, PAMs alter the orthosteric binding site to increase its affinity for specific agonists. This manifests as a leftwards shift in the agonist concentration response curve and an increase in signalling (Christopoulos and Kenakin, 2002). PAMs have been discovered and developed for a number of GPCRs, including the adenosine A_1, M_2-muscarinic and calcium-sensing GPCRs (Hill et al., 2014; Christopoulos, 2014). In contrast, negative allosteric modulators decrease the affinity of orthosteric sites for endogenous agonists, reducing ligand sensitivity

and downstream signalling (Kenakin, 2004). Allosteric compounds can also have multiple mechanisms of action though the ability to bind the orthosteric site. Hence, these compounds exhibit intrinsic agonist or antagonist activity in the absence of an orthosteric ligand (Jarvis et al., 1999; Knudsen et al., 2007). The ability to influence agonist selectivity presents an attractive opportunity to fine-tune downstream signalling. This has led to the development of biopic ligands that can simultaneously occupy and influence both the orthosteric and allosteric sites (Valant et al., 2012).

1.4.1.2 Dimerisation and bivalent ligands

Thus far this study has considered GPCRs as monomeric complexes. Indeed, some GCPRs such as the β_1-adrenergic receptor have been shown to solely act as monomers. However, the related β_2 adrenergic receptor forms homodimeric complexes (Lohse, 2010). This is far from an isolated case. Many GPCRs form homodimeric, heterodimeric or higher order complexes though interactions between the TM domains (Milligan et al., 2007; Rivero-Müller et al., 2013) Oligomerisation has many advantages for GPCRs, particularly for trafficking and membrane localisation. Dimerisation can occur in the endoplasmic reticulum, allowing complexed receptors to be transported to the membrane together (reviewed by Milligan (2009)). Indeed, dimerisation is essential for Class C GPCR function where one protomer binds ligand while the other binds and activates a G protein (Romano et al., 1996; Bai et al., 1998; Okamoto et al., 1998; Zhang et al., 2014).

The presence of GPCR oligomers presents both pharmacological challenges and opportunities. Higher order complexes complicate ligand-binding and pharmacology, especially where one protomer can allosterically influence the other (Rozenfeld and Devi, 2010; Hill et al., 2014). However, the development of bitopic ligands allows specific targeting and activation of particular GPCR dimers. These compounds contain two distinct ligand domains connected by a short linker domain that can simultaneously activate multiple binding sites across the dimer (Narlawar et al., 2010; Valant et al., 2012, 2014)

1.4.2 Receptor internalisation

The duration and localisation of a receptor is key to proper signalling. Consequently, the spatial and temporal regulation of GPCRs is tightly controlled in the cell through expression, trafficking and internalisation. Defects in the latter process lead to overexpression of a receptor at the cell surface, excess signalling and a number of disease states. In the case of the protease activated receptor-1 (PAR-1) GPCR, defects in receptor trafficking have been linked to cancer (Marchese et al., 2008). Internalisation varies between receptors and organisms, but the C-terminal tail of the GPCR is a key, conserved feature of this process (Wolfe and Trejo, 2007; Croft et al., 2013).

GPCR internalisation can be agonist dependent or constitutive. Agonist-bound receptor complexes have a high affinity for G protein-coupled receptor kinases (GRKs). There are at least 7 GRKs in mammalian cells that phosphorylate key serine and threonine, but rarely tyrosine, residues on the C-terminus and ICL3 region of the receptor. The phosphorylated GPCR can then engage with a family of proteins known as β-arrestins (Lefkowitz, 2005). This small family consists of β-arrestins-1-4. Confusingly, β-arrestins 2 and 3 are also known as β-arrestins 1 and 2 (Shenoy and Lefkowitz, 2011). β-arrestins consist of structurally distinct N and C-termini flanking a core of 12 polar residues (Hirsch et al., 1999). The core binds binds the phosphorylated residues of the GPCR, exposing the C-terminus of the β-arrestin to the cytosol. This allows the arrestin to perform two functions; inhibition of G protein signalling and to serve as a scaffold for other protein complexes. Typically, the C-terminus binds clathrin and various adaptor proteins, such as AP-2 or the dynamin GTPase, required for clathrin-mediated endocytosis. The GPCR can remain in the endosome for rapid recycling to the cell surface. This allows for quick desensitisation and response to the ligand. Indeed, GPCRs such as the β_2-adrenergic receptor are capable of signalling from the endosome (Shenoy et al., 2006). Alternatively, the receptor can be targeted for lysosomal or proteasomal degradation (Marchese et al., 2008; Correll and McKittrick, 2014) (Figure 1.8).

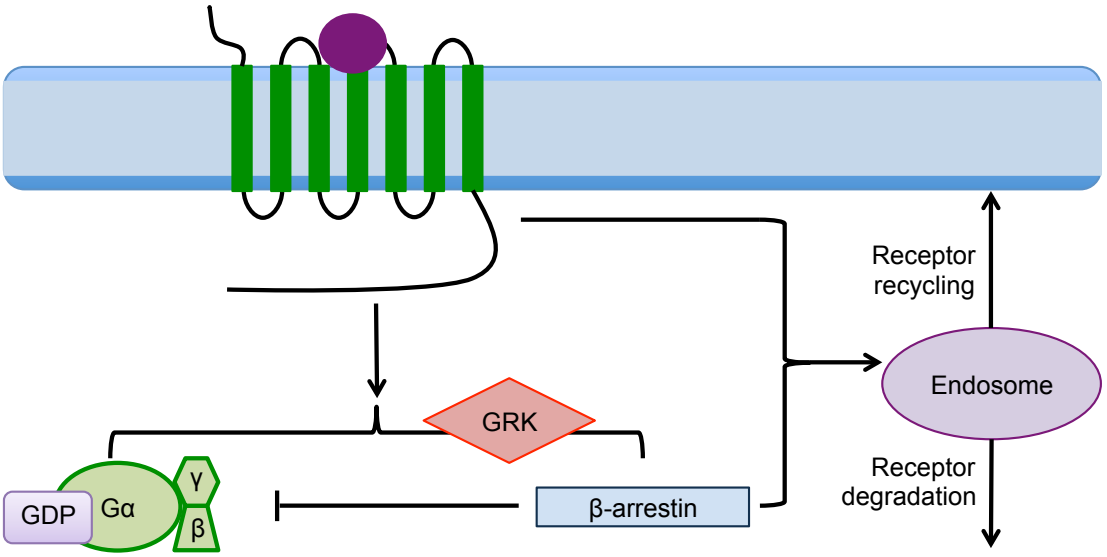

Figure 1.8: **GPCR interactions with β-arrestins and internalisation.** The C-terminus active, agonist-bound GPCR serves as a substrate for GRKs. GRKs phosphorylate specific serines and threonines, enabling β-arrestin recruitment. β-arrestins inhibit G protein activation while serving as a scaffold for internalisation machinery. The internalised GPCR can be held in the endosome for rapid receptor recycling or targeted for degradation. β-arrestins can also trigger signalling in various kinases in response to an active GPCR. Figure adapted from Correll and McKittrick (2014)

However, β-arrestin-independent mechanisms of internalisation exist. Some GPCRs, such PAR-1, can directly interact with the AP-2 adapter protein to shuttle back and forth between the endosome and plasma membrane independent of ligand (Paing et al., 2004). GPCRs, such as the M3-muscarinic receptors can also internalise through clathrin-independent mechanisms (Scarselli and Donaldson, 2009).

1.4.3 β-arrestin signalling

Historically, β-arrestins have been viewed as negative regulators of GPCR signalling and as scaffolds for clathrin-mediated endocytosis. However, β-arrestins also serve as scaffolds for a range of kinases and are becoming increasingly prominent as signalling molecules in their own right. The specificity of this scaffold varies between receptors. The most well-characterised β-arrestin signalling pathways are mitogen activated protein kinases (MAPK) pathways, particularly the extracellular signal-regulated kinases (ERK) pathways activated by the β-adrenergic receptor (reviewed by Shenoy and Lefkowitz (2011)). Here, the agonist-bound GPCR recruits β-arrestin-2. This forms a scaffold for the endocytotic machinery and for the MAPK kinase kinase (MAPKKK) Raf-1. This phosphorylates the MAPK kinase (MAPKK) MEK-1 that activates the MAPK ERK1/2. Phosphorylated ERK1/2 can then activate a range of downstream effectors. However, the MAPK pathway activated is receptor specific. For instance, the angiotensin II GPCR triggers the sequential phosphorylation of Ask1, MKK4 and JNK through β-arrestins (Charest et al., 2005). The activity

of β-arrestins as signalling scaffolds is not limited to MAPK pathways. β-arrestins have also been shown to have both inhibitory and stimulatory effects on PI3K and downstream effects on IP_3 signalling. These signalling scaffolds have also been reported to interact with phosphodiesterases, counteracting cAMP generation and influencing downstream G protein-mediated signalling (DeFea, 2011).

1.5 GPCR signalling bias

Some GPCRs, such as the neurotensin receptor, couple to and activate a single G protein ($G\alpha_i$) to influence downstream signalling (Mustain et al., 2011). However, many GPCRs are promiscuous, binding and activating multiple effectors. Such non-selective pathway activation through a single drug target can greatly contribute to adverse effects. However, the ligand bound to a GPCR can preferentially activate various signalling pathways. This is thought to be through the existence and stabilisation of multiple active receptor states, each with a different affinity for a given signalling effector. This could manifest as preferential activation of G proteins over β-arrestins. This ability to control downstream signalling through ligand alone is termed bias, functional selectivity or agonist-directed trafficking (Figure 1.9). This has signifiant implications for the pharmaceutical industry in terms of rational drug design and reduced adverse effects (reviewed by Shonberg et al. (2014)).

An excellent example of G protein/ β-arrestin signalling bias is the μ-opioid receptor (MOR). This GPCR is a powerful target for pain and exploited by analgesics such as morphine. Like many GPCRs, the MOR is capable of signalling through multiple pathways, both G protein dependent and G protein-independent. The analgesic properties of morphine arise through $G\alpha_{12}$ activation (Pradhan et al., 2010, 2012). However, adverse drug effects include addiction, nausea and inflammation at high sustained doses. β-arrestin knockout mouse models (Raehal, 2005) show greater sensitivity to morphine with reduced adverse effects. This suggests that the adverse effects of MOR ligands are due to unwanted activation of the β-arrestin mediated signalling. Consequently, ligands have been developed that bias MOR signalling through G protein-dependent pathways with reduced adverse effects (Chen et al., 2013; DeWire et al., 2013). Thus, ligand bias has significant implications for rational drug design and is of significant interest to the pharmaceutical industry.

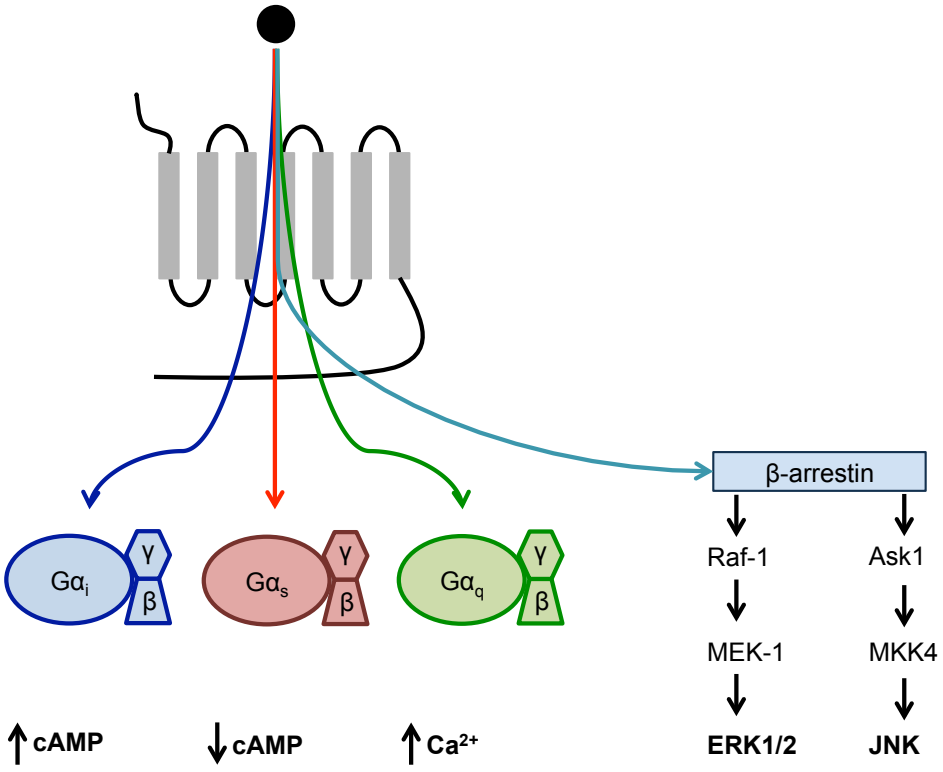

Figure 1.9: **GPCR signalling bias.** Many GPCRs are capable of signalling through multiple effectors, G proteins and β-arrestins to regulate a variety of downstream processes. In these cases, the bound ligand can directly influence the signalling pathway activated. This is termed bias, functional selectivity or agonist-directed trafficking.

Ligand bias is not limited to preferentially signalling via G protein-dependent or G protein-independent mechanisms. Many GPCRs are capable of selective G protein activation in response to ligand. An excellent example of this is the GLP-1R. The GLP-1R responds to the peptide hormone GLP-1 to influence blood glucose homeostasis *in vivo*. Consequently, the GLP-1R is an attractive target for the treatment of Type-2 diabetes. This receptor is capable of signalling through $G\alpha_s$ and $G\alpha_i$ and can both stimulate and inhibit adenylate cyclase. Weston et al. (2014) demonstrated that the preferential activation of $G\alpha_s$ and $G\alpha_i$ is a function the ligand, varying between GLP-1 and its degradation product. Further, they hypothesise that this bias is a negative feedback mechanism for rapid termination of signal.

1.6 Modelling GPCR pharmacology

The precise mechanisms underlying bias are unclear. X-ray crystallography has produced a multitude of active and inactive receptor structures with remarkably consistent TM helix arrangements (Palczewski et al., 2000; Tsuchiya et al., 2002; Park et al., 2008; Chien et al., 2010). This would appear to favour the two-state model of activation. While it is hypothesised that multiple active receptor conformations exist these models only account for the receptor and not the effector; G protein or β-arrestin. Consequently, the contribution of the effector is ignored. This study aims to understand the kinetic contribution of the ligand, the GPCR and the effector in determining signalling bias. However, this information is not easily accessible experimentally. Systems pharmacology, and by extension systems biology, combine experimental and theoretical approaches to elucidate details not available through either method alone. Here, mathematical models are applied to experimental data to understand the changes in ligand binding, receptor activation and downstream signalling. Fortunately, GPCRs are extremely well characterised and there are a number of mathematical models available for use.

1.6.1 Structural models

There are approximately 130 crystal structures of GPCRs solved to date and this number is growing rapidly. Consequently, there is a vast amount of structural information available to inform mathematical models. For example, homology modelling uses a known crystal structure as a template for a receptor whose structure is unknown. The amino acid sequence, and potential transmembrane domains, are aligned and mapped onto the equivalent regions and residues of a known structure (Tuccinardi et al., 2006). This allows for a range of predictions to be made about the unknown structure including its potential docking interactions with ligands and other proteins (Córdova-Sintjago et al., 2012). This approach has generated a model of the active adenosine A_1 receptor using the crystal structure of the active, ligand-bound, adenosine A_{2A} receptor. This model was used to predict the ligand binding characteristics of a range of novel agonists (Knight *et al., in preparation*). However, homology modelling has a number of limitations. The selection of the correct template is crucial and can be difficult or counterintuitive. Additionally, the template structure may require editing before a homology model can be developed. While the TM domains are largely conserved, the ECL and ICL regions of GPCRs are highly variable and and conformationally flexible. The conformation of the ECL regions in particular has significant implications for the ligand binding pocket. These limitations present difficulties in generating an accurate homology model (Costanzi, 2012, 2013).

Even after the generation of a successful homology model, consequent mechanistic information is lacking. The best a homology model can do is predict whether two molecules can dock in a given conformation. How they interact is often elusive. Structural studies, whether generated by homology modelling or X-ray crystallography, can be extended by more complex modelling techniques. An example of this is molecular dynamics simulation. These models can provide atomistic levels of data on a protein structure and its potential conformational changes and movements as a function of time. The potential interactions between different residues and atoms are stored in a force field that dictates both the complexity and progression of the simulation. However, this method is incredibly expensive in terms of both time and raw computational power. Consequently, the majority of simulations are in the nano to μ-second range and are limited to a small subset of molecules (Linderman, 2009). To date there are no molecular dynamics studies that include the ligand, the receptor and the G protein. While molecular dynamics modelling could potentially be used to identify the functional unit of functional selectivity, computational expense limits its feasibility at this time. However, simpler modelling techniques can be employed to understand the kinetics of bias.

1.6.2 Equilibrium models

Equilibrium models typically use one or more simple equations to evaluate a system at steady state. These models can be fitted to experimental data through algorithms such as least squares regression to estimate a number of parameters. These approaches are an essential part of modern pharmacology. For example, the logistic equation has been used extensively to quantitate the features of sigmoidal concentration-response curves in response ligands. These include basal ligand-independent signal, the maximum level of signal (E_{max}) and EC_{50} (the ligand concentration required to elicit half maximal response, a measure of sensitivity) (Goutelle et al., 2008). This model is an excellent system to explore and compare ligands and basic details of their mechanisms. Comparing E_{max} allows for full/ partial agonism to be determined while the basal allows the level of constitutive activity to be measured. While this model is extremely useful, it can be limited. For example, the EC_{50} is a measure of sensitivity on a system level. This includes contributions from the ligand, the GPCR and the effector that cannot be distinguished by this equation. However, slightly more complex equilibrium models that describe systems at steady-state can separate these processes (Motulsky and Christopoulos, 2004). This has advantages when studying ligand bias.

1.6.2.1 The Operational Model of Pharmacological Agonism

Black and Leff (1983) revolutionised quantitative pharmacology with the development of the operational model of pharmacology (hereby referred to as the operational model). This model assumes a very simple reaction scheme where a ligand binds a receptor with an affinity K_A. The active, ligand-bound, receptor (LR) then triggers downstream signalling to bring about a response with a signal transduction coefficient, K_E (Figure 1.10). However, the efficiency of signal transduction is also dependent on the concentration of active receptor. Consequently, a new term was used to define the efficiency of downstream signalling. This is known as efficacy or τ and is calculated as $\frac{[LR]}{K_E}$. This reaction scheme was evaluated at steady state, where all reactions are at equilibrium.

$$Response = Basal + \frac{E_{max} - Basal \cdot \tau^n \cdot [A]^n}{\tau^n \cdot [A]^n + ([A] + K_A)^n} \tag{1.1}$$

Here n represents the slope of the exponential phase of the concentration-response curve or the proportionality of response between $Basal$ and E_{max}. Generally it is assumed that the response is linearly proportional to ligand concentration in this range and n is constrained to 1.

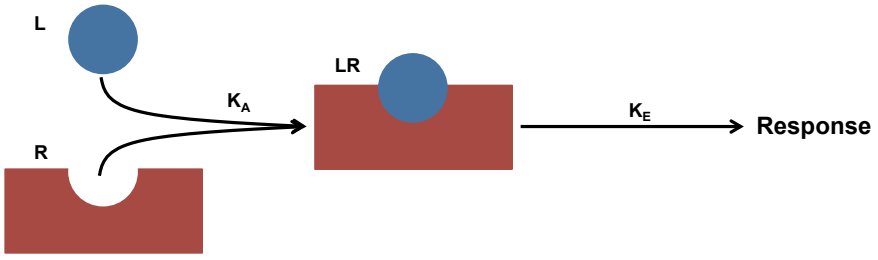

FIGURE 1.10: **The Operational Model of Pharmacological Agonism.** Ligand (L) binds receptor, with an affinity K_A to form and active ligand receptor (LR) complex. This complex can then induce downstream signalling with a signal transduction coefficient K_E. However, the efficiency of signal transduction is also dependent on the amount of LR available. Consequently, efficacy or τ, determined as $\frac{[LR]}{K_E}$, is used as a measure of downstream signalling efficiency.

This simple model is extremely powerful. Its simplicity allows it to be applied to any system where a drug binds a target to induce a quantitative signalling response. When applied to GPCR signalling, K_A represents ligand binding and τ is essentially a black box containing both G protein activation and all downstream signalling. This distinction between ligand binding and downstream signal allows this model to be used to quantitate bias. Rajagopal et al. (2011) used this model to develop a method to directly compare and quantify signalling bias between different signalling pathways for various ligands targeting a single receptor.

Since its publication in 1983 the operational model has had profound effects on pharmacology. Indeed, it has been adapted to new ligands, new applications and even to include allosterism as evidenced by the collected works of Prof. Terry Kenakin and Prof. Arthur Christopoulos (Christopoulos and Kenakin, 2002; Kenakin, 2004; Kenakin et al., 2012; Christopoulos, 2014; Shonberg et al., 2014). Thanks to their efforts, this model remains a central tenet of GPCR pharmacology. However, this model does have some significant limitations. This model effectively separates EC_{50} into K_A and τ, splitting a system level response into ligand binding and downstream signal transduction.

$$EC_{50} = \frac{K_A}{1+\tau} \tag{1.2}$$

As K_A and τ represent two intrinsically linked, but potentially unknown, variables one cannot be accurately calculated without knowledge of the other. While this does not affect the calculation of bias factors as described by Rajagopal et al. (2011) it does hinder the usefulness of this model in looking at the contribution of the ligand, receptor and G protein to functional selectivity. However, more complicated models can overcome this limitation as outlined below.

1.6.3 Ordinary differential equation models

Biochemical reactions and pathways are highly dynamic processes in which concentrations of various species are continuously changing with respect to time and position. The simplicity of equilibrium models is both their greatest strength and greatest weakness. While they are extremely versatile their predictions can be ambiguous, such as the K_A and τ values of the operational model. However, differential equation models study non-equilibrium processes that might be important. The most basic form of differential equation is the ordinary differential equation (ODE), a deterministic model that describes the change of a variable with respect to time. These models are well-suited for modelling biochemical processes, such as signal transduction pathways, and are relatively easy to construct. For example, the reaction scheme of Figure 1.11 denotes a simple pathway with a series of interacting components. Each interaction has an intrinsic rate of activity. Here A is converted to B with a rate of K_1, B becomes C with a rate of K_2, C inhibits A with a rate of K_3 and A is continuously generated with a rate of K_4.

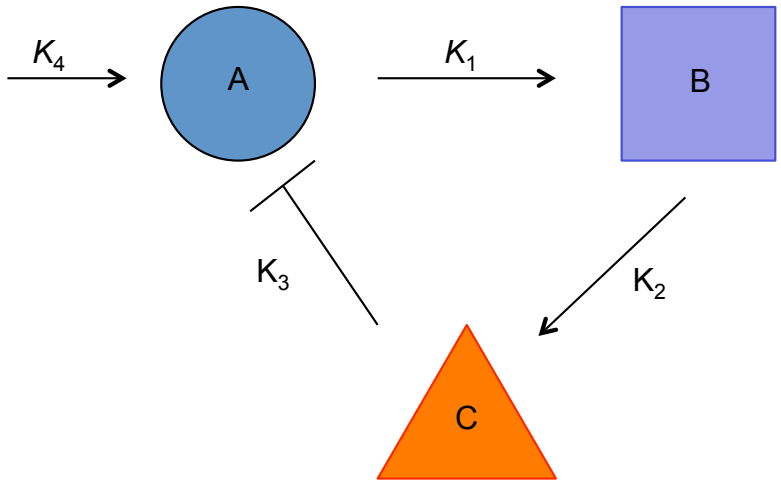

FIGURE 1.11: **A basic biochemical reaction scheme.** In this simple scheme, A is converted to B. B becomes C which inhibits A. A is automatically generated. Each of these processes has an intrinsic rate, K.

The laws of mass action dictate that a reaction, with a single mechanistic step, is a product of the concentration of the reactants and the intrinsic reaction rate. By assuming mass action kinetics an expression, ν, can be generated for each reaction.

$$\nu_1 = [A] \cdot K_1 \tag{1.3}$$

$$\nu_2 = [B] \cdot K_2 \tag{1.4}$$

$$\nu_3 = [C] \cdot K_3 \tag{1.5}$$

$$\nu_4 = K_4 \tag{1.6}$$

ODEs can then be built using positive or negative forms of these expressions depending on whether the species of interest is being generated or depleted.

$$\frac{d[A]}{dt} = \nu_4 - \nu_1 - \nu_3 \tag{1.7}$$

$$\frac{d[B]}{dt} = \nu_1 - \nu_2 \tag{1.8}$$

$$\frac{d[C]}{dt} = \nu_2 - \nu_3 \tag{1.9}$$

These simple deterministic models can be extended to include spatial regulation of the species being modelled. This can be achieved through either modelling two forms of a given species, each representing a different compartment, as implemented by Croft et al. (2013), or by extending the differential equation model to include two dimensions of movement, space and time. These are known as partial differential equations. A further extension of this model type is to include a term for stochasiticity that draws its parameters from a

probability distribution. The consequent stochastic model never reproduces the same data twice and better represents the inherent complexity, variability and unpredictability of biological systems. Despite these extensions, the simple ODE model remains an extremely powerful tool in quantitatively exploring GPCR pharmacology (Linderman, 2009).

1.6.3.1 Ordinary differential equation models of GPCRs

A notable example of a GPCR ODE model is the cubic ternary complex model (Weiss et al., 1996). This model was designed to be thermodynamically complete, containing a distinct number of receptor states and interconversions between them, each with an associated rate constant. Here the receptor can exist in R or R* conformation. Each of these conformations can also bind a G protein (G) or agonist (A). The ability of this model to include an inactive GPCR binding a G protein touches upon an outlying question in GPCR pharmacology: does the receptor precouple to a G protein?

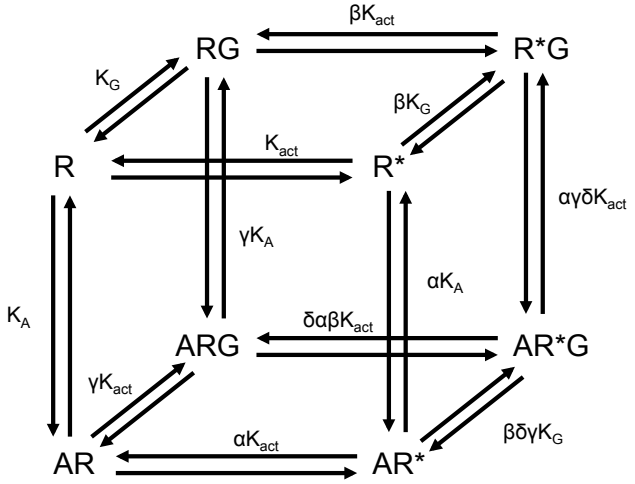

FIGURE 1.12: **The cubic ternary complex model.** This model describes the conversion of a GPCR between inactive (R) and active (R*) states. This model also incorporates association with the G protein (G) both prior to and following agonist (A) binding. Here K_A, K_G and K_{act} represent the equilibrium constants of agonist binding, G protein recruitment and receptor activation respectively. α, β, γ and δ are thermodynamic constants that influence the interactions between individual components. Figure adapted from Linderman (2009).

If an endogenous GPCR is removed from a simple system there is a significant increase in the basal level of signal (Davey, 1998). This would suggest that the GPCR can act as a negative regulator of signalling and must couple to the G protein while inactive. Indeed, studies using fluorescent proteins suggest that GPCRs and G proteins precouple (Galés et al., 2005; Nobles et al., 2005). However, the traditional collision-coupling model suggests a transient interaction between an active GPCR and G protein with a reaction-diffusion based mechanism (Tolkovsky and Levitzki, 1978; Brinkerhoff et al., 2008). The cubic ternary complex model includes both collision-coupling and precoupling. By setting

the rates of R and G association to zero, this model condenses to a collision-coupling mechanism. However, while this model describes the kinetics of receptor activation and G protein recruitment it does not include the G protein cycle. Thus, it would require extension to make predictions of downstream signalling. Shea et al. (2000) used this approach to suggest that collision coupling alone can be used to explain experimentally observed trends. However, the authors also accepted that this study does not completely eliminate pre-coupling as a precursor to agonist binding and downstream signalling.

Kinetic ODE models are very powerful tools when combined with experimental approaches. However, the cubic ternary complex model contains 24 reactions between 8 different species governed by 4 thermodynamic parameters and 3 kinetic rate constants in various combinations. All to describe one ligand binding one receptor to activate one G protein. The promiscuity of GPCRs and crosstalk between competing signalling components hinders the application of these models to mammalian systems. This limitation can be circumvented by turning to much simpler experimental systems.

1.7 Unravelling complexity: Yeast as a model system

Unicellular yeast G protein signalling pathways are highly conserved with those of mammalian systems. While the mechanisms are consistent, yeast signalling pathways contain far fewer components. This, combined with an experimental robustness, low cost and an inherent genetic tractability result in an excellent experimental system with which to modify, dissect and explore cellular processes (Ladds et al., 2005b). The resulting findings and hypotheses can then be applied to equivalent mammalian systems.

The budding yeast *Saccharomyces cerevisiae* has proven to be an excellent system to study the mechanisms of GPCR signalling. *Sc. cerevisiae* has two GPCR signalling pathways; a glucose-sensing pathway and a pheromone-response pathway. There is very little interaction between these two processes. Thus, either of these pathways can serve as an model to study a G protein signalling cascade in isolation. The pheromone-response pathway in particular has proved to be exceptionally useful in this regard. For example, RGS proteins were first discovered in *Sc. cerevisiae* leading to the identification of RGS proteins in mammalian cells (Chan and Otte, 1982a,b; Dohlman et al., 1995).

1.7.1 *Saccharomyces cerevisiae* pheromone response

When undergoing vegetative growth *Sc. cerevisiae* cells exist in a haploid state with either an **a** or α mating type. The mating types share the same G protein signal transduction machinery but express different GPCRs (Figure 1.13). **a**-cells are defined by the expression of STE3 that responds to the peptide pheromone **a**-factor, while α-cells respond to the α-factor pheromone via STE2. Pheromone binding the relevant GPCR causes the activation of a heterotrimeric G protein consisting of GPA1 (the Gα) and the STE4-STE18 G$\beta\gamma$ dimer. Negative regulation of the G protein cycle is achieved through the intrinsic GTPase activity of GPA1 and the prototypical RGS protein SST2. Negative regulation at the receptor level is achieved through the yeast casein kinases 1 and 2 (YCK1 and YCK2). Active STE2 recruits YCK1 and YCK2 to promote receptor ubiquitination, internalisation and ultimately destruction (Roth and Davis, 1996).

In *Sc. cerevisiae* the G$\beta\gamma$ is the effector, triggering signal transduction through binding STE20 and activating a MAPK cascade. Here, STE11, STE7 and STE12 are sequentially phosphorylated. However, in this pathway the STE11 STE7 and FUS3 are complexed with the STE5 scaffold protein. Scaffolding the MAPK cascade ensures proper membrane localisation of signaling components and has implications for regulation. The scaffold limits the number of proteins each MAPK can activate, thus limiting amplification of signal (Shao et al., 2006; Chen and Thorner, 2007; Thomson et al., 2011). Once phosphorylated FUS3, now FUS3PP, dissociates from the MAPK scaffold to activate a number of downstream targets to prime the cell for mating.

FUS3PP binds and activates the STE12 transcription factor to activate a number of pheromone-responsive genes, including the agglutinin FUS1 required for cell fusion, SST2 and the STE2 or STE3 GPCRs depending mating type. BAR1 expression is also under the control of the pheromone-response-pathway. This protease is secreted to the extracellular space where it breaks down the ligand, terminating the signal (MacKay et al., 1988).

FUS3PP also activates the cyclin inhibitor FAR1 and CDC28 to initiate G1-phase cell cycle arrest, an essential step required to ensure haploidy and efficient mating (Tyers and Futcher, 1993). FUS3PP also phosphorylates the formin BNI1 to induce cytoskeletal reorganisation and cell polarisation. The cell begins to grow towards the source of the pheromone through the development of a projection known as a shmoo. The shmoo of one mating partner meets one of the opposite mating type, forming a new diploid cell. These cells undergo sporulation under conditions of nutrient starvation until resources become less scarce (Merlini et al., 2013).

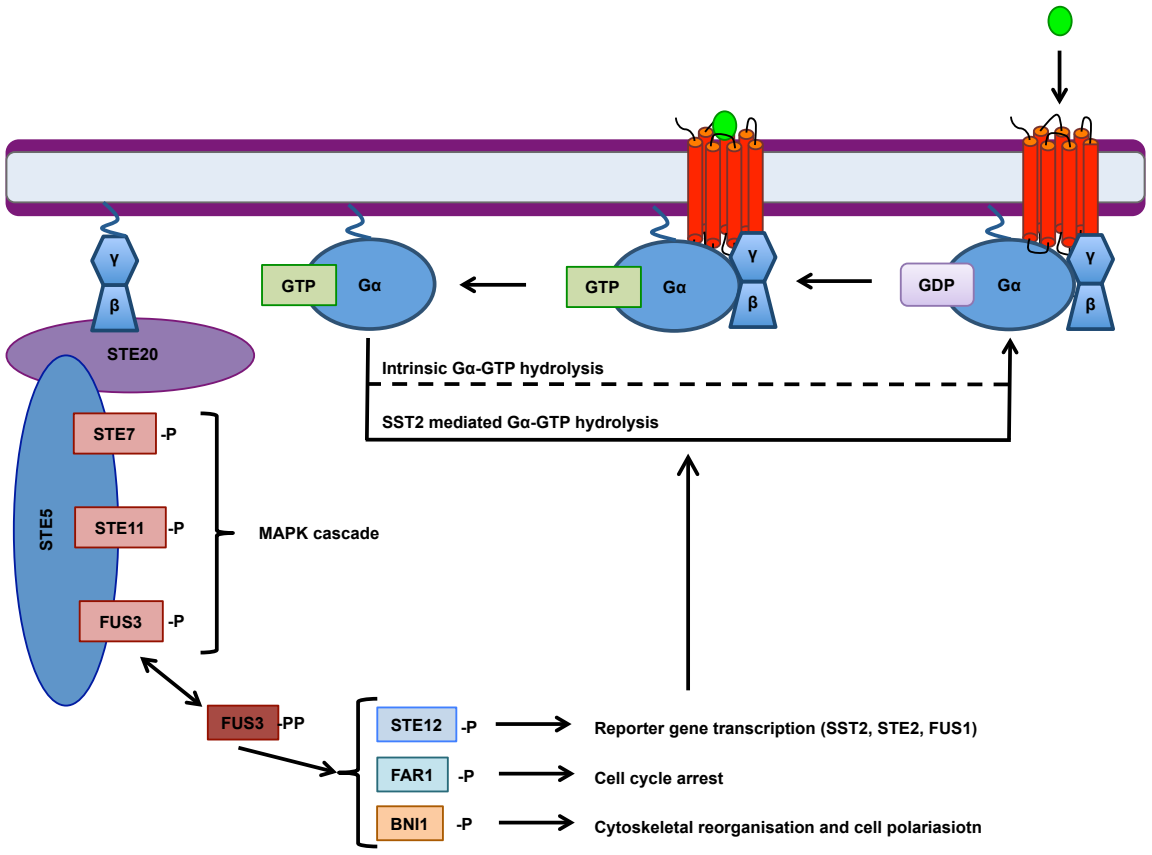

FIGURE 1.13: **The *Saccharomyces cerevisiae pheromone response*** Haploid *Sc. cerevisiae* cells exist as either the α or **a** mating type that express the STE2 or STE3 GPCR, respectively. The active receptor activates a heterotrimeric G protein consisting of GPA1 and a STE4 STE18 G$\beta\gamma$ dimer. Free G$\beta\gamma$ recruits STE20 and activates a scaffolded MAPK cascade consisting of STE11, STE7 and FUS3. Phosphorylated FUS3 dissociates from the scaffold and activates a range of effectors to induce changes in gene expression, cell cycle arrest, cell polarisation and movement.

1.7.2 Yeast transplant strains

The *Sc. cerevisiae* pheromone response has done much to elucidate the mechanisms of G protein signalling. The expression of a single yeast GPCR in a simple pathway has limited implications for our understanding of mammalian receptor pharmacology and bias. However, the yeast pheromone response is capable of responding to mammalian GPCRs. For example, the neurotensin receptor is capable of interacting with GPA1 and promotion of signal through this pathway (Leplatois et al., 2001). While, this artificial interaction can elucidate receptor level effects, the information gained on mammalian G protein signalling in response to ligand is limited. The yeast pheromone response can also signal through mammalian G proteins, such as the Gα_s. This approach was used to functionally couple the β_2-adrenergic receptor to this pathway (King et al., 1990). While the GPCR G protein interaction is closer to a mammalian system, the efficiency of signal transduction in yeast is greatly reduced relative to the endogenous GPA1 (Price et al., 1996).

Mammalian GPCRs can be expressed and coupled to the yeast pheromone response while maintaining a mammalian receptor-G protein interaction through the use of transplant G proteins. A number of studies have shown that the specificity of the GPCR G protein interaction is determined by the C-terminus of the Gα, particularly the last 5 residues (Brown et al., 2000; Ladds et al., 2003; Sunahara et al., 2012).

A series of transplant strains have been generated in *Sc. cerevisiae* and the fission yeast *Schizosacchromyces pombe* where the Gα has been removed and replaced with a counterpart that contains the 5 C-terminal amino acids of a mammalian Gα. These have been used to study individual mammalian GPCR G protein interactions in isolation (Olesnicky et al., 1999; Brown et al., 2000; Ladds et al., 2003). The *Sz. pombe* pheromone response shares many basic similarities with that of *Sc. cerevisiae* but there are key mechanistic differences between them. Most notably, the *Sz. pombe* pheromone response utilises the Gα as an effector that stimulates an unscaffolded MAPK cascade (Hoffman, 2005).

Transplant *Sc. cerevisiae* strains have been far more extensively used to study mammalian GPCRs. To date, *Sc. cerevisiae* has been used to study a wide range of mammalian GPCRs including the β_2-adrenergic (King et al., 1990) μ-opioid (Lagane et al., 2000), vasopressin (Erlenbach et al., 2001b) and C5a receptors (Klco et al., 2005). The Frizzled receptors deserve particular note as it was the yeast pheromone response that was used to identify its interactions with various G proteins (Dirnberger and Seuwen, 2007; Nichols et al., 2013). Of the various transplant yeast systems available, the strains developed by Brown et al. (2000) have been widely used to study GPCR mediated signalling in multiple G protein backgrounds. Here they developed a panel of yeast strains containing one of eleven G protein transplants, each representing an individual isolated mammalian G protein (Table 1.2). These strains were initially validated using somatostatin, serotonin, purinergic, melatonin and adenosine A_{2B} receptors where mammalian pharmacology was faithfully replicated. Since their creation, these strains have been to study a wide range of GPCRs. These include the nicotinic (Wise et al., 2003), muscarinic (Erlenbach et al., 2001a; Stewart et al., 2010) and adenosine receptor families in addition to Family B GPCRs such as GLP-1 (Stewart et al., 2009; Peeters et al., 2011, 2012; Bertheleme et al., 2013, 2014; Weston et al., 2014).

However, these receptors have been extensively characterised in mammalian systems. The yeast transplant system of Brown et al. (2000) has proven to be particularly powerful in studying orphan GPCRs that have no known ligand or function. Consequently, they are extremely difficult to study in a mammalian setting. Expressing an orphan GPCR in a series of yeast transplant strains and treating them with millions of compounds using high throughput screening technology can elucidate which G protein signalling pathways may be activated by a given ligand. Indeed, this approach was used to identify ligands and roles for GPR41, GPR43 and GPR55 (Brown, 2002; Brown et al., 2011).

TABLE 1.2: **Gα transplants and their C-terminal residues.** Strains developed by Brown et al. (2000)

Gα transplant	**C-terminal residues**
GPA1	KIGII
GPA1/Gα_q	EYNLV
GPA1/Gα_{12}	DIMLQ
GPA1/Gα_{13}	QLMLQ
GPA1/Gα_{14}	EFNLV
GPA1/Gα_{16}	EYNLV
GPA1/Gα_o	GCGLY
GPA1/G$\alpha_{i1/2}$	DCGLF
GPA1/Gα_{i3}	ECGLY
GPA1/Gα_z	YIGLC
GPA1/Gα_s	QYELL

The *Sc. cerevisiae* transplant strains are an excellent tool to study mammalian pharmacology. The simplicity of the yeast system, the availability of the strains developed by Brown et al. (2000) and the ability to isolate mammalian receptor G protein interactions presents an opportunity to model signalling bias. However, it must be noted that the yeast system has one crucial limitation when studying GPCR signalling bias. Yeast do not signal through β-arrestins. Instead receptor internalisation is mediated through ubiquitination. Consequently, studies of functional selectivity in the yeast system are strictly limited to G-protein bias.

1.7.3 Models of yeast signal transduction

The yeast pheromone response is a model pathway upon which our knowledge of GPCR signalling has been constructed. Consequently, this pathway has been very well characterised experimentally and computationally. Thus, there is a wide array of data and theoretical frameworks available with which to model G protein bias in the *Sc. cerevisiae* transplant system. This includes a number of ODE models of the yeast G protein cycle.

The most influential of these studies was conducted by Yi et al. (2003). Here, they developed a fluorescence resonance energy reporter (FRET) reporter system to study G protein signalling dynamics. This technique exploits pairs of fluorescent proteins to measure the rate at which two proteins dissociate or associate. A FRET pair was generated where GPA1 was fused to cyan fluorescent protein (CFP) and STE18 was fused to yellow fluorescent protein (YFP). The rate at which this FRET pairing moved beyond a certain radius was measured as a change in fluorescence in response to ligand. This led to the development of an ODE model that was fitted to the experimental data of the FRET reporter strains. This study, and the calculated rate constants, laid the foundation for a number of other theoretical studies.

One such model is that of Hao et al. (2003) (Figure 1.14). This model represents one of the first examples of combining mathematical and experimental approaches to the yeast system. Here a simple model was devised to explore the RGS protein, SST2, and its effects on $G\alpha^{GTP}$ hydrolysis. This model consists of GDP and GTP-bound $G\alpha$, free $G\beta\gamma$ and the heterotrimeric G protein in addition to SST2. Typically, RGS proteins accelerate $G\alpha^{GTP}$ hydrolysis, desensitising the system to G protein activation and therefore ligand. This model allows SST2 activation to promote its own internalisation and destruction. This would manifest as a desensitisation of the system and positive feedback on a pathway level. This prediction shows good agreement with experimental data, an excellent example of the systems biology approach. However, the model of Hao et al. (2003) does not include any signalling processes downstream of the G protein cycle. Yildirim et al. (2004) extended this model to include downstream transcriptional responses including up regulation of SST2, GPA1, STE18 and β-galactosidase.

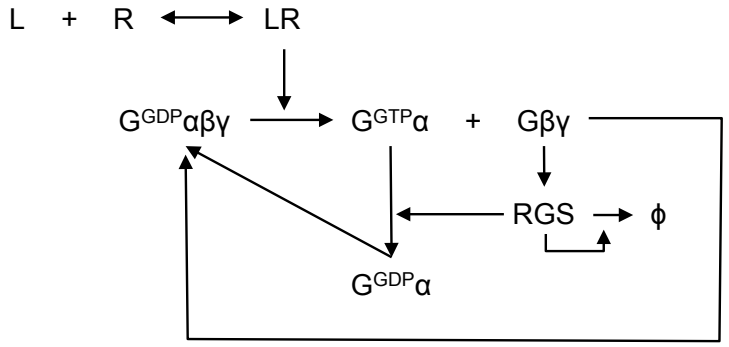

FIGURE 1.14: **The Hao model of yeast GPCR signalling.** The ligand (α-factor) binds to the STE2 receptor (R) to form LR. LR catalyses the conversion of $G^{GDP}\alpha\beta\gamma$ to the $G\alpha^{GTP}$ and $G\beta\gamma$ effector. $G\beta\gamma$ induces activation of the RGS. The RGS can potentiate its own degradation (ϕ denotes a null set) or catalyse the conversion of $G\alpha^{GTP}$ to $G\alpha^{GDP}$. This can combine with $G\beta\gamma$ to reform the inactive $G^{GDP}\alpha\beta\gamma$. Figure adapted from Hao et al. (2003).

Despite this extension by Yildirim et al. (2004) the actual processes of downstream signalling were summarised into single non-linear terms. A more comprehensive ODE model was generated by Kofahl and Klipp (2004). This ambitious study attempted to accurately recreate the temporal dynamics of 35 individual species in the *Sc. cerevisiae* pheromone response through 47 separate reactions governed by 47 individual parameters (Figure 1.15). Many of these parameters were derived from Yi et al. (2003). This model contains receptor activation, the G protein cycle, the MAPK scaffold formation, MAPK signalling and activation of FAR1 as cells enter cell cycle arrest and prepare to mate. To date, the detail of this model has not yet been surpassed, although Shao et al. (2006) used a derivation of this model to study the dynamics of the MAPK scaffold.

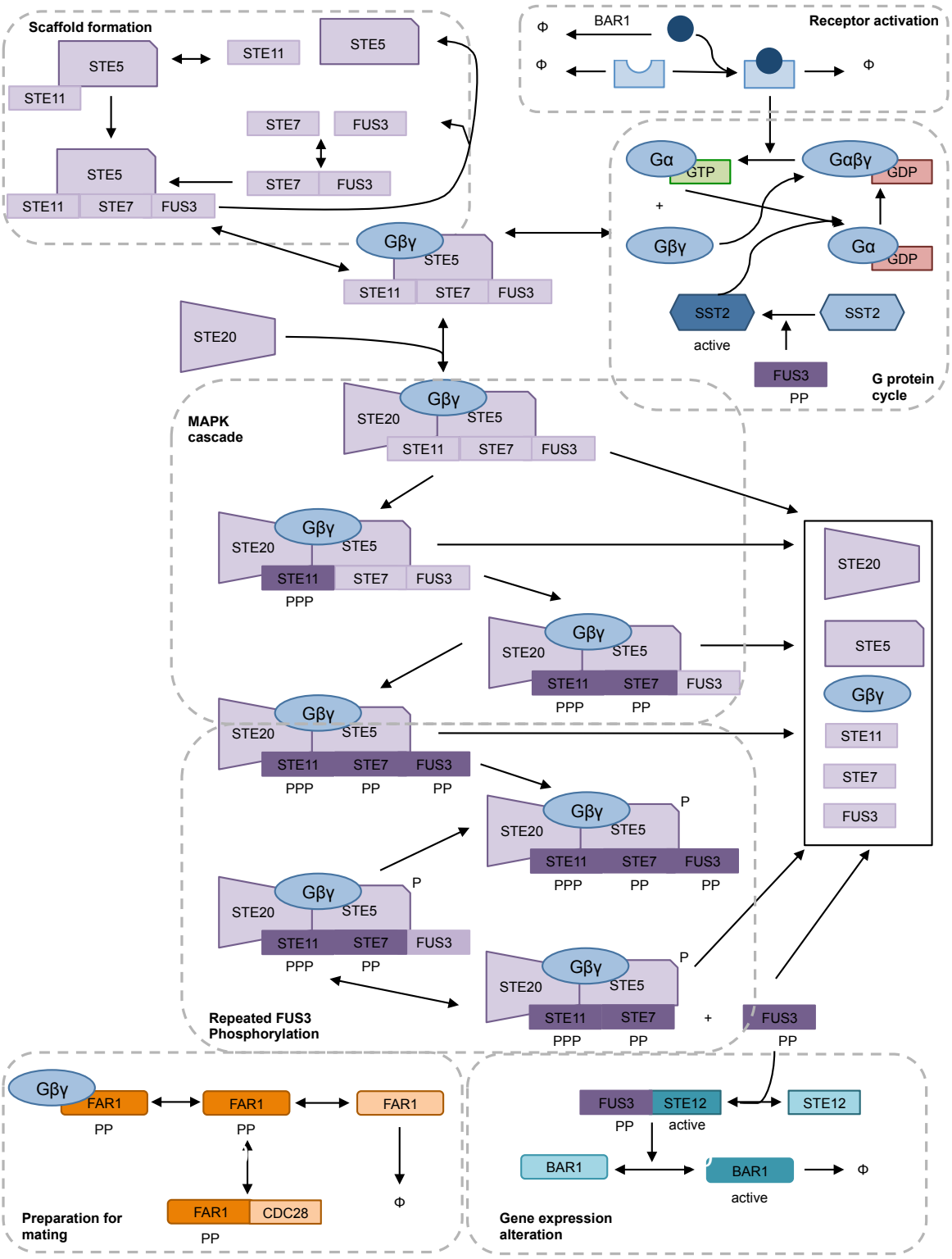

FIGURE 1.15: **The Kofahl and Klipp model of yeast GPCR signalling.** A detailed reaction scheme showing every interaction within the *Sc. cerevisiae* pheromone response considered by this model. These can grouped into scaffold formation, receptor activation, G protein cycle, the MAPK cascade, repeated FUS3 phosphorylation, preparation for mating by cell cycle arrest and changes in gene expression. ϕ denotes degradation or loss of a species. Figure adapted from Kofahl and Klipp (2004).

While this model represents a powerful tool to study the *Sc. cerevisiae* pheromone response on a system level it does have a number of limitations. For example, there is no true gene expression alteration in this model. BAR1 and SST2 are pheromone responsive genes, under the control of the STE12 transcription factor. However, in this model, latent BAR1 is activated by a FUS3PP:STE12$_{active}$ complex. Similarly, active SST2 is generated from inactive SST2 by FUS3PP. These terms were designed to mimic the effects of transcription but do not replicate transcription itself.

The interaction between the receptor and the G protein in this model shares both a strength and a weakness with earlier models. Ligand activates the receptor, but does not dissociate. However, the active receptor does not bind and activate the G protein. G protein activation simply has the concentration of active receptor influence the rate of reaction without actively participating (i.e. the GPCR concentration is not increased or decreased by this reaction). This precludes a great deal of mechanistic detail. Consequently, this model cannot distinguish between receptor G protein-binding and G protein-activation and how these separate processes may be affected by different ligands. However, this also allows this model to accommodate both pre-coupling and collision coupling without including them directly.

The Smith et al. (2009) model of the yeast pheromone response has much more comprehensive G protein cycle, reminiscent of the cubic ternary complex model, that includes both pre-coupling and collision coupling as mechanisms for G protein activation (Figure 1.16). While this model was developed to describe the *Sz. pombe* pheromone response it uses parameters and initial conditions from the Hao et al. (2003); Yi et al. (2003); Kofahl and Klipp (2004) studies of the *Sc. cerevisiae* pathway. This model, where Gα is the effector, qualitatively replicates a counterintuitive feature of the *Sz. pombe* pheromone response. RGS proteins are negative regulators of signalling. Deletion of RGS results in an increased E_{max} and an increased sensitivity to ligand, as observed with SST2 in *Sc. cerevisiae* (Hao et al., 2003). However, in *Sz. pombe* RGS deletion results in a decreased E_{max} and an increased sensitivity to ligand. The Smith model predicts that this is the result of the Gα entering an inert state after activation of the MAPK cascade despite still being GTP bound. This would result in a refractory period where signalling cannot occur. This model can qualitatively recreate this effect in *Sz. pombe*. This model can also be modified to reproduce trends in the *Sc. cerevisiae* system by using G$\beta\gamma$ as an effector, albeit with reduced sensitivity to ligand (Smith et al., 2009).

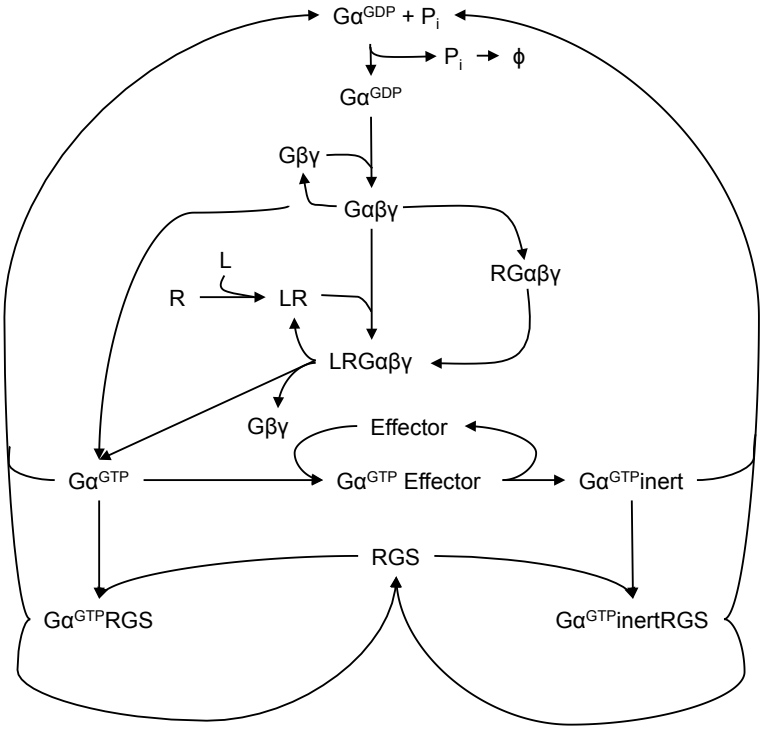

FIGURE 1.16: **The Smith model of *Sz. pombe* GPCR signalling.** This reaction scheme details the model of Smith et al. (2009). This model uses both collision and pre coupling where ligand (L) can bind a receptor (R) bound or unbound to the inactive G protein ($G\alpha\beta\gamma$). $G\alpha\beta\gamma$ dissociates to $G\alpha^{GTP}$ and $G\beta\gamma$. $G\alpha^{GTP}$ interacts with an effector to promote downstream signalling before entering and inert GTP-bound state. $G\alpha$ or $G\alpha^{GTP}$ are hydrolysed to $G\alpha^{GDP}$ through intrinsic GTP hydrolysis or under the influence of the RGS. $G\alpha^{GDP}$ then reassociates with $G\beta\gamma$ to form the inactive $G\alpha\beta\gamma$.

1.7.4 Adenosine receptors

It is a central tenet of systems biology that a mathematical model is only as good as the predictions it can make. As we have observed with the operational model, these predictions can be limited by lack of experimental information or unknown parameters. Thus, the modelling of signalling bias presented here must be based on an appropriate receptor. Ideally, this receptor would have been well characterised in both yeast and mammalian systems. The range of pharmacological tools available for this receptor are also crucial. For instance, the ability to measure ligand binding rates would greatly inform modelling studies. A member of a receptor family would also be advantageous to this thesis due to the inherent opportunities to expand the modelling studies.

The adenosine receptors are a small family of class A GPCRs, consisting of the A_1, A_{2A}, A_{2B} and A_3 receptor subtypes. These receptors all respond to the purinergic nucleoside adenosine. Adenosine has an extremely wide tissue distribution and equally varied roles across throughout the body. Consequently, the adenosine receptors influence a variety of processes. However, the roles, tissue distribution and pharmacology of these receptors differ greatly.

1.7.4.1 The Adenosine A_1 receptor

The adenosine A_1 receptor (A_1R) has a wide tissue distribution but prominent roles in the central nervous system (CNS) and cardiovascular system. This is a predominantly $G\alpha_{i/o}$-coupled GPCR, inhibiting adenylate cyclase with downstream effects on PKA in response to ligand, but can also regulate other effectors. For example, ERK phosphorylation has been reported in response to the A_1R, a β-arrestin mediated process (Gracia et al., 2013). The A_1R interacts with voltage-dependent K^+ channels in the cardiovascular system and has consequently been a target for supra ventricular bradycardia. This receptor also modulates neurotransmitter release throughout the brain, notably in the cerebellum, hippocampus and forebrain. Thus the A_1R has presented an attractive target for sleep disorders (Verzijl and IJzerman, 2011).

Due to its therapeutic relevance to cardiovascular and cerebral disorders a wide range of selective A_1R ligands have been developed. These include agonists, allosteric modulators and antagonists. A_1R agonists are typically derivatives of adenosine while theophylline based compounds such as xanthines are antagonists. Caffeine is an extremely widely consumed A_1R antagonist globally and this has had a direct impact on clinical trials targeting this receptor. Poor patient compliance through the consumption of tea, coffee and chocolate, can affect the pharmacology and efficacy of the compound being trialled (Ribeiro and Sebastiao, 2010).

Crucially this receptor has been well characterised in both mammalian cells and yeast in response to a number of ligands. Stewart et al. (2009) in particular used both experimental systems to demonstrate $G\alpha_{i/o}$-coupling and evidence, but not direct quantification, of signalling bias. Studies of A_1R ligands have been far more extensively characterised in mammalian cells and a vast database exists to validate predictions generated in yeast (Sharman et al., 2011).

There has also been significant interest in the development of fluorescent A_1R ligands. By covalently attaching fluorophores to agonists and antagonists ligand binding can be observed in real time on a single cell or population level. There have been a range of A_1R selective agonists created over the years but only one has been commercially available during this project (Briddon et al., 2004; Middleton et al., 2007; Baker et al., 2010; Kozma et al., 2013). This tool has profound implications for modelling GPCR pharmacology and improving the accuracy of their predictions. Indeed, a significant part of the data presented here aids the development of novel fluorescent compounds with Dr. Jennifer Hemmings and Prof. Martin Lochner of the University of Bern, Switzlerland.

Due to its extensive characterisation, functional expression in the yeast system and range of pharmacological tools available, the A_1R is an excellent candidate to develop and implement a model of ODE bias. However, the other adenosine receptor subtypes are pharmacologically diverse and also of significant interest.

1.7.4.2 The Adenosine A_{2A} receptor

In contrast to the A_1R, the $A_{2A}R$ is a primarily $G\alpha_s$ coupled receptor, however $G\alpha_{olf}$ and $G\alpha_q$ coupling has been reported with downstream effects on adenylate cyclase and PLC-β. The $A_{2A}R$ has also been reported to activate $G\alpha_i$ in mammalian systems when dimerised with the A_1R (Casadó et al., 2010). Like the A_1R, it has a broad tissue distribution with a particular presence in platelets, cardiac muscle, blood vessels and peripheral nerves. It is also located within the striatum and olfactory bulb of the CNS (Lynge and Hellsten, 2000; Sheth et al., 2014). Consequently, the $A_{2A}R$ has received therapeutic interest for coronary dilation and Parkinson's disease via agonists and antagonists respectively. The $A_{2A}R$ also has a role in angiogenesis, a vital step in tumour formation and is an attractive target for anticancer drugs (Sachdeva and Gupta, 2013).

This receptor receives particular attention for its high constitutive activity, due in part to its lack of ionic lock. Mutagenesis studies have identified regions crucial to constitutive activity that can be applied to other GPCRS. Two studies identified key residues responsible for GPCR thermostability and constitutive activation, demonstrating a negative correlation between the two (Bertheleme et al., 2013, 2014). Encouragingly, these studies exploited the yeast transplant system. However, these studies used a GPA1/$G\alpha_i$ transplant G protein that may not have an equivalent mammalian interaction with the $A_{2A}R$.

To date, the $A_{2A}R$ is the only adenosine receptor with a solved crystal structure in both the presence and absence of ligand (Lebon et al., 2011; Xu et al., 2011) (Figure 1.17). These structural studies have suggested a roles for TM3, TM5 and TM7 in receptor activation that are shared amongst all GPCRs (Lebon et al., 2011). These structures have had particular relevance for the other adenosine receptors and has served as a template for the generation of homology models.

1.7.4.3 The Adenosine A_{2B} receptor

In contrast to the A_1R and $A_{2A}R$, the $A_{2B}R$ is a low affinity receptor that is normally dormant under physiological extracellular adenosine concentrations. Consequently, the $A_{2B}R$ is activated in high stress conditions *in vivo* such as adenosine release from cells undergoing apoptosis. Its tissue distribution is restricted to gastrointestinal, cardiovascular and mast cells with a particular role in immuno- and inflammatory disorders including asthma and chronic obstructive pulmonary disease. However, the $A_{2B}R$ is the least characterised of the adenosine receptor subytpes (Jacobson, 2009).

Like the $A_{2A}R$, the $A_{2B}R$ is known to activate adenylate cyclase and PLC-β through $G\alpha_s$ and $G\alpha_q$ respectively but has also been reported to signal through MAPK cascades. The $A_{2B}R$ has also been shown to functionally couple to the yeast system. Indeed this was one of the first receptors to be used in the system developed by Brown et al. (2000) and functional couplings have been reported in the strains representing $G\alpha_q$, $G\alpha_o$, $G\alpha_{i1}$, $G\alpha_{i3}$, $G\alpha_s$, $G\alpha_{14}$ and $G\alpha_{16}$. However, this receptor has been more extensively studied using the GPA1/$G\alpha_{i3}$ strain (Peeters et al., 2011; Liu et al., 2014). To date there is little evidence that the $A_{2B}R$ couples to $G\alpha_i$ *in vivo*.

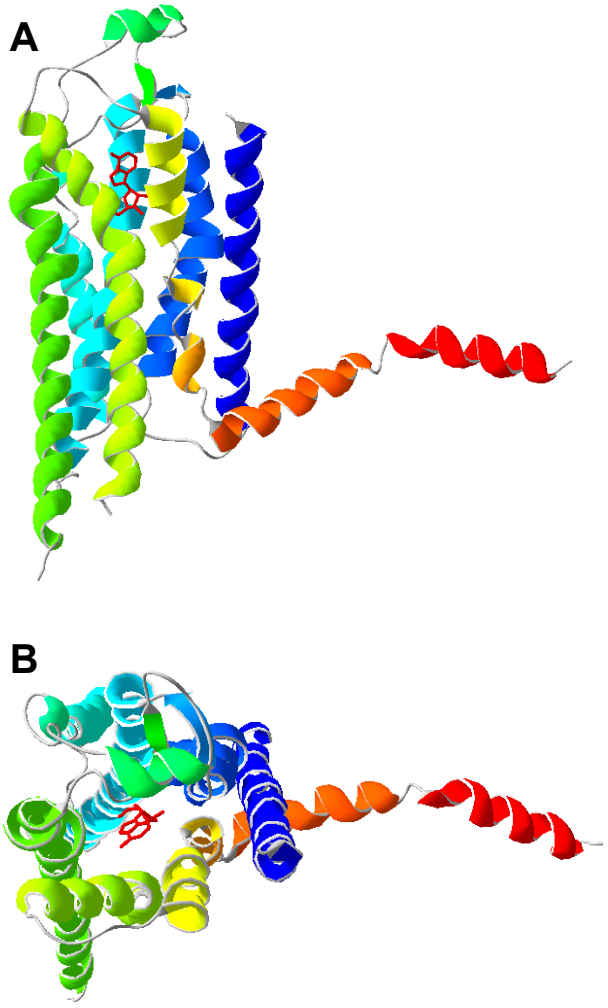

FIGURE 1.17: **The crystal structure of adenosine-bound $A_{2a}R$.** PDB ID 2YDO (Lebon et al., 2011). $A_{2A}R$ represented as ribbon structure. Ball and stick representation of adenosine shown in red. **A.** "Side-on" view of receptor. **B.** "Top-down" view of receptor.

1.7.4.4 The Adenosine A_3 receptor

The adenosine A_3 receptor (A_3R) is a primarily $G\alpha_i$ and $G\alpha_q$ coupled GPCR. In addition to inhibition of adenylate cyclase and activation of PLC-β this receptor has also been reported to signal through MAPK. ERK1/2 and WNT signalling pathways. Like the other adenosine receptor subtypes, the A_3R has a broad tissue distribution and a myriad of roles. It is known to be expressed throughout the immune and cardiovascular systems in addition to the CNS. Consequently, this receptor has been implicated in a number of inflammatory and immune disorders including asthma, glaucoma and hypoxia (Antonioli et al., 2014). Its activity in the CNS has presented an attractive target for Parkinson's disease whereas its involvement in MAPK mediated apoptosis has potential for an anticancer treatment (Jacobson and Gao, 2006; Wagner et al., 2010).

The A_1R and $A_{2A}R$ have comparable high affinities while the $A_{2B}R$ is a low affinity receptor. The A_3R is an intermediate affinity receptor. However this receptor was the last to be discovered and studies of the A_3R are still in their infancy. Regardless, there has been a great deal of attention paid to this receptor and, while the crystal structure of this structure is still unknown, many homology and structural models of the A_3R have been generated (Cheong et al., 2013). To date no studies have reported functional expression of the A_3R in the yeast system. The presents an attractive goal for this study of adenosine receptor pharmacology in *Sc. cerevisiae*.

1.8 Aims

This study aims to understand the contribution of the ligand, the receptor and the G protein to functional selectivity of the A_1R in yeast. To achieve this, this study aims to:

- **Express and characterise all four adenosine receptor subtypes.**
  Determine G protein coupling in yeast.
  Examine bias and receptor selectivity of adenosine receptor agonists.

- **Screen novel adenosine receptor agonist**
  Screen precursor compounds to inform novel fluorescent agonist development in collaboration with Dr. Jennifer Hemmings (University of Bern).

- **Model G protein signalling bias of the A_1R in yeast**
  Develop a minimal ODE model of G protein signalling in yeast guided by existing theoretical frameworks. Apply this model to experimental data to predict the contribution of the ligand, receptor and G protein to signalling bias.

Chapter 2

Materials and Methods

2.1 Materials

2.1.1 General laboratory reagents

Analytical grade laboratory reagents were purchased from Sigma-Aldrich Co. Ltd. (Poole, Dorset, UK) and Merck BDH Laboratory Supplies (Poole, Dorset, UK)

2.1.2 Molecular Biology Reagents

Restriction enzymes, T4 DNA ligase and *Taq* DNA polymerase (from *Thermus aquaticus*) were supplied by Life Technologies Ltd. (Paisley, Scotland, UK). Bacterial alkaline phosphatase and FastStart high fidelity enzyme blend were purchased from Fermentas (York, UK) and Roche Diagnostics Ltd (Lewes, East Sussex, UK) respectively. All oligonucleotides were synthesised by Sigma-Alrich Co. Ltd. (Poole, Dorset, UK).

2.1.3 Ligands

Adenosine was purchased from Sigma-Aldrich Co. Ltd. (Poole, Dorset, UK). 5'-N-Ethyl carboxyamidoadenosine (NECA), 2-chloro-N^6-cyclopentyladenosine (2CCPA), CGS21680, di-propylcyclopentylxanthine (DPCPX), SLV-320 and PD81723 were purchased from R&D Systems (Bristol, UK). CAS200623 was purchased from CellAura (Nottingham, UK). All compounds with a JH prefix were synthesised by Dr. Jennifer Hemmings (University of Bern, Switzerland).

2.1.4 Photographic Supplies

DNA gels were visualised using a G:Box iChemi gel documentation system with GeneTool analysis software (Syngene, Cambridge, UK).

2.1.5 Growth media

Luria broth, yeast extract (YE) and agar were supplied by Life Technologies Ltd. (Paisley, Scotland, UK). All components of Amino Acid (AA) selective medium (detailed in Table 2.3) were purchased from Sigma-Aldrich Co. Ltd. (Poole, Dorset, UK) Plates and liquid media for the selective growth of yeast were made using AA media. Rich (YE) medium containing (250 μg/ml) adenine, leucine and uracil was used for non-selective growth of yeast. The following media were made by dissolving the reagents in reverse osmotically filtered (RO) water. Plates were made by supplementing liquid media with 1.5 % (w/v) agar.

Table 2.1: Yeast extract medium (YE) (per litre)

Yeast extract	5 g
Glucose	30 g

Table 2.2: Selective medium (AA) (per litre)

Yeast nitrogen base (without amino acids)	6.7 g
Glucose	20 g
Amino acid mix	1.5 g
Selection amino acid mix	0.5 g

2.1.6 Bacterial Strain

Escherichia coli (E. coli) strain DH5α (*E. coli*; genotype: *supE44 hsdR17 endA96 thi-1 relA1 recA1 gyrA96*) was used for amplification of plasmids. Strain supplied by Stratagene (Cambridge, UK).

2.1.7 *Saccharomyces cerevisiae* strains

Standard nomenclature has been used to describe the *Sc. cerevisiae* strains used in this thesis (Table 2.5). Gene deletions at the *yfg* locus are denoted *yfgΔ*. Gene integrations at specific loci, for example the ADE2 adenine biosynthesis gene, are denoted as *yfgΔ::ADE2*. Creation of strains with a MMY prefix are described in Olesnicky et al. (1999) and Brown et al. (2000). Strains with a SC prefix are unique to this thesis.

his3, leu2, trp1 and *ura3* were deleted to allow histidine, leucine, tryptaphan and uracil to be used as nutritional markers for selection respectively. *can1* encodes arginine permease

Table 2.3: Amino acid mix

L-alanine	2 g
L-arginine	2 g
L-asparagine	2 g
L-cysteine	2 g
L-glutamine	2 g
L-glutamate	2 g
L-glycine	2 g
L-isoleucine	2 g
L-lysine	2 g
L-phenylalanine	2 g
L-proline	2 g
L-serine	2 g
L-threonine	2 g
L-tryptophan	2 g
L-tyrosine	2 g
L-valine	2 g
myo-inositol	2 g
para-amino benzoic acid	0.4 g

Table 2.4: Select amino acid mix (components as required)

Adenine	2 g
L-histidine	2 g
L-leucine	4 g
Uracil	2 g
L-methionine	2 g

and has been deleted to prevent basic amino acid transport into the cell, thus maintaining the appropriate nutritional markers (Whelan et al., 1979).

The *gpa1* locus has been deleted to prevent expression of GPA1, the Gα endogenous to this pathway. Genes encoding GPA1 transplants, with the 5 C-terminal amino acids replaced with those of mammalian G proteins, were integrated into these strains using a tryptophan selection marker to allow mammalian GPCRs to signal through this pathway (Brown et al., 2000).

These strains are *Δste2* to prevent expression of the native GPCR, STE2, that signals through this pathway. Yeast cells can also switch mating type and express the GPCR STE3, which also signals through the MAPK pathway of the pheromone response. Thus, these strains are *MAT*a deficient to prevent mating type switching. The gene encoding the endogenous RGS protein, *sst2*, has been deleted to increase the sensitivity of the yeast system to receptor activation (Brown et al., 2000; Yildirim et al., 2004).

Sc. cerevisiae enters cell-cycle arrest in response to pheromone. This is under the control of FAR1, which interacts with cyclin-dependent kinases to bring about cell-cycle arrest in response to the MAPK FUS3 (Tyers and Futcher, 1993). *far1* has been deleted and *his3* placed under the control of the pheromone-responsive *fus1* promoter. *his3* encodes imidazoleglycerol-phosphate dehydratase - a key step in the histidine biosynthesis pathway. Thus HIS3 expression, and therefore growth in histidine deficient media, can be used as a transcriptional reporter of pathway activation. Alternatively, β-galactosidase has also been placed under the control of the *fus1* promoter and integrated into these strains. This allows β-galactosidase to be used as a quantitative measure of pathway activation.

The *ADORA1* gene, encoding the adenosine A_1 receptor, has been integrated at the *ura3* locus in the SC195, SC197, SC199 and SC222 strains using the pRS306GPD expression factor. A C-terminal A_1R^{GFP} fusion was cloned into the pRS306GPD expression vector and integrated into the *ura3* locus of MMY22, MMY23, MMY24 and MMY25 to create SC209, SC211, SC213 and SC215 respectively.

Table 2.5: ***Sc. cerevisiae* strains.** Standard names of *Sc. cerevisiae* strains and their corresponding genotypes as used in this study. Strains with a MMY prefix are described in Brown et al. (2000) and used under license from GlaxoSmithKline, Stevenage, UK.

Strain	**Genotype**
MMY9	*MAT*a, *his3 leu2 trp1 ura3 can1 gpa1Δ::ADE2 far1Δ::ura3Δ sst2Δ::ura3Δ fus1::FUS1-HIS3 LEU2::FUS1-lacZ*
MMY11	*MAT*a, *his3 leu2 trp1 ura3 can1 gpa1Δ::ADE2 far1Δ::ura3Δ sst2Δ::ura3Δ fus1::FUS1-HIS3 LEU2::FUS1-lacZ ste2ΔG418^R*
MMY12	*MAT*a, *his3 leu2 trp1 ura3 can1 gpa1Δ::ADE2 far1Δ::ura3Δ sst2Δ::ura3Δ fus1::FUS1-HIS3 LEU2::FUS1-lacZ ste2ΔG418^R TRP::GPA1*
MMY14	*MAT*a, *his3 leu2 trp1 ura3 can1 gpa1Δ::ADE2 far1Δ::ura3Δ sst2Δ::ura3Δ fus1::FUS1-HIS3 LEU2::FUS1-lacZ ste2ΔG418^R TRP::GPA1/Gα$_{q(5)}$*
MMY16	*MAT*a, *his3 leu2 trp1 ura3 can1 gpa1Δ::ADE2 far1Δ::ura3Δ sst2Δ::ura3Δ fus1::FUS1-HIS3 LEU2::FUS1-lacZ ste2ΔG418^R TRP::GPA1/Gα$_{16(5)}$*
MMY19	*MAT*a, *his3 leu2 trp1 ura3 can1 gpa1Δ::ADE2 far1Δ::ura3Δ sst2Δ::ura3Δ fus1::FUS1-HIS3 LEU2::FUS1-lacZ ste2ΔG418^R TRP::GPA1/Gα$_{12(5)}$*
MMY20	*MAT*a, *his3 leu2 trp1 ura3 can1 gpa1Δ::ADE2 far1Δ::ura3Δ sst2Δ::ura3Δ fus1::FUS1-HIS3 LEU2::FUS1-lacZ ste2ΔG418^R TRP::GPA1/Gα$_{13(5)}$*
MMY21	*MAT*a, *his3 leu2 trp1 ura3 can1 gpa1Δ::ADE2 far1Δ::ura3Δ sst2Δ::ura3Δ fus1::FUS1-HIS3 LEU2::FUS1-lacZ ste2ΔG418^R TRP::GPA1/Gα$_{14(5)}$*
MMY22	*MAT*a, *his3 leu2 trp1 ura3 can1 gpa1Δ::ADE2 far1Δ::ura3Δ sst2Δ::ura3Δ fus1::FUS1-HIS3 LEU2::FUS1-lacZ ste2ΔG418^R TRP::GPA1/Gα$_{o(5)}$*
MMY23	*MAT*a, *his3 leu2 trp1 ura3 can1 gpa1Δ::ADE2 far1Δ::ura3Δ sst2Δ::ura3Δ fus1::FUS1-HIS3 LEU2::FUS1-lacZ ste2ΔG418^R TRP::GPA1/Gα$_{i1/2(5)}$*
MMY24	*MAT*a, *his3 leu2 trp1 ura3 can1 gpa1Δ::ADE2 far1Δ::ura3Δ sst2Δ::ura3Δ fus1::FUS1-HIS3 LEU2::FUS1-lacZ ste2ΔG418^R TRP::GPA1/Gα$_{i3(5)}$*
MMY25	*MAT*a, *his3 leu2 trp1 ura3 can1 gpa1Δ::ADE2 far1Δ::ura3Δ sst2Δ::ura3Δ fus1::FUS1-HIS3 LEU2::FUS1-lacZ ste2ΔG418^R TRP::GPA1/Gα$_{z(5)}$*
MMY28	*MAT*a, *his3 leu2 trp1 ura3 can1 gpa1Δ::ADE2 far1Δ::ura3Δ sst2Δ::ura3Δ fus1::FUS1-HIS3 LEU2::FUS1-lacZ ste2ΔG418^R TRP::GPA1/Gα$_{s(5)}$*
SC195	*MAT*a, *his3 leu2 trp1 ura3 can1 gpa1Δ::ADE2 far1Δ::ura3Δ sst2Δ::ura3Δ fus1::FUS1-HIS3 LEU2::FUS1-lacZ ste2ΔG418^R TRP::GPA1/Gα$_{i1/2(5)}$ URA3::ADORA1*
SC197	*MAT*a, *his3 leu2 trp1 ura3 can1 gpa1Δ::ADE2 far1Δ::ura3Δ sst2Δ::ura3Δ fus1::FUS1-HIS3 LEU2::FUS1-lacZ ste2ΔG418^R TRP::GPA1/Gα$_{i3(5)}$ URA3::ADORA1*
SC199	*MAT*a, *his3 leu2 trp1 ura3 can1 gpa1Δ::ADE2 far1Δ::ura3Δ sst2Δ::ura3Δ fus1::FUS1-HIS3 LEU2::FUS1-lacZ ste2ΔG418^R TRP::GPA1/Gα$_{z(5)}$ URA3::ADORA1*
SC209	*MAT*a, *his3 leu2 trp1 ura3 can1 gpa1Δ::ADE2 far1Δ::ura3Δ sst2Δ::ura3Δ fus1::FUS1-HIS3 LEU2::FUS1-lacZ ste2ΔG418^R TRP::GPA1/Gα$_{o(5)}$ URA3::ADORA1-GFP*
SC211	*MAT*a, *his3 leu2 trp1 ura3 can1 gpa1Δ::ADE2 far1Δ::ura3Δ sst2Δ::ura3Δ fus1::FUS1-HIS3 LEU2::FUS1-lacZ ste2ΔG418^R TRP::GPA1/Gα$_{i1/2(5)}$ URA3::ADORA1-GFP*
SC213	*MAT*a, *his3 leu2 trp1 ura3 can1 gpa1Δ::ADE2 far1Δ::ura3Δ sst2Δ::ura3Δ fus1::FUS1-HIS3 LEU2::FUS1-lacZ ste2ΔG418^R TRP::GPA1/Gα$_{i3(5)}$ URA3::ADORA1-GFP*
SC215	*MAT*a, *his3 leu2 trp1 ura3 can1 gpa1Δ::ADE2 far1Δ::ura3Δ sst2Δ::ura3Δ fus1::FUS1-HIS3 LEU2::FUS1-lacZ ste2ΔG418^R TRP::GPA1/Gα$_{z(5)}$ URA3::ADORA1-GFP*
SC222	*MAT*a, *his3 leu2 trp1 ura3 can1 gpa1Δ::ADE2 far1Δ::ura3Δ sst2Δ::ura3Δ fus1::FUS1-HIS3 LEU2::FUS1-lacZ ste2ΔG418^R TRP::GPA1/Gα$_{o(5)}$ URA3::ADORA1*

2.1.8 Plasmids and Constructs

Table 2.6 lists the DNA constructs used in this thesis.

Table 2.6: **Names of DNA constructs used in this thesis.**

Name	Construct (Selection)	Source
JD1778	pKS-pREP-MCS-GFP	G. Ladds (unpublished)
JD2131	pREP3xr-adenosine A_{2A} receptor	R. Forfar, PhD thesis, 2007
JD2226	pKS-pREP-mcs-A_1R-GFP	R. Forfar, PhD thesis, 2007
JD2227	pKS-pREP-mcs-A_{2A}R-GFP	R. Forfar, PhD thesis, 2007
JD3706	p426GPD-A_1R	Stewart et al. (2009)
JD3736	p426GPD	GlaxoSmithKline
JD3748	p426GPD-A_{2A}R	This study
JD3756	pcDNA3.1+-adenosine A_{2B} receptor	cDNA.org
JD3775	p426GPD-adenosine A_{2B} receptor	This study
JD3785	p426GPD-A_1R^{GFP}	This study
JD3818	p426GPD-$A_{2A}R^{GFP}$	This study
JD3823	pRS306-STE2 leader	C. Weston (unpublished)
JD3825	pKS-pREP-mcs-$A_{2B}R^{GFP}$	This study
JD3826	p426GPD-$A_{2B}R^{GFP}$	This study
JD3830	p426GPD-STE2 leader	C. Weston (unpublished)
JD3831	pRS306	Dowell and Brown (2009)
JD3865	pcDNA3.1+ adenosine A_3 receptor	cDNA.org
JD3883	pRS306-adenosine A_3 receptor	This study
JD3885	pRS306-STE2 leader-adenosine A_3 receptor	This study
JD3887	p426GPD-adenosine A_3 receptor	This study
JD3889	p426GPD-STE2 leader-adenosine A_3 receptor	This study
JD3932	pRS306-GPD-CYC1	G. Ladds (unpublished)
JD3954	pRS306-GPD-CYC1-A_1R	This study
JD3984	pRS306-GPD-CYC1-A_1R^{GFP}	This study

2.2 Experimental Methods

2.2.1 Cloning techniques

Standard techniques were used to manipulate DNA (Sambrook et al., 1989). Restriction digests were performed according to manufacturer's recommendations. DNA fragments were analysed by electrophoresis on 1 % (w/v) agarose gels stained with 0.5 μg/ml ethidium bromide. DNA fragments were recovered from agaorse gels using the QIAquick Gel Extraction Kit (Qiagen, West Sussex, UK).

2.2.2 Transformation of *Escherichia coli*

Chemically competent *E. coli* DH5α cells were produced and transformed by heat shock with plasmid DNA as described by Sambrook et al. (1989).

2.2.3 Transformation of *Saccharomyces cerevisiae*

Sc. cerevisiae was transfomed with circularised plamid DNA, or linear DNA fragments for integration, using the lithium acetate/ single straded DNA/polyethylene glycol method described by Gietz and Schiestl (2007).

2.2.4 Polymerase Chain Reaction (PCR)

Taq DNA polymerase (Life Technologies Ltd, Paisley, Scotland, UK) was used to amplify products for analysis. Amplication of DNA fragments for cloning was performed using the FastStart high fidelity polymerase blend (Roche Diagnostics Ltd). All polymerases were used according to manufacturers recommendations.

2.2.4.1 PCR amplification of DNA for cloning

50μl PCR reactions were prepared using 1μg of sense and antisense primer, 10-50 ng template DNA and 0.2 mM of deoxyribonucleoside triphosphates (dNTPs) consisting of dATP, dCTP, dGTP and dTTP (purchased from Fermentas, Hanover, MD, USA). PCRs typically consisted of 30 cycles of a 0.5min, 94°C denaturation step and a 1 min annealing step at 94°C. Extension was performed at 72°C for 1 min per 1kbp of template DNA. Final extension was achieved through a 7 min incubation at 72°C.

2.2.4.2 Screening Plasmid DNA from bacterial cells

A single bacterial colony was suspended in 100 μl water and stored at 4°C. 1 μl of this suspension was used as the template in a 10 μl PCR reaction.

2.2.5 Double-stranded DNA sequencing

Sanger sequencing was outsourced to GATC Biotech (London, UK) to check no mutations were introduced during PCR and DNA manipulation.

2.2.6 Cloning strategies

Directional cloning strategies for the constructs developed in this thesis are summarised in the following schematics.

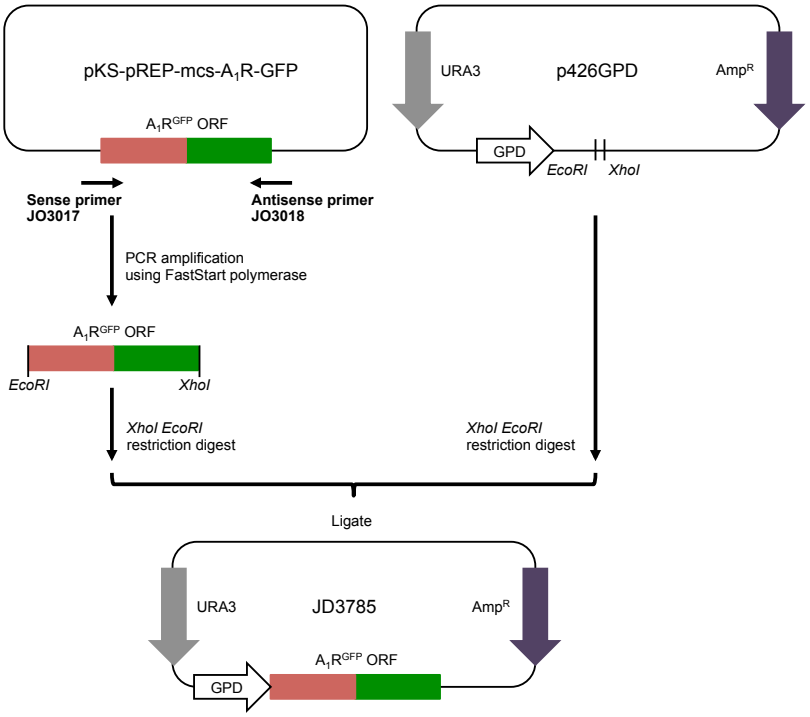

Figure 2.1: **Cloning A_1R^{GFP} into the p426GPD expression vector.** A_1R^{GFP} was amplified from the pKS-pREP-mcs-A_1R^{GFP} vector by PCR. This product was digested by *EcoRI* and *XhoI* before ligation into *EcoRI XhoI* cut p426GPD expression vector. Cloning was confirmed by PCR, restriction digest and sequencing.

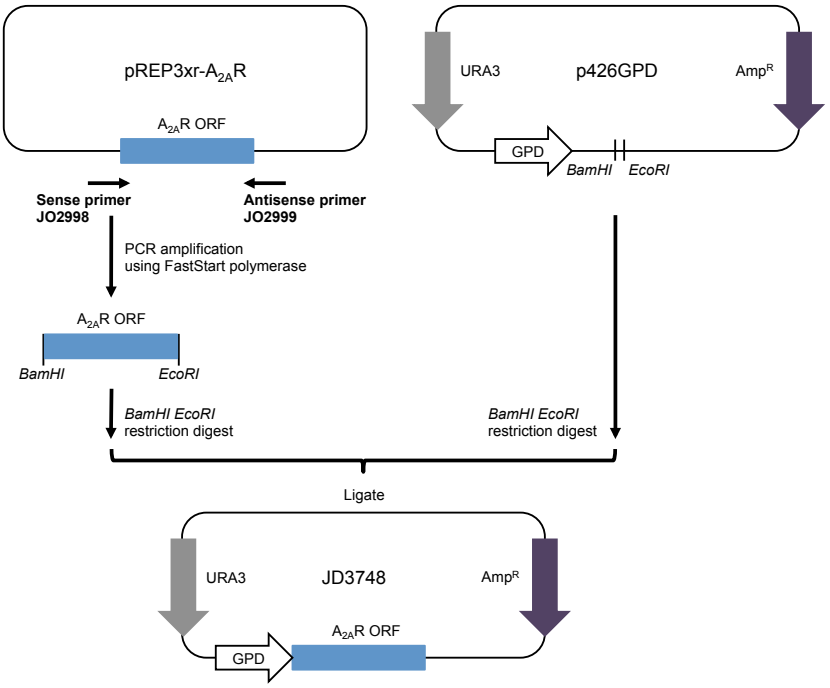

Figure 2.2: **Cloning A_{2A}R into the p426GPD expression vector.** The A_{2A}R was amplified from the pREP3xr-A_{2A}R vector by PCR. This product was digested by *BamHI* and *EcoRI* before ligation into *BamHI EcoRI* cut p426GPD. Cloning was confirmed by PCR, restriction digest and sequencing.

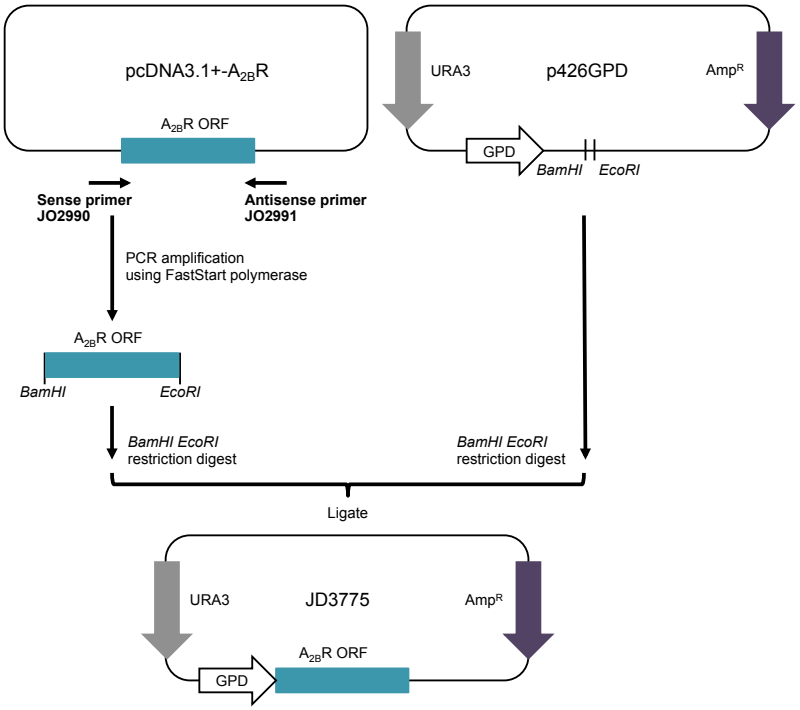

Figure 2.3: **Cloning A_{2B}R in the p426GPD expression vector.** The A_{2B}R was amplified from the pcDNA3.1+-A_{2B}R vector by PCR. This product was digested by *BamHI* and *EcoRI* before ligation into *BamHI EcoRI* cut p426GPD. Cloning was confirmed by PCR, restriction digest and sequencing.

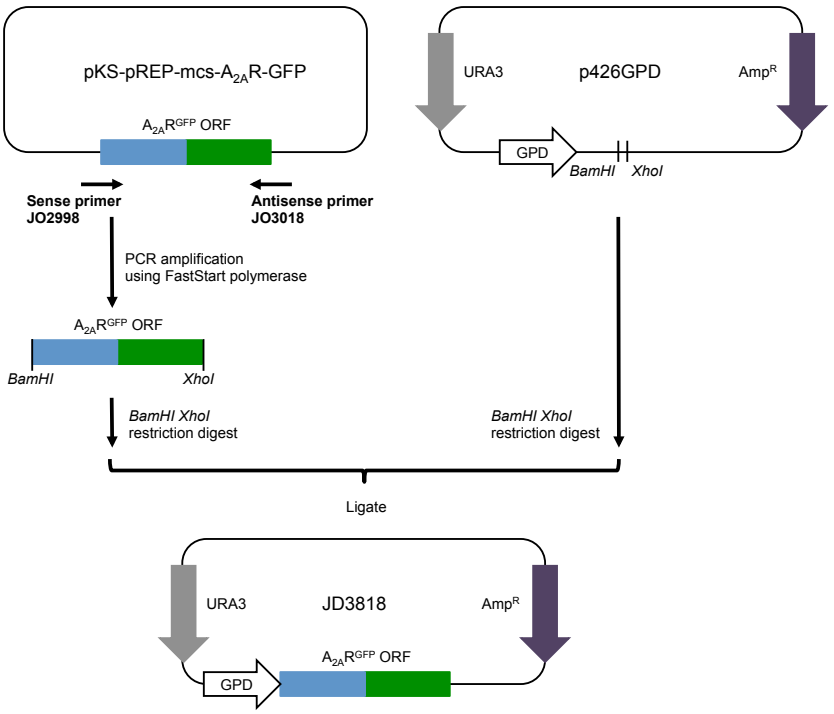

FIGURE 2.4: **Cloning $\mathbf{A_{2A}R^{GFP}}$ into the p426GPD expression vector.** The $A_{2A}R^{GFP}$ was amplified from the pKS-pREP-mcs-$A_{2A}R^{GFP}$ vector by PCR. This product was digested by *BamHI* and *XhoI* before ligation into *BamHI XhoI* cut p426GPD. Cloning was confirmed by PCR, restriction digest and sequencing.

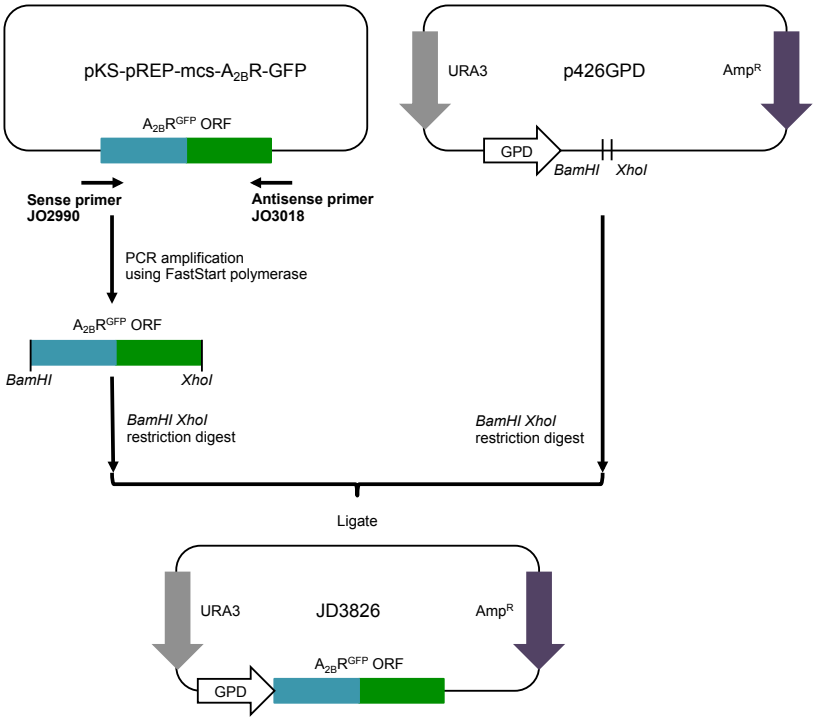

FIGURE 2.5: **Cloning $\mathbf{A_{2B}R^{GFP}}$ in the p426GPD expression vector.** The $A_{2B}R^{GFP}$ was amplified from the pKS-pREP-mcs-$A_{2B}R^{GFP}$ vector by PCR. This product was digested by *BamHI* and *XhoI* before ligation into *BamHI XhoI* cut p426GPD. Cloning was confirmed by PCR, restriction digest and sequencing.

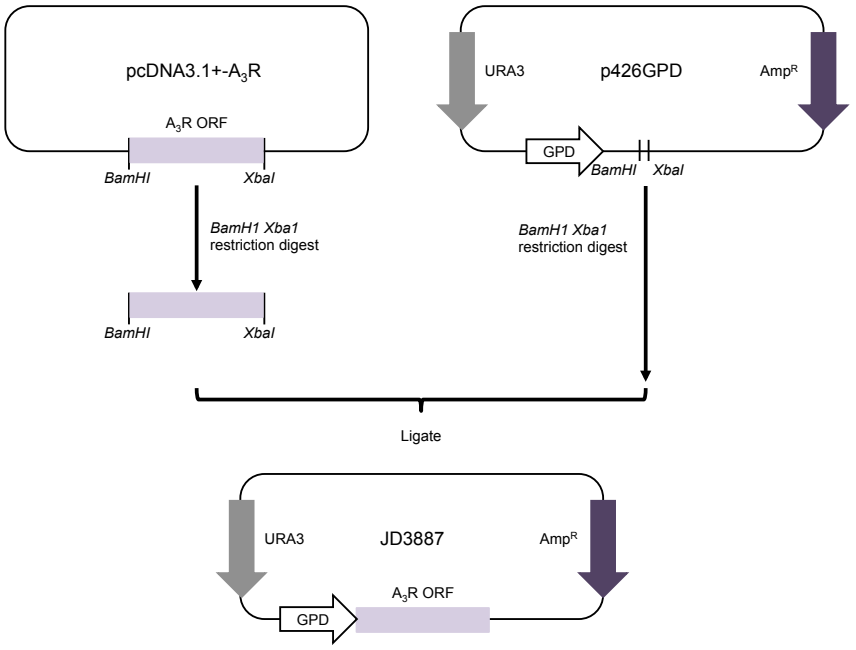

Figure 2.6: **Cloning A_3R in the p426GPD expression vector.** The A_3R was excised from pcDNA3.1+-A_3R by *BamHI XbaI* digest. The product was gel purified and ligated into *BamHI XbaI* cut p426GPD. Cloning was confirmed by PCR and restriction digest.

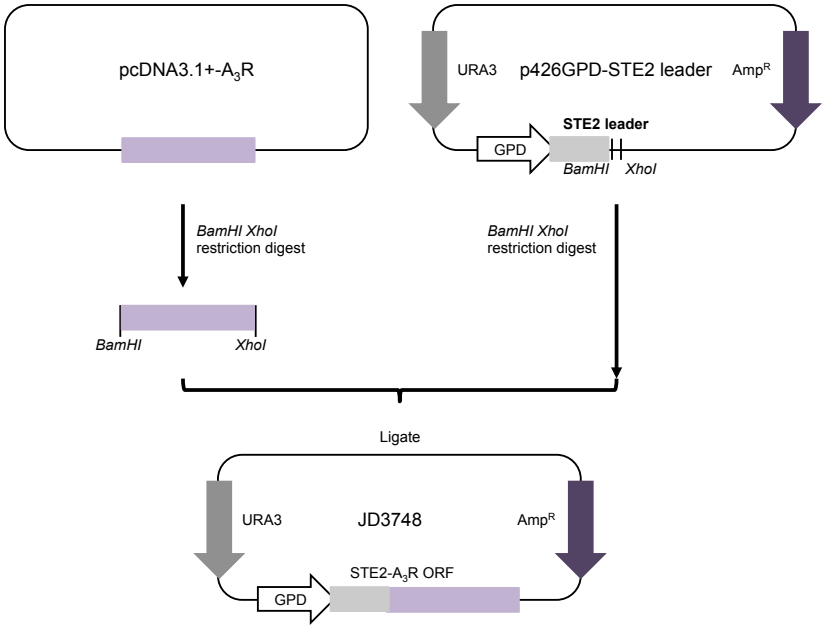

Figure 2.7: **Cloning STE2-A_3R into the p426GPD expression vector.** The A_3R was excised from pcDNA3.1+-A_3R by *BamHI XhoI* digest. The product was gel purified and ligated into *BamHI XhoI* cut p426GPD-STE2 expression vector in frame with the STE2 leader sequencing. Cloning was confirmed by PCR and restriction digest.

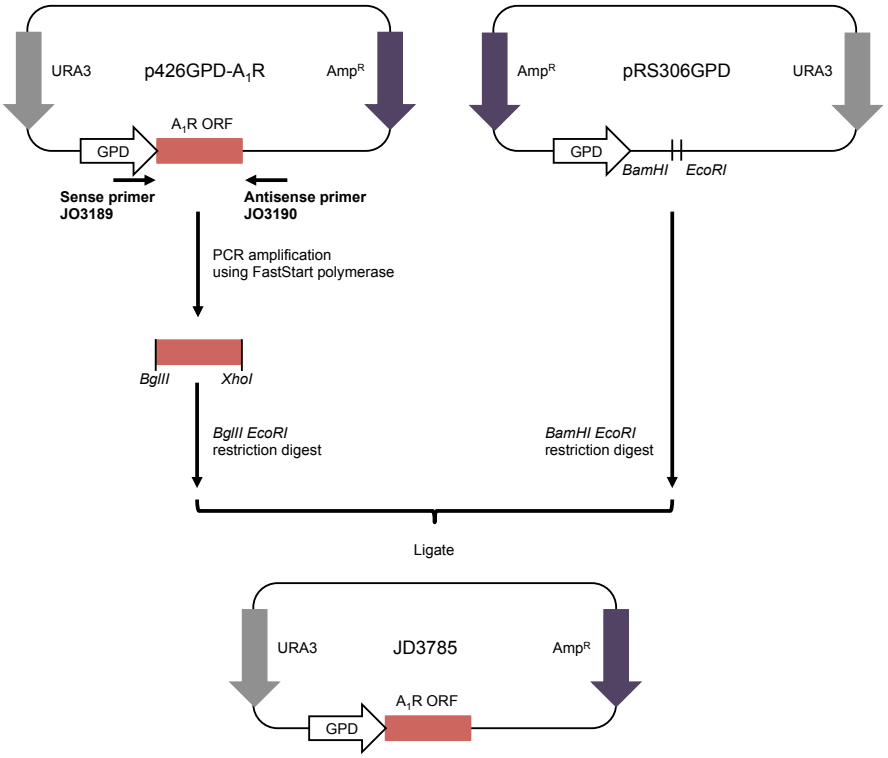

FIGURE 2.8: **Cloning A_1R into the pRS306GPD integration vector.** The A_1R was amplified from p426GPD-A_1R by PCR before digestion by *BglII* and *EcoR1*. The product was ligated into *BamHI EcoRI* cut pRS306GPD integration vector. Cloning was confirmed by PCR, restriction digest and sequencing.

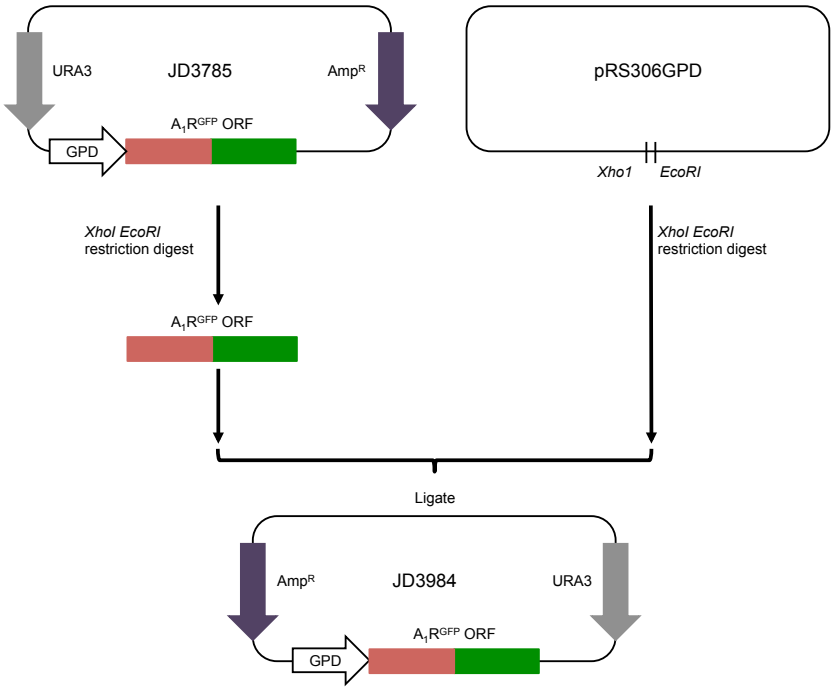

FIGURE 2.9: **Cloning A_1R^{GFP} into the pRS306GPD integration vector.** The A_1R^{GFP} was amplified from p426GPD-A_1R^{GFP} by PCR before digestion by *XhoI* and *EcoRI*. The product was ligated into *XhoI EcoRI* cut pRS306GPD integration vector. Cloning was confirmed by PCR, restriction digest and sequencing.

2.2.7 Pharmacological assays in yeast

Yeast were routinely cultured on AA plates containing 1.5% (w/v) agar lacking the relevant selectable marker. Prior to treatment, yeast cells were incubated in appropriate liquid AA media for 16 hours at 30 °C. Cells were diulted 1:10 in the same media and cultured for 8 hours at 29 °C. Cell density was adjusted to an optical density at 600nm (OD_{600}) of 0.02 as determined by a photospectrometer. 100 μl cells were treated with 1 μl of the appropriate compound stock in a clear 96-well plate at 29 °C. Where possible compound stocks were prepared in DMSO. Where compounds were not soluble in DMSO cells were also incubated with 1 % (v/v) DMSO.

2.2.7.1 β-galactosidase assays

Yeast cells were treated as described in section 2.2.7 for 16 hours at 29 °C. β-galactosidase assays were performed using a method adapted from Dohlman et al. (1995). 20 μl yeast cells were transferred to clear 96-well plates and incubated with 260 μl Z-buffer (Table 2.7) containing 2.25mM O-nitrophenyl-β-D-galactopyranoside (ONPG, a chromogenic reporter for β-galactosidase; purchased from Sigma-aldrich Co. Ltd.) for 90 minutes at 29 °C. Reactions were halted by addition of 70 μl 2M sodium carbonate. Plates were analysed using a Mithras LB940 microplate reader (Berthold Technologies, Harpenden, UK). β-galactosidase activity was detected by OD_{430}. The strains are *Δfar1* and incapable of cell cycle arrest induced by the pheromone-response. Consequently, these cells grow throughout treatment. Cell density was measured by OD_{620}. To compensate for variability in cell number and bleed through through overlapping absorption spectra, β-galactosidase activity (mU) was calculated as $\frac{OD_{430} - OD_{620}}{OD_{620}}$.

Table 2.7: Z buffer

$NaPO_4$ (pH 7.0)	0.1 M
KCl	10 mM
$MgSO_4$	1 mM
β-mercaptoethanol	50 mM
(v/v) chloroform	0.5 %
(w/v) SDS	0.005 %

2.2.7.2 Growth assays

Yeast cells were cultured for 16 hours in the appropriate liquid AA media for 16 hours at 29 °C. Cells were diluted 1:10 in liquid AA media lacking histidine and cultured for 24 hours. Cells were again diluted 1:10 in liquid AA media lacking histidine and cultured at at 29 °C for a further 6-8 hours. Cell density was adjusted to OD_{600} = 0.02 in the

same media and incubated with the appropriate concentration of ligand, or 1 % (v/v) DMSO, in a 96-well plate. Growth was quantified by OD_{620} in a Mithras LB940 microplate reader (Berthold Technologies, Harpenden, UK) at appropriate intervals. Alternatively, growth was quantified using the fluorescent substrate fluorescein di-β-D-Glucopyrnaoside (FDGlu; purchased from Sigma-Aldrich Co. Ltd, Poole, Dorset, UK). FDGlu is converted to fluorescein by exoglucanase that is secreted by dividing cells (Dowell and Brown, 2009; Weston et al., 2014). Fluorescein signal was detected using a Mithras LB940 or TECAN Infinite M200 microplate reader (TECAN Ultra Evolution, Reading, UK) using excitation and emission wavelengths of 485 nm and 535 nm respectively. Data was expressed as percentage basal signal to compensate for differences in relative fluorescent units between the two machines.

2.2.8 Fluorescence microscopy

Cells were cultured in AA for 12-16 hours, washed in phosphate buffered saline (PBS) and briefly sonicated. 2μl was transferred directly to a solid AA pad, containing 2 % w/v agarose, on a CoverWell^{TM} imaging chamber (Grace Bio-Labs, Oregon, USA). A coverslip was placed over the cells on the agar pad and sealed with a Vaseline, Lanolin and Paraffin equal parts by weight mixture (VALAP) to prevent drying of the cells. Images were obtained using a True Confocal Scanner Leica TCS SP5 microscope (Leica Microsystems Ltd., Milton Keynes, UK) or a DeltaVision system wide-field deconvolution microscope as described by Ladds et al. (2005a) and Croft et al. (2013).

2.2.8.1 Image analysis

Image acquisition and subsequent deconvolution of images from the DeltaVision microscope were performed using softWoRx (applied precision) software. Deconvolution was performed with the following settings; Ratio = conservative, Number of cycles = 8 and Noise filtering = high. All other image processing was performed using the open source software ImageJ (http://rsb.info.nih.gov/ij/).

2.2.9 Flow cytometry

Cells were cultured in AA for 12-16 hours, washed in PBS and briefly sonicated. Upto 30,000 particles were analysed for fluorescence intensity per sample using a Beckton, Dickson and Company (BD) LSR II flow cytometer (BD Biosciences, Oxford, UK). To measure GFP constructs, excitation was achieved using a 488 nm laser, and emission detected using a 530/30 nm band pass filter with a 505 nm long pass filter. For the fluorescent ligand CAS200623, excitation was achieved using a 488 nm laser and emission detected using a 575/26 nm band pass filter with a 550 nm long pass filter.

2.3 Computational methods

2.3.1 Statistical methods

Data were analysed using Graphpad Prism software version 6.0e for Mac OS X (GraphPad Software Inc., San Diego, CA, USA). Statistical differences were assessed using one-way ANOVA with Bonferroni's or Dunnett's multiple comparison tests or Student's T-test as appropriate. A probability $(P) < 0.05$ was considered significant.

2.3.2 Non-linear regression of simple models

Equilibrium models were implemented in Graphpad Prism. This software is able to fit simple models to experimental data through non-linear regression and to perform simulations based on a steady-state.

Non-linear regression of the logistic equation (2.1) was used to determine *Basal* (unstimulated level of signal), E_{max} (maximum level of signal), $LogEC_{50}$ (the ligand concentration required to induce half maximal response, a measure of system sensitivity to ligand or potency) and n. n is known as the Hill Slope and represents the proportionality of response to drug concentration between *Basal* and E_{max}. Generally, it is assumed that a response is linearly proportional to drug concentration in this range and n is constrained to 1.

$$Response = Basal + \frac{E_{max} - Basal}{(LogEC_{50} - [A])^n} \tag{2.1}$$

The operational model of pharmacological agonism (Black and Leff, 1983) effectively splits potency into two new parameters; ligand binding affinity (K_A) and efficacy (τ, a measure of G protein activation and downstream signal transduction). This model was applied to experimental concentration-response curves through non-linear regression.

$$Response = Basal + \frac{E_{max} - Basal \cdot \tau^n \cdot [A]^n}{\tau^n \cdot [A]^n + ([A] + K_A)^n} \tag{2.2}$$

$$EC_{50} = \frac{K_A}{1 + \tau} \tag{2.3}$$

2.3.2.1 Bias plots

The method of Rajagopal et al. (2011) was used to quantify ligand bias in the yeast system. τ and K_A were calculated through non-linear regression of the operational model of pharmacological agonism using Graphpad Prism. $\Delta\frac{\tau}{K_A}$ was calculated for each ligand in each yeast strain. NECA was used as a reference ligand to compensate for experimental and system bias.

$$\Delta log\frac{\tau}{K_A} = log\frac{\tau}{K_{A\,ligand}} - log\frac{\tau}{K_{A\,reference}} \tag{2.4}$$

$\Delta\Delta\frac{\tau}{K_A}$, a measure of ligand bias, was determined as the difference in $\Delta\frac{\tau}{K_A}$ for a given ligand between two yeast strains.

$$\Delta\Delta log\frac{\tau}{K_A} = \Delta log\frac{\tau}{K_{A\,pathway1}} - \Delta log\frac{\tau}{K_{A\,pathway2}} \tag{2.5}$$

2.3.2.2 Schild analysis

Schild analyses were performed to elucidate competitive antagonism (Schild, 1947, 1949). Dose ratios (DR) were calculated by comparing the EC_{50} of agonist concentration-response curves with and without various concentrations of antagonist (2.6).

$$DR = \frac{EC_{50}^{agonist}}{EC_{50}^{antagonist}} \tag{2.6}$$

Schild plots were created by plotting *Log(DR-1)* against *Log [Antagonist] M* in Graphpad Prism. Linear-regression or non-linear regression of the exponential equation were applied to concentration response curves as appropriate.

2.3.3 Systems of ordinary differential equations

Ordinary differential equation (ODE) models were constructed from biological reaction schemes by assuming the laws of mass action kinetics. These models were written and implemented in Matlab 2012a (Mathworks, Cambridge, UK). The models of Kofahl and Klipp (2004) and Smith et al. (2009) were implemented as described by the authors. Models constructed here assumed initial inactive receptor and G protein concentrations of 160nm, except Kofahl and Klipp (2004) that specific a receptor concentration of 1.6μM. Systems of ODEs were solved using the in-built ODE23s solver and a step size of 0.001 hours. A second-order Runge-Kutta algorithm was chosen to reduce computational time. Concentration-response curves were created from simulated time course data at 16 hours, consistent with the experimental data presented here, unless stated otherwise. The model of Smith et al. (2009) was equilibrated through 14 hours simulation in the absence of ligand. Equilibrium was assumed for all other models implemented here and no equilibration performed prior to addition of ligand.

2.3.3.1 Model analysis

Structural identifiability analysis was performed to determine whether a given model output is the result of a unique combination of parameters. If so the framework is termed globally and structurally identifiable and was an essential prerequisite of all models developed here. This was determined using the GenSSI toolbox for Matlab 2012a (Chis et al., 2011a).

Parameter sensitivity analysis was performed by individually increasing and decreasing each rate constant, K, 10^6 fold and performing 16 hour timecourse simulations. In these simulations all other parameters were constrained to the values as implemented by Kofahl and Klipp (2004) and experimentally determined by Yi et al. (2003) . Each species of the model was plotted as a function of time to assess the influence of a given rate constant throughout the simulated pathway. Concentration-response curves were calculated using the solutions of a 16 hour simulation, consistent with the experimental studies presented here.

2.3.3.2 Model fitting

Multivariate fitting to experimental time course data was performed using the Potter's Wheel toolbox for Matlab (Maiwald and Timmer, 2008; Raue et al., 2009). This platform allows models to be input directly or through a graphical user interface where individual species, K and their respective values are defined by the user. Potter's wheel then optimises specific parameters to decrease the distance between experimental data points and the model prediction, χ^2 (Maiwald et al., 2012). When fitting the time course data of multiple

ligand concentrations $\chi^2 < 300$ was considered an acceptable fit. When fitting the data of a single ligand concentration $\chi^2 < 8$ was considered a reasonable fit.

Chapter 3

Establishing the System: Expression and Characterisation of Adenosine Receptors in Yeast

3.1 Background

The adenosine receptor family are a pharmacologically diverse class of GPCRs that respond to the purinergic nucleoside adenosine. The adenosine A_1 and adenosine A_3 receptors typically inhibit adenylate cyclase activity through activation of the inhibitory $G\alpha_{i/o}$ proteins. In contrast, the adenosine A_{2A} and A_{2B} receptors stimulate adenylate cyclase through the stimulatory $G\alpha_s$ proteins. The pharmacology of these receptors has been well-characterised in mammalian cells. Consequently, they have generated significant interest as a clinical target for a diverse range of conditions including sleep apnoea, Parkinson's disease and cardiopulmonary arrhythmia (reviewed by Jacobson and Gao (2006)). To date, the A_1R, $A_{2A}R$ and $A_{2B}R$ have been functionally expressed in *Sc. cerevisiae* strains containing transplant $G\alpha$ subunits (Brown et al., 2000; Stewart et al., 2009; Peeters et al., 2011; Bertheleme et al., 2013). These G proteins contain the 5 C-terminal residues, and therefore GPCR coupling specificity, of mammalian counterparts. However, no functional studies of the A_3R in yeast have been reported.

The focus of this study is to model A_1R pharmacology in yeast to estimate the contribution of the ligand, receptor and G protein to mammalian functional selectivity. In this chapter the yeast system is established and validated as a paradigm for adenosine receptor pharmacology. These receptors are expressed in the transplant yeast strains and their signalling in response to a number of ligands compared.

3.2 Characterisation of the Adenosine A_1 Receptor in Yeast

The A_1R was one of the first receptors successfully expressed in, and functionally coupled to, the yeast G protein transplant strains (Brown et al., 2000). In recent years, yeast has been used to learn a great deal about A_1R pharmacology. Stewart et al. (2009) showed that the A_1R functionally couples to GPA1/Gα_o, GPA1/G$\alpha_{i1/2}$ and GPA1/Gα_{i3}. These represent inhibitory G proteins that inhibit adenylate cyclase in a mammalian setting. Indeed, Stewart et al. (2009) showed that the pharmacology of the A_1R in yeast, in response to a range of agonists and antagonists, is in good agreement with mammalian cAMP accumulation assays. Further, Peeters et al. (2012) expressed a range of A_1R mutants in the MMY24 (GPA1/Gα_{i3}) strain to elucidate the significance of the extracellular loops in agonist binding and allosterism. Thus, there is a wealth of data available to validate experimental and computational studies of this receptor in yeast.

The A_1R was expressed in the panel of GPA1 transplant yeast strains under the control of the constitutive glyceraldehyde phosphate dehydrogenase (*GAPDH*) promoter using the p426GPD vector. These strains contain β-galactosidase under the control of the *FUS1* promoter. This is activated by STE12, a transcription factor downstream of the yeast pheromone response. Brown et al. (2000) and Stewart et al. (2009) used β-galactosidase as a transcriptional reporter to assess A_1R pharmacology in yeast. Thus, this established method is ideal to investigate adenosine receptor pharmacology in yeast. 8-16 colonies of each transformed strain were isolated and incubated with the potent, non subtype-selective agonist 5'-N-ethylcarboxyamidoadenosine (NECA) for 16 hours and β-galactosidase activity determined using the chromogenic substrate ONPG. (Figure 3.1). Consistent with previous studies (Brown et al., 2000; Stewart et al., 2009; Peeters et al., 2012) significant activity was detected in the GPA1/Gα_o, GPA1/G$\alpha_{i1/2}$ and GPA1/Gα_{i3} strains ($P < 0.05$, Student's T-test). However, a previously unreported coupling of the A_1R to GPA1/Gα_z was also observed.

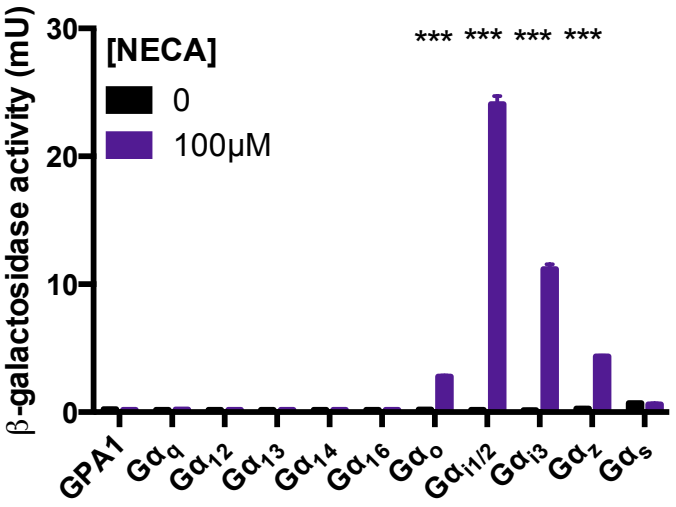

Figure 3.1: **Expression and coupling-profiles of the A_1R in yeast.** The A_1R was expressed in a panel of yeast strains using the p426GPD vector selected for uracil biosynthesis. n = 8 - 16 colonies were picked and incubated with either the agonist NECA, or 1 % DMSO for 16 hours. Cells were assayed for β-galactosidase activity (mU). Significant responses were determined by Student's T-test. $P < 0.05$ was considered significant. ***P < 0.0005.

Figure 3.1 shows that the responding strains have varying levels of β-galactosidase activity in response to 100μM NECA (GPA1/Gα_o = 2.8±0.1 mU, GPA1/G$\alpha_{i1/2}$ = 24.1±0.6 mU, GPA1/Gα_{i3} = 11.2±0.4 mU and GPA1/Gα_z = 4.4±0.1 mU). The differing levels of signal between strains may be indicative of G protein-coupling. Strains that demonstrated a significant response to NECA ($P < 0.05$) were isolated for further pharmacological characterisation in response to a number of ligands.

3.2.1 β-galactosidase assays to investigate A_1R pharmacology

To validate the pharmacology of the A_1R in yeast concentration-response curves were constructed for a range of ligands; NECA, adenosine, 2-chloro-N^6-cyclopentyladenosine (2CCPA) and the A_2R selective ligand CGS21680. Each strain was incubated with the ligand for 16 hours at 30°C. Cells were lysed and β-galactosidase activity determined.

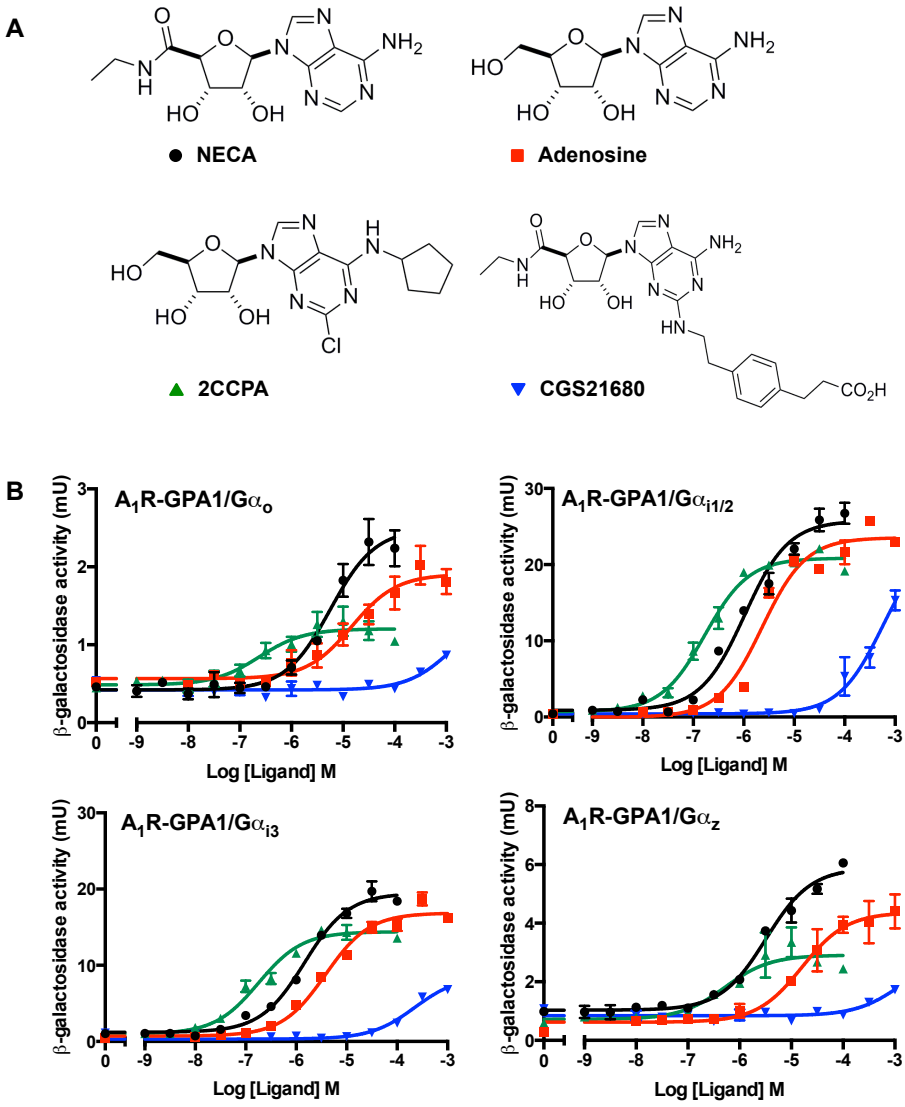

Figure 3.2: **β-galactosidase concentration-response curves of the A_1R in yeast**. **A.** The chemical structures of 5'-N-ethylcarboxyamidoadenosine (NECA), adenosine, 2-chloro-N^6-cyclopentyladenosine and CGS21680. **B.** The A_1R-GPA1/Gα_o, A_1R-GPA1/G$\alpha_{i1/2}$, A_1R-GPA1/Gα_{i3} and A_1R-GPA1/Gα_z strains were incubated with various concentrations of NECA, 2CCPA, adenosine and CGS21680 for 16 hours at 30°C. Cells were assayed for β-galactosidase activity (mU). Data is represented as the mean of triplicate repeats ± S.E.M fitted with the logistic equation.

Concentration-response curves, such as Figure 3.2 yield a myriad of information. NECA elicits the highest response in A_1R-GPA1/Gα_o, A_1R-GPA1/G$\alpha_{i1/2}$, A_1R-GPA1/Gα_{i3} and A_1R-GPA1/Gα_z. Thus, NECA was assumed to be a full agonist in all strains. Encouragingly, the A_2R-selective agonist CGS21680 only induces a response through the A_1R at very high concentrations. Observations such as these can be useful, but much quantitative insight can be gained through the application of simple mathematical models such as the logistic equation. This was fitted to the experimental data of Figure 3.2 by non-linear regression to determine $Basal$, E_{max} and pEC_{50}. These parameters were compared by One-Way ANOVA and a $P < 0.05$ considered significant.

The pEC_{50} of NECA is remarkably conserved between strains but the E_{max} varies significantly (Table 3.1). For NECA, this is highest in the GPA1/G$\alpha_{i1/2}$ strain and progressively lower for GPA1/Gα_{i3}, GPA1/Gα_z and GPA1/Gα_o (E_{max} = 25.8±0.6, 19.5±0.4, 5.8±0.2 and 2.5±0.1 respectively), further suggesting differences in G protein-coupling efficiency between strains.

Adenosine yields consistent potency values between yeast strains that are lower than those of NECA (Table 3.1). This is in agreement with mammalian data (IJzerman et al., 2014a). The adenosine E_{max} values do not significantly differ from those of NECA. This suggests that adenosine is also a full agonist against A_1R-GPA1/Gα_o, A_1R-GPA1/G$\alpha_{i1/2}$, A_1R-GPA1/Gα_{i3} and A_1R-GPA1/Gα_z. However, 2CCPA shows more variable trends between strains.

2CCPA elicits a higher potency than NECA or adenosine in all strains, consistent with mammalian data. While the rank order of 2CCPA E_{max}s remains A_1R-GPA1/G$\alpha_{i1/2}$ > A_1R-GPA1/Gα_{i3} > A_1R-GPA1/Gα_z >A_1R-GPA1/Gα_o their statistical differences from NECA vary between strains. In A_1R-GPA1/G$\alpha_{i1/2}$ there is no significant difference between 2CCPA and NECA E_{max}, suggesting that 2CCPA is a full agonist in this strain. However, the 2CCPA E_{max} is significantly lower than that of NECA for all other strains Table 3.1. This would suggest that 2CCPA is a partial agonist of the A_1R in GPA1/Gα_o, Gα_{i3} and Gα_z backgrounds. This may suggest partial agonism as a function of the G protein. But, statistical differences in E_{max} do not necessarily translate to physiological differences. For example, the NECA, adenosine and 2CCPA E_{max} values are 19.5±0.4, 16.5±0.5 and 14.4±0.3, respectively, in A_1R-GPA1/Gα_{i3}. This relative consistency may in fact render 2CCPA a full agonist in this strain. The same may be true of A_1R-GPA1/Gα_o and Gα_z given the low magnitude of response and the difficulties in distinguishing between Gα_i subtypes *in vivo*

Regardless, 2CCPA has a consistently higher pEC_{50} but lower maximal signal than adenosine and NECA in all strains . pEC_{50} is a measure of system sensitivity to ligand, while E_{max} denotes the downstream signalling in response. This suggests that the system is more sensitive to 2CCPA but has a reduced ability to respond. This hints at a distinction

between ligand binding and G protein activation. Indeed it is possible to separate pEC_{50} into ligand binding and signal transduction using the operational model of pharmacology (Black and Leff, 1983).

This equation effectively splits potency into two new parameters, ligand binding affinity (K_A) and a signal transduction coefficient known as efficacy (τ). In the yeast system τ is a measure of G protein activation and downstream signalling. The operational model of pharmacology was applied to the data of Figure 3.2 by non-linear regression to obtain pK_A and $log\tau$ values (Table 3.1).

Table 3.1: **Pharmacological parameters of the A_1R.** The logistic equation and the operational model of pharmacological agonism were applied to the data of Figure 3.2 by non-linear regression. $pEC_{50} = -Log\ EC_{50}$ (potency), E_{max} = maximum level of signal, pK_A = −Log K_A (ligand binding affinity) and τ = efficacy. N.D. = not determined due to insufficient response. Significant differences were assessed by One-Way ANOVA with Dunnett's multiple comparisons test. P < 0.05 was considered significant. *P < 0.05, **P < 0.005, ***P < 0.005 compared to NECA in the same strain.

Strain	**Ligand**	**pEC$_{50}$**	**E$_{max}$**	pK_A	$log\tau$
GPA1/Gα_o	NECA	5.2±0.1	2.5±0.1	4.4±0.1	0.9±0.1
	Adenosine	4.8±0.1	1.9±0.1	4.5±0.2	0.4±0.1*
	2CCPA	6.6±0.2	1.2±0.1*	6.5±0.2***	−0.2±0.0***
	CGS21680	2.9±0.8*	1.5±0.5	N.D.	N.D.
GPA1/G$\alpha_{i1/2}$	NECA	6.0±0.1	25.8±0.6	4.4±0.1	1.5±0.1
	Adenosine	5.6±0.1	23.5±0.7	4.6±0.2***	0.9±0.1*
	2CCPA	6.7±0.1*	20.9±0.4	6.1±0.1***	0.6±0.1***
	CGS21680	3.2±0.1***	23.5±3.6	N.D.	N.D.
GPA1/Gα_{i3}	NECA	5.8±0.1	19.5±0.4	5.1±0.1	0.7±0.1
	Adenosine	5.7±0.1	16.5±0.5*	5.1±0.1	0.4±0.0
	2CCPA	6.7±0.1**	14.4±0.3**	6.4±0.1***	0.2±0.1
	CGS21680	3.7±0.2***	8.6±1.0***	N.D.	N.D.
GPA1/Gα_z	NECA	5.5±0.1	5.8±0.2	4.4±0.3	1.2±0.3
	Adenosine	4.8±0.2	3.9±0.3**	4.3±0.2	0.3±0.1*
	2CCPA	6.3±0.2	2.9±0.2***	6.1±0.2**	−0.2±0.1**
	CGS21680	2.9±0.5**	2.9±1.5	N.D.	N.D.

Interestingly, the pK_A values for each ligand do not significantly differ between each Gα transplant (P < 0.05, one-way ANOVA). This predicts that the G protein does not affect the affinity of the A_1R to ligands. However $log\ \tau$ varies considerably between strains. For the most part, A_1R-GPA1/Gα_o and A_1R-GPA1/Gα_z have lower $log\ \tau$ values than the A_1R-GPA1/Gα_i strains. This may indicate that the observed differences in E_{max} are the result of lower signal transduction capacity. This could be the result of the efficiency of G protein-coupling and downstream signalling, whereby the A_1R couples most strongly to GPA1/G$\alpha_{i1/2}$. Further, the efficiency of G protein-induced signalling is progressively lower for GPA1/G$\alpha_{i1/2}$ > GPA1/Gα_{i3} > GPA1/Gα_z > GPA1/Gα_o as indicated by $log\tau$ (Table 3.1).

3.2.2 Investigating G protein bias in the A_1R

Functional selectivity has been investigated, with regard to G protein bias, for the A_1R in yeast (Stewart et al., 2009). However, while concentration-response curves of different ligands have been compared for different G proteins, to our knowledge the degree of bias has never been directly quantified for the A_1R in yeast. Rajagopal et al. (2011) developed an excellent method for quantifying signalling bias, between G proteins or between G proteins and β-arrestins (reviewed by Shonberg et al. (2014)). This method uses a reference ligand to compensate for bias as a result of assay or experimental system differences. NECA is a consistent full agonist for all strains tested and was used as the reference ligand in calculating bias. By subtracting this value for that from the another pathway a normalised value for bias can be calculated.

Bias plots were created comparing the A_1R signalling bias for GPA1/Gα_o, GPA1/G$\alpha_{i1/2}$, GPA1/Gα_{i3} and GPA1/Gα_z relative to each other (Figure 3.3). Consistent trends between the ligands were observed in terms of bias. Adenosine is biased GPA1/Gα_o = GPA1/Gα_{i3} > GPA1/G$\alpha_{i1/2}$ > GPA1/Gα_z. 2CCPA is similar, but shows a significant bias between GPA1/Gα_o and GPA1/Gα_{i3} such that GPA1/Gα_o > GPA1/Gα_{i3} > GPA1/G$\alpha_{i1/2}$ > GPA1/Gα_z. These measurements of G protein signalling bias of the A_1R are not possible in mammalian systems due to the difficulties in distinguishing between different Gα_i *in vivo*.

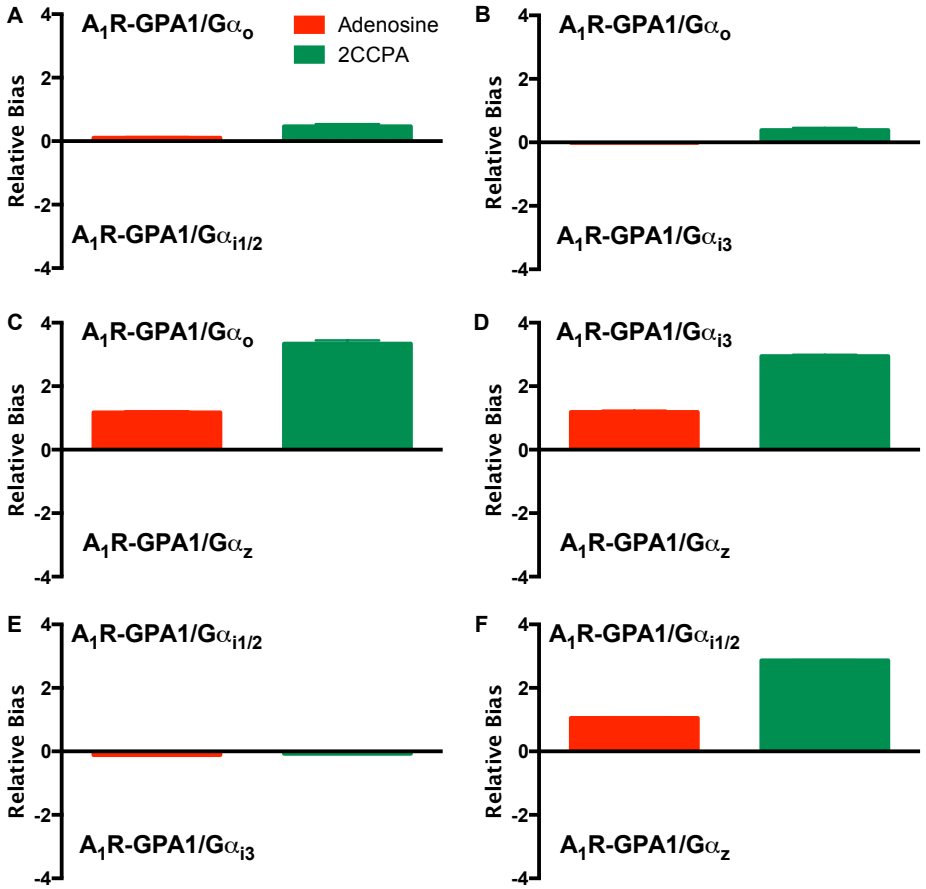

Figure 3.3: **Calculating A_1R bias in yeast.** A normalised measure of bias, was calculated using the method of Rajagopal et al. (2011) and the data of Figure 3.2 and parameters of Table 3.1. NECA was used as the reference ligand to compensate for system bias. Data represents mean ± S.E.M of triplicate repeats. **A.** A_1R-GPA1/Gα_o vs. A_1R-GPA1/Gα_{i3}. **B.** A_1R-GPA1/Gα_o vs. A_1R-GPA1/G$\alpha_{i1/2}$. **C.** A_1R-GPA1/Gα_o vs. A_1R-GPA1/Gα_z. **D.** A_1R-GPA1/Gα_{i3} vs. A_1R-GPA1/Gα_z. **E.** A_1R-GPA1/Gα_{i3} vs.A_1R-GPA1/G$\alpha_{i1/2}$. **F.** A_1R-GPA1/G$\alpha_{i1/2}$ vs. A_1R-GPA1/Gα_z.

3.2.3 Growth assays to investigate A_1R Pharmacology

Thus far our studies of A_1R pharmacology in the yeast system have exploited the *FUS1*> *β-galactosidase* reporter. However, the transplant yeast strains also contain *HIS3* under the control of the *FUS1* promoter (*FUS1>HIS3*). *HIS3* encodes imidazoleglycerol-phosphate dehydratase - a key step in the histidine biosynthesis pathway. This allows growth in histidine deficient media to be used as a transcriptional reporter of pathway activation. This has many advantages over β-galactosidase such as sensitivity. The yeast growth assay has previously been shown to yield higher potencies than β-galactosidase assays (Dowell and Brown, 2009). This is particularly advantageous when expressing receptors such as GLP-1 in yeast, which have been shown to have weak β-galactosidase activity in response to ligands (Weston et al., 2014). Another advantage is β-galactosidase assays typically require cell lysis and normalisation to cell density to be effective. However, growth assays require a single measurement of cell density, i.e. OD_{600}. This assay has successfully been exploited by drug screening programmes and pharmacological investigation of a variety of receptors (Brown, 2002; Brown et al., 2011; Peeters et al., 2011, 2012; Liu et al., 2014). Alternatively, many studies use a Fluorescein-Di-β-D-glucopyranoside (FDGlu) to quantify growth (Brown et al., 2011; Bertheleme et al., 2013; Weston et al., 2014). FDGlu is processed to fluorescein by Exg1p, a yeast exoglucanase that is ubiquitously and constitutively expressed during cell division (Dowell and Brown, 2009). Thus, fluorescein concentration, and therefore fluorescence, are a direct indication of cell density. FDGlu overcomes several limitations of growth assays compared to simple measurements of OD_{600}. As cells settle on the bottom of the plate, the pathlength and refractive index are altered, affecting the reliability of absorbance measurements. Fluorescence does not have the same limitation. FDGlu provides the means to measure growth without having to resuspend the cultures and provides a means to obtain timecourse data. Therefore FDGlu was chosen to quantify growth in our transplant yeast strains in response to adenosine receptor activation.

A_1R transplant strains were cultured in AA-Ura overnight and subcultured in histidine deficient media (AA-Ura-His) for a further 24-48 hours, as described by Weston et al. (2014), to histidine starve the yeast cells. This was intended to significantly reduce the rate of growth in unstimulated cells. Cells were then incubated with NECA, adenosine, 2CCPA or CGS21680 and 20μM FDGlu for 16 hours at 30°C. Fluorescence was detected using a TECAN Infinite M200 microplate reader (excitation wavelength = 485nm, emission wavelength = 535nm, Figure 3.4).

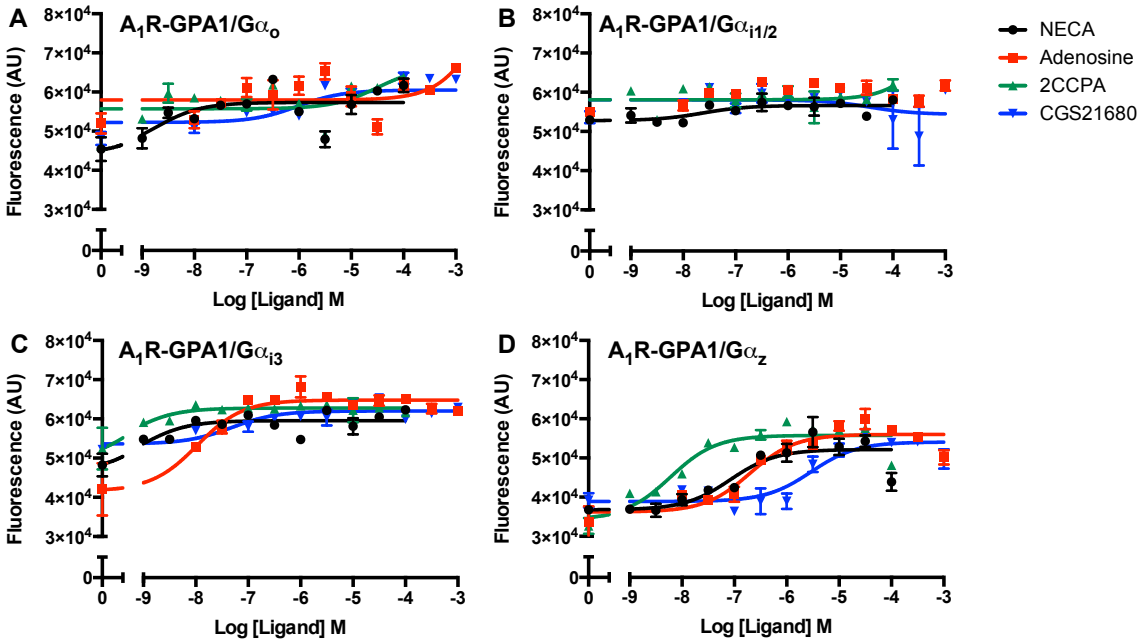

Figure 3.4: **Histidine starvation of A_1R expressing yeast transplants.** Responding A_1R strains identified in Figure 3.1 were cultured in AA-Ura overnight and subcultured into AA-Ura-His for 24-48 hours. Cell density was then adjusted to OD_{600} = 0.02 and cells incubated in AA-Ura-His containing the approriate concentration of ligand and 20μM FDGlu for 16 hours at 30°C.Fluorescence was detected using a TECAN Infinite M200 microplate reader (excitation wavelength = 485nm, emission wavelength = 535nm). **A.** A_1R-GPA1/Gα_o measured at 14 hours. **B.** A_1R-GPA1/G$\alpha_{i1/2}$ measured at 14 hours. **C.** A_1R-GPA1/Gα_{i3} measured at 12 hours. **D.** A_1R-GPA1/Gα_z

The growth data of Figure 3.4 is a remarkable contrast to the β-galactosidase data of Figure 3.2. Concentration-response curves could only be determined for A_1R-GPA1/Gα_z and here the signalling window (the relative difference between basal and maximum signal) is greatly reduced compared to Figure 3.2. However, the GPA1/Gα_z yielded higher potencies in a growth assay relative to β-galactosidase assay (pEC_{50} = 7.1±0.3, 6.7±0.2, 8.2±0.2 and 5.5±0.2 for NECA, adenosine, 2CCPA and CGS21680 respectively). Interestingly all compounds in the A_1R-GPA1/Gα_z transplant act as full agonists in this assay. The lack of significant response in the A_1R-GPA1/Gα_o, A_1R-GPA1/G$\alpha_{i1/2}$ and A_1R-GPA1/Gα_{i3} strains is inconsistent with their β-galactosidase activity in response to the same ligands ($P > 0.05$, one-way ANOVA).

3.2.3.1 Using 3-amino triazole to generate concentration-response curves for A_1R growth assays

Figure 3.4 suggests that histidine starvation is insufficient to generate concentration-response curves for the A_1R in yeast by growth assay. However, Peeters et al. (2011) successfully created concentration-response curves by growth assay for the A_1R in the GPA1/Gα_{i3} strain using 7mM 3-amino-triazole (3-AT). 3-AT is a competitive inhibitor of imidazoleglycerol-phosphate dehydratase, the *HIS3* gene product and a rate limiting step in the histidine biosynthesis pathway. This greatly reduces basal growth, allowing the formation of concentration-response curves as MAPK signalling in yeast increases HIS3 expression, overcoming the 3-AT inhibition. Therefore, 3-AT affects the rate at which the cells grow. A timecourse experiment was performed to assess the effect of yeast cell growth in response to NECA and 3AT. The A_1R transplant strains were cultured in AA-Ura overnight at 30°C and then subcultured in AA-Ura-His for 8 hours. Cell density was adjusted to OD_{600} = 0.02 and cells incubated with the appropriate concentration of ligand, 7mM 3-AT and 20μM FDGlu. Fluorescence was measured every 15 minutes for 20 hours.

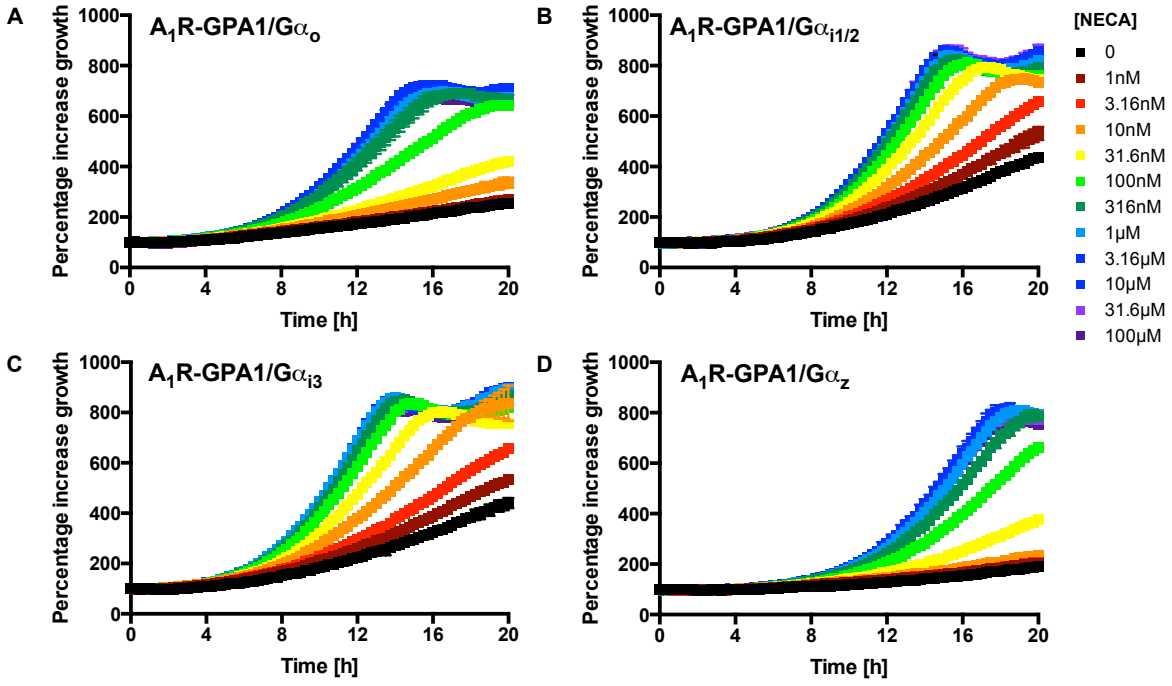

Figure 3.5: **Growth timecourse assays of A_1R expressing yeast cells.** Responding A_1R strains identified in Figure 3.1 were cultured in AA-Ura overnight at 30°C and subcultured in AA-Ura-His for 8 hours. Cell density was adjusted to OD_{600} = 0.02 and cells incubated in AA-Ura-His containing the appropriate concentration of NECA, 7mM 3-AT and 20μM FDGlu. Fluorescence was measured every 15 minutes for 20 hours using a TECAN Inifinte M200 microplate reader (excitation wavelength = 485nm, emission wavelength = 535nm). **A.** A_1R-GPA1/Gα_o. **B.** A_1R-GPA1/G$\alpha_{i1/2}$. **C.** A_1R-GPA1/Gα_{i3}. **D.** A_1R-GPA1/Gα_z. Data represents mean of tripicate repeats ± S.E.M.

In contrast to Figure 3.4, all strains respond to NECA in a concentration-dependent manner in the presence of 3AT. The timecourse data of Figure 3.5 suggests that the A_1R transplant strains reach stationary phase at different times. Therefore, the optimal time to calculate concentration-response curves varies. For A_1R-GPA1/Gα_o and A_1R-GPA1/G$\alpha_{i1/2}$ this occurs at 14 hours when the difference between stimulated and unstimulated growth is highest. Concentration-response curves were created for A_1R-GPA1/Gα_{i3} and A_1R-GPA1/Gα_o at 12 and 16 hours respectively (Figure 3.5). Non-linear regression of the logistic equation to Figure 3.5 yielded pEC_{50}, E_{max} and basal growth in response to NECA (Table 3.2).

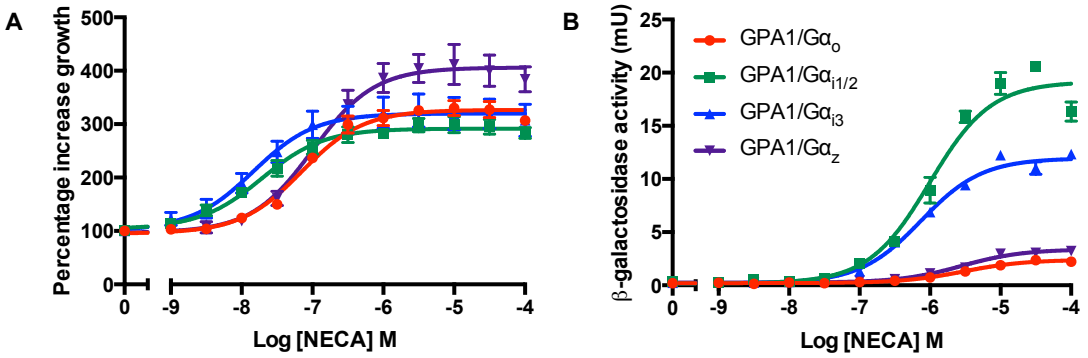

Figure 3.6: **NECA growth concentration-response curves of A_1R expressing yeast cells. A.** Concentration-response curves were constructed from the timecourse data of Figure 3.5 at 14, 14, 12 and 16 hours for A_1R-GPA1/Gα_o, A_1R-GPA1/G$\alpha_{i1/2}$, A_1R-GPA1/Gα_{i3} and A_1R-GPA1/Gα_z respectively. **B.** A_1R-GPA1/Gα_o, A_1R-GPA1/G$\alpha_{i1/2}$, A_1R-GPA1/Gα_{i3} and A_1R-GPA1/Gα_z were incubated with various concentrations of NECA for 16 hours, lysed and assayed for β-galactosidase activity. Data represents the mean of triplicate repeats ± S.E.M and were fitted using the logistic equation.

Table 3.2: **Basal, potency and E_{max} of A_1R strains in response to NECA**. The logistic equation was applied to the data of Figure 3.6 to obtain basal levels of signalling, potency, a measure of sensitivity to ligand, and maximum signal E_{max}. β-galactosidase activity (mU) has been included for comparison.

Strain	**Basal Growth**	**pEC$_{50}$ Growth**	**E$_{max}$ Growth**	**Basal mU**	**pEC$_{50}$ mU**	**E$_{max}$ mU**
GPA1/Gα_o	96±10	7.2±0.1	327±10	0.21±0.1	5.53±0.1	2.40±0.1
GPA1/G$\alpha_{i1/2}$	105±10	7.7±0.1	292±10	0.17±0.4	6.00±0.1	19.15±0.6
GPA1/Gα_{i3}	103±10	7.8±0.1	320±10	0.19±0.1	6.13±0.1	11.95±0.2
GPA1/Gα_z	97±10	7.0±0.1	406±10	0.26±0.1	5.55±0.1	3.39±0.1

A_1R-GPA1/Gα_z shows a similar pEC_{50} value for NECA with 3-AT relative to histidine starvation alone (7.0±0.1 compared to 7.1±0.3 respectively). With 7mM 3-AT, potencies are consistently 15-fold higher for growth assay relative to β-galactosidase activity in all strains (Table 3.2). Interestingly, there is a split between the strains with regard to potency. A_1R-GPA1/Gα_o and A_1R-GPA1/Gα_z have remarkably similar potencies, as do A_1R-GPA1/G$\alpha_{i1/2}$ and A_1R-GPA1/Gα_{i3} which share higher pEC$_{50}$ values. This trend

is consistent with their respective β-galactosidase data and may represent functional selectivity. However, E_{max} is far more consistent between strains for growth than for β-galactosidase activity.

3.2.3.2 Pharmacological characterisation of the A_1R by growth assay

Having established the necessity of 3-AT to perform growth assays for A_1R activity in the yeast system, growth was explored as an avenue to elucidate the pharmacology of NECA, adenosine, 2CCPA and CGS21680. Yeast cells were incubated in AA-Ura-His containing the appropriate concentration of ligand and 7mM 3-AT. 20μM FDGlu was used to quantify growth by fluorescence (Figure 3.7). The resulting concentration-response curves were fitted using the logistic equation (Table 3.3).

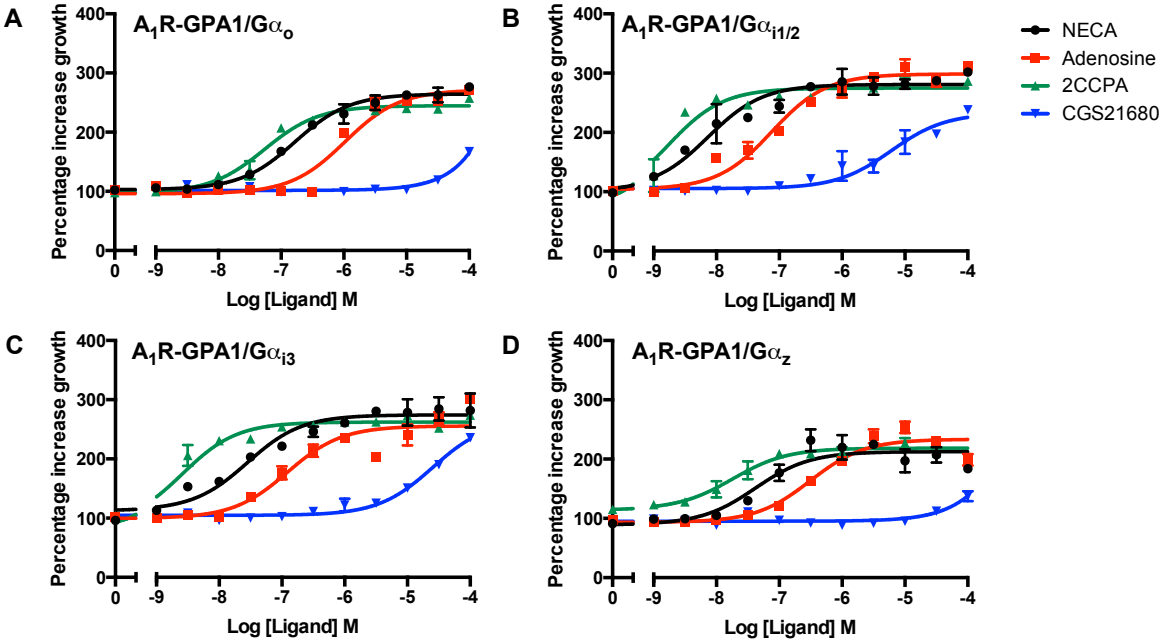

Figure 3.7: **Concentration-response curves for A_1R growth assay in yeast.** Yeast transplant strains expressing the A_1R were incubated in AA-Ura-His containing 7mM 3-AT, 20μM FDGlu and the appropriate concentration of ligand. Fluorescence was measured at the appropriate time to construct a concentration-response curve. **A.** A_1R-GPA1/Gα_o measured at 14 hours. **B.** A_1R-GPA1/G$\alpha_{i1/2}$ measured at 14 hours. **C.** A_1R-GPA1/Gα_{i3} measured at 12 hours. **D.** A_1R-GPA1/Gα_z measured at 16 hours.

There are clear differences between the growth assay data of Figure 3.7 and the β-galactosidase data of Figure 3.2. The β-galactosidase data suggests that adenosine and 2CCPA are partial agonists, although E_{max} relative to NECA varied between strains. However, growth assay data suggests that NECA, adenosine and 2CCPA are full agonists and that strain differences in E_{max} are not as pronounced as the β-galactosidase data of Figure 3.2. This feature is likely to be a consequence of the assay. The E_{max} of the system is determined by the stationary phase and nutritional availability of the culture. Thus, it

Table 3.3: **Pharmacological parameters of the A_1R growth assay.** The logistic equation (2.1) was applied to the data of Figure 3.7 by non-linear regression. $pEC_{50} = -Log\ EC_{50}$ (potency) and E_{max} = *maximum level of signal.* Equivalent β-galactosidase data (mU) has been included for comparison.

Strain	**Ligand**	**pEC$_{50}$ Growth**	**E$_{max}$ Growth**	**pEC$_{50}$ mU**	**E$_{max}$ mU**
GPA1/Gα_o	NECA	6.8±0.1	2.6±0.0	5.2±0.1	2.5±0.1
	Adenosine	6.0±0.1	2.7±0.1	4/8±0.1	1.9±0.1
	2CCPA	7.3±0.	2.4±0.0	6.6±0.2	1.2±0.1
GPA1/G$\alpha_{i1/2}$	NECA	8.13±0.1	2.8±0.1	6.0±0.1	25.8±0.6
	Adenosine	7.1±0.1	3.0±0.1	5.6±0.1	23.5±0.7
	2CCPA	8.8±0.1	2.8±0.1	6.7±0.1	20.9±0.4
GPA1/Gα_{i3}	NECA	7.6±0.1	2.7±0.1	5.8±0.1	19.5±0.4
	Adenosine	6.9±0.2	2.6±0.1	5.7±0.1	16.5±0.5
	2CCPA	8.6±0.1	2.6±0.1	6.7±0.1	14.4±0.3
GPA1/Gα_z	NECA	7.4±0.2	2.1±0.1	5.5±0.1	5.8±0.2
	Adenosine	6.5±0.1	2.3±0.1	4.8±0.2	3.9±0.3
	2CCPA	7.7±0.1	2.2±0.0	6.3±0.2	2.9±0.2

is likely that the cells are reaching their maximum rate of growth and therefore stationary phase at lower ligand concentrations. This may present difficulties differentiating partial and full agonists.

pEC_{50} values vary between strains by growth assays. However, pEC_{50} values are higher for all ligands and strains in growth assays relative to β-galactosidase assays. The values of Table 3.3 are consistent with mammalian studies (IJzerman et al., 2014a). However, this increase in sensitivity could be the result of limits on signalling windows imposed by the stationary phase of the culture. Signalling hits maximum levels at lower ligand concentrations because pathway and signalling capacity have reached the limits of the system with regard to growth. This could result in increased pEC_{50} values.

There are clear differences in A_1R pharmacology between the two transcriptional reporters. Growth appears to be more sensitive and yield potency values closer to mammalian systems. However, all ligands tested behave as full agonists according to growth assay and E_{max} is broadly similar between A_1R strains. In contrast, β-galactosidase assays are less sensitive but show clearer differences between G protein subtypes and full/ partial agonism. Given that the aim of this study is to model functional selectivity between ligands and G protein subtypes in yeast, we elected to continue with β-galactosidase assays as the primary method to explore adenosine receptor pharmacology in yeast.

3.2.4 Characterisation of a C-terminal A_1R^{GFP} fusion protein

Thus far we have explored the pharmacology of the A_1R in yeast and have identified a series of responding and non-responding strains. We have shown that β-galactosidase E_{max} varies significantly between strains. However, expression and trafficking of the A_1R to the cell membrane could vary between strains and influence signalling profiles. This could manifest in the observed variation in E_{max}. Fusing a protein of interest with the *Aequoria victoria*-derived green fluorescent protein (GFP) allows protein localisation to be measured in real-time. Thus we sought to use a fluorescent A_1R^{GFP} construct to assess differences in receptor expression and localisation between responding and non-responding strains. C-terminal GPCR-GFP fusion constructs have been powerful tools to study the trafficking and internalisation of a range of receptors without affecting ligand binding or signal transduction. This includes the adenosine receptor family (Bevan et al., 1999; Niebauer and Robinson, 2006; Sitaraman et al., 2002; May et al., 2011).

Previously, a C-terminal A_1R^{GFP} fusion construct, linked by a single isoleucine residue, was created to explore adenosine receptor trafficking in the fission yeast *Sz. pombe* (Forfar, PhD Thesis). This study showed that while the A_1R does not function in *Sz. pombe*, it is trafficked to the cell membrane. As this construct was readily available, it was cloned into the p426GPD expression vector and expressed in the panel of *Sc. cerevisiae* yeast transplant strains. 8-16 colonies of each strain were isolated and screened for β-galactosidase activity in response to 100μM NECA. These responses were compared to those induced by DMSO alone by Student's T-test where a $P < 0.05$ was considered significant.

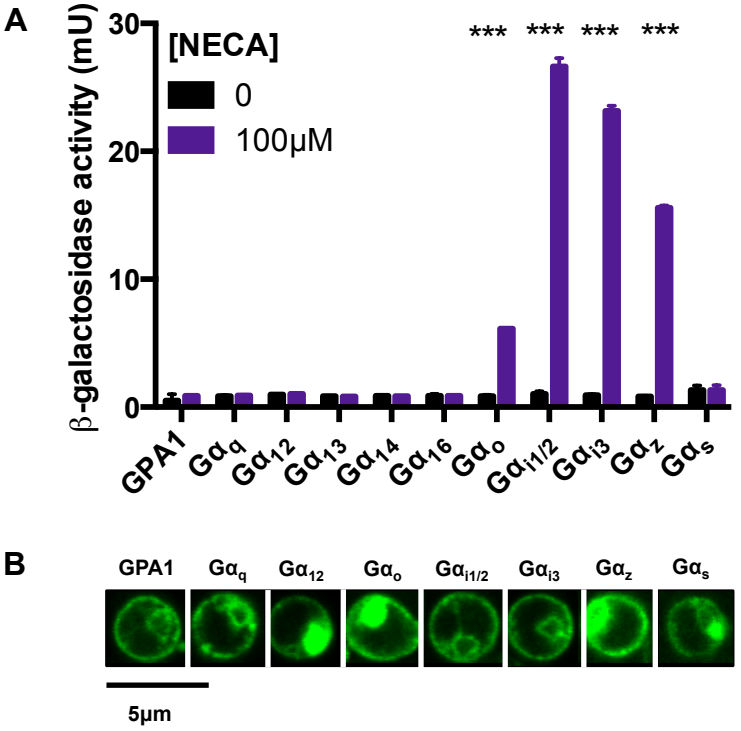

Figure 3.8: **Determining A_1R^{GFP} coupling in yeast. A**. A C-terminal A_1R^{GFP} fusion construct was expressed in a panel of yeast strains using the p426GPD vector selected for uracil biosynthesis. n = 8 - 16 colonies were picked and incubated with either the full agonist NECA, or 1 % DMSO for 16 hours. Cells were lysed and assayed for β-galactosidase activity (mU). Significant responses were determined by Student's T-test (***P $<$ 0.0005). **B.** Responding and non-responding strains were imaged using a Leica SP5 confocal microscope. ImageJ was used to compensate for background fluorescence. Single cells, representative of the fluorescent population, have been selected to demonstrate receptor localisation.

Consistent with the A_1R, the A_1R^{GFP} only upregulated β-galactosidase activity in response to NECA in four strains; GPA1/Gα_o, GPA1/G$\alpha_{i1/2}$, GPA1/Gα_{i3} and GPA1/Gα_z (Figure 3.8A). However, the level of upregulation in the GPA1/Gα_o and GPA1/Gα_z has increased considerably (6.1±0.0 mU and 15.6±0.2 mU for compared to 2.8±0.1 and 4.4±0.1 for A_1R-GPA1/Gα_o and A_1R-GPA1/Gα_z respectively. The order of response (GPA1/G$\alpha_{i1/2}$ $>$ GPA1/G$\alpha_{i1/2}$ $>$ GPA1/G$\alpha_{i1/2}$ $>$ GPA1/G$\alpha_{i1/2}$) is shared by the A_1R and A_1R^{GFP}. Given this similarity, the GFP fluorophore can be used to determine if differences in maximal activity are the result of receptor localisation.

Responding and non-responding strains were imaged by confocal microscopy to determine receptor localisation (Figure 3.8B). Clear membrane localisation was observed in responding and non-responding strains alike as were consistent patterns. This suggests that the level of response is not a consequence of receptor trafficking.

3.2.4.1 Measuring cell-to-cell variation in A_1R^{GFP} flow cytometry

Even in a genetically identical population, cell-to-cell variation can arise. Indeed, phenotypic variability confers an adaptability to a genetically limited population and may in fact be selected for in yeast (Neildez-Nguyen et al., 2007; Zhang et al., 2009). Our expression system may further contribute to this variability. The copy number of the constitutive p426GPD could vary amongst a population thus promoting differences in receptor expression. It is possible that the differences in E_{max} may be due to differences in receptor expression across a population. Flow cytometry assesses the fluorescence of thousands of individual cells in a matter of seconds allowing a larger scale investigation of population level effects than traditional microscopy (Hawley et al., 2004). This approach was used to explore the expression of A_1R^{GFP} in the GPA1/Gα_o, GPA1/G$\alpha_{i1/2}$, GPA1/Gα_{i3} and GPA1/Gα_z strains (Figure 3.9).

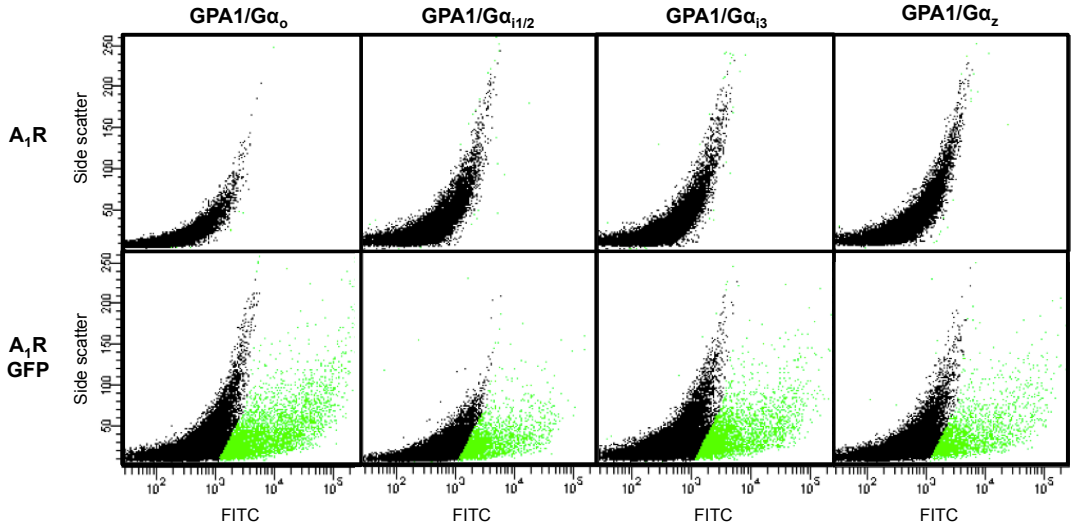

Figure 3.9: **Flow cytometry of A_1R^{GFP} in yeast.** Responding A_1R and A_1R^{GFP} strains were analysed using a LSRII flow cytometer. 3x10^4 cells were analysed and fluorescence intensity in the GFP channel quantified for each cell. The graphs show fluorescence intensity vs. side scatter (a measure of cell width). Thresholds were set using the equivalent A_1R expressing strains. Cells with fluorescence below the threshold are shown in black. Cells with GFP fluorescence above the threshold are shown in green.

Table 3.4: **A_1R^{GFP} flow cytometry.** The percentage of the population showing detectable fluorescence, the average fluorescence units (FU) of the responding populations and the average FU of the total populations were calculated from Figure 3.9 using FACSDiva software. Data collected from 3x10^4 cells per sample. Error bars represent S.E.M.

Strain	**Percentage Fluorescent**	**Average FU x 10^4 Fluorescent Population**	**Average FU x 10^4 Total Population**
GPA1/Gα_o	14.8	16.3±0.5	2.9±0.1
GPA1/G$\alpha_{i1/2}$	8.6	7.7±0.3	1.1±0.1
GPA1/Gα_{i3}	11.3	11.3±0.3	1.8±0.1
GPA1/Gα_z	7.5	12.9±0.5	1.4±0.1

Figure 3.9 shows the presence of a mixed population of fluorescent and non-fluorescent cells. 14.8%, 8.6%, 11.3% and 7.5% of the A_1R^{GFP}-GPA1/Gα_o, A_1R^{GFP}-GPA1/G$\alpha_{i1/2}$, A_1R^{GFP}-GPA1/Gα_{i3} and A_1R^{GFP}-GPA1/Gα_z populations, respectively, show detectable fluorescence respectively (Table 3.4). The variation between the strains is inconsistent with their respective levels of signal (Figure 3.8). Similarly, the differences in average fluorescence per cell, in both the responding and total populations, do not reflect the signalling profiles in response to NECA. Taken together, these data suggest that differences in expression level do not account for differences in signalling in the A_1R^{GFP} strains despite the high variability in expression across a population.

3.2.4.2 Pharmacological characterisation of the A_1R^{GFP}

To further examine the effects of the GFP fluorophore on the A_1R and downstream signalling, β-galactosidase activity concentration-response curves were generated for the responding strains of Figure 3.8. The logistic equation and the operational model of pharmacological agonism were applied to these data.

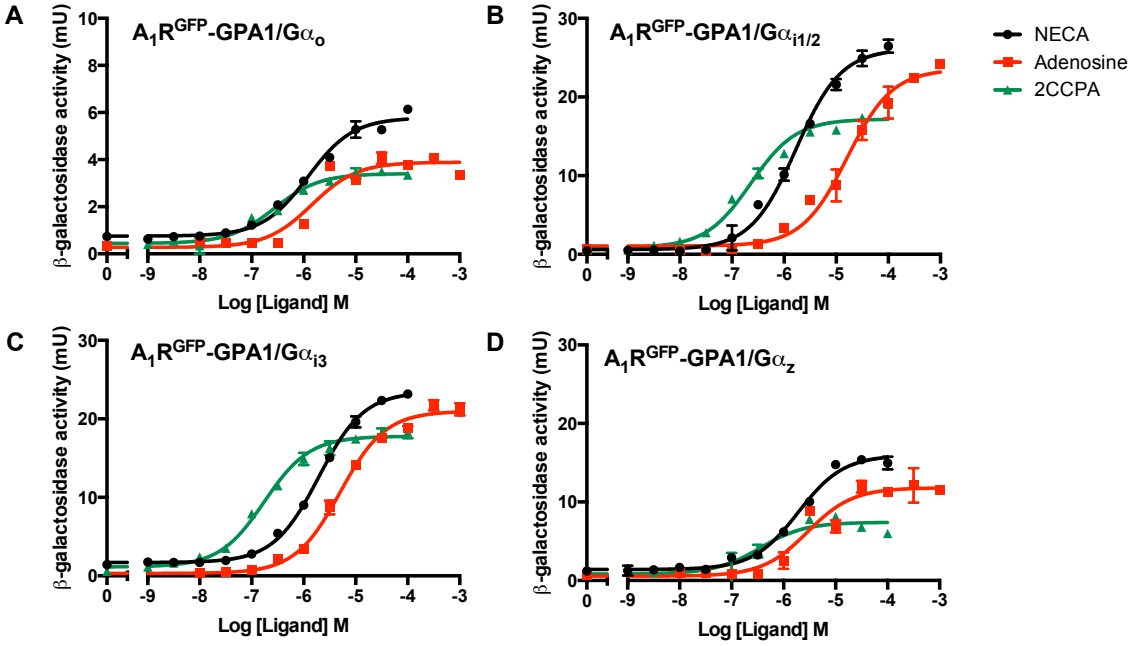

Figure 3.10: **β-galactosidase concentration-response curves of the A_1R^{GFP} in yeast.** Yeast cells expressing A_1R^{GFP} were incubated with various concentrations of NECA, 2CCPA and adenosine for 16 hours at 30°C. Cells were lysed and assayed for β-galactosidase activity(mU). Data is represented as the mean of triplicate repeats ± S.E.M fitted with the logistic equation. **A.** A_1R-GFP-GPA1/Gα_o. **B.** A_1R-GFP-GPA1/G$\alpha_{i1/2}$. **B.** A_1R-GFP-GPA1/Gα_{i3}. **D.** A_1R-GFP-GPA1/Gα_z.

Table 3.5: **Pharmacological parameters of the A_1R^{GFP}.** The logistic equation and the operational model of pharmacological agonism were applied to the data of Figure 3.10 by non-linear regression. $pEC_{50} = -Log\ EC_{50}$ (potency), E_{max} = maximum level of signal, $pK_A = -\text{Log } K_A$ (ligand binding affinity) and τ = efficacy. Significant differences were assessed by One-Way ANOVA with Dunnett's multiple comparisons test. *P < 0.05, **P < 0.005, ***P < 0.005 compared to NECA in the same strain.

Strain	**Ligand**	**pEC$_{50}$**	E_{max} **mU**	pK_A	$log\tau$
GPA1/Gα_o	NECA	5.9±0.1	5.8±0.1	4.1±0.1	1.8±0.1
	Adenosine	5.8±0.2	3.9±0.2***	5.3±0.1***	0.3±0.1***
	2CCPA	6.6±0.1*	3.4±0.1***	6.2±0.1***	0.1±0.1***
GPA1/G$\alpha_{i1/2}$	NECA	5.8±0.1	26.1±0.5	4.4±0.1	1.4±0.1
	Adenosine	4.8±0.1***	23.5±0.7**	3.8±0.2*	0.9±0.1*
	2CCPA	6.6±0.1**	17.2±0.4***	6.2±0.1***	0.3±0.1***
GPA1/Gα_{i3}	NECA	5.7±0.1	23.4±0.2	5.1±0.0	1.0±0.1
	Adenosine	5.3±0.1	20.1±0.5**	4.2±0.1***	1.0±0.1
	2CCPA	6.8±0.1***	17.8±0.3***	6.1±0.1***	0.5±0.1*
GPA1/Gα_z	NECA	5.7±0.1	16.0±0.4	4.4±0.1	1.5±0.1
	Adenosine	5.5±0.1	11.8±0.6**	5.0±0.1*	0.4±0.1***
	2CCPA	6.5±0.2*	7.4±0.4***	6.2±0.2***	−0.1±0.1***

The data of Table 3.1 and Table 3.5, for the A_1R and A_1R^{GFP} respectively, are remarkably similar. pEC_{50} and pK_A are consistent between the A_1R and A_1R^{GFP}. However, E_{max} is increased for A_1R^{GFP} in the GPA1/Gα_o and GPA1/Gα_z strains relative to their A_1R counterparts. This effect is present, although less pronounced for the GPA1/Gα_{i3} strain. Here the pharmacology of the A_1R^{GFP} is broadly similar in the presence of GPA1/G$\alpha_{i1/2}$ and GPA1/Gα_{i3}. However, the increased E_{max} in GPA1/Gα_o and GPA1/Gα_z may be due to reduced internalisation of the receptor.

Internalisation is a key regulatory process in GPCR activation and signalling. In *Sc. cerevisiae*, STE2 activation leads to phosphorylation of critical residues at the receptor tail by the yeast casein kinases YCK1 and YCK2 (Hicke et al., 1998). The phosphorylated receptor is then ubiquitinated and targetted for clathrin mediated internalisation and lysosomal degradation (Roth and Davis, 1996). While a $A_{2A}R^{GFP}$ fusion protein has been shown to internalise slowly in yeast (Butz et al., 2003; Niebauer et al., 2004; Niebauer and Robinson, 2006) it has not been shown that this process is is extended to A_1R^{GFP}. This can be measured through fluorescence microscopy. Unfortunately, GFP is sensitive to photobleaching preventing the generation of timecourse data. To circumvent this all A_1R^{GFP} strains were treated with 1% (v/v) DMSO or 100 μM NECA for 16 hours and imaged using a Deltavision widefield microscope (Figure 3.11). Clear membrane localisation of the receptor is maintained after NECA treatment, suggesting that A_1R^{GFP} is not internalised in yeast after 16 hours exposure to NECA. Therefore, it is possible that the lack of internalisation is influencing differences in E_{max} between the A_1R and A_1R^{GFP}.

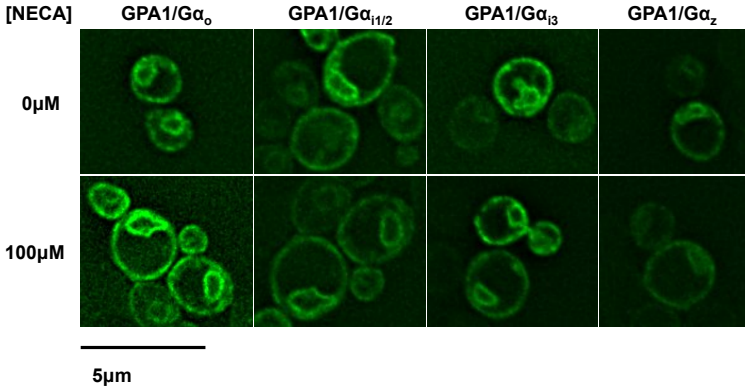

Figure 3.11: **Testing internalisation of A_1R-GFP in yeast by widefield microscopy.** The responding A_1R-GFP strains of Figure 3.8 were cultured overnight in AA-Ura in a shaking incubator at 30°C. Cells were subcultured in AA-Ura for a further 6-8 hours. Cell density adjusted to OD_{600} = 0.02 and cells incubated in AA-Ura containing 1% (v/v) DMSO or 100μM NECA for 16 hours at 30°C. Cells were imaged using a DeltaVision widefield microscope (excitation = 488nm and emission = 535nm). Images were deconvolved using SoftWorxRx and processed in ImageJ.

3.3 Characterisation of the Adenosine A_{2A} Receptor in Yeast

The adenosine A_{2A} receptor ($A_{2A}R$) has gained attention as a therapeutic target in recent years due to its intrinsic constitutive activity. Unlike the other adenosine receptors the crystal structure of the $A_{2A}R$ has been solved (Figure 1.17). Consequently, there is a great deal of structural, in addition to pharmacological, information available about this receptor.

In contrast to the A_1R, the $A_{2A}R$ is primarily $G\alpha_s$-coupled, mediating its activity through activation of adenylate cyclase (reviewed by Jacobson (2009)). However, it has been reported that the $A_{2A}R$ can influence PLC-β through $G\alpha_q$ (Sheth et al., 2014). The $A_{2A}R$ has been shown to signal in yeast through the endogenous G protein, GPA1, or the MMY24 GPA1/$G\alpha_{i3}$ transplant strain used here (Price et al., 1996; Bertheleme et al., 2013, 2014). Interestingly, the $A_{2A}R$ has not been shown to signal through chimeric $G\alpha_s$ subunits in yeast. We sought to expand our studies to include signalling bias and ligand specificity in the $A_{2A}R$. The $A_{2A}R$ was cloned into the p426GPD vector, under the control of the constitutive *GAPDH* promoter and transformed into the panel of yeast transplant strains. 8-16 colonies of each strain were screened for β-galactosidase activity in response to 100μM NECA. Responses were compared to DMSO by Student's T-test and a $P < 0.05$ considered significant (Figure 3.12).

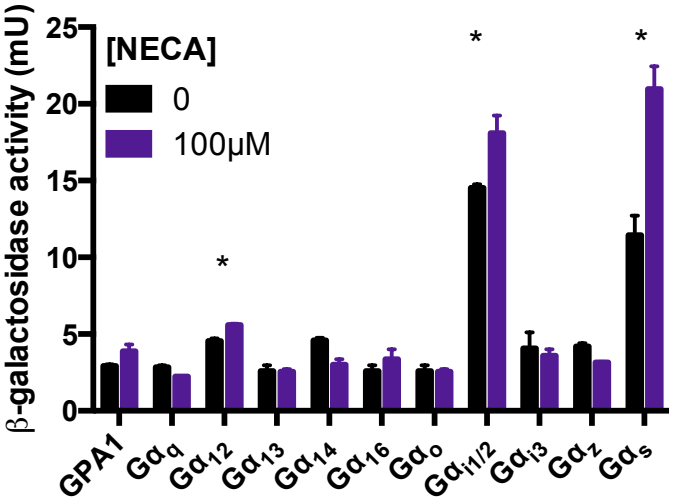

Figure 3.12: **Expression of the adenosine $A_{2A}R$ in yeast.** The $A_{2A}R$ was expressed in a panel of yeast strains using the p426GPD vector selected for uracil biosynthesis. n = 8 - 16 colonies were picked and incubated in AA-Ura containing either 100μM NECA, or 1 % DMSO for 16 hours. Cells were lysed and assayed for β-galactosidase activity. Significant responses were determined by Student's T-test compared to DMSO alone (*$P < 0.05$).

Constitutive activity is the defining feature of the $A_{2A}R$. This is recreated in yeast through enhanced basal activity. Basal activity is higher in all $A_{2A}R$ transformed strains than the untransformed basal (0.5±0.2 mU). Statistically significant responses to NECA were detected for the GPA1/$G\alpha_s$ and GPA1/$G\alpha_{i1/2}$ transplant strains. Interestingly, the basal level of signal is higher in the responding strains (basal = 3.4±0.2 mU, 14.5±0.2 mU and 11.4±1.3 mU for "non-responding", $A_{2A}R$-GPA1/G$\alpha_{i1/2}$ and $A_{2A}R$-GPA1/Gα_s strains respectively). This higher basal in the responding strains could be the result of precoupling, whereas the lower basal of the non-responding strains may represent a more transient interaction between the receptor and the G protein. The novel discovery of a $A_{2A}R$-GPA1/Gα_s coupling in yeast is encouraging given the known role of the $A_{2A}R$ in stimulating adenylate cyclase in mammalian cells. Also, consistent with other studies significant activity in response to ligand was observed in a GPA1/Gα_i strain (Bertheleme et al., 2013, 2014). However, in contrast to Bertheleme et al. (2013, 2014) who have shown activity in GPA1/Gα_{i3}, we observe $A_{2A}R$-mediated activation of GPA1/G$\alpha_{i1/2}$ in response to NECA. The physiological significance of these interactions is unclear as, to the best of our knowledge, the $A_{2A}R$ has not been shown to interact with Gα_i proteins without heterodimerisation with the A_1R (Casadó et al., 2010).

A C-terminal $A_{2A}R^{GFP}$ variant was created to ensure that receptor localisation was consistent between responding and non-responding strains. This construct was transformed into the panel of strains using the p426GPD vector and cells imaged by confocal microscopy (Figure 3.13). Consistent membrane localisation of $A_{2A}R^{GFP}$ between strains was observed in all strains tested.

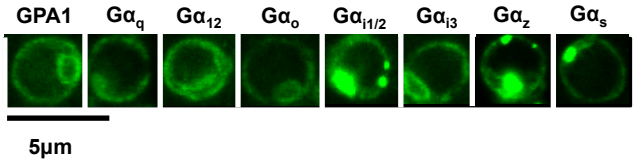

Figure 3.13: **Localisation of the $A_{2A}R^{GFP}$ in yeast.** The $A_{2A}R$ was C-terminally tagged with GFP and cloned into the p426GPD vector. This was transformed into the panel of yeast strains and imaged using a True Confocal Scanner Leica TCS SP5 microscope. Images were processed and background fluorescence compensated for using ImageJ software.

The physiologically significant A_{2A}R-GPA1/Gα_s coupling was characterised in response to a number of ligands. This strain was incubated in AA-Ura containing various concentrations of NECA, adenosine, 2CCPA and CGS21680 for 16 hours at 30°C. Cells were lysed and β-galactosidase activity determined. Concentration-response curves were generated for NECA and CGS21680 (pEC_{50} = 6.5±0.2 and 4.7±0.1, E_{max} = 19.2±0.6 mU and 24.9±0.8 mU for NECA and CGS21680 respectively) but could not be constructed for adenosine or 2CCPA (Figure 3.14).

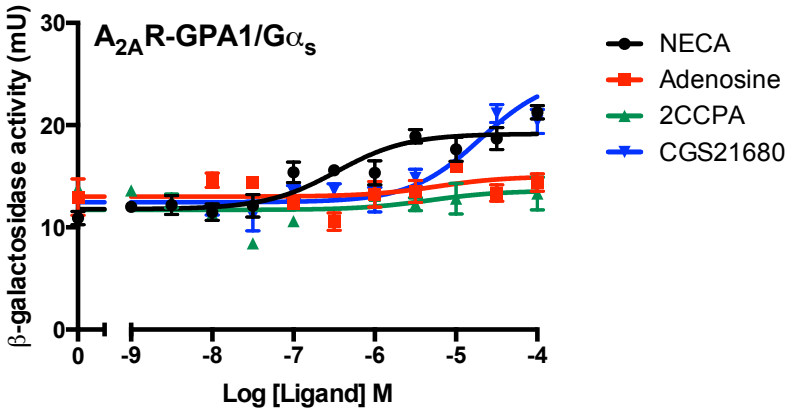

Figure 3.14: **A_{2A}R-GPA1/Gα_s concentration-response curves in yeast.** A_{2A}R-GPA1/Gα_s was incubated with a concentration range of NECA, adenosine, 2CCPA and CGS21680. Cells were lysed and β-galactosidase activity determined. Data represents the mean of quadruplicate repeats ± S.E.M fitted using the logistic equation.

Adenosine is the endogenous ligand of the A_{2A}R. Therefore, a response should have been observed. However, the basal level of signal fluctuated greatly in this strain (basal = 13.09±2.3 mU). This is likely to be the result of cell-to-cell variation. Here we express the A_{2A}R using the p426GPD expression vector. As observed with p426GPD-A_1R^{GFP}, not all cells in a population will express the receptor to the same level and some may not express the receptor at all (Figure 3.9). Also the constitutive activity of the A_{2A}R can contribute to the basal noise in signalling and downstream responses, including transcription of β-galactosidase. As the receptor equilibrium lies closer to the active receptor state there is increased signalling through the pheromone response pathway. Consequently, the effect of cell-to-cell variation on ligand-independent signalling becomes more pronounced. 3-AT reduces the growth of cells lacking signalling downstream of an active receptor, as was observed for the A_1R. 3-AT was explored as a tool to prevent proliferation of low-responding cells to limit variability in the A_{2A}R-GPA1/Gα_s strain.

3.3.1 Optimisation of 3-AT to generate β-galactosidase concentration-response curves in A_{2A}R-expressing yeast

NECA and adenosine concentration-response curves were generated for A_{2A}R-GPA1/Gα_s with varying concentrations of 3-AT (Figure 3.15).

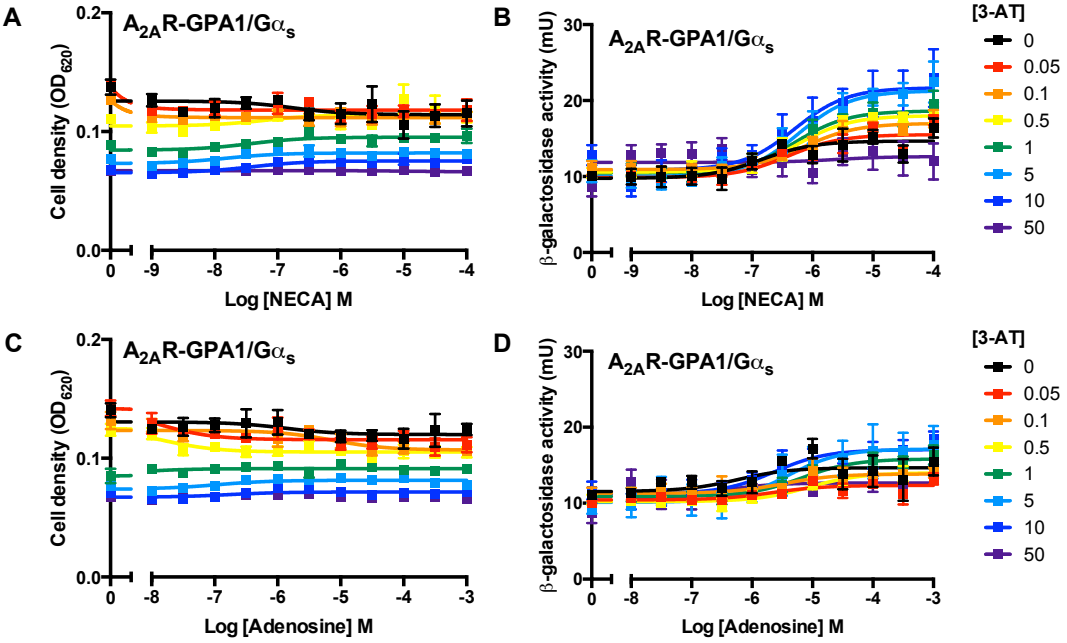

Figure 3.15: **Effect of 3-AT on the adenosine A_{2A}R β-galactosidase activity in yeast.** A_{2a}R-GPA1/Gα_s was incubated in AA-Ura-His containing the appropriate concentrations of 3-AT and ligand for 16 hours at 30°C. Cell density was determined by OD_{620}. Cells were lysed and β-galactosidase activity measured. **A.** OD_{620} and **B.** β-galactosidase activity in response to NECA. **C.** OD_{620} and **D.** β-galactosidase activity in response to adenosine. Data represents the mean of triplicate repeats ± S.E.M fitted with the logistic equation.

3-AT reduced basal growth in these cells, as indicated by the decreasing OD_{620} (Figure 3.15C and D). However, 3-AT did not appear to affect basal β-galactosidase activity (mU) but did result in the emergence of higher E_{max}. This creates a signalling window in which concentration-response curves can be constructed. 5mM 3-AT appears to generate the optimum signalling window and was used for all future experiments on the A_{2A}R. Interestingly, Bertheleme et al. (2013, 2014) generated growth concentration-response curves for the A_{2A}R in the yeast transplant system in the presence of 10mM 3-AT. However, they utilise the GPA1/Gα_{i3} transplant strain. As we observed in the validation of the A_1R, and as described by Weston et al. (2014), the GPA1/Gα_s transplant strain used here has an elevated basal level of β-galactosidase activity. This fundamental difference between the GPA1/Gα_{i3} and GPA1/Gα_s strains may explain this discrepancy.

3.3.2 Pharmacological characterisation of the $A_{2A}R$ in yeast using 3-AT

Having established the 5mM optimal concentration of 3-AT for generating concentration curves for the $A_{2A}R$ in yeast, the $A_{2A}R$-GPA1/Gα_s and $A_{2A}R$-GPA1/G$\alpha_{i1/2}$ strains were characterised in response to NECA, adenosine, 2CCPA and CGS21680 (Figure 3.16).

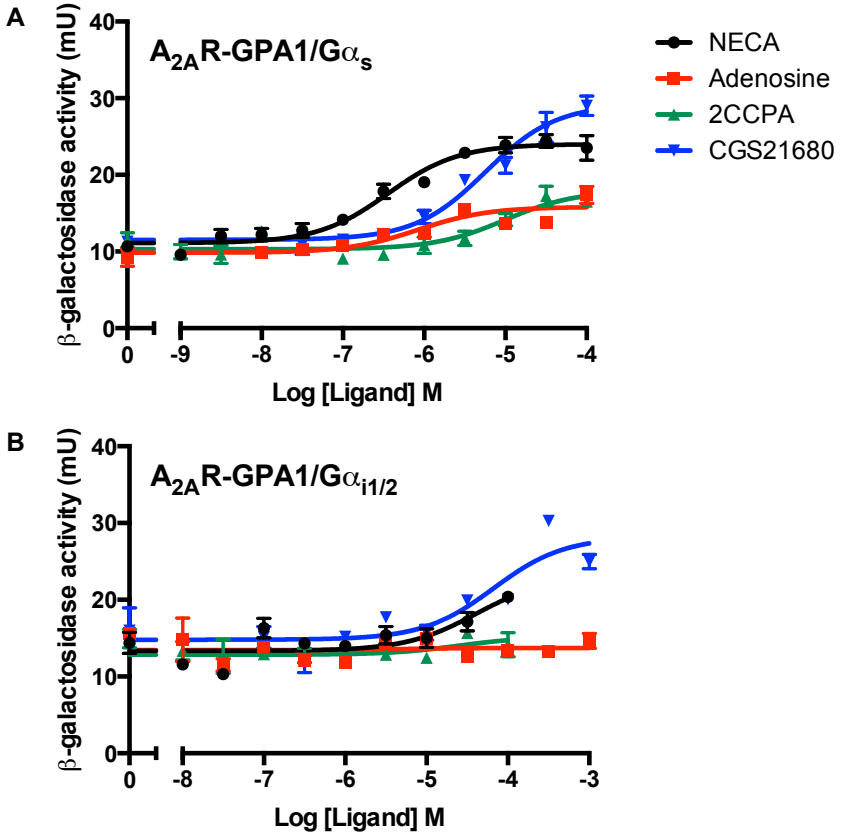

Figure 3.16: **Pharmacology of $A_{2A}R$ in GPA1/Gα_s and GPA1/G$\alpha_{i1/2}$ transplant strains.** Yeast cells were cultured in AA-Ura-His containing the appropriate concentration of ligand and 5mM 3-AT for 16 hours at 30°C. Cells were lysed and β-galactosidase activity determined. Data represents the mean of triplicate repeats ± S.E.M fitted with the logistic equation. **A.** $A_{2A}R$-GPA1/Gα_s. **B.** $A_{2A}R$-GPA1/G$\alpha_{i1/2}$.

Table 3.6: **Pharmacological parameters of the $A_{2A}R$.** The logistic equation and the operational model of pharmacological agonism were applied to the data of Figure 3.16 by non-linear regression. $pEC_{50} = -Log\ EC_{50}$ (potency), E_{max} = *maximum level of signal*, $pK_A = -LogK_A$ (ligand binding affinity) and τ = efficacy. *N.R.* = no response. Significant differences to NECA in the same strain were assessed by One-Way ANOVA with Dunnett's multiple comparisons test. *P < 0.05, **P < 0.005, compared to NECA in the same strain.

Strain	Ligand	pEC_{50}	E_{max}	pK_A	$log\tau$
GPA1/Gα_s	NECA	6.5±0.2	19.2±0.6	5.9±0.2	0.5±0.1
	Adenosine	5.2±0.8	15.0±0.6**	5.6±0.2	0.0±0.3
	2CCPA	5.0±0.2	17.9±1.2*	4.7±0.3	−0.1±0.1
	CGS21680	4.7±0.2*	24.9±0.8	4.9±0.1	−0.3±0.0
GPA1/G$\alpha_{i1/2}$	NECA	4.4±0.5	23.0±4.7	3.3±0.2	1.0±0.2
	Adenosine	N.R.	N.R.	N.R.	N.R.
	2CCPA	N.R.	N.R.	N.R.	N.R.
	CGS21680	4.3±0.2	28.1±1.7	2.8±0.1	1.6±0.1*

The behaviour of the $A_{2A}R$ varies between the GPA1/Gα_s and GPA1/G$\alpha_{i1/2}$ strains. NECA and CGS21680 induced a response in both strains but only $A_{2A}R$-GPA1/Gα_s responded to adenosine and 2CCPA. NECA is the most potent ligand tested (pEC_{50} = 6.5±0.2) and shows strong activity in this strain. CGS21680 may be a full agonist in this strain but has a reduced potency relative to NECA (pEC_{50} = 4.47±0.2). Adenosine and 2CCPA are both partial agonists of the $A_{2A}R$ in the GPA1/Gα_s strain. In contrast, adenosine and 2CCPA do not elicit a response in the $A_{2A}R$-GPA1/G$\alpha_{1/2}$ strain. CGS21680 exhibits broadly similar pharmacology for the $A_{2A}R$ in GPA1/G$\alpha_{i1/2}$ and GPA1/Gα_s backgrounds but pK_A and $log\tau$ values differ. Taken together this data suggests that G protein subtype influences the pharmacology of the $A_{2A}R$. Bias plots could not be created to explore this effect further due to the need for a reference ligand and the poor response of NECA in the $A_{2A}R$-GPA1/G$\alpha_{i1/2}$ strain.

NECA, adenosine, 2CCPA and CGS21680 elicit responses in the $A_{2A}R$-GPA1/Gα_s strain and all A_1R strains tested. In the yeast system, these receptors share the same cell signalling machinery with the exception of the the 5 C-terminal amino acids of GPA1. This allows the use of the Rajagopal et al. (2011) method to create bias plots to describe the selectivity of these compounds for the A_1R relative to the $A_{2A}R$. To our knowledge, this is the first time this method has been used to study the selectivity of ligands for different receptor subtypes. The selectivity of adenosine, 2CCPA and CGS21680 were calculated for A_1R-GPA1/G$\alpha_{i1/2}$ relative to $A_{2A}R$-GPA1/Gα_s using NECA as a reference ligand. The bias plot of Figure 3.17 demonstrates that adenosine and 2CCPA are biased towards A_1R activation while CGS21680 is a $A_{2A}R$ selective ligand.

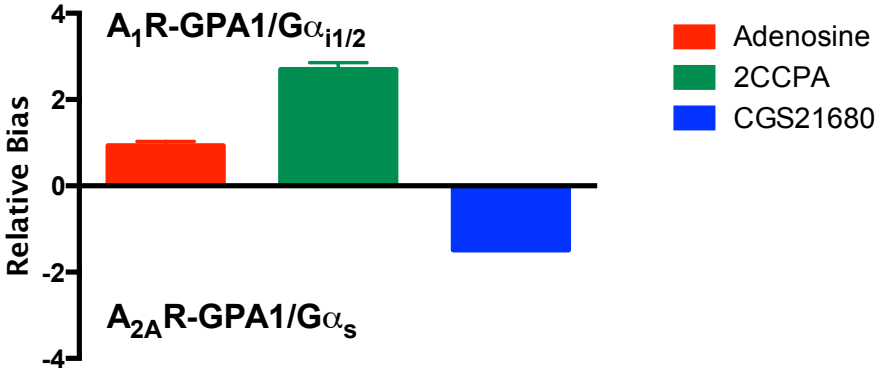

Figure 3.17: **Bias plots to quantify $A_1R/A_{2A}R$ ligand selectivity.** The method of Rajagopal et al. (2011) was used to calculate ligand selectivity using the data of Figure 3.2 and Figure 3.16 and parameters of Table 3.1 and Table 3.6. NECA was used as the reference ligand. Data represents mean ± S.E.M of triplicate repeats.

3.4 Characterisation of the Adenosine A_{2B} Receptor in Yeast

Validation of adenosine receptor subtypes in yeast were extended to include the A_{2B}R. Like the A_{2A}R, the A_{2B}R is primarily coupled to stimulatory G proteins such as Gα_s in mammalian systems but has been shown to couple to inhibitory G protein transplants in the yeast system (Brown et al., 2000; Peeters et al., 2012; Liu et al., 2014). The A_{2B}R is known to be a low affinity adenosine receptor, requiring high concentrations of ligand to induce a response. These concentrations are far higher than basal adenosine concentrations and are typically associated with pathophysiological conditions (Jacobson, 2009). Consequently, the A_{2B}R has been implicated in stress and immunological responses. However, the tissue distribution of the adenosine receptors overlap considerably, particularly in skeletal muscle and the cardiovascular system (Lynge and Hellsten, 2000). It is likely that the pharmacology and physiology of the A_1R and A_{2B}R are tightly linked. Consequently, this receptor warrants further investigation.

The A_{2B}R was cloned into the p426GPD expression vector and expressed in the panel of yeast transplant strains. 8-16 colonies were picked and screened for activity in response to a 100μM NECA by β-galactosidase assay (Figure 3.18). Responses were compared to DMSO alone by Student's T-test and a $P < 0.05$ considered significant

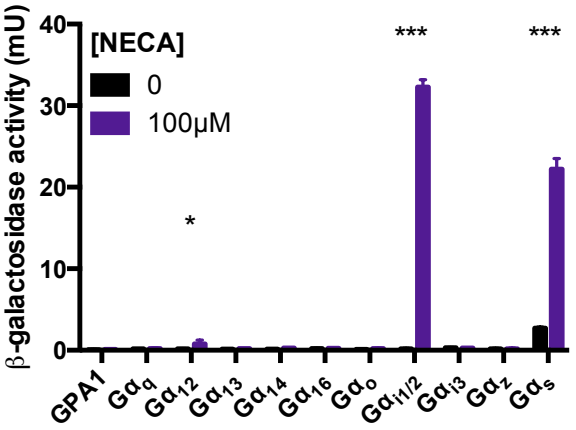

Figure 3.18: **Expression of the adenosine A_{2B}R in yeast.** The A_{2B}R was expressed in a panel of yeast strains using the p426GPD vector. n = 8 - 16 colonies were picked and incubated with either the full agonist NECA, or 1 % DMSO for 16 hours. Cells were lysed and assayed for β-galactosidase activity. Significant responses were determined by Student's T-test (***$P < 0.0005$, **$P < 0.005$, *$P < 0.05$).

Significant upregulation of signal in response to NECA were detected in yeast expressing GPA1/Gα_{12}, GPA1/Gα_{i3} and GPA1/Gα_s. The A_{2B}R-GPA1/Gα_{12} response is limited (1.3±0.3 mU) and may not be physiologically relevant. However, the A_{2B}R responses to 100μM NECA, via GPA1/G$\alpha_{i1/2}$ and GPA1/Gα_s, were much higher (32.3±0.9 mU and 22.2±1.3 respectively). Previous studies have shown the A_{2A}R and the A_{2B}R couple to the GPA1/Gα_{i3} transplant in yeast (Peeters et al., 2011; Bertheleme et al., 2013, 2014). Here

no significant activity was observed for either of these receptors in this strain. However, activity was detected via the $A_{2A}R$ and $A_{2B}R$ in the GPA1/G$\alpha_{i1/2}$ strain.

A C-terminal $A_{2B}R^{GFP}$ fusion protein was created to ensure proper receptor trafficking and membrane localisation. This construct was cloned into the p426GPD vector and expressed in the panel of transplant strains. Individual colonies were picked and imaged by confocal microscopy. Figure 3.19 shows membrane localisation of the receptor is shared by in both responding and non-responding strains alike.

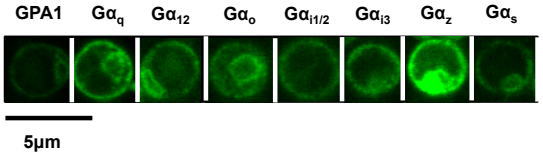

Figure 3.19: **Localisation of the $A_{2B}R^{GFP}$ in yeast.** The $A_{2B}R$ was C-terminally tagged with GFP and cloned into the p426GPD vector. This was transformed into the panel of yeast strains. Cells were imaged using a True Confocal Scanner Leica TCS SP5 microscope. Images were processed using ImageJ software.

Due to the similarity of the $A_{2A}R$ and the $A_{2B}R$ coupling profiles in yeast the $A_{2B}R$-GPA1/G$\alpha_{i1/2}$ and $A_{2B}R$-GPA1/Gα_s strains were selected for further characterisation (Figure 3.20). Quantitative insight into these concentration-response curves was gained through non-linear regression of the logistic equation and the operational model of pharmacological agonism (Table 3.7).

The $A_{2B}R$ induces a higher E_{max} in GPA1/G$\alpha_{i1/2}$ than in GPA1/Gα_s (32.4±1.7 compared to 24.6±0.9). This may indicate a more efficient G protein coupling in the $A_{2B}R$-GPA1/G$\alpha_{i1/2}$ transplant. This is reflected in largely reduced $log\tau$ values for $A_{2B}R$-GPA1/Gα_s. Consistent with this, adenosine is a full agonist of the $A_{2B}R$ in the GPA1/G$\alpha_{i1/2}$ strain but a partial agonist against GPA1/Gα_s based on their responses relative to NECA. In contrast to the $A_{2A}R$, NECA, adenosine, 2CCPA and CGS21680 show similar potencies for both $A_{2B}R$ strains (Table 3.7). Consistent with observations of the A_1R in yeast, all ligands show a 15-fold reduction in potency for the $A_{2B}R$ relative to mammalian systems (IJzerman et al., 2014b), confirming the reduced sensitivity of the yeast β-galactosidase assay relative to mammalian systems.

The lack of plateau in the 2CCPA and CGS21680 presented difficulties in fitting the operational model. The operational model requires a full sigmoidal curve for accurate fitting. However, the operational model variants exist where a reference E_{max} of a full agonist is included to circumvent this limitation (Motulsky and Christopoulos, 2004). Here, NECA was assumed to be approaching its upper plateau. Consequently, the operational model values presented here are estimates that should be used with some caution. The similarity in $A_{2B}R$ potencies in the GPA1/G$\alpha_{i1/2}$ and GPA1/Gα_s strains is reflected by consistent pK_A values for all ligands. However, $log\tau$ values are reduced in $A_{2B}R$-GPA1/Gα_s. This

suggests that the G protein transplant does not affect binding in the $A_{2B}R$ but does affect signal transduction. However, while these predictions are consistent with Figure 3.19 this is speculative without more data points for fitting. However, bias plots may alleviate this problem. As bias plots use $\Delta\Delta\frac{\tau}{K_A}$, and the inherent ambiguity of the operational model, this method is appropriate for the study of bias in the $A_{2B}R$. To confirm this a bias plot was constructed to compare the activity of adenosine, 2CCPA and CGS21680 in the $A_{2B}R$ strains (Figure 3.21). No significant bias was detected between strains for any ligand ($P > 0.05$, Student's T-test).

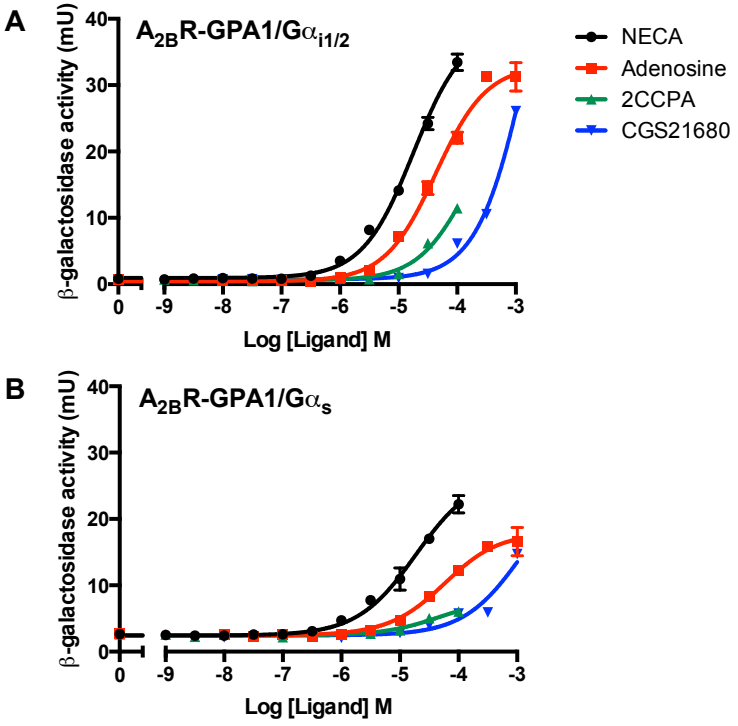

Figure 3.20: **β-galactosidase concentration-response curves of the $A_{2B}R$ in yeast**. Yeast cells were incubated in AA-Ura containing NECA, adenosine, 2CCPA or CGS21680 for 16 hours at 30°C. Cells were lysed and β-galactosidase activity determined. **A.** $A_{2B}R$-GPA1/G$\alpha_{i1/2}$/ **B.** $A_{2B}R$-GPA1/Gα_s. Data represents the mean of triplicate repeats ± S.E.M fitted with the logistic equation.

Table 3.7: **Pharmacological parameters of the A_{2B}R.** The logistic equation (2.1) and the operational model of pharmacological agonism were applied to the data of Figure 3.20 by non-linear regression. $pEC_{50} = -Log\ EC_{50}$ (potency), E_{max} = *maximum level of signal*, $pK_A = -Log\ K_A$ (ligand binding affinity) and τ = efficacy. Significant differences to NECA in the same strain were assessed by One-Way ANOVA with Dunnett's multiple comparisons test. *P < 0.05, **P < 0.005, ***P < 0.005 compared to NECA in the same strain.

Strain	Ligand	pEC_{50}	E_{max}	pK_A	log τ
GPA1/G$\alpha_{i1/2}$	NECA	4.8±0.1	34.7±1.3	4.1±1.0	0.8±0.1
	Adenosine	4.4±0.0*	33.0±0.8	3.5±0.1	0.9±0.1
	2CCPA	3.8±0.1***	28.5±5.1	3.3±0.3	0.4±0.2
	CGS21680	2.7±0.1***	28.1±1.7	3.2±0.2	0.4±0.1
GPA1/Gα_s	NECA	4.8±0.1	24.6±0.9	4.2±0.1	0.6±0.1
	Adenosine	4.3±0.8	17.5±0.6**	3.8±0.1	0.3±0.1
	2CCPA	4.1±0.1	7.5±0.5***	4.4±0.1	3.5±0.1***
	CGS21680	2.2±0.6***	14.7±0.7***	3.4±0.1	−0.2±0.1

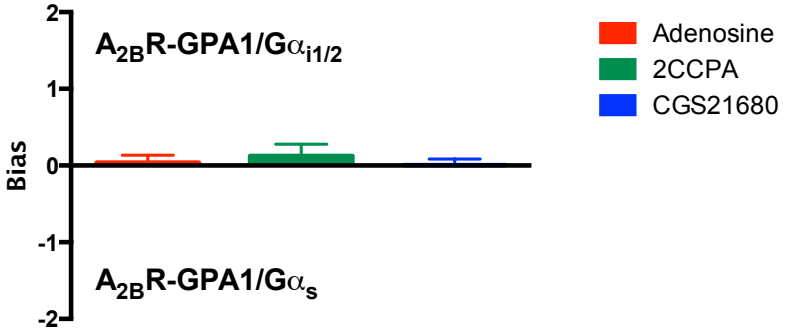

Figure 3.21: **Calculating A_{2B}R bias in yeast.** Bias plots were constructed from Table 3.7 as described by Rajagopal et al. (2011). NECA was used as the reference ligand. Error bars represent S.E.M.

Bias plots were also used to describe the selectivity of adenosine, 2CCPA and CGS21680 for the A_{2B}R compared to the A_1R and A_{2A}R. As no bias was detected for any ligand between the A_{2B}R strains the physiologically relevant A_{2B}R-GPA1/Gα_s strain was compared to A_1R-GPA1/G$\alpha_{i1/2}$ and A_{2A}R-GPA1/Gα_s (Figure 3.22). These bias plots demonstrate that adenosine and 2CCPA are A_1R selective ligands but selectively activate the A_{2A}R compared to the A_{2B}R. In contrast, CGS21680 is a A_2R biased ligand with a preference for the A_{2A}R overall. This is consistent with studies of mammalian systems (Verzijl and IJzerman, 2011).

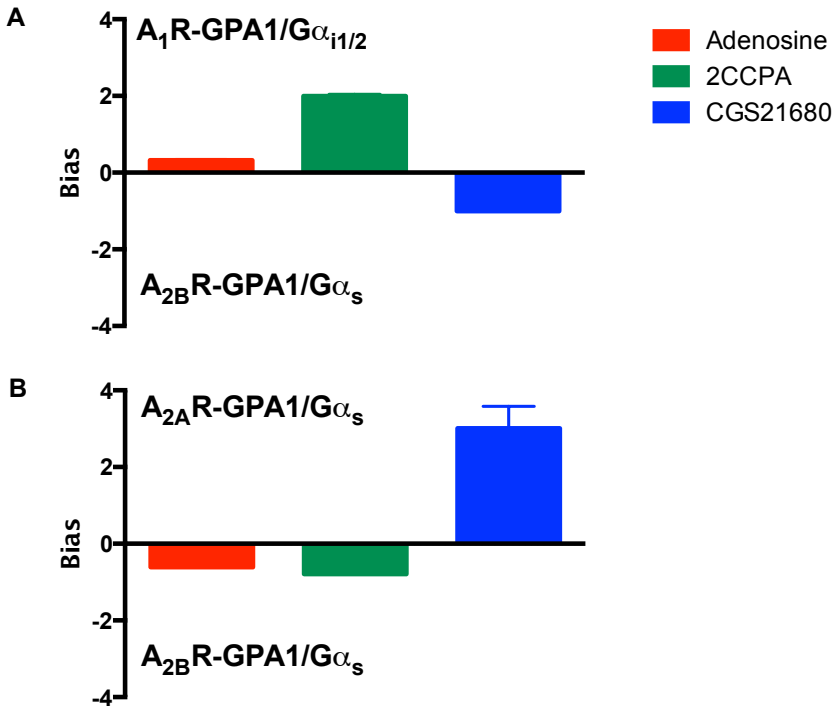

Figure 3.22: **Bias plots to quantify A_{2B}R ligand selectivity.** Bias plots were constructed from Table 3.1, Table 3.6 and Table 3.7 as described by Rajagopal et al. (2011). NECA was used as the reference ligand. Error bars represent S.E.M.

3.5 Characterisation of the Adenosine A_3 Receptor in yeast

To date, there have been no reported studies of the A_3R in yeast. The A_3R, like the A_1R, is a primarily $G\alpha_i$-coupled receptor involved in regulating the immune response (Antonioli et al., 2014). Given the similarity of the A_1R and A_3R G protein-coupling profiles we sought to express and characterise the A_3R in yeast. The A_3R was cloned into the p426GPD expression vector and expressed in the panel of yeast transplant strains. 8-16 colonies were isolated and screened for β-galactosidase activity in response to 100μM NECA. No significant increase in β-galactosidase activity was detected for any strain ($P > 0.05$, Student's T-test, Figure 3.23). As growth is a more sensitive reporter of receptor activity than β-galactosidase in the yeast system, each isolate was rescreened for activity in response to 100μM NECA by growth assay. The assay was performed with and without 3-AT. Once again no significantly responding strains were identified ($P > 0.05$, Student's T-test, Figure 3.23).

It is entirely possible that the lack of A_3R responses to NECA in yeast were the result of inadequate trafficking from the endoplasmic reticulum to the cell surface. Membrane localisation of GPCRs are determined by the N-terminus of the receptor. For instance, the N-terminus of STE2 contains membrane localisation sequences and lipid modification sites essential to membrane expression. Previously, Wedlock et al. (1993) used the STE2 leader sequence to express the human thyroid peroxidase enzymes at the yeast cell membrane. This approach has since been applied to functionally express mammalian GPCRs in the yeast transplant strains (Ladds *et al.,* unpublished data). A p426GPD expression vector was created that contained an in-frame STE2 leader sequencing immediately preceding the multiple cloning site (Figure 3.24).

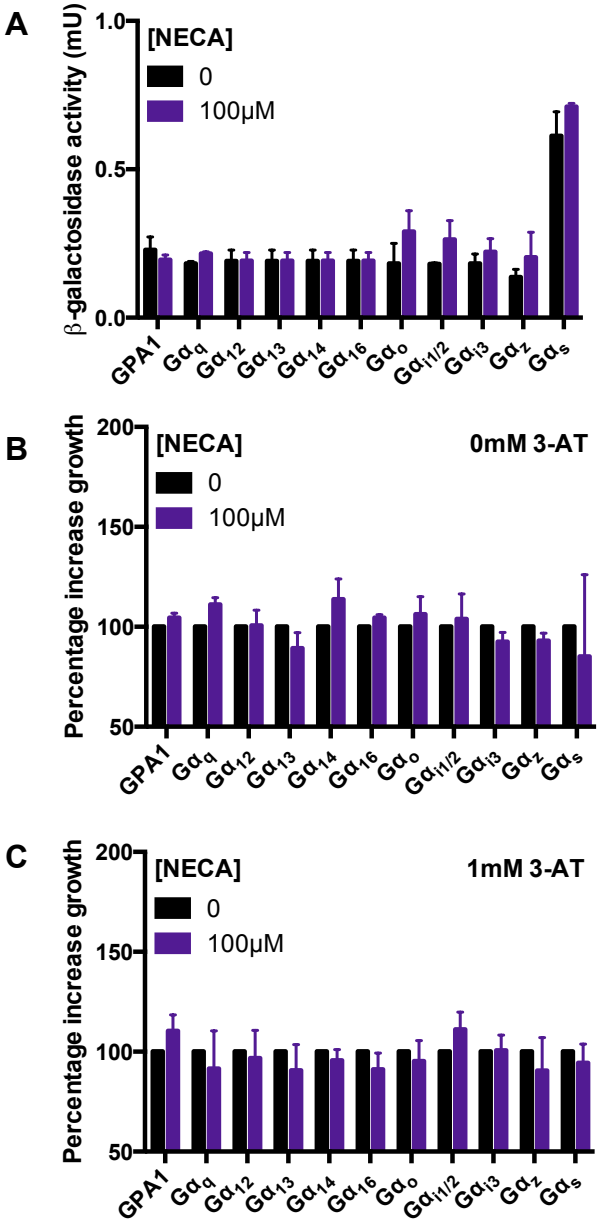

Figure 3.23: **Expression of the adenosine A_3R in yeast. A**. The A_3R was expressed in a panel of yeast strains using the p426GPD vector and selected for uracil biosynthesis. 8 - 16 colonies were picked and incubated with either the full agonist NECA, or 1 % DMSO for 16 hours. **A.** Cells were lysed and screened for β-galactosidase activity. **B.** Cells were cultured in AA-Ura-His containing 20μM FDGlu and 100μM NECA or 1% (w/v) DMSO. Fluorescence was measured after 16 hours (excitation wavelength = 485nm, emission wavelength = 535nm). **C.** Cells were cultured in AA-Ura-His containing 20μM FDGlu, 1mM 3-AT and 100μM NECA or 1% (w/v) DMSO. Fluorescence was measured after 16 hours (excitation wavelength = 485nm, emission wavelength = 535nm).

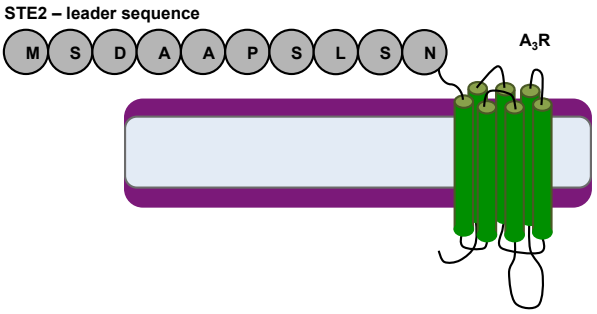

Figure 3.24: **A STE2-A_3R fusion construct for expression in yeast.** A schematic representation of the A_3R containing the N-terminal amino acids of STE2 required for membrane localisation.

The A_3R was cloned into this construct to create an N-terminal STE2 leader-A_3R fusion protein (STE2-A_3R, Figure 3.24). This construct was transformed into the panel of yeast transplant strains. 8-16 colonies were isolated and screened for activity in response to NECA by both β-galactosidase assay and growth assay. Upregulation of β-galactosidase activity in response to NECA was not detected for any strain. However, significant, but marginal, responses were detected by growth assay in the GPA1/Gα_{13} transplant strain in the presence of 1mM 3-AT (Figure 3.25, *P<0.05).

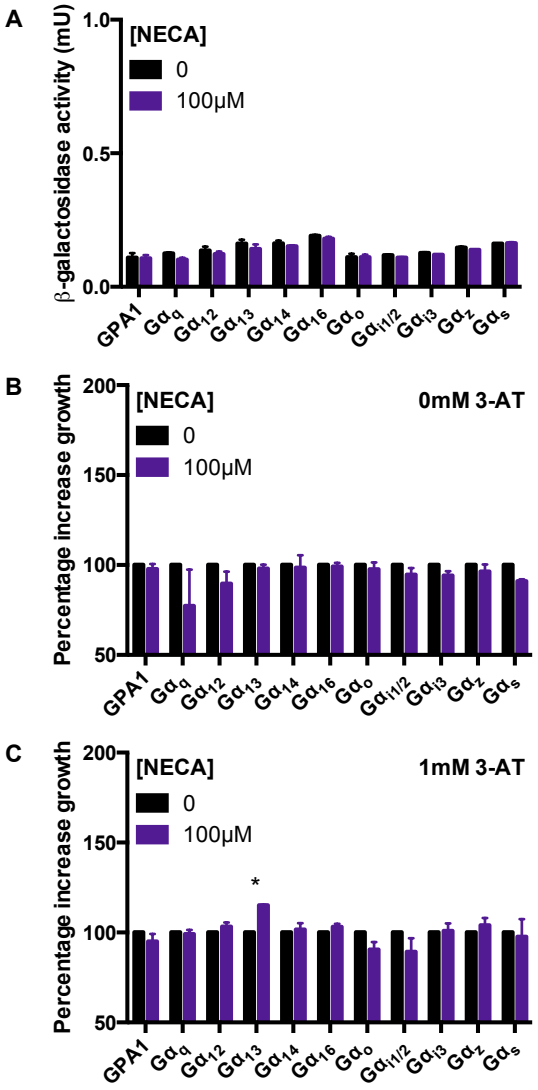

Figure 3.25: **Functional screening of STE2-A_3R construct.** The A_3R was expressed in a panel of yeast strains using the p426GPD vector containing the STE2 leader sequenceand selected for uracil biosynthesis. 8 - 16 colonies were picked and incubated with either the full agonist NECA, or 1 % DMSO for 16 hours. **A.** Cells were lysed and screened for β-galactosidase activity. **B.** Cells were cultured in AA-Ura-His containing 20μM FDGlu and 100μM NECA or 1% (w/v) DMSO. Fluorescence was measured after 16 hours (excitation wavelength = 485nm, emission wavelength = 535nm). **C.** Cells were cultured in AA-Ura-His containing 20μM FDGlu, 1mM 3-AT and 100μM NECA or 1% (w/v) DMSO. Fluorescence was measured after 16 hours (excitation wavelength = 485nm, emission wavelength = 535nm). *P $<$ 0.05.

Weak responses were detected for the STE2-A_3R in GPA1/Gα_{13} only in the presence of 3-AT, suggesting a weak interaction between the A_3R and the yeast transplant system. While the physiological significance of this interaction is unclear this stain may provide a platform to study receptor level effects. Time course data were generated for the STE2-A_3R in these strains in response to NECA, 2CCPA and adenosine in the presence of 3-AT (Figure 3.26) to identify an optimal signalling window in which to generate concentration response curves.

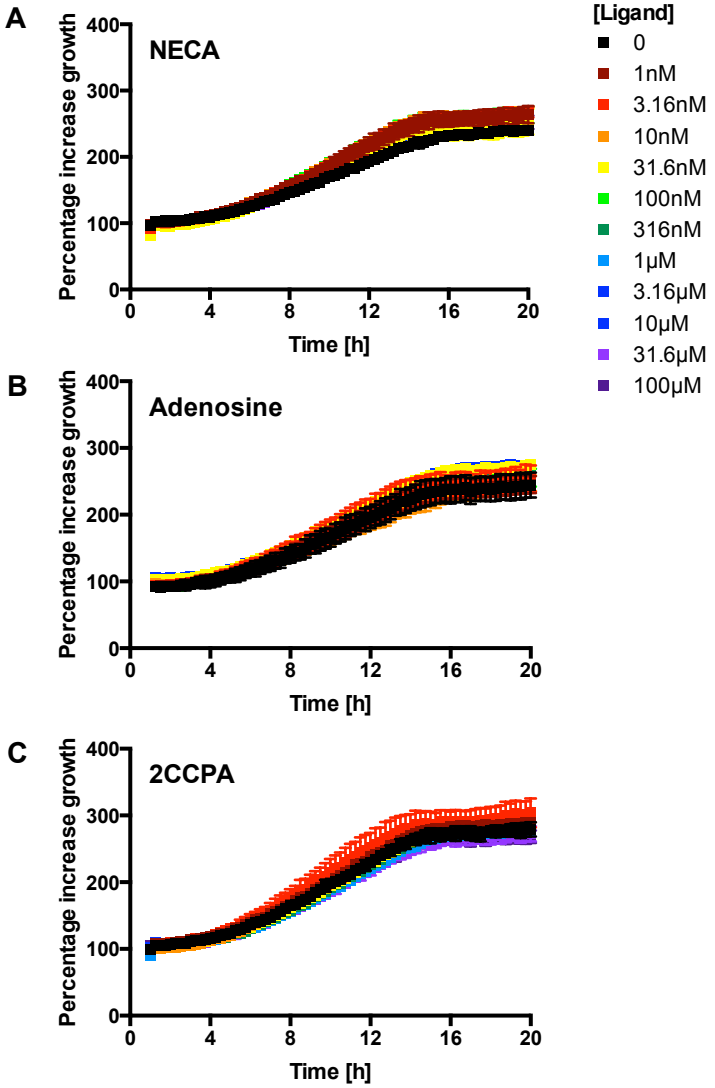

Figure 3.26: **STE2-A_3R-GPA1/Gα_{13} timecourses.** STE2-A_3R-GPA1/Gα_{13} cells were incubated in AA-Ura-His containing the appropriate concentration of ligand, 1mM and 3-AT and 20μM FDGlu. Fluorescence was measured every 15 minutes for 20 hours using a TECAN Infinite M200 microplate reader (excitation wavelength = 488nm, emission wavelength = 535nm). Data represents mean ± S.E.M. of triplicate repeats. **A.** NECA. **B.** Adenosine. **C.** 2CCPA.

The time course data of Figure 3.26 suggest weak responses to NECA in this strain. However, this response was too weak to construct a dose-response curve at any timepoint. No significant responses could be detected in this strain for adenosine or 2CCPA ($P > 0.05$ one-way ANOVA). This study of the A_3R indicates that this receptor does not function sufficiently in the yeast system to generate any pharmacologically meaningful data. Consequently, studies of this receptor were not pursued any further.

3.6 Summary

The ultimate aim of this study is model mammalian GPCR pharmacology to understand the contribution of ligand, receptor and G protein to function selective. The adenosine receptor family, particularly, the A_1R was chosen for this purpose due to demonstrated functional selectivity in yeast and mammalian systems.

A crucial first step of this project was the expression characterisation of the A_1R, $A_{2A}R$, $A_{2B}R$ and A_3R subtypes in yeast. The A_1R signalled in strains containing GPA1/Gα_o, GPA1/Gα_o and GPA1/Gα_o that represent inhibitory G proteins. This is consistent with the known roles of the A_1R in mammalian cells. For the first time a potential A_1R-GPA1/Gα_z interaction was reported. Functional selectivity of the A_1R was explored by applying simple mathematical models to the concentration-response curves of a number of ligands. This suggested that the G protein subtype influenced the signal transduction efficiency of the A_1R but not necessarily the ligand binding affinity.

Studies were extended to include the $A_{2A}R$ and $A_{2B}R$ subtypes. In mammalian cells these are primarily Gα_s coupled. Here, these receptors were functionally expressed in the GPA1/Gα_s transplant strain. However, functional coupling of these receptors to GPA/G$\alpha_{i1/2}$. These have not been reported in mammalian systems but similar GPA1/Gα_{i3} couplings have been reported in yeast. For the first time, A_1R/A_2R selectivity has been directly quantified using the method of Rajagopal et al. (2011). While originally designed to describe signalling bias, the similarity of these strains allows it to be used to describe receptor selectivity.

Unfortunately, the A_3R response was not robust enough to provide any pharmacologically meaningful information. Consequently, studies of this receptor were pursued no further.

Chapter 4

Compound screening and characterisation in yeast

4.1 Introduction

Fluorescent technologies have revolutionised pharmacology and molecular biology. Fluorescent ligands have proven to be particularly powerful. Traditionally ligand binding has been determined *in vivo* and *in vitro* using radiolabelled compounds. However, these approaches are typically high cost, low speed and technically demanding (Lohse et al., 2012). In contrast, fluorescent compounds are non-invasive and allow ligand binding and localisation to be quantified on both single-cell and population levels. Thus fluorescent A_1R selective compounds would greatly advantageous from both pharmacological and computational standpoints. Fluorescent ligands would allow quantification of ligand binding in real-time. Ligand binding rates would allow us to overcome a limitation of the operational model of pharmacological agonism and improve our parameter estimation studies. A range fluorescent A_1R-selective agonists have been synthesised and characterised (Macchia et al., 1998, 2002; Briddon et al., 2004; Baker et al., 2010; Dale et al., 2012; Kozma et al., 2013).

The need for ligand-binding data and the existence of fluorescent agonists were powerful incentives to use the A_1R to understand functional selectivity. However, only one, CAS200623, was available during this study in limited quantities and at great expense (Middleton et al., 2007). Dr Jennifer Hemmings and Prof Martin Lochner (University of Bern, Switzerland) were seeking to develop and synthesise novel A_1R-selective fluorescent ligands. Here, yeast has been demonstrated as an excellent system to study A_1R/A_2R selectivity in the absence of cross-talk. Indeed, these strains were initially developed as a drug-screening platform (Brown et al., 2000). Our desire for easy access to fluorescent ligands led to a collaboration with Dr Jenniifer Hemmings and Prof Martin Lochner. Here, the compounds they synthesised were screened and characterised in the yeast system. The data generated was used to guide fluorescent agonist development.

4.1.1 The linker region: N^6 purine substituents

The majority of fluorescent adenosine receptor agonists consist of three regions; a ligand domain, a linker domain and a fluorophore (Figure 4.1). The ligand domain is typically based on NECA or adenosine in the case of agonists or a xanthine-core for antagonists. A range of fluorophores have been tested including BODIPY, FITC or TAMRA which fluoresce in the red, green and yellow channels respectively (Jacobson et al., 1987; Middleton et al., 2007; Kumar et al., 2011; Kozma et al., 2013).

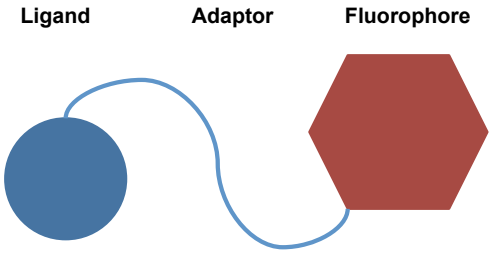

FIGURE 4.1: **Fluorescent agonist schematic.** Fluorescent adenosine receptor agonists typically consist of a ligand domain that binds the receptor, based on agonists such as adenosine or NECA and a fluorophore. To prevent the large fluorophore affecting ligand binding a linker domain, such as a hydrocarbon chain, connects the fluorescent group to the ligand.

The majority of published A_1R fluorescent ligands have their fluorophore covalently attached to the N^6 region of the purine moiety (Figure 4.2, reviewed by Kozma et al. (2013)). Previously, this attachment has been achieved using a hydrocarbon chain of varying lengths and these compounds have been shown to have good activity in the A_1R and A_3R subtypes (Baker et al., 2010; May et al., 2010). The N^6-region has also been associated with adenosine A_1R selectivity (Shearer et al., 2009; Colca, 2012). For instance, 2CCPA and R-PIA contain covalent N^6 modifications and have higher potencies at the A_1R than other adenosine receptors (IJzerman et al., 2014a). These compounds contain N^6-conjugated cyclopentyl and phenyl groups respectively.

In this study Dr Hemmings synthesised a range of fluorescent agonist precursors containing covalently attached N^6-cyclopentyl, -azabicyclo and -adamantyl regions (Figure 4.2). Here, these compounds were screened and characterised in yeast. Those with good A_1R activity and selectivity were to be further modified by Dr Hemmings through attachment of the fluorophore.

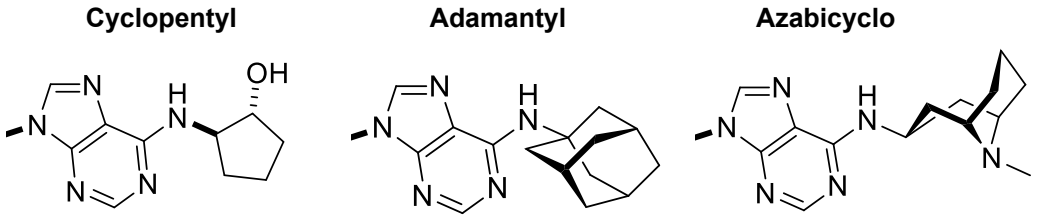

FIGURE 4.2: **N^6 substituents tested.** N^6 substituents, such as the cyclopentyl group of 2CCPA, have been shown to confer a degree of A_1R selectivity. A number of N^6 substituents were added to adenosine receptor ligands by Dr. Jennifer Hemmings. Purine group included to show site of attachment.

4.1.1.1 Investigating N^6-cyclopentyl substituents as adenosine receptor agonists

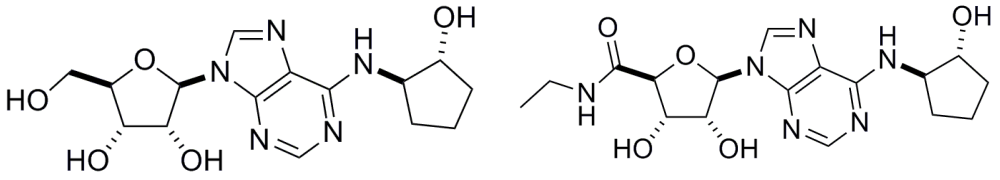

FIGURE 4.3: **N^6-cyclopentyl agonists structures.** JH109 and JH114 are derived from adenosine and NECA respectively.

The first compounds tested were N^6-cyclopentyl substituents. JH109 and JH114 are based on adenosine and NECA respectively (Figure 4.3). These compounds were tested for activity in our panel of A_1R-expressing strains; GPA1/G$\alpha_{i1/2}$, GPA1/Gα_{i3} and GPA1/Gα_z. GPA1/Gα_o was omitted from this study due to its low response to adenosine and 2CCPA (Chapter 3). Each of these strains were incubated with a concentration range of JH109 and JH114 in AA-Ura for 16 hours at 30°C. Transcriptional responses were then determined by β-galactosidase assays (Figure 4.4). Non-linear regression of the operational model of pharmacological agonism and the logistic equation were used to calculate pEC_{50}, E_{max}, pK_A and τ (Table 4.1).

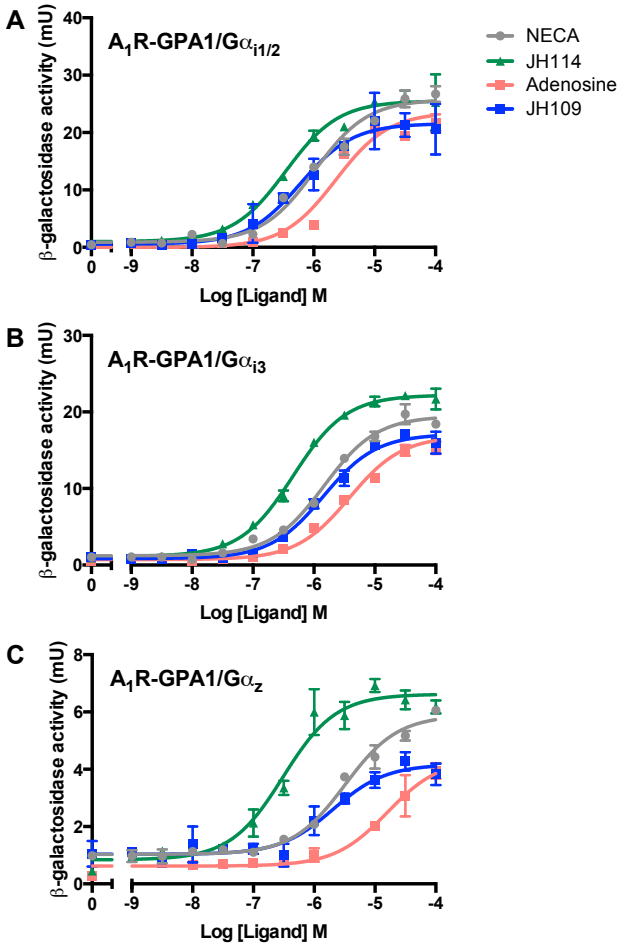

FIGURE 4.4: **N^6-cyclopentyl agonist pharmacology of the A$_1$R in yeast.** Yeast cells were incubated in AA-Ura containing an appropriate concentration of ligand for 16 hours at 30°C. Cells were lysed and β-galactosidase activity determined. Data represents mean ± S.E.M of triplicate repeats fitted with the logistic equation. **A.** A$_1$R-GPA1/G$\alpha_{i1/2}$. **B.** A$_1$R-GPA1/Gα_{i3}. **C.** A$_1$R-GPA1/Gα_z.

TABLE 4.1: **Pharmacological parameters of the A$_1$R in response to N^6 cyclopentyl agonists.** The logistic equation and the operational model of pharmacological agonism were applied to the data of Figure 4.4 by non-linear regression. $pEC_{50} = -Log\ EC_{50}$ (potency), E_{max} = maximum level of signal, $pK_A = -\text{Log}\ K_A$ (ligand binding affinity) and τ = efficacy. NECA and adenosine values have been included for comparison. * P < 0.05, *** P < 0.0005, Student's T-test relative to precursor compound.

Strain	Ligand	pEC_{50}	E_{max}	pK_A	$log\tau$
GPA1/G$\alpha_{i1/2}$	NECA	6.0±0.1	25.8±0.6	4.4±0.1	1.5±0.1
	JH114	6.5±0.1*	25.5±0.7	4.8±0.5	1.6±0.5
	Adenosine	5.6±0.1	23.5±0.7	4.6±0.2	0.9±0.1
	JH109	6.2±0.1*	21.6±1.1	5.5±0.1*	0.7±0.1
GPA1/Gα_{i3}	NECA	5.8±0.0	19.5±0.4	5.1±0.1	0.7±0.1
	JH114	6.3±0.1***	22.0±0.4	4.7±0.3	1.6±0.2*
	Adenosine	5.7±0.1	16.5±0.5	5.1±0.1	0.4±0.0
	JH109	5.8±0.1	17.1±0.4	5.3±0.1	0.4±0.1
GPA1/Gα_z	NECA	5.5±0.1	5.8±0.2	4.4±0.3	1.2±0.3
	JH114	6.8±0.1	5.5±0.2	3.8±0.3	0.8±0.2
	Adenosine	4.8±0.2	3.9±0.3	4.3±0.2	0.3±0.1
	JH109	5.1±0.1	3.8±0.2	5.0±0.2	0.1±0.1

The data of Figure 4.4 and Table 4.1 show JH109 and JH114 are more potent than adenosine and NECA respectively in all A_1R strains tested. No significant increases in E_{max} for JH109 or JH114 relative to their precursor compounds were observed ($P > 0.05$, Student's T-test). Consistently, there is a modest increase in pK_A ($P > 0.05$, Student's T-test). There was no appreciable increase in $log\tau$ for JH109 or JH114 compared to adenosine and NECA respectively in A_1R-GPA1/Gα_{i3} or A_1R-GPA1/Gα_z. Taken together these data suggest that N^6-cyclopentyl modifications increase A_1R ligand sensitivity. However, there were differences in pK_A and $log\tau$ for JH109 and JH114 in the A_1R strains compared to their respective precursors (Table 4.4). Bias plots were constructed for these compounds in the A_1R strains using NECA as a reference compound. These suggest that JH109 exhibits a bias of GPA1/G$\alpha_{i1/2}$ > GPA1/Gα_{i3} > GPA1/Gα_z whereas JH114 is biased GPA1/G$\alpha_{i1/2}$ = GPA1/Gα_{i3} > GPA1/Gα_z for the A_1R in yeast (Figure 4.5).

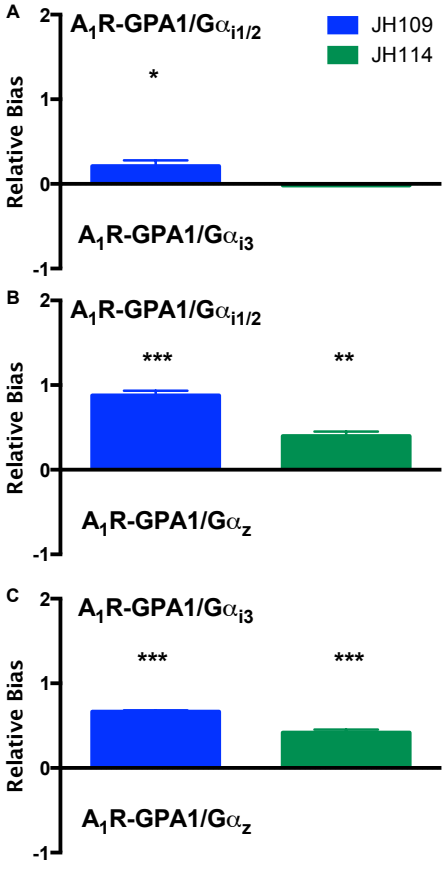

FIGURE 4.5: **A_1R bias for N^6-cyclopentyl agonists.** Bias plots were prepared for the data of Table 4.1 as described by Rajagopal et al. (2011). NECA was used as the reference compound to compensate for system bias. **A.** A_1R-GPA1/G$\alpha_{i1/2}$ vs. A_1R-GPA1/Gα_{i3}. **B.** A_1R-GPA1/G$\alpha_{i1/2}$ vs. A_1R-GPA1/Gα_z. **C.** A_1R-GPA1/Gα_{i3} vs. A_1R-GPA1/Gα_z. *$P < 0.05$, **$P < 0.005$, ***$P < 0.0005$, one-way ANOVA with Dunnett's multiple comparison test compared to NECA bias.

The subtype specificities of JH109 and JH114 were further explored using the yeast transplant system. As the physiological significance of $A_{2A}R$ and $A_{2B}R$ GPA1/G$\alpha_{i1/2}$ couplings in yeast is unclear, the A_2R-GPA1/Gα_s strains were chosen for novel compound characterisation. The $A_{2A}R$-GPA1/Gα_s and $A_{2B}R$-GPA1/Gα_s strains were incubated with JH109 or JH114 in AA-Ura for 16 hours at 30°C and β-galactosidase activity determined (Figure 4.6). pEC_{50}, E_{max}, pK_A and $log\tau$ were calculated through non-linear regression of the logistic equation and the operational model of pharmacological agonism respectively (Table 4.2).

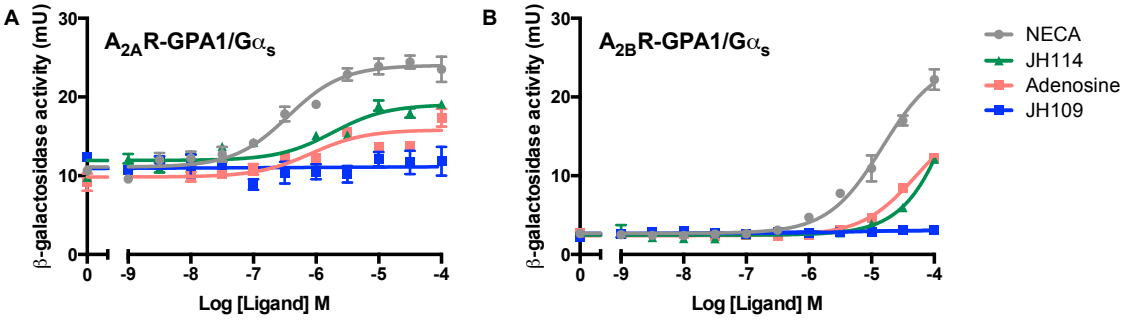

FIGURE 4.6: **N^6-cyclopentyl agonist pharmacology of the $A_{2A}R$ and $A_{2B}R$ in yeast.** $A_{2A}R$ and $A_{2B}R$ expressing yeast strains were incubated in AA-Ura-His or AA-Ura, respectively, containing an appropriate concentration of ligand for 16 hours at 30°C. $A_{2a}R$ expressing cells were also incubated with 5mM 3-AT. Cells were lysed and β-galactosidase activity determined. Data represents the mean of triplicate repeats ± S.E.M fitted with the logistic equation. **A.** $A_{2A}R$-GPA1/Gα_s. **B.** $A_{2B}R$-GPA1/Gα_s.

TABLE 4.2: **Pharmacological parameters of the $A_{2A}R$ and $A_{2B}R$ in response to N^6 cyclopentyl agonists.** The logistic equation and the operational model of pharmacological agonism were applied to the data of Figure 4.6 by non-linear regression. $pEC_{50} = -Log\ EC_{50}$ (potency), E_{max} = maximum level of signal, $pK_A = -\text{Log } K_A$ (ligand binding affinity) and τ = efficacy. *N.R.* denotes no response. NECA and adenosine values have been included for comparison. Student's T-test relative to precursor compound where P < 0.05 was considered significant. *** P < 0.0005

Strain	Ligand	pEC_{50}	E_{max}	pK_A	log τ
$A_{2A}R$-GPA1/Gα_s	NECA	6.5±0.2	19.2±0.6	5.9±0.2	0.5±0.1
	JH114	5.3±0.3	19.5±1.1	4.6±0.4	0.3±0.1
	Adenosine	4.2±0.1	15.0±0.6	5.6±0.2	0.0±0.3
	JH109	N.R.	N.R.	N.R.	N.R.
$A_{2B}R$-GPA1/Gα_s	NECA	4.8±0.1	24.6±0.9	4.2±0.1	0.6±0.1
	JH114	3.5±0.3	12.1±0.1	4.2±0.1	−0.2±0.1***
	Adenosine	4.3±0.8	17.5±0.6	3.8±0.1	0.3±0.1
	JH109	N.R.	N.R.	N.R.	N.R.

JH109 yielded no detectable response via the $A_{2A}R$ or the $A_{2B}R$. However, JH114 induced a response via these receptors but with reduced potency, E_{max}, pK_A and $log\tau$ relative to NECA (Table 4.2). Taken together, these data suggest that N^6-cyclopentyl moeities increase the A_1R selectivity of purinergic agonists compared to their NECA and adenosine precursors in yeast.

4.1.1.2 Investigating N^6-azabicyclo compounds as adenosine receptor agonists

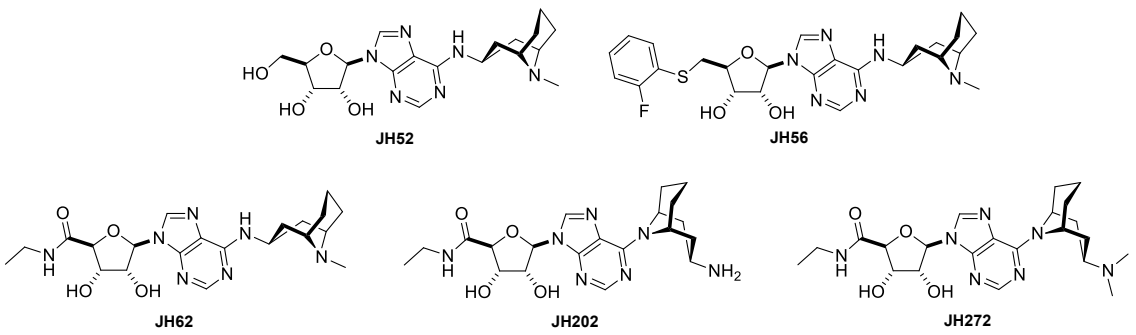

FIGURE 4.7: **N^6-azabicyclo structures.** JH52 uses adenosine as a ligand domain. JH56 also includes a 5' covalent modification to the ribose group. JH62, JH202 and JH272 use NECA as a ligand domain with various N^6-azabicyclo regions. Compounds synthesised by Dr. Jennifer Hemmings, University of Bern, Switzerland.

Further to our investigation of N^6-cyclopentyl substituents, Dr. Hemmings synthesised a series of N^6-azabicyclo compounds as potential fluorescent A_1R agonist precursors (Figure 4.7). These compounds were tested for activity in the A_1R-GPA1/G$\alpha_{i1/2}$, A_1R-GPA1/Gα_{i3} and A_1R-GPA1/Gα_z yeast strains. Each of these strains were incubated with a concentration range of JH52, JH56, JH62, JH202 and JH272 in AA-Ura for 16 hours at 30°C. Transcriptional responses were determined by β-galactosidase assay (Figure 4.8). One-way ANOVA showed no significant upregulation of signal in response to any N^6-azabicyclo agonist ($P>0.05$).

Despite the lack of A_1R-mediated signalling, the $A_{2A}R$ and $A_{2B}R$ strains were assayed for activity in response to the N^6-azabicyclo ligands. $A_{2A}R$-GPA1/Gα_s and $A_{2B}R$-GPA1/Gα_s were incubated with JH52, JH56, JH62, JH202 and JH272 in AA-Ura for 16 hours at 30°C and β-galactosidase activity determined (Figure 4.9). Once again no significant upregulation of signal in response to ligand was detected ($P>0.05$, one-way ANOVA with Dunnett's post-test). Due to the lack of significant activity in any strain tested this class of compound was not developed or studied any further.

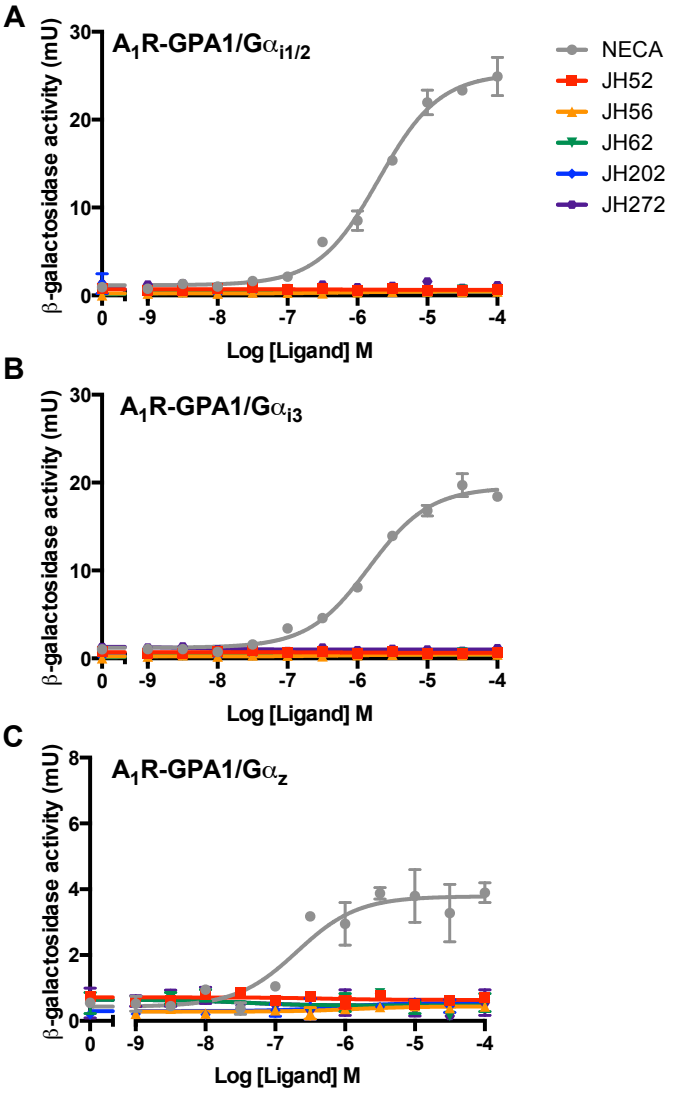

Figure 4.8: **N^6-azabicyclo agonist pharmacology of the A_1R in yeast.** Yeast cells were incubated in AA-Ura containing an appropriate concentration of ligand for 16 hours at 30°C. Cells were lysed and β-galactosidase activity determined. Data represents mean ± S.E.M of triplicate repeats fitted with the logistic equation. **A.** A_1R-GPA1/G$\alpha_{i1/2}$. **B.** A_1R-GPA1/Gα_{i3}. **C.** A_1R-GPA1/Gα_z.

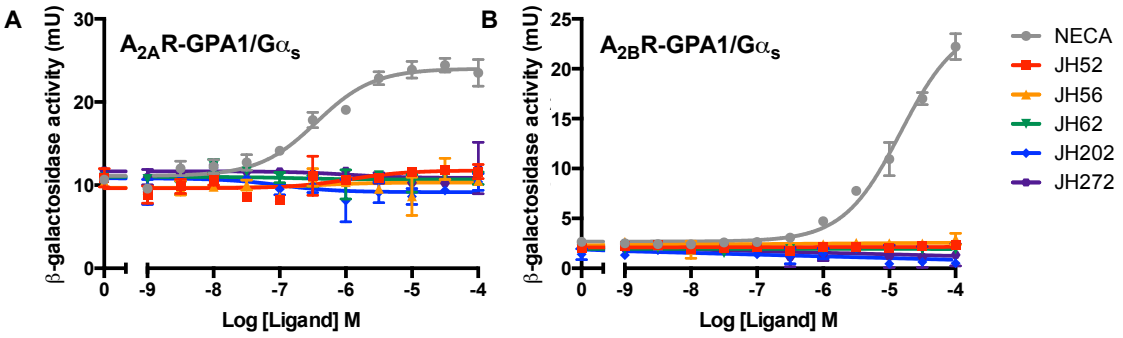

FIGURE 4.9: **N^6-azabicyclo agonist pharmacology of the $A_{2A}R$ and $A_{2B}R$ in yeast.** Yeast cells were incubated in AA-Ura containing an appropriate concentration of ligand for 16 hours at 30°C. Cells were lysed and β-galactosidase activity determined. Data represents mean ± S.E.M of triplicate repeats fitted with the logistic equation. **A.** $A_{2A}R$-GPA1/Gα_s. **B.** $A_{2B}R$-GPA1/Gα_s.

4.1.1.3 Investigating N^6-adamantyl agonists

Previously, N^6-adamantyl adenosine receptor agonists have been shown to have good A_1R selectivity over the $A_{2A}R$, $A_{2B}R$ and A_3R in rats (Daly et al., 1986; Gao et al., 2003). A selective partial A_1R agonist containing an N^6-adamantyl agonist (CVT-3619/ GS-9667) has also undergone clinical trials but has been discontinued due to inadequate pharmacokinetics (Shearer et al., 2009; Colca, 2012). Consequently, N^6-adamantyl nucleosides show promise as fluorescent ligand precursors. A range of N^6-adamantyl agonists were synthesised by Dr. Hemmings and provided for screening in yeast (Figure 4.10).

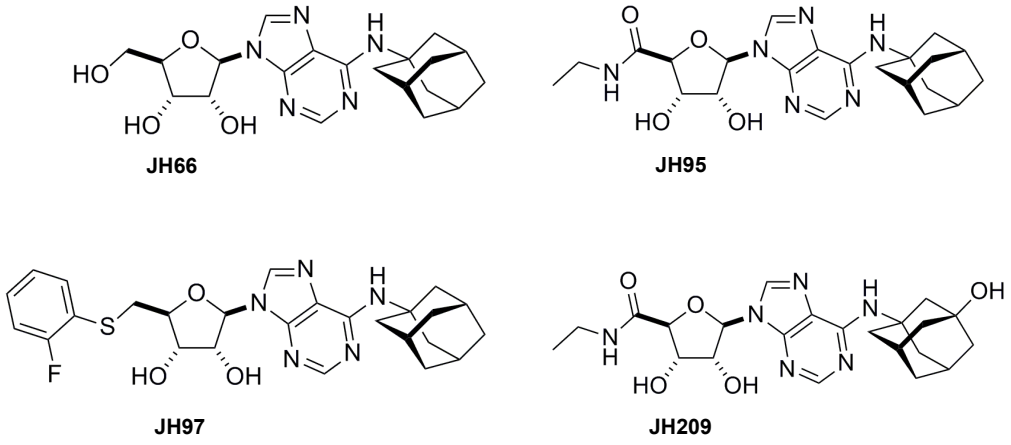

FIGURE 4.10: **N^6-adamantyl structures.** JH66 and JH95 are N^6-adamantyl substituents of adenosine and NECA respectively. JH97 also contains a 5' modification of the ribose group. JH209 is derived from JH95 but contains a hydroxyl group on the adamantyl region. Compounds synthesised by Dr. Jennifer Hemmings, University of Bern, Switzerland.

The N^6-adamantyl agonists of (Figure 4.10) were tested for activity in strains representing A_1R-GPA1/G$\alpha_{i1/2}$, A_1R-GPA1/Gα_{i3} and A_1R-GPA1/Gα_z. Each of these strains were incubated with a concentration range of JH52, JH56, JH62, JH202 and JH272 in AA-Ura for 16 hours at 30°C. Transcriptional responses were determined by β-galactosidase assay (Figure 4.11). pEC50, E_{max}, pK_A and τ were determined through non-linear regression of the logistic equation and the operational model of pharmacology (Table 4.3).

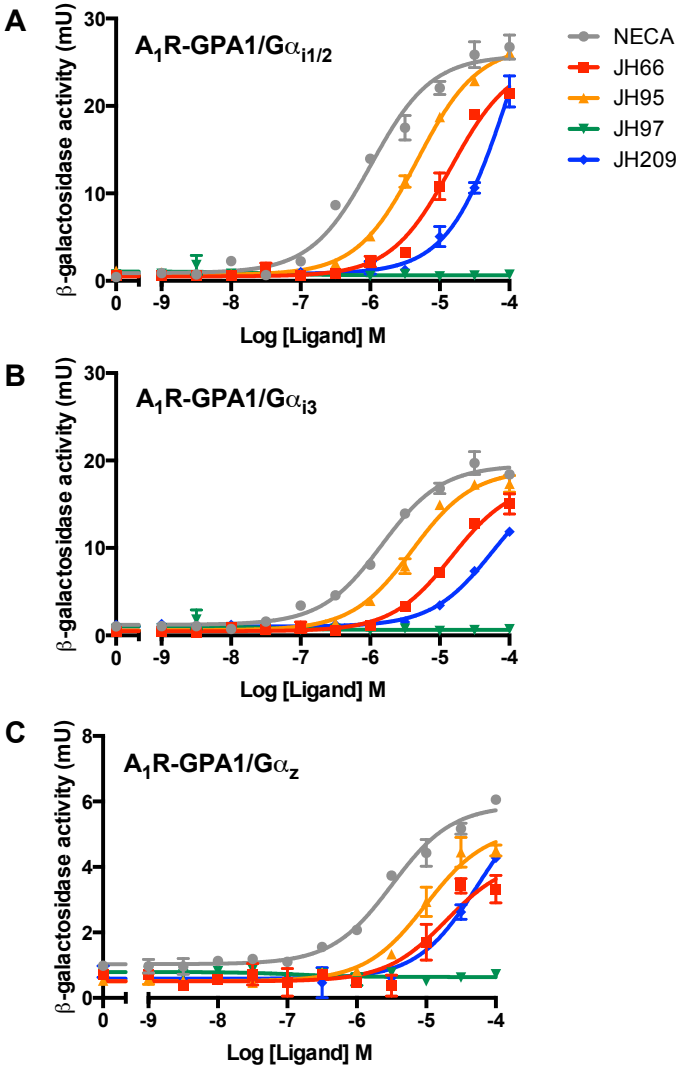

FIGURE 4.11: **N^6-adamantyl agonist pharmacology of the A_1R in yeast.** Yeast cells were incubated in AA-Ura containing an appropriate concentration of ligand for 16 hours at 30°C. Cells were lysed and β-galactosidase activity determined. Data represents mean ± S.E.M. of triplicate repeats fitted with the logistic equation. **A.** A_1R-GPA1/G$\alpha_{i1/2}$. **B.** A_1R-GPA1/Gα_{i3}. **C.** A_1R-GPA1/Gα_z.

TABLE 4.3: **Pharmacological parameters of the A_1R in response to N^6-adamantyl agonists.** The logistic equation and the operational model of pharmacological agonism were applied to the data of Figure 4.11 by non-linear regression. $pEC_{50} = -Log\ EC_{50}$ (potency),E_{max} = maximum level of signal, $pK_A = -\text{Log}\ K_A$ (ligand binding affinity) and τ = efficacy. N.R. denotes no response. JH66 and JH95 are derivatives of adenosine and NECA respectively. Therefore, NECA and adenosine have been included for comparison. * P < 0.05, ** P < 0.005, *** P < 0.0005, Student's T-test or one-way ANOVA with Dunnett's multiple comparison test as appropriate, relative to precursor compound

Strain	**Ligand**	**pEC$_{50}$**	E_{max}	pK_A	$log\tau$
A_1R-GPA1/G$\alpha_{i1/2}$	Adenosine	5.6±0.1	23.5±0.7	4.6±0.2	0.9±0.1
	JH66	4.8±0.1**	25.4±1.0	3.0±1.1	1.8±1.1
	NECA	6.0±0.1	25.8±0.6	4.4±0.1	1.5±0.1
	JH95	5.4±0.0**	26.9±0.3	4.2±0.3	1.2±0.3
	JH97	N.R.	N.R.	N.R.	N.R.
	JH209	4.0±0.1***	25.7±6.1	3.5±0.1**	1.0±0.1*
A_1R-GPA1/Gα_{i3}	Adenosine	5.7±0.1	16.5±0.5	5.1±0.1	0.4±0.0
	JH66	4.8±0.1**	17.6±0.6	4.2±0.1**	0.5±0.1
	NECA	5.8±0.0	19.5±0.4	5.1±0.1	0.7±0.1
	JH95	5.3±0.1**	19.0±0.7	4.6±0.1*	0.7±0.1
	JH97	N.R.	N.R.	N.R.	N.R.
	JH209	4.2±0.1***	18.1±0.9	3.7±0.1*	0.5±0.1
A_1R-GPA1/Gα_z	Adenosine	4.8±0.2	3.9±0.3	4.3±0.2	0.3±0.1
	JH66	4.4±0.1	2.8±0.2*	4.1±0.2	−0.2±0.1*
	NECA	5.5±0.1	5.8±0.2	4.4±0.3	1.2±0.3
	JH95	4.9±0.1*	4.5±0.2*	4.5±0.2	0.4±0.1
	JH97	N.R.	N.R.	N.R.	N.R.
	JH209	3.4±0.6*	2.8±0.3**	3.8±0.3	−0.1±0.2*

The behaviour of the N^6-adamantyl agonists is remarkably consistent between the G protein transplant strains (Figure 4.11). In particular the potency of these compounds for the A_1R appears to be largely G protein-independent in yeast (Table 4.3). Differences in E_{max} between strains is consistent with all other compounds tested and is likely to be a consequence of G protein-coupling efficiency. Trends in $log\tau$ would agree with this.

JH66 and JH95 are derivatives of adenosine and NECA respectively. These compounds show a reduced potency compared to their precursors (Table 4.3). This is in direct contrast to the N^6-cyclopentyl agonists JH109 and JH114 that show increased potency relative to adenosine and NECA respectively. This may be the result of steric hinderence as the operational model predicts variation in ligand sensitivity (pK_A) but not necessarily efficacy ($log\tau$). The lack of structural information regarding the A_1R makes this difficult to determine. However, JH209 is a modified form of JH95 containing an adamantyl-hydroxyl group. This compound shows reduced potency relative to JH95. The 5'-modified JH97 shows no response in any A_1R strain tested (Figure 4.11).

Bias plots were constructed to investigate the influence of G protein subtype on N^6-adamantyl agonist pharmacology (Figure 4.12). These compounds do little to bias signal between GPA1/G$\alpha_{i1/2}$ and GPA1/Gα_{i3}. However, JH95 promotes a slight bias towards GPA1/Gα_{i3} through the A_1R in yeast. Consistent with all other compounds tested, N^6-adamantyl agonists promote GPA1/Gα_i bias relative to GPA1/Gα_z.

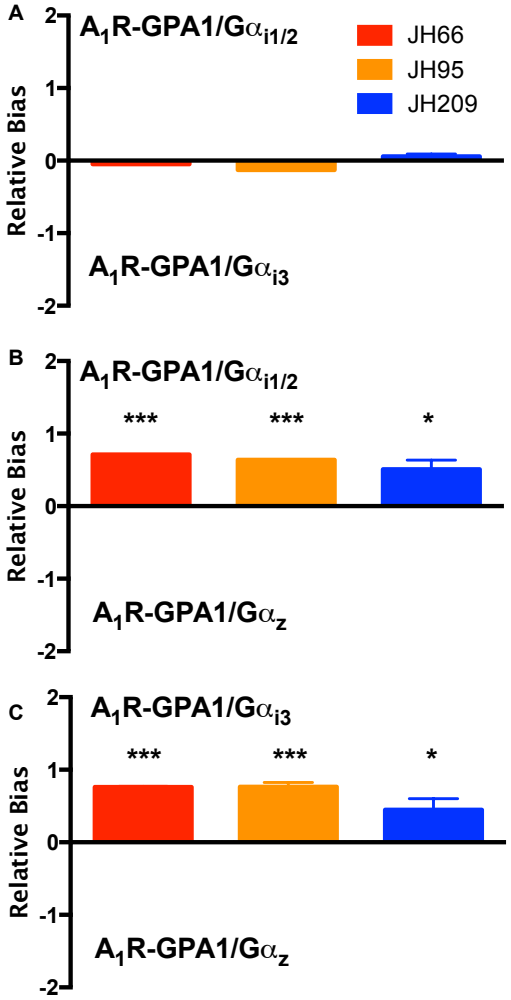

FIGURE 4.12: **A_1R bias for N^6-adamantyl agonists.** Bias plots were prepared for the data of Table 4.3 as described by Rajagopal et al. (2011). NECA was used as the reference ligand to compensate for system bias. **A.** A_1R-GPA1/G$\alpha_{i1/2}$ vs. A_1R-GPA1/Gα_{i3}. **B.** A_1R-GPA1/G$\alpha_{i1/2}$ vs. A_1R-GPA1/Gα_z. **C.** A_1R-GPA1/Gα_{i3} vs. A_1R-GPA1/Gα_z. $P < 0.05$, *** $P < 0.0005$ one-way ANOVA with Dunnett's multiple comparison test compared to NECA bias.

The A_{2A}R-GPA1/Gα_s and A_{2B}-GPA1/Gα_s strains were used to elucidate the subtype specificity of the N^6-adamantyl agonists. Strains were incubated with a concentration range of JH66, JH95, JH97 or JH209 for 16 hours in the appropriate media. Cells were lysed and β-galactosidase activity determined (Figure 4.13).

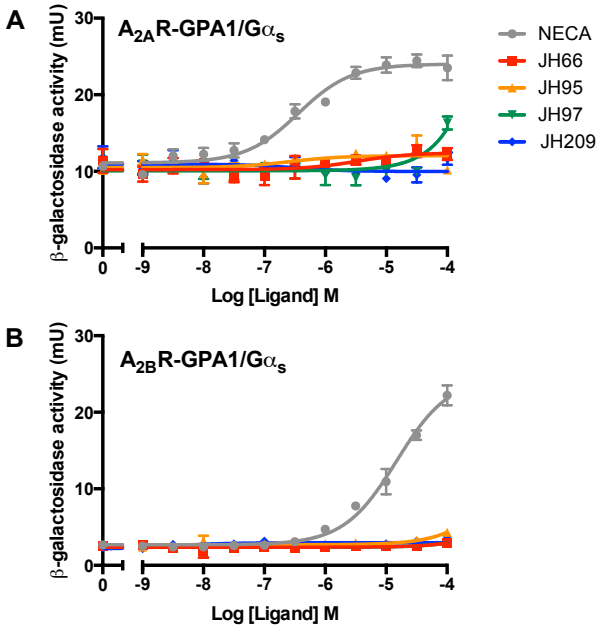

FIGURE 4.13: **N^6-adamantyl agonist pharmacology of the $A_{2A}R$ and $A_{2B}R$ in yeast.** $A_{2A}R$ and $A_{2B}R$ expressing yeast strains were cultured in AA-Ura and AA-Ura-His, respectively, containing an appropriate concentration of ligand for 16 hours at 30°C. $A_{2A}R$ expressing cells were also incubated with 5mM 3-AT. Cells were lysed and β-galactosidase activity determined. **A.** $A_{2A}R$-GPA1/Gα_s. **B.** $A_{2B}R$-GPA1/Gα_s.

No significant increase in signal was detected in response to JH66, JH95 or JH209 in $A_{2A}R$-GPA1/Gα_s or $A_{2B}R$-GPA1/Gα_s (one-way ANOVA, P>0.05). However, JH97 up-regulated signal in $A_{2A}R$-GPA1/Gα_s at high concentrations (β-galactosidase activity = 16.3±0.9 in response to 100μM JH97 compared to 10.7±0.3 for DMSO alone). JH97 contains an aromatic group covalently attached to the 5' region of the compound. This may suggest that 5'-modifications of the nucleotide region of adenosine receptor agonists can influence $A_{2A}R$ selectivity in yeast.

4.1.2 CAS200623: an established fluorescent compound

In our efforts to develop novel fluorescent compounds an existing ligand was characterised in yeast. CAS200623 is a commercially available fluorescent adenosine receptor agonist. This compound uses NECA as a ligand domain and a BODIPY (630/650) fluorophore connected by a hydrocarbon chain (Baker et al. (2010), Figure 4.14). CAS200623 has already been established in mammalian systems as an agonist to the A_1R and the A_3R (Briddon et al., 2004; May et al., 2010, 2011; Baker et al., 2010). Indeed, cAMP accumulation assays have demonstrated that CAS200623 inhibits adenylate cyclase in A_1R-transfected cell lines (Middleton et al., 2007). However, the potency of CAS200623 was lower than that of NECA in this study (pEC_{50} = 9.44 and 8.47 M for NECA and CAS200623, respectively). To our knowledge, no fluorescent adenosine receptor agonists, including CAS200623, have been tested in yeast.

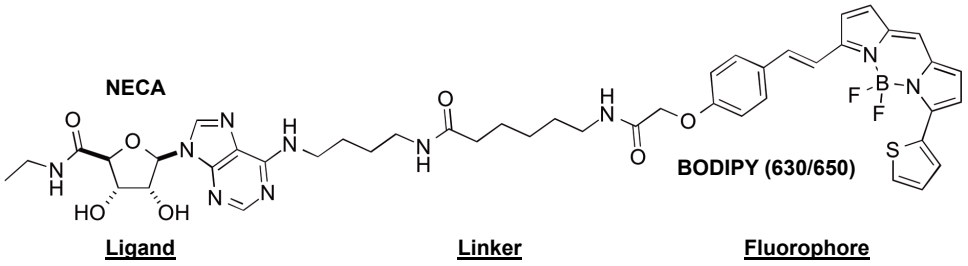

FIGURE 4.14: **CAS200623 structure.** NECA is covalently linked to a BODIPY fluorophore via an extended hydrocarbon chain. Chemical structure derived from Middleton et al. (2007) and Baker et al. (2010).

A_1R-GPA1/G$\alpha_{i1/2}$, $A_{2A}R$-GPA1/Gα_s, and $A_{2B}R$-GPA1/Gα_s were used to establish the pharmacology and selectivity of CAS200623 in yeast. These strains were incubated with concentration-response curves of CAS200623 for 16 hours in the appropriate media and β-galactosidase activity determined (Figure 4.15).

CAS200623 induces high signal in the A_1R and $A_{2A}R$ in yeast (β-galactosidase activity = 29.0±0.8 and 16.8±0.1 for the A_1R and $A_{2A}R$ respectively in response to 100μM CAS200623). However, this compound has a low potency for these receptors in yeast (pEC_{50} = 4.5±0.1 and 4.4±0.1 for the A_1R and $A_{2A}R$ respectively). The $A_{2B}R$ showed a modest response to 100μM CAS200623 (β-galactosidase activity = 4.5±0.1 mU). However, the $A_{2B}R$ is known to be a low affinity receptor compared to the A_1R and $A_{2A}R$. Given the low potency of of CAS200623 for these receptors, a low response in $A_{2B}R$-GPA1/Gα_s is unsurprising. Taken together, these data suggest that CAS200623 is a low potency agonist with poor A_1R/A_2R selectivity in yeast.

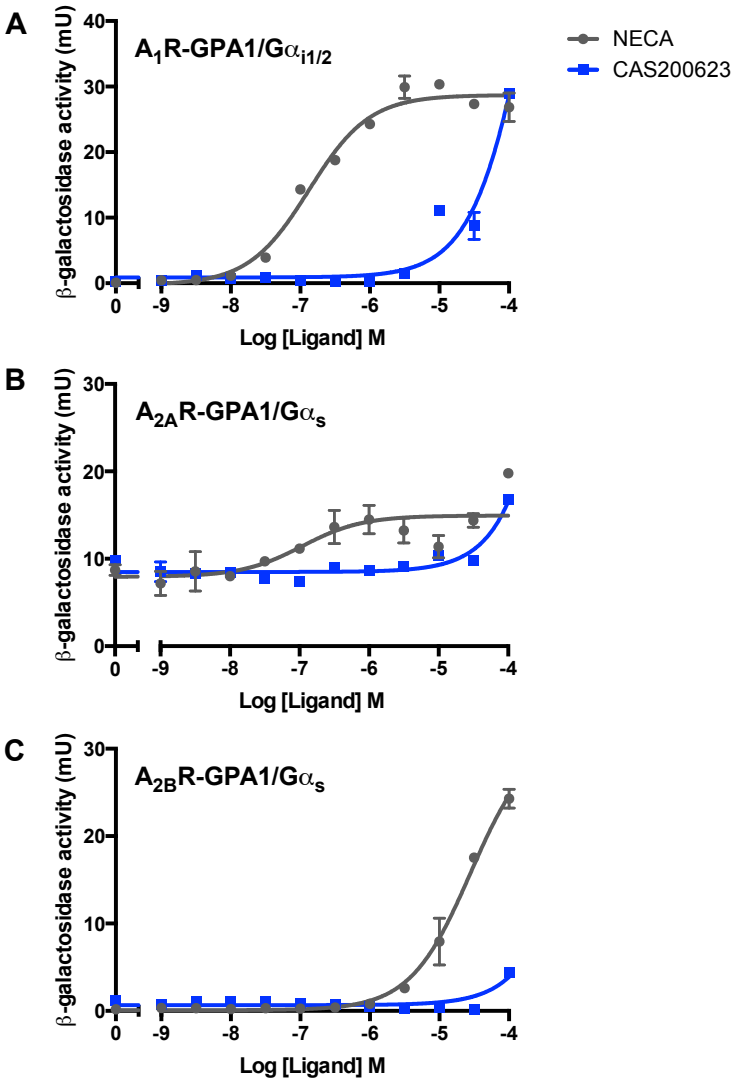

FIGURE 4.15: **CAS200623 pharmacology in yeast.** Yeast strains were cultured in AA-Ura overnight in a shaking incubator at 30°C. Cells were subcultured in AA-Ura and allowed to grow for a further 6 - 8 hours. Cell density was adjusted to OD_{600} = 0.02 and cells incubated in AA-Ura containing an appropriate concentration of ligand or 1% DMSO. A_{2A}R-GPA1/Gα_s was maintained in AA-Ura-His and supplemented with 5mM DMSO upon agonist treatment. Cells were lysed and β-galactosidase activity determined. **A.** A_1R-GPA1/G$\alpha_{i1/2}$. **B.** A_{2A}R-GPA1/Gα_s. **C.** A_{2B}R-GPA1/Gα_s.

CAS200623 clearly interacts with the A_1R given the transcriptional responses observed in the presence of a high concentration of ligand. The A_1R^{GFP} construct provides an excellent tool to assess the specificity of ligand bindingas 8.6% of the population are expressing the fluorescent receptor to a detectable level (Figure 3.9). Therefore, flow cytometry can be used to assess fluorescent ligand binding across a mixed population and elucidate the specificity of A_1R/A_1R^{GFP} binding by CAS200623.

Cells were incubated in AA-Ura overnight in a shaking incubator at 30°C. Cultures were centrifuged at 2000RPM for 5 minutes and the pellet washed with ice cold PBS before sonication to ensure measurement of single cells and not aggregates. Cells were incubated with 100μM CAS200623 and fluorescence measured periodically. Cells transformed with p426GPD alone were supplemented with 1% (v/v) DMSO and used as a gating control for fluorescence due to GFP or the red fluorescent ligand (Figure 4.16).

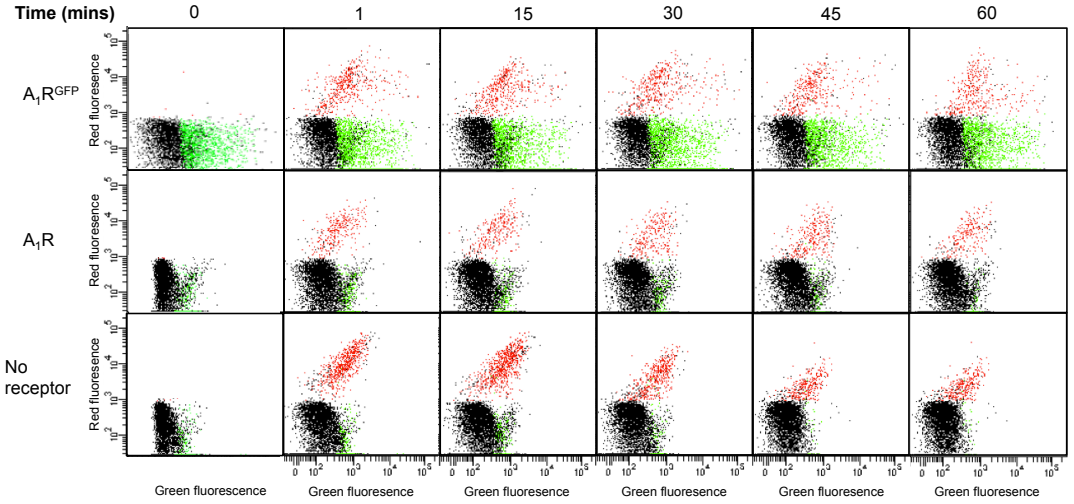

FIGURE 4.16: **Flow cytometry of CAS200623 in yeast.** GPA1/G$\alpha_{i1/2}$ transformed with p426GPD-A$_1$R, p426GPD-A$_1$R^{GFP} or p426GPD alone were cultured in AA-Ura overnight in a shing incubator at 30°C. Cells were harvested by centrifugation at 2000RPM for 5 minutes and washed in ice-cold PBS before sonication. Cells were incubated with 100μM CAS200623 and fluorescence measured in 30,000 cells periodically. Cells transformed with p426GPD alone were used as a gating control to set thresholds. Cells below this threshold are shown in black, cells showing fluorescence in response to ligand are shown in red and those showing GFP fluorescence are shown in green.

The flow cytometry data of Figure 4.16 shows a distinct subpopulation of red fluorescent cells emerge with CAS200623 treatment in all strains tested. This subpopulation represents 5.5±0.7%, 2.6±0.1% and 4.1±0.2% of the A$_1$R, A$_1$R-GFP and vector alone populations respectively. This suggests that the ligand is binding to the yeast cell surface regardless of receptor expression. Consistent with this there is little correlation of red fluorescence with A$_1$R^{GFP} fluorescence. Figure 4.16 also suggests 8.2±0.3% of the A$_1$R^{GFP} populations are expressing the fluorescently-tagged receptor.

Taken together, these data suggest that CAS200623 non-specifically binds to the yeast cell surface. Whether the yeast cell wall, a cellular feature mammalian cells lack, is a contributing factor remains unclear.

4.1.2.1 Development of novel fluorescent compounds

In yeast, CAS200623 activates the A_1R, $A_{2A}R$ and $A_{2B}R$ and non-specifically binds the yeast cell surface. However, cyclopentyl and adamantyl modifications of the N^6 region of the purine affect A_1R/A_2R selectivity of adenosine receptor agonists. Consequently, N^6-modifed adenosine receptor agonists were used as a basis for novel fluorescent compounds. A small amount of JH282 and JH294 were kindly created and provided by Dr. Jennifer Hemmings. JH282 and JH294 both use NECA as the ligand domain but contain N^6-cyclopentyl and N^6-adamantyl groups respectively. Both of these compounds contain a TAMRA fluorophore connected to the ligand by a 4C hydrocarbon chain (Figure 4.17).

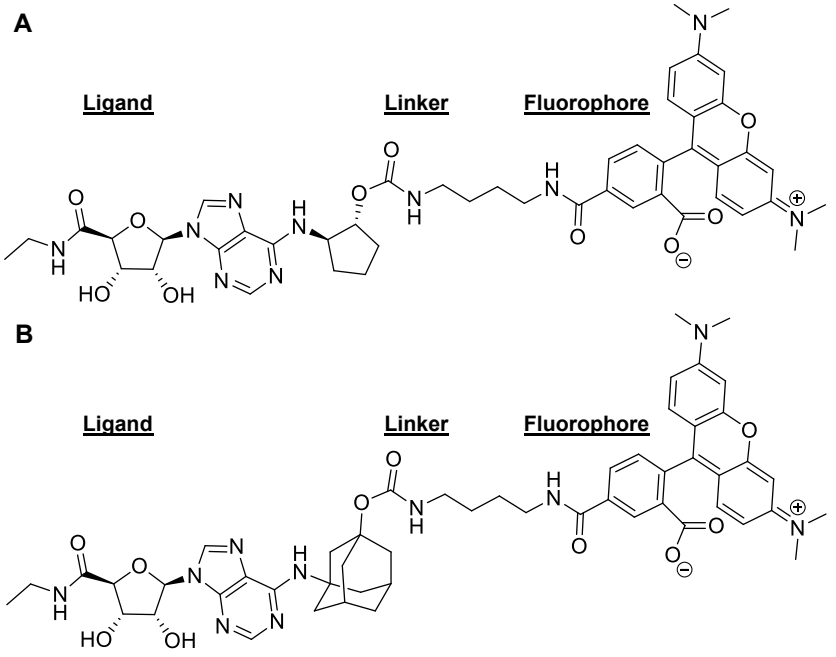

FIGURE 4.17: **Novel fluorescent compound structures. A.** JH282 and **B.** JH294 are derived from JH114 and JH95 respectively. Both compounds use TAMRA as a fluorophore.

JH282 and JH294 were assayed for activity and selectivity using the A_1R-GPA1/G$\alpha_{i1/2}$, $A_{2A}R$-GPA1/Gα_s and $A_{2B}R$-GPA1/Gα_s strains. Cells were incubated in the appropriate media containing a concentration range of JH282 or JH294 for 16 hours at 30°C. β-galactosidase activity was used as a measure of pathway activation (Figure 4.18). No significant upregulation of signal was detected in the $A_{2B}R$-GPA1/Gα_s strain in response to either JH282 or JH294 ($P > 0.05$ one-way ANOVA). However, JH282 appeared to show full agonism against the A_1R and $A_{2A}R$. Non-linear regression of the logistic equation and the operational model of pharmacological agonism was used to explore the pharmacology of this compound (Table 4.4).

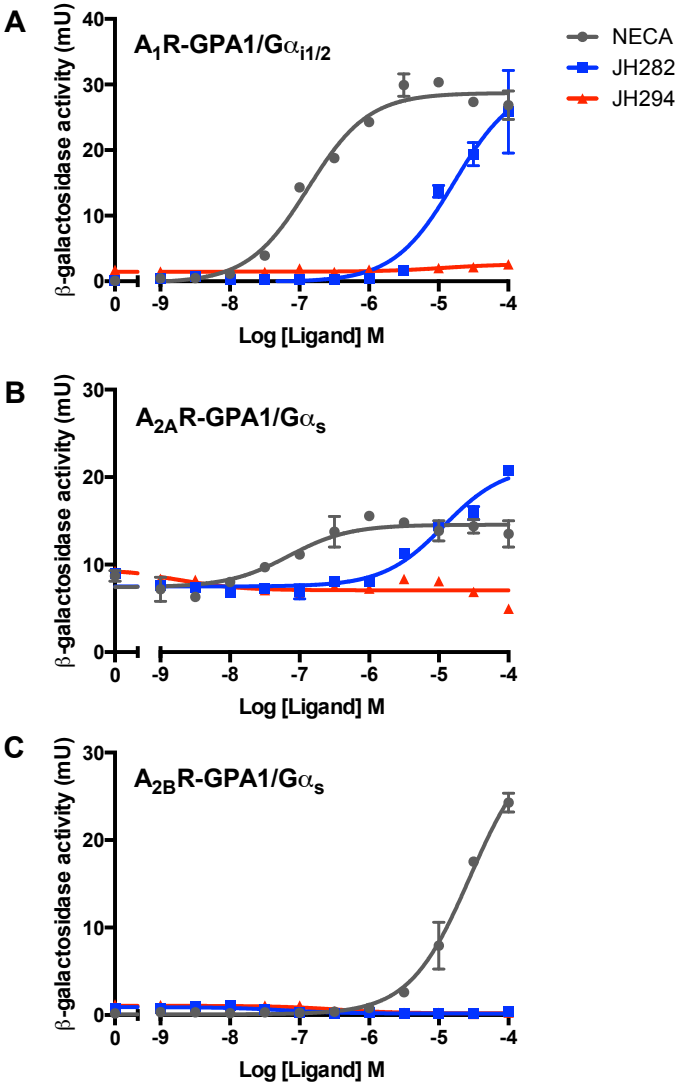

FIGURE 4.18: **Novel fluorescent compound pharmacology in yeast.** Yeast strains were s incubated in AA-Ura containing an appropriate concentration of ligand. A_{2A}R-GPA1/Gα_s was maintained in AA-Ura-His and supplemented with 5mM DMSO upon agonist treatment. Cells were lysed and β-galactosidase activity determined. Data represents the mean of triplicate repeats ± S.E.M fitted with the logistic equation. A_1R-GPA1/G$\alpha_{i1/2}$. **B.** A_{2A}R-GPA1/Gα_s. **C.** A_{2B}R-GPA1/Gα_s.

TABLE 4.4: **Pharmacological parameters of the A_1R and A_{2A}R in response to JH282.** The logistic equation and the operational model of pharmacological agonism were applied to the data of Figure 4.18 by non-linear regression. $pEC_{50} = -Log\ EC_{50}$ (potency), E_{max} = maximum level of signal, $pK_A = -\text{Log}\ K_A$ (ligand binding affinity) and τ = efficacy. NECA and JH114 have been included for comparison. **P < 0.005, JH282 compared to NECA as determined by Student's T-test.

Strain	**Ligand**	pEC_{50}	E_{max}	pK_A	$log\tau$
A_1R-GPA1/G$\alpha_{i1/2}$	NECA	6.0±0.1	25.8±0.6	4.4±0.1	1.5±0.1
	JH114	5.4±0.0	26.9±0.3	4.2±0.3	1.2±0.3
	JH282	4.8±0.1**	30±2.8	3.3±0.1**	1.6±0.1
A_{2A}R-GPA1/Gα_s	NECA	6.5±0.2	19.2±0.6	5.9±0.2	0.5±0.1
	JH114	5.3±0.3	19.5±1.1	4.6±0.4	0.3±0.1
	JH282	4.9±0.1**	21.3±1.0	3.7±0.2**	0.7±0.1

Consistent with CAS200623, the hydrocarbon linker and fluorophore reduce the potency of JH282 in both the A_1R and $A_{2A}R$ relative to its JH114 and NECA precursors. E_{max} is relatively well conserved between JH282 and its precursor JH114. This is accompanied by a 10-fold reduction in pK_A in both the A_1R and $A_{2A}R$ suggesting differences in sensitivity to ligand (Table 4.4). This may also explain why no response was detected for JH294. N^6-adamantyl modifications reduce potency for the A_1R. It is possible that the addition of the fluorophore (and associated hydrocarbon chain) has further reduced potency beyond the limits of detection in yeast. To explore this further concentration-response curves were constructed for JH282 and JH294 by growth assay in AA-Ura-His supplemented with 7mM 3-AT (Figure 4.19). Cell density was quantified by OD_{620} using a Mithas LB940 microplate reader to avoid the fluorescent ligand interfering with the fluorescein signal from FDGlu. No increase in cell density was observed for any strain for JH294.

Here, yeast has been used to inform and guide fluorescent compound development. The resulting compound, JH282, shows promise as a novel fluorescent agonist despite its low potency in yeast. Studies with this compound, and the development of others, are ongoing.

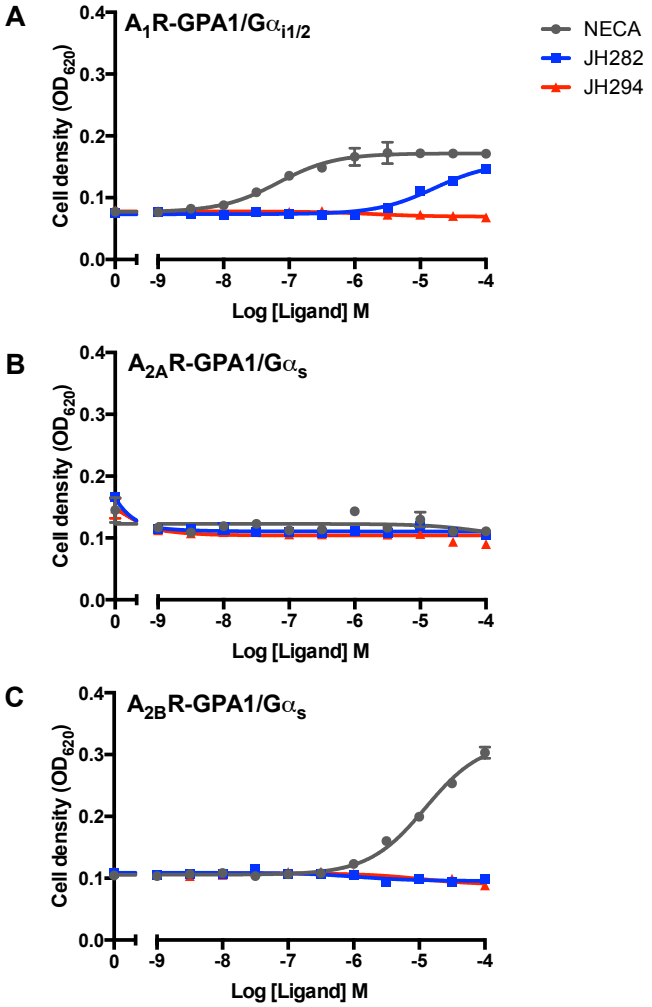

Figure 4.19: **Novel fluorescent compound screening by growth.** Yeast strains were cultured AA-Ura-His containing an appropriate concentration of ligand and 7mM 3AT for 16 hours at 30°C. Cell density was determined by OD_{620}.**A**. A_1R-GPA1/G$\alpha_{i1/2}$. **B.** A_{2A}R-GPA1/Gα_s. **C.** A_{2B}R-GPA1/Gα_s.

4.2 Antagonism of the A_1R

Our pharmacological investigation of the adenosine A_1R pharmacology and novel agonists was extended to include their interaction with adenosine receptor antagonists. Competitive antagonists bind the orthosteric site, stabilising the inactive receptor confirmation and preventing agonist binding. At sufficient concentrations the agonist can displace the antagonist. This manifests itself in a rightward shift in the concentration-response curve (Figure 1.7B).

There are a range of adenosine receptor antagonists available with caffiene being the most widely consumed globally. The majority of A_1R antagonists are xanthines based around a theophylline core (Figure 4.20), a product of adenosine metabolism *in vivo*. Many have entered clinical trials for a range of pathologies including heart failure and renal impairment (Hocher, 2010; Sachdeva and Gupta, 2013). However, these trials are typically met with little success due to complications from a range of factors, including off-target effects and poor patient compliance due to caffeine intake from tea, coffee and chocolate (Ribeiro and Sebastiao, 2010). Here a range of A_1R agonists are characterised in the presence of antagonists in the yeast system.

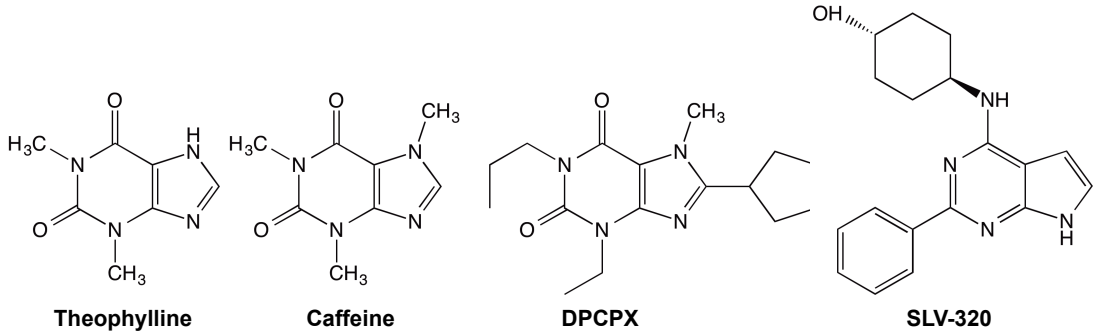

FIGURE 4.20: **Adenosine receptor antagonist structures.** A_1R antagonists such as caffeine are based around a theophylline core. This thesis exploits dipropylcyclopentylxanthine (DPCPX) and SLV-320 as pharmacological tools. These potent antagonists also contain a theophylline core.

4.2.1 Biphasic antagonism with established agonists

Initial studies of A_1R agonism focussed on the full agonist NECA in the presence of the potent antagonist dipropylcyclopentylxanthine (DPCPX) (Figure 4.20). The A_1R-GPA1/G$\alpha_{i1/2}$ strain was used due to its strong response (Figure 4.21). DPCPX induces a rightward shift in the concentration-response curves of the full agonist NECA but does not significantly affect E_{max} ($P<0.05$, one-way ANOVA). The nature of the agonist antagonist interaction was further explored by Schild analysis. This analysis assumes that the shift in pEC_{50} is linearly proportional to the antagonist concentration. For a competitive antagonist, binding the same site as an agonist, this results in a linear Schild plot of unity

slope. However, while the pEC_{50} of NECA is linearly proportional to the concentration of DPCPX, linear regression yields a non-unity slope. This suggests that DPCPX does not compete with NECA for a single site.

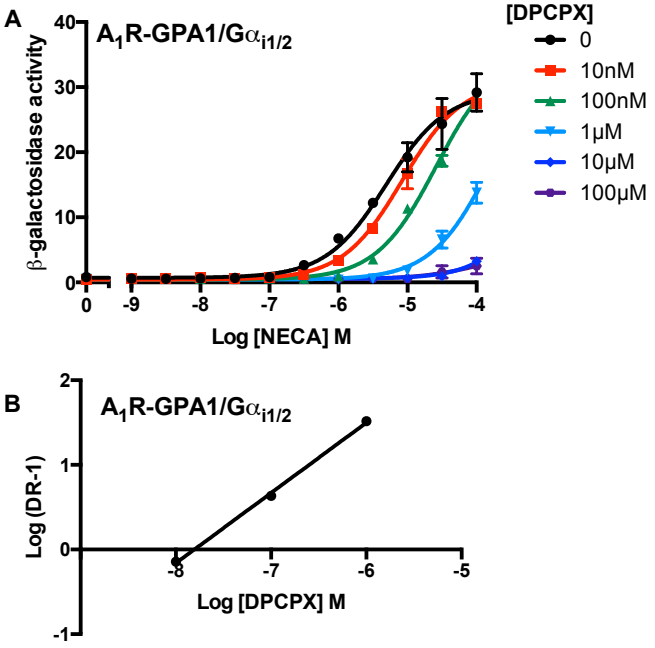

FIGURE 4.21: **Simultaneous treatment of A_1R-GPA1/G$\alpha_{i1/2}$ with NECA and DPCPX.** The A_1R-GPA1/G$\alpha_{i1/2}$ strain was incubated in AA-Ura containing the appropriate concentration of NECA and DPCPX for 16 hours at 30°C. Cells were lysed and β-galactosidase activity determined. Data represents mean ± S.E.M. of triplicate repeats fitted with the logistic equation. **A.** NECA concentration-response curves in the presence of DPCPX. **B.** A Schild plot constructed from the NECA DPCPX concentration-response curves.

This study was extended to include adenosine, a full agonist in this strain. Here there is no significant change in E_{max} ($P > 0.05$, one-way ANOVA) and Schild analysis yielded a slope that does not significantly deviate from unity (0.85 ± 0.18). While this may suggest that DPCPX is a competitive antagonist of adenosine, the behaviour of 2CCPA is an interesting contrast. Here, E_{max} increases significantly as a function of DPCPX, a counterintuitive finding for an antagonist ($P < 0.05$, one-way ANOVA). Consistent with NECA and adenosine, Schild analysis yielded a linear relationship between 2CCPA and DPCPX. However, non-linear regression suggested a non-unity slope (Figure 4.22, Table 4.5). treftab:SC13DPCPX). This suggests that competitive antagonism is insufficient to describe the relationship between 2CCPA and DPCPX in the A_1R-GPA1/G$\alpha_{i1/2}$ yeast strain.

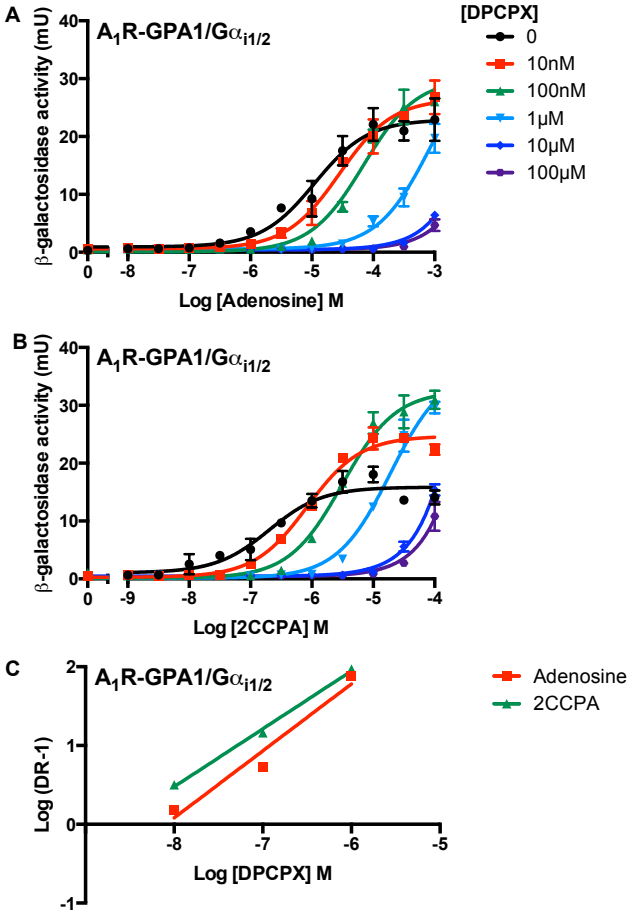

FIGURE 4.22: **Simultaneous treatment of A_1R-GPA1/G$\alpha_{i1/2}$ with adenosine or 2CCPA and DPCPX.** The A_1R-GPA1/G$\alpha_{i1/2}$ strain was incubated in AA-Ura containing the appropriate concentration of agonist and DPCPX for 16 hours at 30°C. Cells were lysed and β-galactosidase activity determined. Data represents mean ± S.E.M. of triplicate repeats fitted with the logistic equation. **A.** Adenosine and DPCPX. **B.** 2CCPA and DPCPX. **C.** Schild plots were contructed from the adenosine and 2CCPA concentration-curves in the presence of DPCPX.

TABLE 4.5: **Pharmacological parameters of DPCPX in combination with NECA, adenosine or 2CCPA in A_1R-GPA1/G$\alpha_{i1/2}$.** E_{max} and for agonist alone and antagonised yeast strains were determined by non-linear regression of the logistic equation. pEC_{50} values were used to perform a Schild analysis. Slope was determined by linear regression. Statistical deviation of the antagonist E_{max} from the agonist alone, or the comparison of slope to unity, were determined by one-way ANOVA. $P < 0.05$ was considered significant. *P<0.05, **P<0.005 and ***P<0.005.

Ligand	**Agonist** E_{max}	**Antagonised** E_{max}	**Schild Slope**
NECA	29.3±1.2	30.9±0.9	0.83±0.03**
Adenosine	22.9±1.1	30.1±0.2*	0.85±0.18
2CCPA	15.6±0.7	32.5±0.9***	0.73±0.04**

The A_1R-specific antagonist SLV-320 (Figure 4.20) was used to assess if non-competitive antagonism of NECA, or the biphasic interaction with 2CCPA, is a DPCPX-specific effect. A_1R-GPA1/G$\alpha_{i1/2}$ was incubated with agonist and SLV-320 simultaneously for 16 hours. Cells were lysed and β-galactosidase activity determined (Figure 4.23). Consistent with DPCPX, SLV-320 has no significant effect on NECA or adenosine E_{max} ($P > 0.05$, one-way ANOVA) and Schild analysis yields non-unity and unity slopes for NECA and adenosine respectively. Once again, 2CCPA shows a significant increase in E_{max} in this strain in the presence of antagonist ($P > 0.05$, one-way ANOVA) and a Schild plot with a non-unity slope. Taken together, this suggests that non-competitive antagonism is not limited to DPCPX.

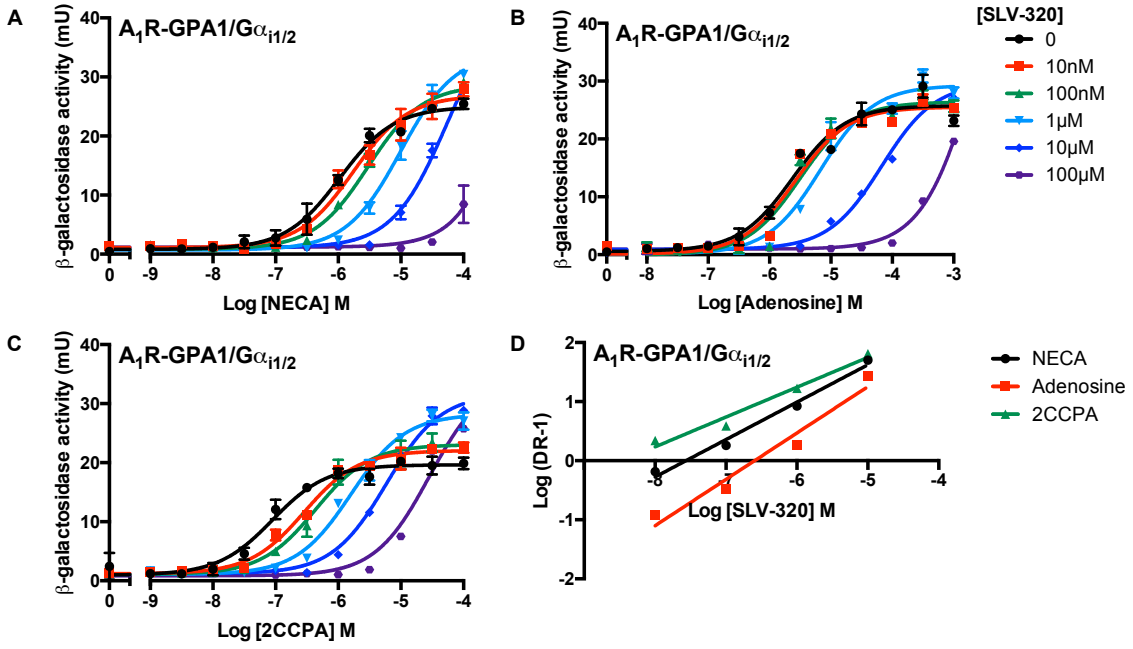

FIGURE 4.23: **Simultaneous treatment of A_1R-GPA1/G$\alpha_{i1/2}$ with NECA, adenosine or 2CCPA and SLV-320.** The A_1R-GPA1/G$\alpha_{i1/2}$ strain was incubated in AA-Ura containing the appropriate concentration of agonist and SLV-320 for 16 hours at 30°C. Cells were lysed and β-galactosidase activity determined. Data represents mean ± S.E.M. of triplicate repeats fitted with the logistic equation. **A.** NECA and SLV-320. **B.** Adenosine and SLV-320. **C.** 2CCPA and SLV-320 **D.** Schild plots were constructed from the adenosine and 2CCPA concentration-curves in the presence of SLV-320.

The yeast transplant system presented an attractive opportunity to explore this apparent non-competitive antagonism as a function of G protein. Consequently, the A_1R-GPA1/Gα_{i3} strain was treated with NECA, adenosine or 2CCPA in the presence of various concentrations of DPCPX or SLV-320 (Figure 4.24).

TABLE 4.6: **Pharmacological parameters of SLV-320 in combination with NECA, adenosine or 2CCPA in A_1R-GPA1/G$\alpha_{i1/2}$.** E_{max} and for agonist alone and antagonised yeast strains were determined by non-linear regression of the logistic equation. pEC_{50} values were used to perform a Schild analysis. Slope was determined by linear regression. Statistical deviation of the antagonist E_{max} from the agonist alone, or the comparison of slope to unity, were determined by one-way ANOVA. *P < 0.05, **P < 0.005 and ***P < 0.005.

Ligand	Agonist E_{max}	Antagonised E_{max}	Schild Slope
NECA	25.0±0.7	34.2±1.1**	0.63±0.05**
Adenosine	25.8±0.8	29.3±1.0*	0.78±0.11**
2CCPA	19.6±0.5	31.7±0.7***	0.50±0.06**

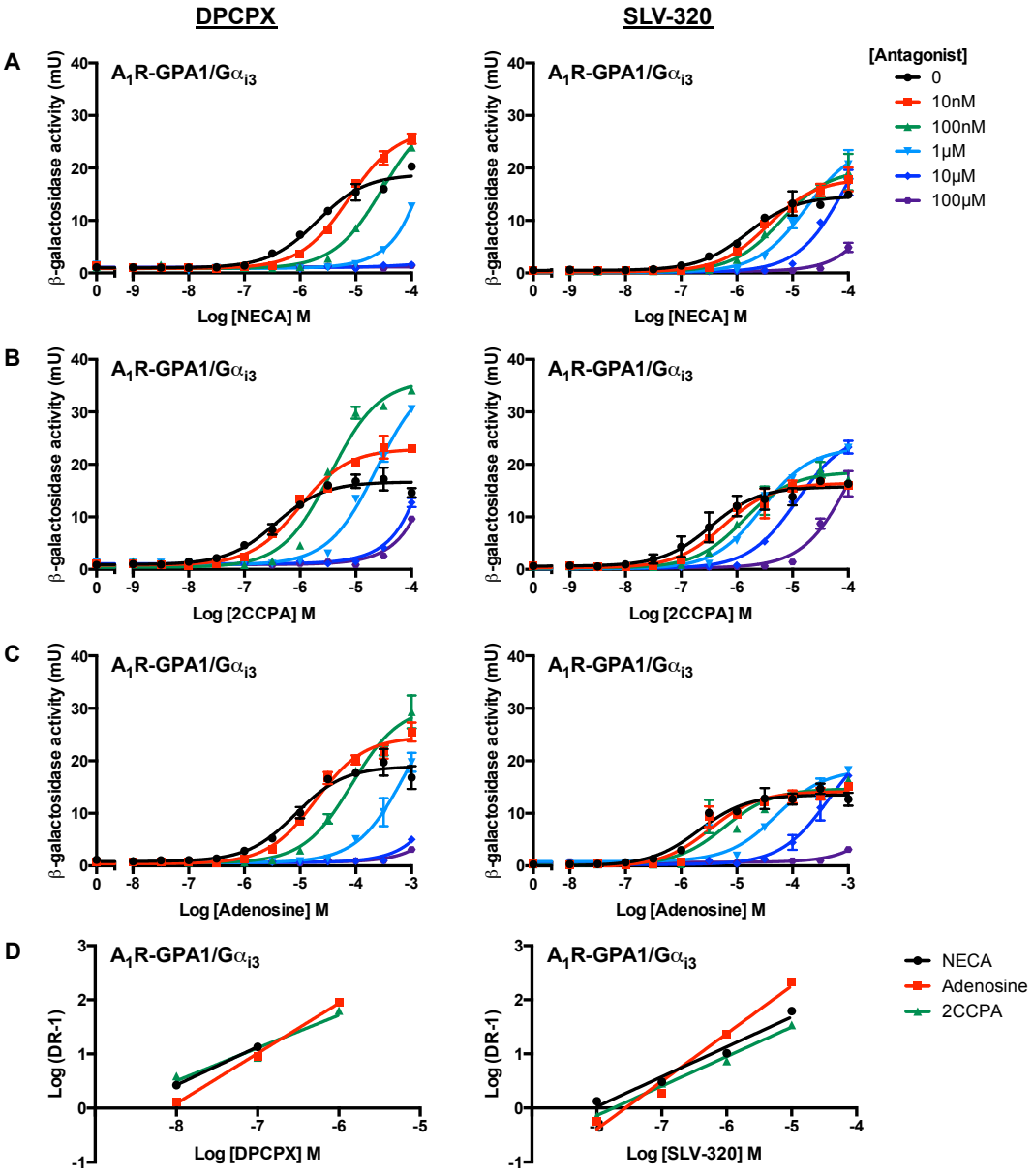

FIGURE 4.24: **Simultaneous treatment of A_1R-GPA1/Gα_{i3} with NECA, adenosine or 2CCPA and DPCPX or SLV-320**. The A_1R-GPA1/Gα_{i3} strain was incubated in AA-Ura containing the appropriate concentration of agonist and antagonist for 16 hours at 30°C. Cells were lysed and β-galactosidase activity determined. Data represents mean ± S.E.M. of triplicate repeats fitted with the logistic equation. **A.** NECA, **B.** 2CCPA and **C.** adenosine concentration response curves in the presence of DPCPX and SLV-320. **D.** Schild analyses for DPCPX and SLV-320.

In contrast to A_1R-GPA1/G$\alpha_{i1/2}$, A_1R-GPA1/Gα_{i3} shows a significant increase in NECA E_{max} in response to both DPCPX and SLV-320 (P>0.05, one-way ANOVA). Schild analysis also yields non-unity slopes for NECA in response to either antagonist (Table 4.7). 2CCPA shows remarkably similar behaviour. However, while adenosine does shows a significant increases in E_{max} in the presence of either antagonist (P>0.05, one-way ANOVA), Schild analyses yield slopes that do not significantly deviate from unity (Table 4.7).

TABLE 4.7: **Pharmacological parameters of DPCPX or SLV-320 in combination with NECA, adenosine or 2CCPA in A_1R-GPA1/Gα_{i3}.** The data of Figure 4.24 was fitted with the logistic equation to determine E_{max} and pEC_{50}. The highest E_{max} of the antagonised concentration-response curves was compared to the E_{max} of the appropriate agonist alone curve. pEC_{50} values were used to calculate dose ratios (DR). The slope of the resulting Schild plot was determined by linear regression and compared to unity by one-way ANOVA. *P < 0.05, **P < 0.005 and ***P < 0.005. Error bars represent S.E.M.

Antagonist	**Ligand**	**Agonist** E_{max}	**Antagonised** E_{max}	**Schild Slope**
DPCPX	NECA	18.8±0.5	27.4±0.5**	0.71±0.01**
	Adenosine	18.9±0.6	30.4±1.2*	0.83±0.04
	2CCPA	16.7±0.5	36.1±1.1***	0.61±0.15***
SLV-320	NECA	14.6±0.4	19.8±0.9**	0.55±0.07**
	Adenosine	13.5±0.5	25.2±3.0*	0.88±0.09
	2CCPA	15.7±0.7	26.1±0.7***	0.54±0.03***

Both adenosine and NECA E_{max} increases in the presence of DPCPX or SLV-320 in A_1R-GPA1/Gα_{i3}, but not A_1R-GPA1/G$\alpha_{i1/2}$. This may be a consequence of maximal signalling through the A_1R when expressed from a plasmid. We have observed that all strains, bar GPA1/G$\alpha_{i1/2}$, show a significantly higher E_{max} via a C-terminal A_1R^{GFP} fusion protein in comparison to the unmodified A_1R. In these experiments, the highest observed β-galactosidase activity was 26±0.5 mU. Thus, it is possible that no increase in E_{max} was observed for A_1R-GPA1/G$\alpha_{i1/2}$ in the presence of antagonist as this system is already signalling at maximum in response to agonist alone. A_1R-GPA1/Gα_{i3} shows a lower signal in response to NECA than A_1R-GPA1/G$\alpha_{i1/2}$. This suggests that this strain is not inducing the maximum level of β-galactosidase signal for these strains. Consequently, one would predict that A_1R-GPA1/Gα_z, a low-activity strain, would demonstrate biphasic antagonism for NECA, adenosine and 2CCPA. Therefore, this strain was incubated with combinations of agonist and antagonist for 16 hours and β-galactosidase activity determined (Figure 4.25)

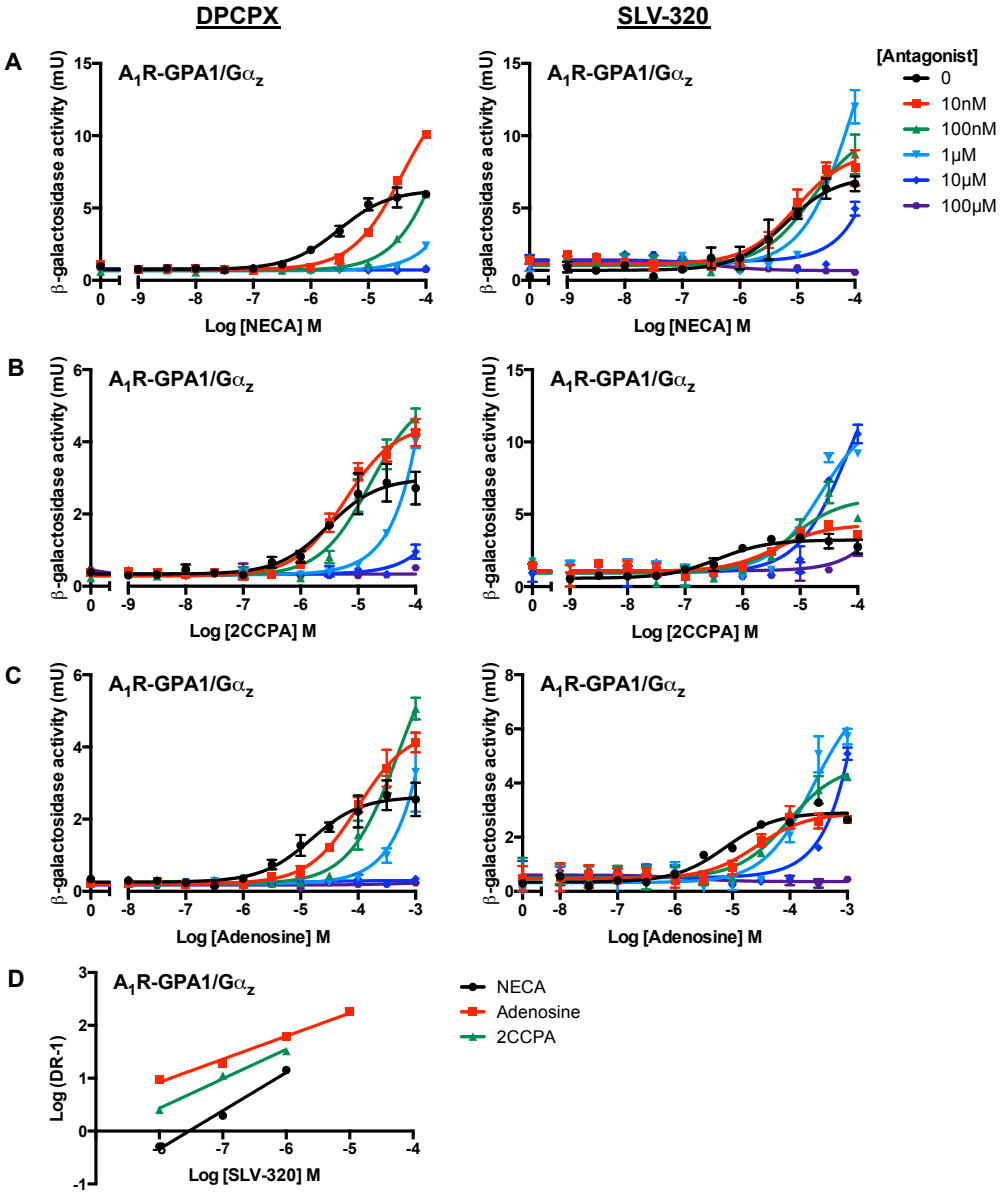

FIGURE 4.25: **Agonist - antagonist interactions against A_1R-GPA1/Gα_z.** The A_1R-GPA1/Gα_z strain was incubated in AA-Ura containing the appropriate concentration of agonist and antagonist for 16 hours at 30°C. Cells were lysed and β-galactosidase activity determined. Data represents mean ± S.E.M. of triplicate repeats fitted with the logistic equation. **A.** NECA, **B.** 2CCPA and **C.** adenosine concentration response curves in the presence of DPCPX and SLV-320. **D.** Schild analysis for SLV-320.

TABLE 4.8: **Pharmacological parameters of DPCPX or SLV-320 in combination with NECA, adenosine or 2CCPA in A_1R-GPA1/Gα_z.** E_{max} and for agonist alone and antagonised yeast strains were determined by non-linear regression of the logistic equation. pEC_{50} values were used to perform a Schild analysis. Slope was determined by linear regression. Statistical deviation of the antagonist E_{max} from the agonist alone, or the comparison of slope to unity, were determined by one-way ANOVA *P < 0.05, **P < 0.005 and ***P < 0.005.

Antagonist	**Ligand**	**Agonist** E_{max}	**Antagonised** E_{max}	**Schild Slope**
DPCPX	NECA	6.3±0.2	13.8±0.5***	N.D.
	Adenosine	2.6±0.1	7.6±0.6**	N.D.
	2CCPA	3.0±0.2	5.4±0.3**	N.D.
SLV-320	NECA	7.2±0.5	13.8±0.9**	0.72±0.08*
	Adenosine	2.9±0.1	7.6±0.9*	0.44±0.03***
	2CCPA	3.2±0.1	5.4±1.3***	0.56±0.06**

Figure 4.25 shows that the E_{max} of NECA, adenosine and 2CCPA are significantly increased by both DPCPX and SLV-320 (P < 0.05, one-way ANOVA) consistent with the other A_1R-expressing strains tested here. A rightward shift in the concentration-response curve of these agonists was observed as a function of antagonist concentration. While a Schild analysis was not possible for DPCPX in combination with any agonist, SLV-320 yielded a significantly non-unity slope with NECA, adenosine and 2CCPA (Table 4.8). This suggests that, in this strain, none of these agonists have a purely competitive relationship with DPCPX or SLV-320.

This biphasic antagonism of the A_1R has been observed in number of previous studies (Alexander et al., 2006; Stewart et al., 2009) with little attention drawn to the data. However, Gracia et al. (2013) performed the first comprehensive study of this phenomena. This study used radioligand-binding and ERK phosphorylation assays to study the interaction between agonists, such as R-PIA, and the antagonists DPCPX and caffeine. The data of this study is remarkably consistent with our observed trends in yeast. ERK phosphorylation occurs as a direct result of β-arrestin recruitment and can be considered G protein independent. However, GPCRs do not signal through β-arrestins in yeast. This suggests that the biphasic antagonism of the A_1R is a receptor level effect. This is supported by consistent potentiation of signal across all G protein transplant strains.

To confirm that this is a receptor, and not yeast, specific effect these studies were repeated for the A_{2B}R-GPA1/Gα_s strain. SLV-320 had a limited effect on the agonist pharmacology of the A_{2B}R. However, DPCPX induces a rightward shift in the concentration-response curves of NECA and adenosine (Figure 4.26). Further, Schild analysis yielded straight lines with unity slope for NECA and adenosine. This suggests that the non-competitive interaction of the agonists and antagonists is an A_1R-specific effect.

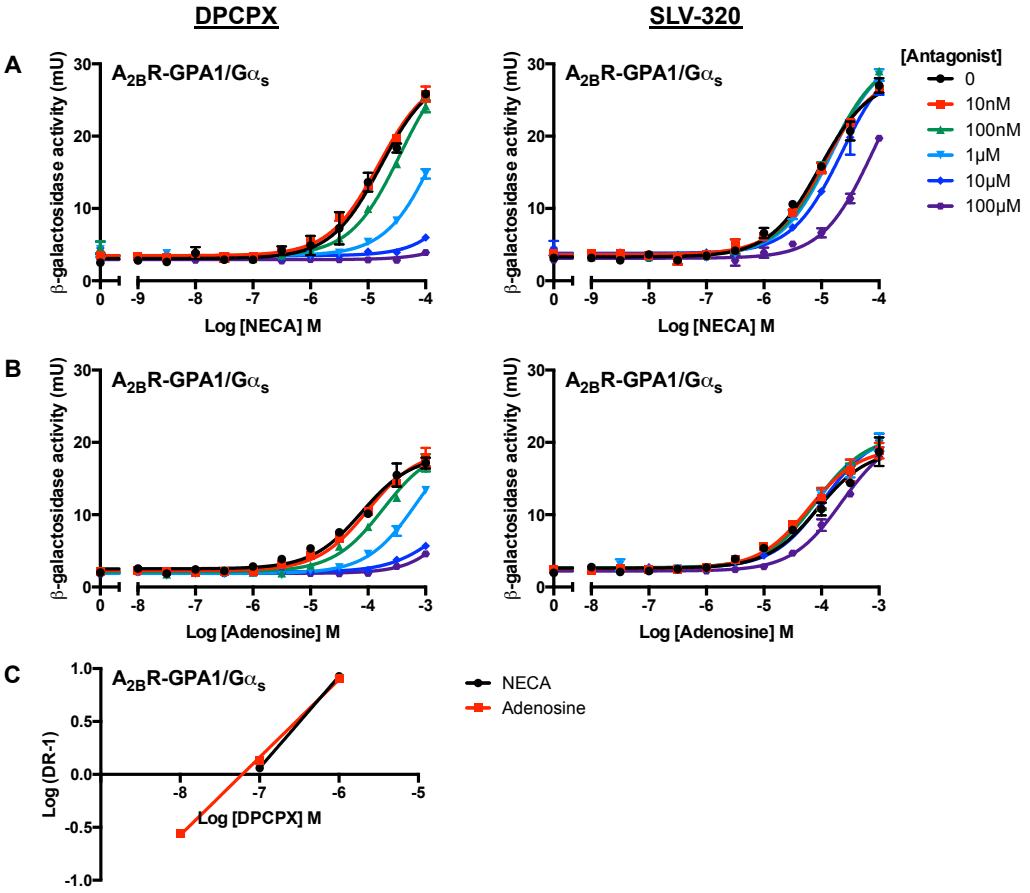

FIGURE 4.26: **Agonist - antagonist interactions against A_{2B}R-GPA1/Gα_s.** The A_{2B}R-GPA1/Gα_s strain was iincubated in AA-Ura containing the appropriate concentration of agonist and antagonist for 16 hours at 30°C. Cells were lysed and β-galactosidase activity determined. Data represents mean ± S.E.M. of triplicate repeats fitted with the logistic equation. **A.** NECA and **B.** adenosine concentration-response curves in the presence of DPCPX and SLV-320. **C.** Schild analysis of NECA and adenosine with DPCPX.

Schild analyses of A_1R antagonism in yeast suggest non-cooperativity between agonist and antagonist. This implicates multiple binding sites and suggests two hypotheses; dimerisation or allosterism (Figure 4.27). Gracia et al. (2013) use a BRET reporter system to confirm that the A_1R does form homodimers *in vivo* and strongly suggest that the biphasic response is a consequence of an interaction between two orthosteric sites across a dimer (Figure 4.27A). However, no causal relationship is established experimentally and the conclusions of their study are premature without studying the effect in purely monomeric A_1R variants. There is currently no crystal structure available for the A_1R and the dimerisation interface is unknown. Consequently, it is impossible to assess if this effect is shared by monomeric receptors.

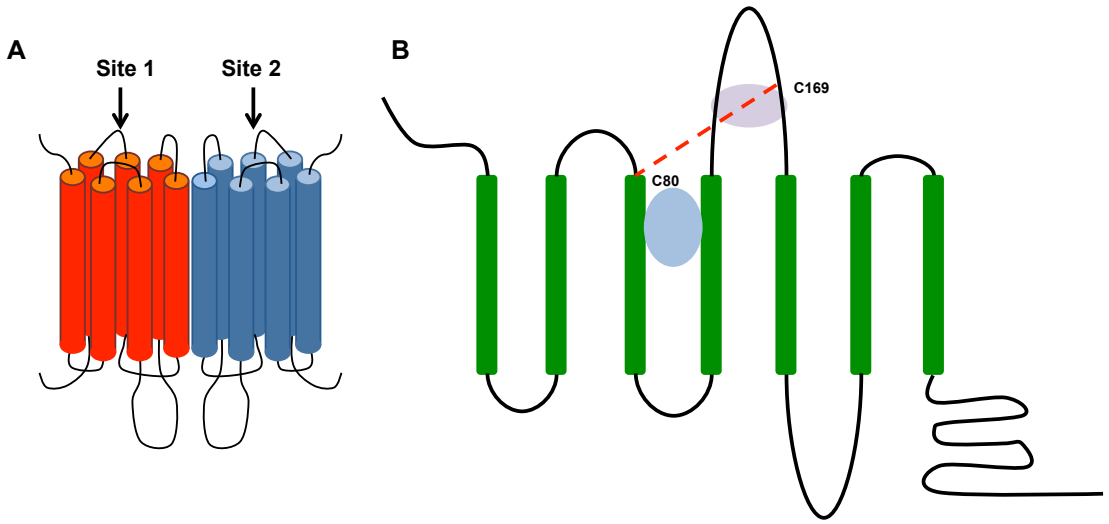

FIGURE 4.27: **Potential mechanisms of biphasic antagonism of the A_1R. A.** Dimerisation between two receptors and interaction between two orthosteric sites. **B.** Allosteric antagonism. The potential orthosteric and allosteric sites are shown in blue and purple respectively. The disulphide bridge linking the two sites are shown as a red line. Figure adapted from Peeters et al. (2012).

An alternative hypothesis is allosteric antagonism (Kenakin et al., 2006). Like many GPCRs, the A_1R has both orthosteric and allosteric ligand binding sites. Allosteric antagonists can bind the orthosteric and allosteric site separately. Orthosterically bound ligand acts as an antagonist while allosterically bound ligands promote agonist binding and receptor activation (Figure 4.27B). Peeters et al. (2012) performed an alanine scan of the extracellular loops of the A_1R. The pharmacology of the A_1R mutants were established using the MMY24 (GPA1/Gα_{i3}) yeast strain. Extracelluar loop 2 (ECL2), in particular a disulphide bridge between C^{80} of TM3 and C^{169} of ECL2, has been shown to be crucial to allosterism of the A_1R (Peeters et al., 2012). Thus, it is likely that the allosteric site of the A_1R is in ECL2 (Figure 4.27). Disruption of ECL2 also compromised orthosteric ligand binding. Docking studies of an A_1R homology model suggest that the orthosteric ligand binding site lies within the TM domains with particularly strong interactions with TM3 and TM4 (Narlawar et al., 2010). This suggests that the orthosteric and allosteric sites are closely associated. This is also supported by computational studies using bivalent ligands consisting of linked orthosteric and allosteric domains (Narlawar et al., 2010). Given the experimental data and lack of solely monomeric A_1R variant, allosteric antagonism may be easier to assess than dimerisation.

Allosteric agents of the A_1R have been established and characterised in mammalian cells (May et al., 2010). One such compound is PD81723, which was originally identified in an A_1R antagonist screen but acts as an allosteric regulator of the A_1R at sub-μM concentrations. Consequently, PD81723 is widely considered to be an allosteric antagonist (Bruns and Fergus, 1990; Jarvis et al., 1999). We hoped to exploit the dual pharmacology of this compound to elucidate if the biphasic antagonism observed is the result of allosterism. Peeters et al. (2012) used growth assays to assess A_1R pharmacology in response to 1μM PD81723. Preliminary studies used the same strain in the presence and absence of 7mM 3-AT. In the presence of 7mM 3-AT no significant increase in pEC_{50} for NECA in presence of 1μM PD81723 was observed by growth assay (Figure 4.28A). However, the growth response is greatly reduced at >10μM PD81723. β-galactosidase activity in response to NECA is unaffected by PD81723 in the sub μM range but is greatly reduced by >10μM PD81723 (Figure 4.28B). When repeating this assay without 3-AT cell density was greatly reduced in response to high concentrations of PD81723, suggesting that this compound is toxic to yeast or inhibits their growth (Figure 4.28C). The detrimental effect of PD81723 on yeast growth limits its usefulness as a pharmacological tool to study allosteric antagonism. Consequently, these studies were pursued no further and the precise mechanism of biphasic A_1R antagonism remains a mystery.

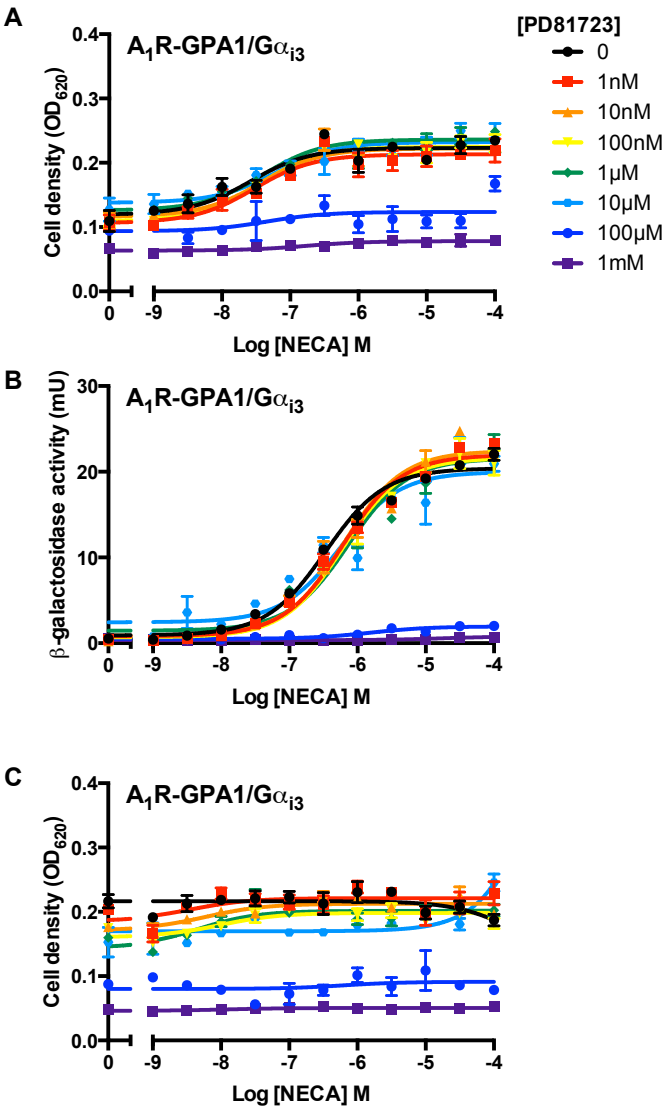

Figure 4.28: **The effects of PD81723 on yeast.** A_1R-GPA1/Gα_{i3} cells were incubated in AA-Ura-His containing appropriate concentrations of NECA and PD81723 and 7mM 3-AT for 16 hours at 30°C. **A.** Cell density as determined by OD_{620}. **B.** β-galactosidase activity. **C.** Cells were incubated in AA-Ura-His containing the appropriate concentration of NECA and PD81723 but lacking 3-AT. Cell density was determined by OD_{620}.

4.2.2 Investigating A_1R antagonist pharmacology in the presence of novel N^6-substituted agonists

The N^6-cyclopentyl substituents JH109 and JH114 were assessed for activity in yeast in the presence of the antagonists DPCPX and SLV-320. The A_1R-GPA1/$G\alpha_{i1/2}$ and A_1R-GPA1/$G\alpha_z$ strains were selected for these studies. Potentiation of signal by antagonists is difficult to see in the GPA1/$G\alpha_{i1/2}$ due to the high activity of the A_1R in this strain. Activity is significantly lower for the A_1R-GPA1/$G\alpha_z$ but the potentiation is more obvious. Consequently, these strains were incubated with JH109 or JH114 in combination with DPCPX or SLV-320 for 16 hours and β-galactosidase activity determined (Figure 4.29, Figure 4.30)

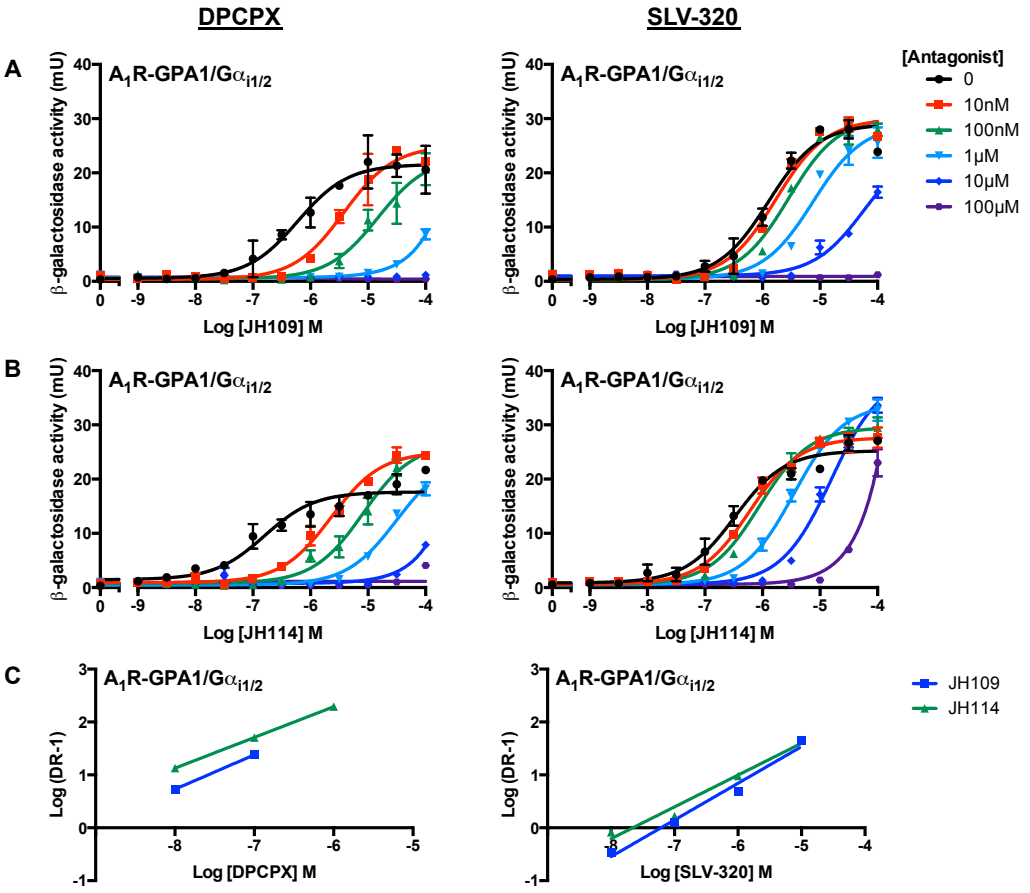

FIGURE 4.29: **N^6-cyclopentyl agonist and antagonist interactions in A_1R-GPA1/$G\alpha_{i1/2}$.** GPA1/$G\alpha_{i1/2}$ transplant yeast cells expressing the A_1R were incubated with N^6-cyclopentyl agonists and antagonists simulataneously for 16 hours at 30°C. Cells were lysed and β-galactosidase activity determined. Data represents the mean ± S.E.M of triplicate repeats fitted with the logistic equation. **A.** JH109 and **B.** JH114 concentration-response curves in the presence of DPCPX and SLV-320. **C.** Schild analyses for DPCPX and SLV-320 in the presence of JH109 and JH114.

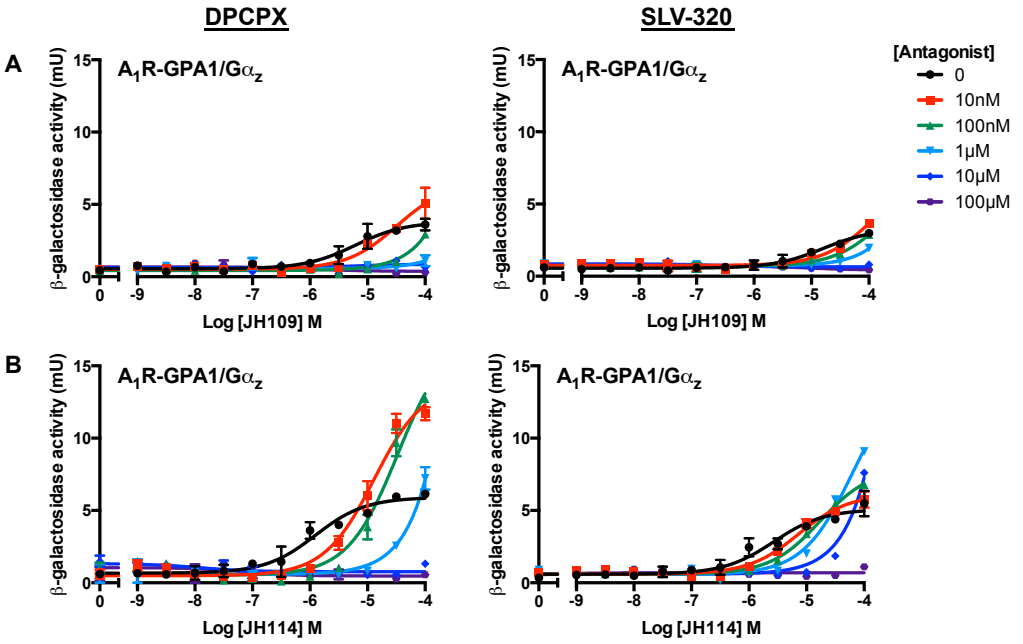

FIGURE 4.30: **N^6-cyclopentyl agonist and antagonist interactions in A$_1$R-GPA1/Gα_z.** A$_1$R-GPA1/Gα_z transplant yeast cells expressing the A$_1$R were incubated with N^6-cyclopentyl agonists and antagonists simulataneously for 16 hours at 30°C. Cells were lysed and β-galactosidase activity determined. Data represents the mean ± S.E.M of triplicate repeats fitted with the logistic equation. **A.** JH109 and **B.** JH114 concentration-response curves in the presence of DPCPX and SLV-320.

No significant increase in the E_{max} of the adenosine derivative JH109 was observed in combination with SLV-320 or DPCPX in A$_1$R-GPA1/G$\alpha_{i1/2}$ (P > 0.05 one-way ANOVA, Figure 4.29A). However, significant potentiation of signal was observed when JH114, derived from NECA, was used in combination with these ligands. However, Schild analysis of these data does not provide a straight line of unity slope. Similarly, in A$_1$R-GPA1/Gα_z no significant in increase in E_{max} was observed for JH109 in combination with either antagonist tested compared to agonist alone (Figure 4.30). This is in contrast to JH114, which does show an increase in signal when used in combination with either antagonist in this strain. Unfortunately, the low response of the this strain and limited shift in potency prevented the accurate calculation of dose ratios. This prevented the construction of Schild plots.

In contrast to its adenosine precursor, the N^6-cyclopentyl agonist JH109 does not appear to share the biphasic antagonism seen in the presence of DPCX and SLV-320 in yeast. The N^6-adamantyl agonists JH66, JH95 and JH209 were used to further investigate the effect of N^6-substituents on biphasic antagonism in the A$_1$R-GPA1/G$\alpha_{i1/2}$ (Figure 4.31) and A$_1$R-GPA1/Gα_z (Figure 4.32).

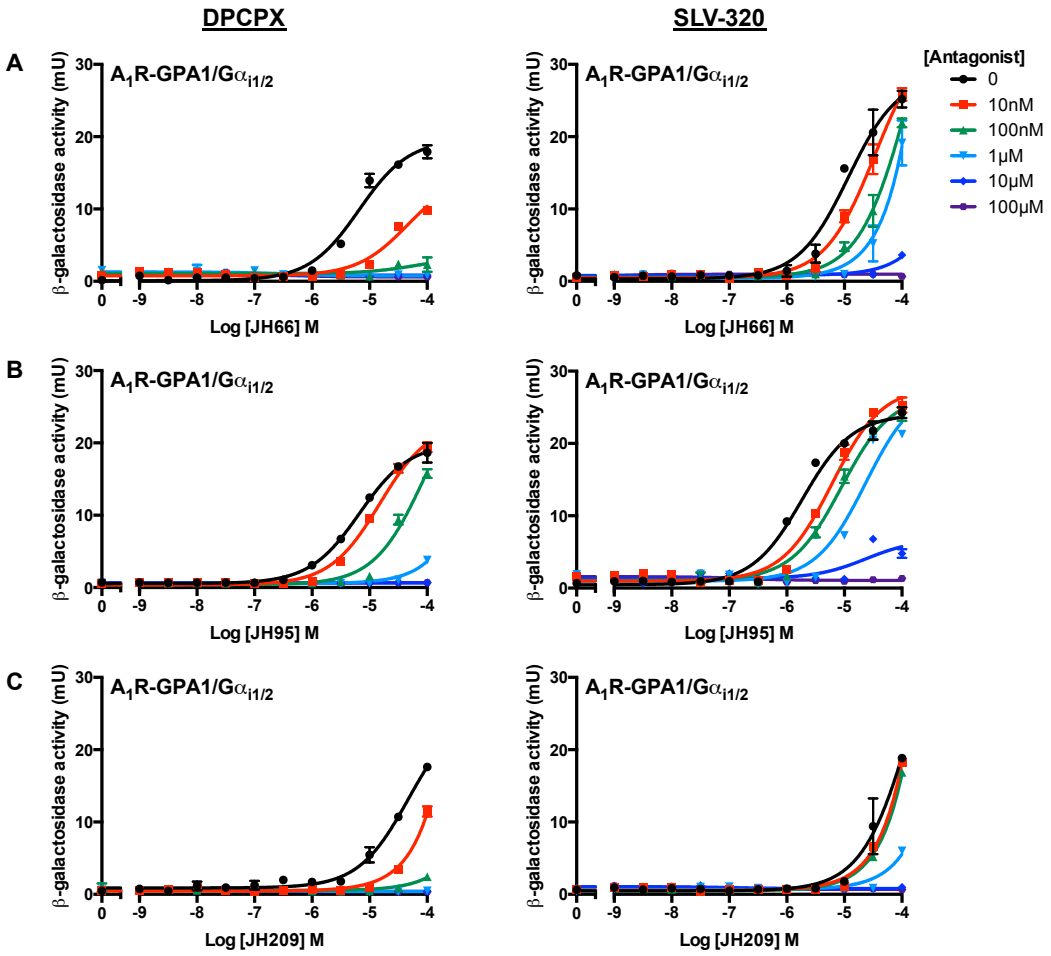

FIGURE 4.31: **Antagonising N^6-adamantyl agonists in A_1R-GPA1/G$\alpha_{i1/2}$.** GPA1/Gα_{i3} transplant yeast cells expressing the A_1R were incubated with N^6-cyclopentyl agonists and antagonists simulataneously for 16 hours at 30°C. Cells were lysed and β-galactosidase activity determined. Data represents the mean ± S.E.M of triplicate repeats fitted with the logistic equation. **A.** JH66, **B.** JH95 and **C.** JH209 concentration-response curves in the presence of DPCPX and SLV-320.

In A_1R-GPA1/G$\alpha_{i1/2}$ neither JH66, JH95 or JH209 promote a significant increase in E_{max} in the presence of either antagonist compared to agonist alone (Figure 4.31, $P > 0.05$, one-way ANOVA). This may suggest that these agonists directly compete with DPCPX and SLV-320. However, Schild analysis was hindered by the low potency of these agonists in yeast. Consequently, shifts in pEC_{50} could not be used to calculate a dose ratio and competitive interaction cannot be established for JH66, JH95 or JH209 with either antagonist.

Consistent with A_1R-GPA1/G$\alpha_{i1/2}$, neither JH66, JH95 or JH109 increase E_{max} in the presence of DPCPX or SLV-320 relative to agonists alone ($P < 0.05$, one-way ANOVA). However, the low potency of these ligands and reduced response of this strain prevented the calculation of dose-ratios for Schild analysis. Consequently, how the N^6-adamantyl modifications of JH66 and JH95 affect the biphasic antagonism of their adenosine and NECA precursors remains unclear. This effect warrants further study. For example, using the A_1R mutants of Peeters et al. (2012) that show compromised allosterism in the same yeast background used here.

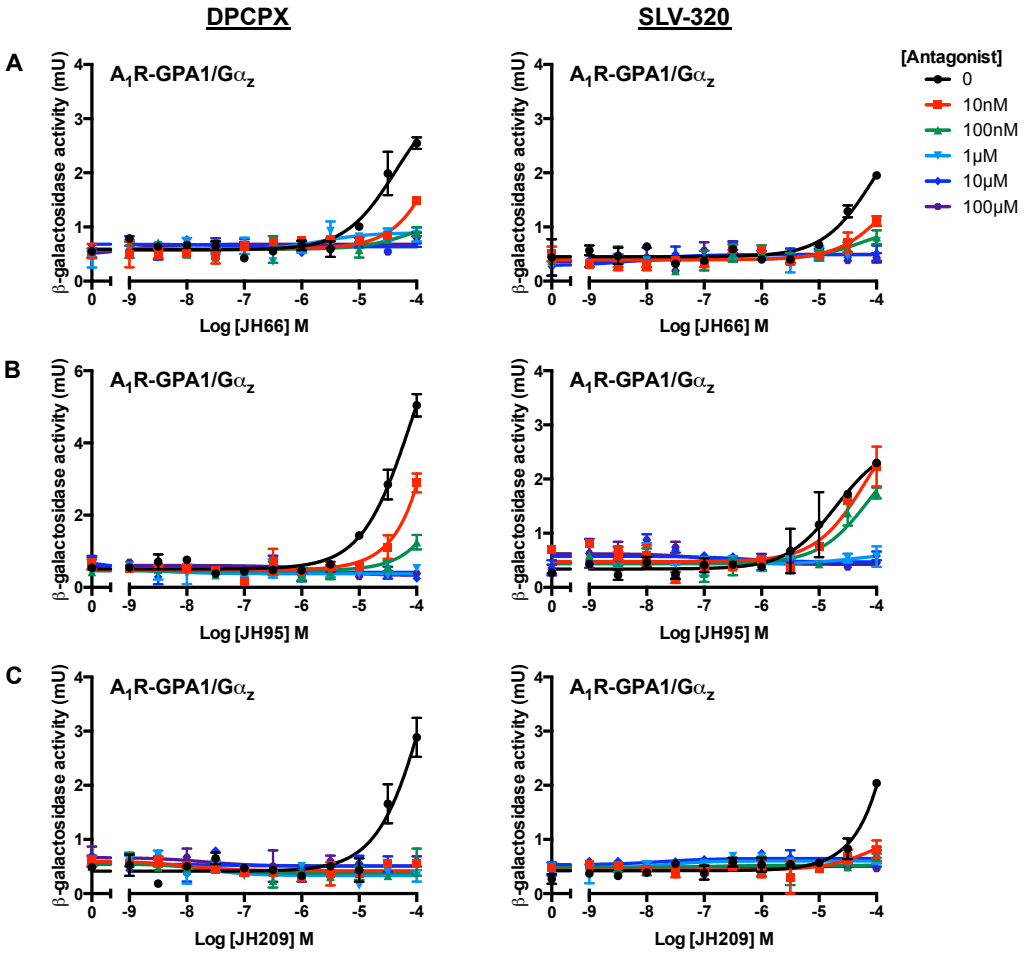

FIGURE 4.32: **N^6-adamantyl agonist and antagonist interactions in A_1R-GPA1/Gα_z.** A_1R-GPA1/Gα_z transplant yeast cells expressing the A_1R were incubated with N^6-cyclopentyl agonists and antagonists simulataneously for 16 hours at 30°C. Cells were lysed and β-galactosidase activity determined. Data represents the mean *pm* S.E.M of triplicate repeats fitted with the logistic equation. **A.** JH66, **B.** JH95 and **C.** JH209 concentration-response curves in the presence of DPCPX and SLV-320.

4.3 Summary

This study ultimately aims to combine experimental and theoretical approaches to understand functional selectivity. However, dynamic experimental data is required to inform theoretical studies. For instance, the operational model can only accurately distinguish ligand-binding and downstream signalling if one of these parameters are already determined. Fluorescent ligands can be used to measure ligand-binding in real time. Indeed, the existence of fluorescent ligands were a powerful driver for the selection of the A_1R as a tool to study functional selectivity. However, only one of these compounds were available in limited availability at great expense. Fortunately, Dr Jennifer Hemmings and Prof Martin Lochner (University of Bern, Switzerland) were looking to develop novel fluorescent A_1R agonists. Their need for an experimental system to test their compounds, our need for a cheap and easy supply of fluorescent agonists and the development of these yeast strains as a drug screening platform naturally led to the collaboration described here.

Covalent modification of the N^6 position of the purine group have been shown to confer subtype specificity in adenosine receptors. Dr Hemmings synthesised a range of agonists modified to include N^6-azabicyclo, -cyclopentyl and -adamantyl groups. Here, these compounds were characterised in the yeast transplant system. N^6-adamantyl substituents exhibited total A_1R/A_2R selectivity while N^6-cyclopentyl agonists showed increased A_1R potency relative to their precursor compounds. The operational model suggests these effects a consequence of ligand-binding rather than signal transduction. N^6-cyclopentyl and N^6-adamantyl NECA derivatives were chosen for fluorescent-compound attached

Here, covalent attachment of fluorophores to purine nucleosides such as adenosine or NECA reduces potency against the A_1R. A commercially-available fluorescent agonist, CAS200623, was screened for activity in A_1R and A_2R expressing yeast and shown to have a low potency with poor A_1R/A_2R selectivity. Flow cytometry showed that this compound binds to the yeast cell surface in cells not expressing an adenosine receptor. Further, novel N^6-cyclopentyl and N^6-adamantyl fluorescent compounds were screened for activity in yeast. The N^6-cyclopentyl fluorescent agonist provided a robust response against the A_1R and $A_{2A}R$ in yeast, albeit with low potency.

Finally, this chapter explores biphasic antagonism of the A_1R. Here, theA_1R antagonists DPCPX and SLV-320 increase E_{max} while shifting the concentration-response curve to the right. This effect has been documented in mammalian systems through ERK1/2 phosphorylation and is faithfully reproduced here in yeast, a G protein mediated effect. Therefore, biphasic antagonism is likely to be a receptor specific effect. This study hypothesises that this may be a consequence of dimerisation or allosteric antagonism, a known pharmacological characteristic of the A_1R. However, this effect is not shared by N^6-adamantyl agonists. While the underlying mechanism remains unclear, the N^6-adamantyl fluorescent precursor compounds could represent a means to elucidate this.

Chapter 5

An interdisciplinary approach to A_1R pharmacology in yeast

5.1 Introduction

A systems pharmacology approach integrates experimental and computational methods to investigate the action of drugs on a system level. Here we, and others, have demonstrated that the *Sc. cerevisiae* transplant strains are an excellent platform to investigate the pharmacology of GPCRs.

This study ultimately aims to understand functional selectivity of GPCRs with regard to G protein bias with a particular focus on the kinetic contribution of the ligand, receptor and G protein. Indeed, the operational model allows ligand binding and signal transduction efficiency, τ, to be estimated. However, τ is effectively a black box that, in this case, describes the receptor-G protein interaction and all downstream responses up to the transcriptional reporter. Thus, this model does not isolate the individual contributions of the ligand, GPCR and G protein to functional selectivity. Indeed, to properly distinguish these processes biological rate constants need to be estimated. Equilibrium models are effective but limited. ODE models however, describe a biochemical reaction scheme with the desired level of complexity. This includes the number of interacting species and the biochemical parameters that govern this interaction.

Here, a mathematical framework is developed to describe the pharmacology of the A_1R in different G protein backgrounds. By fitting a minimal ODE model to experimental data generated in yeast it is possible to extract multiple kinetic parameters, i.e. rate constants, simultaneously. However, before this can be achieved several considerations need to be addressed. These include:

- Variability in the experimental system
- Ambiguity of model predictions
- Complexity of the model

Variability in the experimental system, at least with regard to receptor expression from the p426GPD vector, is clear from the flow cytometry data of the A_1R^{GFP}. However this may be addressed by changing the expression system.

5.1.1 Refining the experimental system

Yeast is an excellent, robust system for the screening and characterisation of agonists and antagonists. Clear differences were observed in adenosine receptor activity between strains, particularly the A_1R, when expressed from the p426GPD plasmid. However, flow cytometry of C-terminal A_1R^{GFP} fusion proteins suggest that receptor expression varies between individual cells and that the majority of the population do not express the A_1R to a detectable level.

ODE models are deterministic. Those based on population data, such as β-galactosidase assays, represent an average cell in that population. Variation in receptor expression, the primary messenger of the pheromone response, therefore poses difficulties. This is especially true if a proportion of the population do not express the receptor at all. Therefore, uniform expression of the A_1R across the population is essential for meaningful model predictions. This may be influenced by an unequal distribution of a high copy number plasmid across a population. The p426GPD expression vector uses the *URA3* uracil biosynthesis selection marker. *URA3* has not been deleted in these strains but silenced through a single base pair mutation (Olesnicky et al., 1999; Brown et al., 2000). Reversion is an issue with this selection marker and may also contribute to variation in plasmid copy number and receptor expression across the population (Chattoo et al., 1979).

Chromosomal expression ensures that each cell in a population has the same copy number of a given gene and therefore expression is uniform between cells. Further, integration is stable and not easily removed. Therefore reversion of the $\Delta URA3$ genotype should not affect receptor expression. Thus, chromosomal integration provides a convenient avenue to refine the experimental system to increase its amenability to deterministic modelling.

5.1.1.1 Characterisation of yeast strains chromosomally expressing the A_1R

The A_1R was cloned into the pRS306GPD expression vector under the control of the constitutive *GAPDH* promoter. The construct was linearised by restriction digest and integrated into the *URA3* locus as described by Gietz and Schiestl (2007). The GPA1/Gα_o, GPA1/G$\alpha_{i1/2}$, GPA1/Gα_{i3} and GPA1/Gα_z strains were selected due to their response to the A_1R when expressed from a plasmid. 8-16 colonies were isolated and incubated with 100μM NECA for 16 hours. Cells were lysed and β-galactosidase activity determined (Figure 5.1). The equivalent strains expressing the A_1R from the p426GPD plasmid, using the same promoter, were included for comparison.

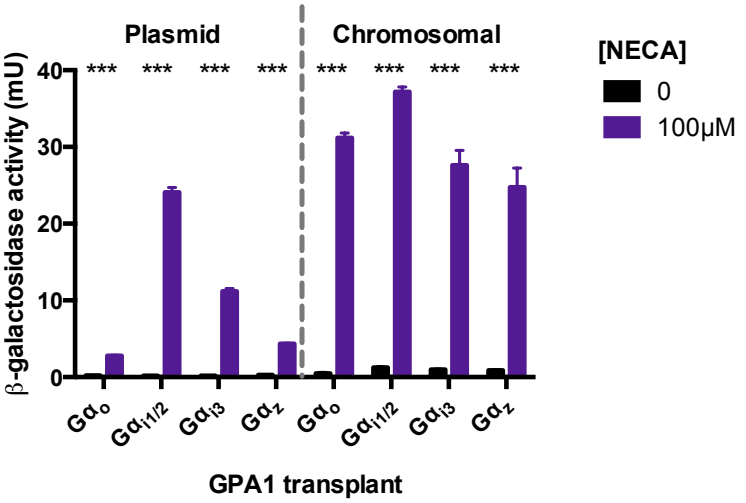

Figure 5.1: **Screening yeast chromosomally-expressing the A_1R for β-galactosidase activity in response to NECA.** The A_1R was placed under the control of the constitutive *GAPDH* promoter and integrated into the *URA3* locus of the GPA1/Gα_o, GPA1/G$\alpha_{i1/2}$, GPA1/Gα_{i3} and GPA1/Gα_z transplant strains. 8-16 colonies were selected and incubated with 100μM NECA for 16 hours. Cells were lysed and β-galactosidase activity determined. The equivalent strains expressing the A_1R from the p426GPD expression plasmid were included for comparison. Student's T-test compared to DMSO alone control. $P < 0.05$ was considered significant. *** $P < 0.0005$.

All strains assayed showed a significant upregulation of β-galactosidase activity in response to NECA ($P<0.05$, Student's T-test). Interestingly, the level of signal is higher in the chromosomal-expression strains relative to their plasmid counterparts, including GPA1/G$\alpha_{i1/2}$ (β-galactosidase activity = 31.2$\pm$0.6 mU and 37.2$\pm$0.6 mU for the plasmid and integrate strains respectively). This suggests that the observed E_{max} of the adenosine receptors expressed via plasmid is not the overall maximum β-galactosidase activity of the yeast transplant system. Concentration-response curves were created for NECA, adenosine and 2CCPA using the integrated strains. To better distinguish them from their plasmid counterparts these strains will be referred to as A_1R::GPA1/Gα_o, A_1R::GPA1/G$\alpha_{i1/2}$, A_1R::GPA1/Gα_{i3} and A_1R::GPA1/Gα_z.

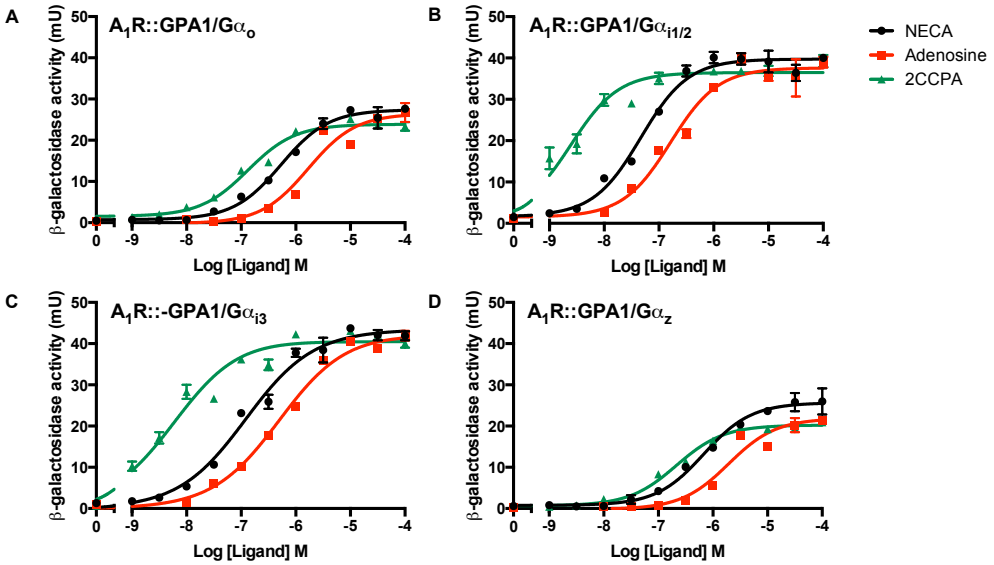

FIGURE 5.2: **Pharmacology of chromosomally-expressed A_1R in yeast.** The integrate strains were incubated with NECA, adenosine or 2CCPA for 16 hours. Cells were lysed and β-galactosidase activity determined. **A.** A_1R::GPA1/Gα_o. **B.** A_1R::GPA1/G$\alpha_{i1/2}$. **C.** A_1R::GPA1/Gα_{i3}. **D.** A_1R::GPA1/Gα_z. Data represents the mean of triplicate repeats ± S.E.M fitted with the logistic equation.

TABLE 5.1: **Pharmacological parameters of chromosomally-expressed A_1R.** The logistic equation the operational model were applied to the data of Figure 5.2 by non-linear regression. $pEC_{50} = -Log\ EC_{50}$ (potency), E_{max} = *maximum level of signal*, $pK_A = -$Log K_A (ligand binding affinity) and τ = efficacy. Equivalent plasmid parameters have been included for comparison. * P < 0.05, ** P < 0.005, *** P < 0.0005, Student's T-test comparing parameter for chromosomal-expression to plasmid counterpart.

Strain	**Ligand**	pEC_{50}	E_{max}	pK_A	$log\tau$
A_1R::GPA1/Gα_o	NECA	6.3±0.1*	27.4±0.5***	4.4±0.1	1.9±0.3*
(Chromosomal)	Adenosine	5.8±0.1**	26.4±0.1***	4.2±0.5	1.5±0.5
	2CCPA	6.9±0.1	23.9±0.4**	6.1±0.2	0.8±0.1**
A_1R-GPA1/Gα_o	NECA	5.2±0.1	2.5±0.1	4.4±0.1	0.9±0.1
(Plasmid)	Adenosine	4.8±0.1	1.9±0.1	4.5±0.2	0.4±0.1
	2CCPA	6.6±0.2	1.2±0.1	6.5±0.2	−0.2±0.1
A_1R::GPA1/G$\alpha_{i1/2}$	NECA	7.3±0.1***	39.7±0.7***	4.8±0.5	2.6±0.6
(Chromosomal)	Adenosine	6.8±0.1**	37.6±0.8***	5.4±0.3	1.4±0.3
	2CCPA	8.6±0.1***	36.5±0.7***	7.4±0.2**	1.2±0.2
A_1R-GPA1/G$\alpha_{i1/2}$	NECA	6.0±0.1	25.8±0.6	4.4±0.1	1.5±0.1
(Plasmid)	Adenosine	5.6±0.1	23.5±0.7	4.6±0.2	0.9±0.1
	2CCPA	6.7±0.1	20.9±0.4	6.1±0.1	0.6±0.1
A_1R::GPA1/Gα_{i3}	NECA	6.9±0.1**	41.7±0.9***	4.1±1.0	2.8±0.6*
(Chromosomal)	Adenosine	7.3±0.1**	41.3±0.6***	5.2±0.6	2.1±0.6*
	2CCPA	8.3±0.1***	39.5±1.0***	6.6±0.2	1.6±0.2**
A_1R-GPA1/Gα_{i3}	NECA	5.8±0.1	19.5±0.4	5.1±0.1	0.7±0.1
(Plasmid)	Adenosine	5.7±0.1	16.5±0.5	5.1±0.1	0.4±0.1
	2CCPA	6.7±0.1	14.4±0.3	6.4±0.1	0.2±0.1
A_1R::GPA1/Gα_z	NECA	6.2±0.1**	25.7±0.6***	4.4±0.1	1.8±0.1
(Chromosomal)	Adenosine	5.7±0.1*	21.9±0.8***	4.7±0.2	0.8±0.1**
	2CCPA	6.7±0.1	20.2±0.3***	5.9±0.1	0.6±0.1**
A_1R-GPA1/Gα_z	NECA	5.5±0.1	5.8±0.2	4.4±0.3	1.2±0.3
(Plasmid)	Adenosine	4.8±0.2	3.9±0.3	4.3±0.2	0.3±0.1**
	2CCPA	6.3±0.2	2.9±0.2	6.1±0.2	−0.2±0.1**

The data for the chromosomally-expressed A_1R demonstrates considerable differences from the strains expressing the receptor using the p426GPD vector (Figure 5.2). Notably, E_{max} is significantly increased by chromosomal-expression for all ligands relative to their plasmid counterparts. pEC_{50} is broadly consistent for NECA, adenosine and 2CCPA between plasmid and integrate GPA1/Gα_o and GPA1/Gα_z strains. However, this difference between plasmid and integrated expression system pEC_{50} values is far more pronounced in the GPA1/Gα_i strains. Variation in pEC_{50} suggests that integration of the A_1R increases the sensitivity of these strains to NECA, adenosine and 2CCPA (Table 5.1). Interestingly, pK_A is remarkably conserved for all ligands between chromosomal-expression systems and plasmid counterparts. However, $log\tau$ is greatly increased for the integrated strains. This suggests that the ligand sensitivity of the system is unaffected by chromosomal integration but the signal transduction efficiency of the population has increased.

However, at present the maximum level of β-galactosidase activity of these strains, regardless of receptor or ligand, is unknown. It is entirely possible that the observed shift in pEC_{50} for the A_1R::GPA1/Gα_i strains is due to signalling reaching the maximum limit of either the experimental system or the β-galactosidase assay at lower ligand concentrations. To eliminate the latter, the same samples were diluted 1:5 in AA-Ura and the assay repeated. Raw β-galactosidase activity, independent of cell density, was measured by OD_{430} (Figure 5.3). pEC_{50} and normalised responses for all ligands are preserved after sample dilution but the OD_{430} E_{max} is reduced, suggesting that the assay itself is not limiting the maximal signal (Table 5.2).

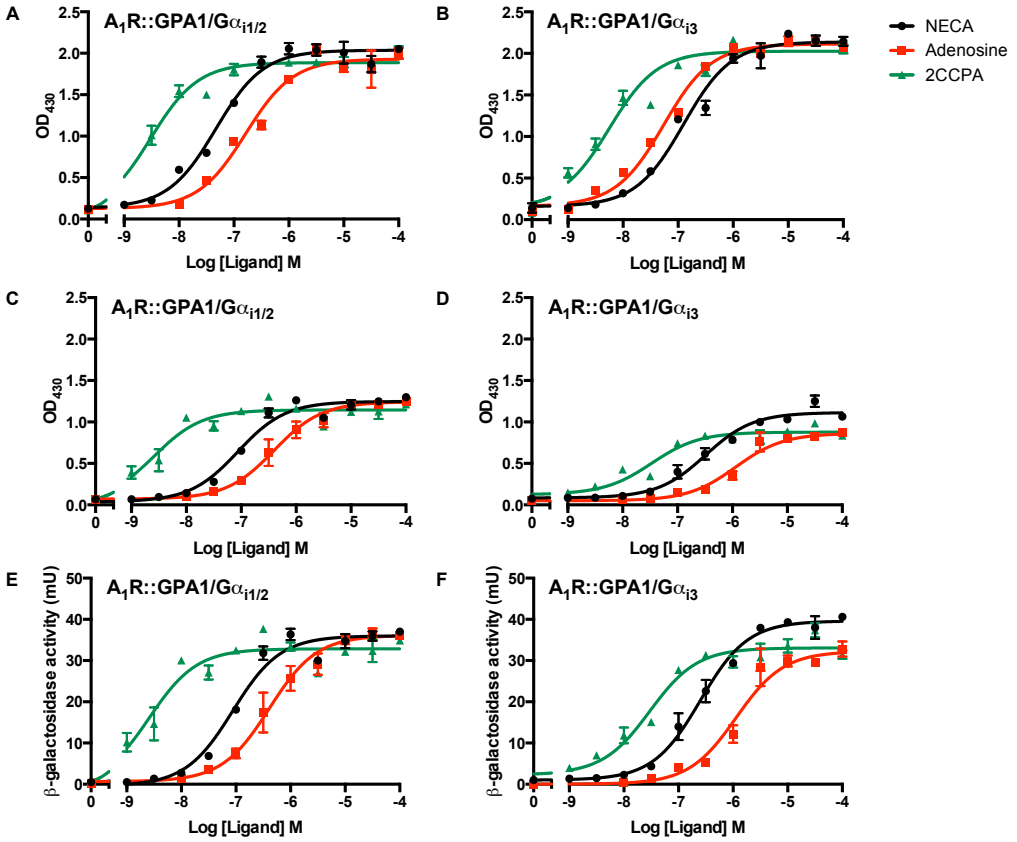

FIGURE 5.3: **A_1R integrate pharmacology in yeast after dilution.** The samples used to generate Figure 5.2 were diluted 1:5 in AA-Ura and the β-galactosidase assay repeated. β-galactosidase activity, regardless of cell density, was quantified by OD_{430}. **A.** A_1R::GPA1/G$\alpha_{i1/2}$ and **B.** A_1R::GPA1/Gα_{i3} before 1:5 dilution. **C.** A_1R::GPA1/G$\alpha_{i1/2}$ and **D.** A_1R::GPA1/Gα_{i3} after 1:5 dilution. **E.** A_1R::GPA1/G$\alpha_{i1/2}$ and **F.** A_1R::GPA1/Gα_{i3} after 1:5 dilution normalised to cell density, quantified by OD_{620}. Data represents the mean of triplicate repeats ± S.E.M fitted with the logistic equation.

TABLE 5.2: **Pharmacological parameters of the integrated A_1R before and after dilution.** The logistic equation and the operational model were applied to the data of Figure 5.3 by non-linear regression. $pEC_{50} = -Log\ EC_{50}$ (potency) and E_{max} = maximum level of signal.

Strain	**Ligand**	**pEC$_{50}$**	**E$_{max}$**
A_1R::GPA1/G$\alpha_{i1/2}$ (Undiluted)	NECA	7.3±0.1	2.0±0.1
	Adenosine	6.8±0.1	1.9±0.1
	2CCPA	8.6±0.1	19±0.1
A_1R-GPA1/G$\alpha_{i1/2}$ (Diluted)	NECA	7.1±0.1	1.3±0.1
	Adenosine	6.4±0.1	1.2±0.1
	2CCPA	8.6±0.1	1.1±0.1
A_1R::GPA1/Gα_{i3} (Undiluted)	NECA	6.9±0.1	2.1±0.1
	Adenosine	7.3±0.1	2.1±0.1
	2CCPA	8.3±0.1	2.0±0.1
A_1R-GPA1/Gα_{i3} (Diluted)	NECA	6.5±0.1	1.1±0.1
	Adenosine	5.9±0.1	0.9±0.1
	2CCPA	7.5±0.1	0.9±0.1

5.1.2 Dynamic ODE models require time course data

End-point data, such as concentration response curves, represent a measure that can be a consequence of any number of time course profiles. For a truly quantitative fit, a model must capture time course data and not just concentration response curves. An example of this is the operational model of pharmacological agonism. While this is an excellent tool to gain insight into end-point measurements it is still an equilibrium model designed to capture data at steady state. Consequently, at best it can only accurately calculate ratios of K_A:τ, limiting its usefulness.

Due to their differences in pharmacology, but consistency in pEC_{50} with their plasmid counterparts, time course data was generated for the A_1R::GPA1/Gα_{i3} and A_1R::GPA1/Gα_z integrates in response to NECA, adenosine and 2CCPA (Figure 5.4 and Figure 5.5 respectively). Both strains produced sigmoidal time course profiles in the presence of all agonists. These data suggest that, in these strains, β-galactosidase activity plateaus after 8-10 hours incubation in ligand. Constructing concentration-response curves for the 12 hour data points faithfully replicates the data of Figure 5.2 (Figure 5.4D and Figure 5.5D).

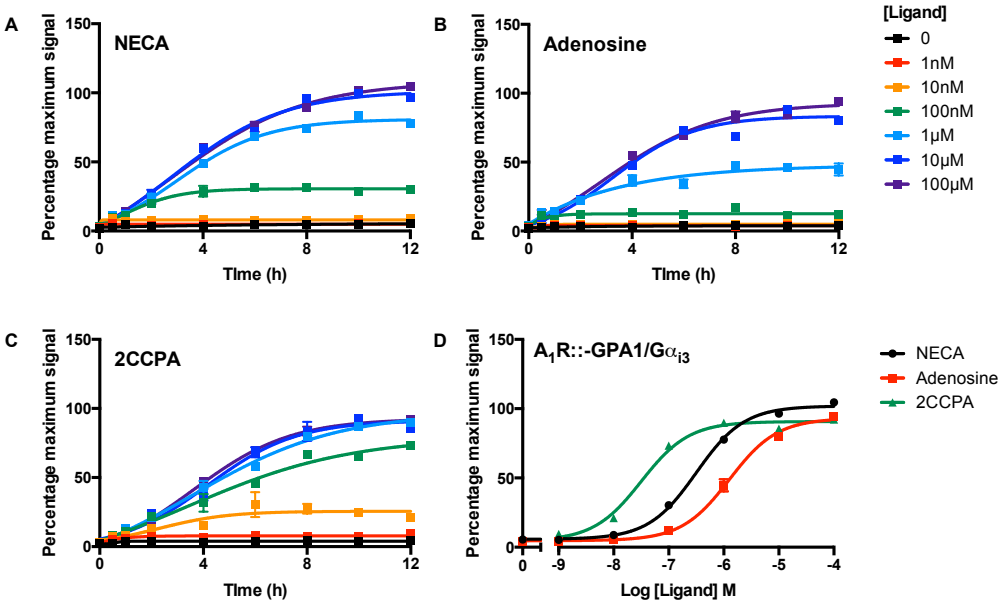

FIGURE 5.4: **β-galactosidase time courses of the A_1R-GPA1/Gα_{i3} integrate strain.** Yeast cells expressing the A_1R were incubated with AA-Ura containing ligand for 0, 0.5, 1, 2, 4, 6, 8, 10 or 12 hours. Cells were lysed and β-galactosidase activity determine. The A_1R::GPA1/G$\alpha_{i1/2}$ integrate, the highest responding strain, was incubated with NECA to determine a maximal response. Data represents mean ± S.E.M. of triplicate repeats fitted with the logistic equation. **A.** NECA. **B.** Adenosine **C.** 2CCPA **D.** Concentration-response curves determined by β-galactosidase activity after 12 hours incubation with ligand.

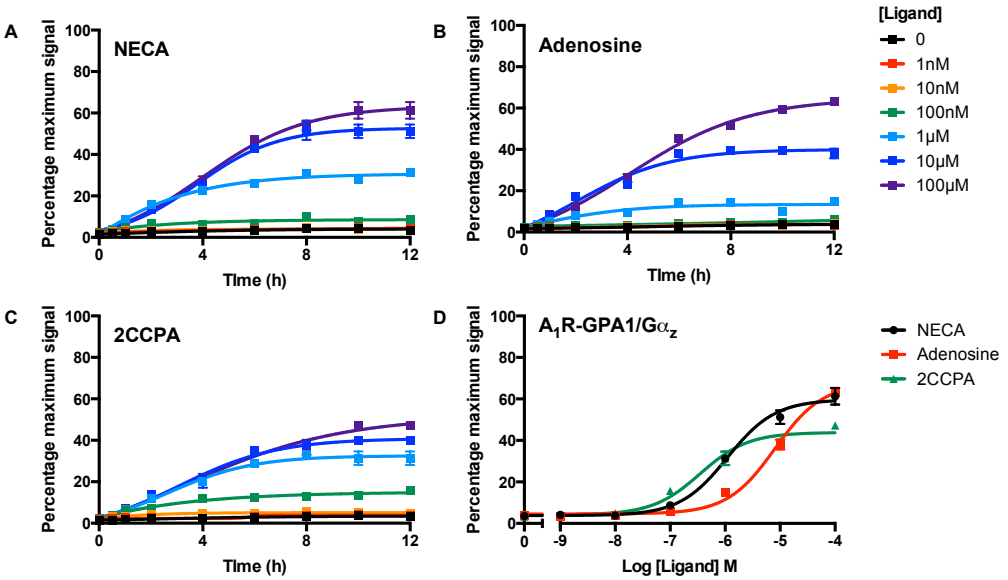

FIGURE 5.5: **β-galactosidase time courses of the A_1R-GPA1/Gα_z integrate strain.** Yeast cells expressing the A_1R were incubated with AA-Ura containing ligand for 0, 0.5, 1, 2, 4, 6, 8, 10 or 12 hours. Cells were lysed and β-galactosidase activity determine. The A_1R::GPA1/G$\alpha_{i1/2}$ integrate, the highest responding strain, was incubated with NECA to determine a maximal response. Data represents mean ± S.E.M. of triplicate repeats fitted with the logistic equation. **A.** NECA. **B.** Adenosine **C.** 2CCPA **D.** Concentration-response curves determined by β-galactosidase activity after 12 hours incubation with ligand.

5.2 Model templates

Having established and further refined the experimental system for mathematical modelling, the next step was to generate a novel framework specifically for fitting time course experimental data. As many known initial conditions and parameters as possible would be a significant advantage. For example, ODE models assume the laws of mass action kinetics. Therefore, the initial species concentrations of the model will influence the predicted parameters. Fortunately, the *Sc. cerevisiae* pheromone response has been very well characterised and the concentrations of various signalling components and the rates with which they interact are already known (Blumer et al., 1988; Bardwell and Thorner, 1996; Bardwell et al., 1996; Ferrell and Bhatt, 1997; van Drogen et al., 2001; Yi et al., 2003).

This information has been used to construct a number of models of the *Sc. cerevisiae* pheromone response. Consequently, there are many model frameworks that can be used to inform minimal model development here. The most notable and complete of these models is that of Kofahl and Klipp (2004).

5.2.1 The Kofahl and Klipp model of the *Sc. cerevisiae* pheromone response

The Kofahl and Klipp (2004) model was designed to emulate the dynamic time course data of the pheromone response, in its entirety, in the presence of 1μM α-factor pheromone. Consequently, it is a rather large model consisting of 47 expressions denoting 47 interactions between 35 signalling components. For the reader's convenience, schematic of the receptor-G protein cycles of model is repeated (Figure 5.6). While the rates of reaction are faithful to experimental studies, this model uses a receptor concentration of 1.6 μM. This is 10-fold higher than the elucidated value of 160nM (Bardwell et al., 1996). The reasons why the authors deviated from the experimentally-determined value are unclear and represent a weakness of this study as a quantitative model.

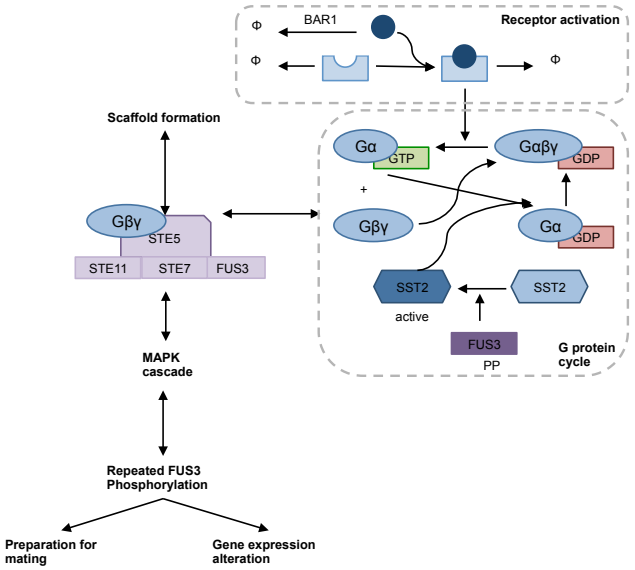

FIGURE 5.6: **The Kofahl and Klipp model of the *Sc. cerevisiae* pheromone response.** This model to be developed here is only concerned with receptor and G protein-level aspects of this model. For simplicity, scaffold formation, MAPK cascade and downstream effects have been condensed. The full reaction scheme is shown in Figure 1.15.

To explore the strengths and weakness of this framework, the Kofahl and Klipp model was implemented in Matlab using the parameters and initial conditions specified by the authors (Kofahl and Klipp, 2004). $SST2$ (the RGS) has been deleted to improve sensitivity to ligand. A $\Delta FAR1$ genotype prevents cell cycle arrest in response to ligand, allowing growth to be used as a transcriptional reporter of pathway activation. Also, a $\Delta BAR1$ genotypes prevents proteolytic degradation of the endogenous yeast pheromone. This was to increase the sensitivity of these strains to pheromone during their original development (Olesnicky et al., 1999; Brown et al., 2000). Model variants were generated to mimic the $\Delta SST2$ and $\Delta SST2\Delta FAR1\Delta BAR1$ phenotypes through setting the initial SST2 activation rate and initial BAR1 and FAR1 concentrations to zero.

The Kofahl and Klipp (2004) model accurately recreates the dynamics of the G protein cycle in response to 1μM ligand (Yi et al. (2003), Figure 5.7A). The G protein cycle terminates within 30 minutes. The rapid G$\beta\gamma$ dynamics may be a consequence of competition between the MAPK cascade and Gα^{GDP}). However, the activation of the STE12 transcription factor is relatively prolonged, as one would expect of a process downstream of the MAPK cascade that transduces and perpetuates signal *in vivo* (Figure 5.7B).

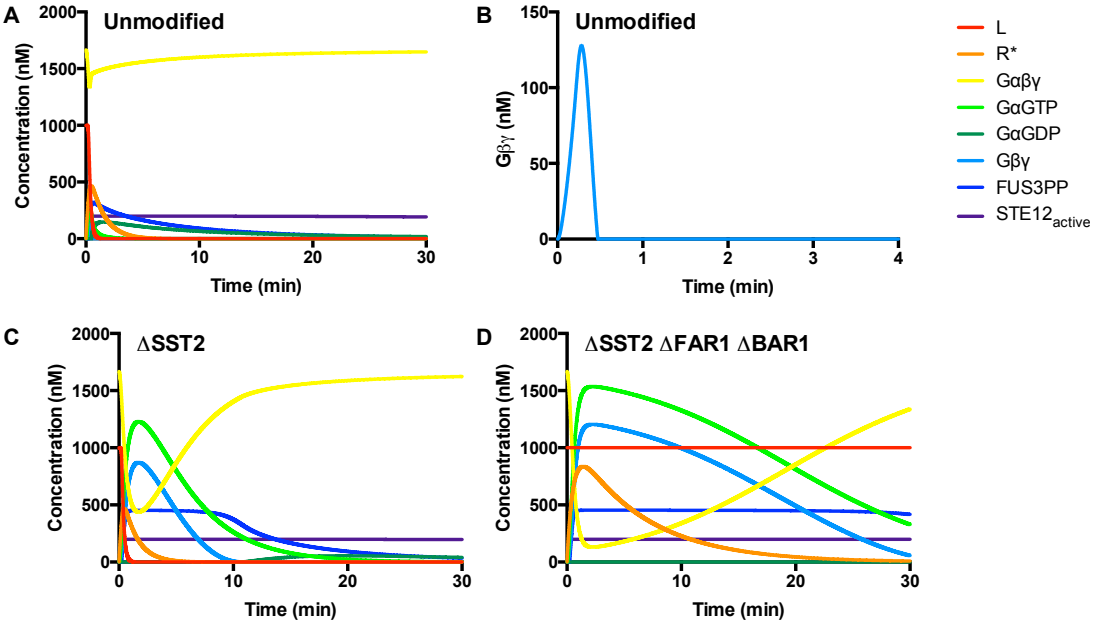

FIGURE 5.7: **Timecourses of the Kofahl and Klipp *Sc. cerevisiae* pheromone response model.** The Kofahl and Klipp model was implemented in Matlab as described by the authors. Simulations were performed using the ODE23s solver with a time step of 0.01 hours. Ligand concentration was 1μM. **A.** Evolution of the G protein cycle and receptor dynamics in the unmodified model. **B.** The isolated G$\beta\gamma$ time course of the unmodified model. **C.** Time courses of the model modified to replicate the $\Delta SST2$ genotype. **D.** Time courses of the model modified to replicate the $\Delta SST2\Delta FAR1\Delta BAR1$ genotype of the transplant strains.

Modification of the model makes interesting predictions of the G protein cycle in genetically manipulated strains (Figure 5.7). As these dynamic studies were not repeated using $\Delta SST2$ or $\Delta SST2\Delta FAR1\Delta BAR1$ phenotypes there are currently no experimental data to validate this model variant. Consequently, these are only predictions and may not reflect the true experimental situation. The $\Delta SST2$ modification results in a prolonged and amplified G protein cycle, with greater variation in the levels of G$\alpha\beta\gamma$ and free G protein subunits. This effect is further enhanced in the $\Delta SST2\Delta FAR1\Delta BAR1$ model (Figure 5.7D). This is a consequence of greater persistence of ligand in the absence of the BAR1 protease. Further, G$\beta\gamma$ directly activates FAR1 to trigger cell cycle arrest in *in vivo*. $\Delta FAR1$ strains have more free G$\beta\gamma$ to trigger downstream signalling. Consequently, the predictions of the modified model variants, in the presence of 1μM ligand, are biologically feasible.

However, these simulations only represent a single ligand concentration. While dynamic studies of the modified yeast strains are elusive, concentration-response curves of the $\Delta SST2\Delta BAR1$ phenotype have been reported (Hao et al., 2003). Here, as in this study, β-galactosidase was used a measure of transcriptional activation via the *FUS1* promoter. Deletion of SST2 resulted in a rightward shift in the concentration-response curve (pEC_{50} = 8.1 compared to 6.3) and a marginal increase in E_{max}. Consequently, there is end-point experimental data available to validate the modified model predictions.

While the Kofahl and Klipp model contains a term for the activated MAPK FUS3PP and the transcription factor STE12, it does not contain a term for the pheromone-responsive agglutinin FUS1. *FUS1*, and β-galactosidase in the yeast transplant strains, are directly activated by STE12 under the influence of FUS3PP. Consequently, β-galactosidase transcription can be approximated as the accumulation of FUS3PP or active STE12. The Kofahl and Klipp model, and variants, were simulated for either 30 minutes or 16 hours, consistent with the experimental data of Yi et al. (2003) and the experimental data presented here, respectively. $\int_0^t [STE12_{active}]dt$ and $\int_0^t [FUS3PP]dt$ calculated using the trapezium rule (Figure 5.8). Interestingly, $\Delta BAR1\Delta FAR1$ modification has little effect on the $\int_0^t [FUS3PP]dt$ output over either time period.

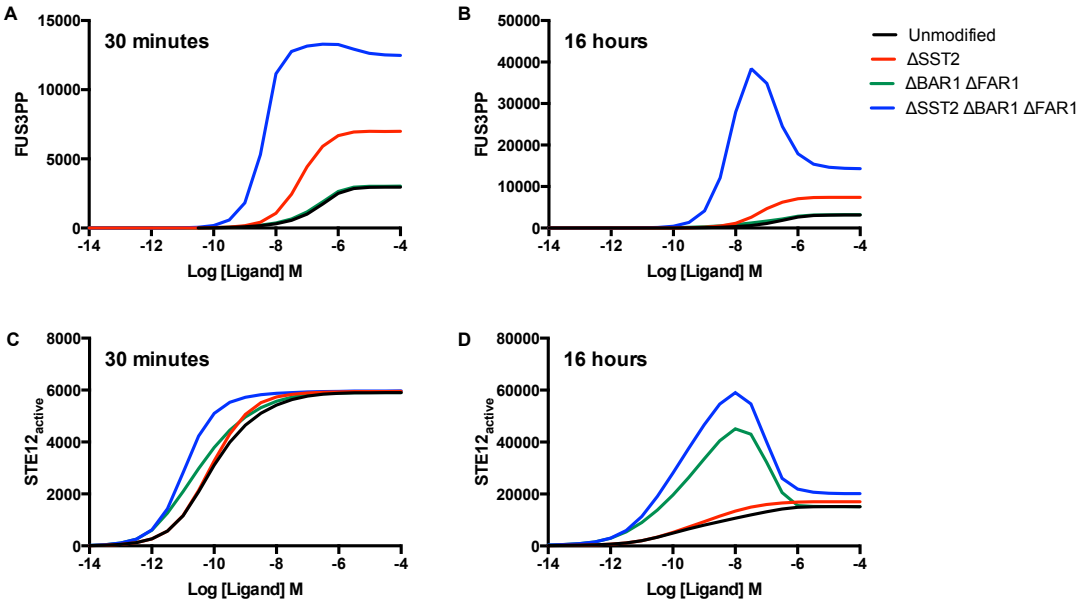

FIGURE 5.8: **Concentration-response curves of the Kofahl and Klipp *Sc. cerevisiae* pheromone response model.** The Kofahl and Klipp model, $\Delta SST2$ and$\Delta SST2\Delta FAR1\Delta BAR1$ variants were implemented in Matlab and simulated for either 0.5 or 16 hours using the ODE23s solver and a variety of ligand concentration. The *FUS1>β-galactosidase* transcriptional reporter was replicated integrating the upstream $STE12_{active}$ and FUS3PP time courses using the trapezium rule. **A.** $\int_0^t [FUS3PP]dt$ over 30 minutes and **B.** 16 hours simulation. **C.** $\int_0^t [STE12_{active}]dt$ over 30 minutes and **D.** 16 hours simulation.

The concentration-response curves of Figure 5.8 show some very interesting differences from the data of Hao et al. (2003). After 30 minutes simulation, the time scale the model was designed for, we show comparable shifts in the FUS3PP curve to the experimental data (pEC_{50} = 6.7, 7.3 and 8.4 for the unmodified, $\Delta SST2$ and $\Delta SST2\Delta BAR1\Delta FAR1$ model variants respectively). However, E_{max} is progressively greater for $\Delta SST2$ and $\Delta SST2\Delta BAR1\Delta FAR1$. In contrast, STE12$_{active}$ E_{max} is consistent between model variants. However, STE12$_{active}$ is much more sensitive to ligand but shifts in the concentration-response curve are much more limited in the model variants compared to the unmodified framework. Taken together, this may suggest that over 30 minutes $\int_0^t [FUS3PP]dt$ is a better estimate of transcriptional activation of β-galactosidase. Consequently, further discussion of this model will use this as measure of pathway activation.

$\int_0^t [FUS3PP]dt$ shows a leftward shift in pEC_{50} for $\Delta SST2$ compared to the unmodified model. However, deleting BAR1 alters the sigmoidal concentration-response curve such that E_{max} is achieved at 10μM pheromone but the level of signal decreases with increasing ligand. This trend is also replicated by STE12$_{active}$. The unmodified model has two forms of negative regulation at the receptor level - proteolytic degradation of the peptide ligand and loss of the active receptor. Without BAR1 there is more ligand in the system, resulting in a greater concentration of R*. As the rate of internalisation is subject to the laws of mass action kinetics, increased R* accelerates internalisation. This manifests as a decrease in signal with increasing ligand. This is in contrast to experimental data generated in modified *Sc. cerevisiae* cells lacking BAR1 (MacKay et al., 1988; Yi et al., 2003). Consequently, this represents a weakness of the Kofahl and Klipp model.

While this model is an excellent framework to study the dynamics of the yeast pheromone response there are a number of other limitations. Firstly, there is no term for spontaneous receptor activation. Consequently, this model does not replicate signalling in the absence of ligand. Another weakness of this model also represents a strength. There is no physical interaction between the active receptor and the G protein. There is simply a term for [R*] in the rate of G protein activation. This allows the Kofahl and Klipp model to represent either or both collision and pre-coupling mechanisms of G protein activation without including either directly..

The Kofahl and Klipp model clearly represents an excellent tool to study the *Sc. cerevisiae* pheromone response. The size and complexity of this model may also present some difficulties in model fitting. Here, the aim is to build a simple model to fit to time course data to understand the rate parameters governing functional selectivity. Of the 47 reactions that build this framework only 11 detail receptor pharmacology, the G protein cycle and interaction with effectors. Consequently, there is scope to minimise this model. The theoretical studies of Smith et al. (2009) may provide the avenue to do so.

5.2.2 The Smith model of the *Sc. cerevisiae* pheromone response

The Kofahl and Klipp model was designed to describe the *Sc. cerevisiae* pheromone response in its entirety. In contrast the Smith et al. (2009) model of the *Sz. pombe* pheromone response has a comprehensive G protein cycle and a minimised approximation of downstream signalling processes. This model draws inspiration from Kofahl and Klipp (2004) and uses the same rate parameters and initial conditions, where applicable. However, *Sz. pombe* uses $G\alpha^{GTP}$ to stimulate downstream signalling in the pheromone response. This model can be modified to use $G\beta\gamma$ to stimulate downstream signalling, thus replicating the *Sc. cerevisiae* G protein cycle (Figure 5.9 (Smith et al., 2009)). Unlike the Kofahl and Klipp model, this model can replicate ligand-dependent receptor activation and downstream basal signalling. Consequently this model does not assume steady state and requires equilibration prior to the introduction of ligand. It is also worth noting that while Kofahl and Klipp (2004) use an excessive 1.6μM receptor concentration, this model uses an experimentally verified 160nM.

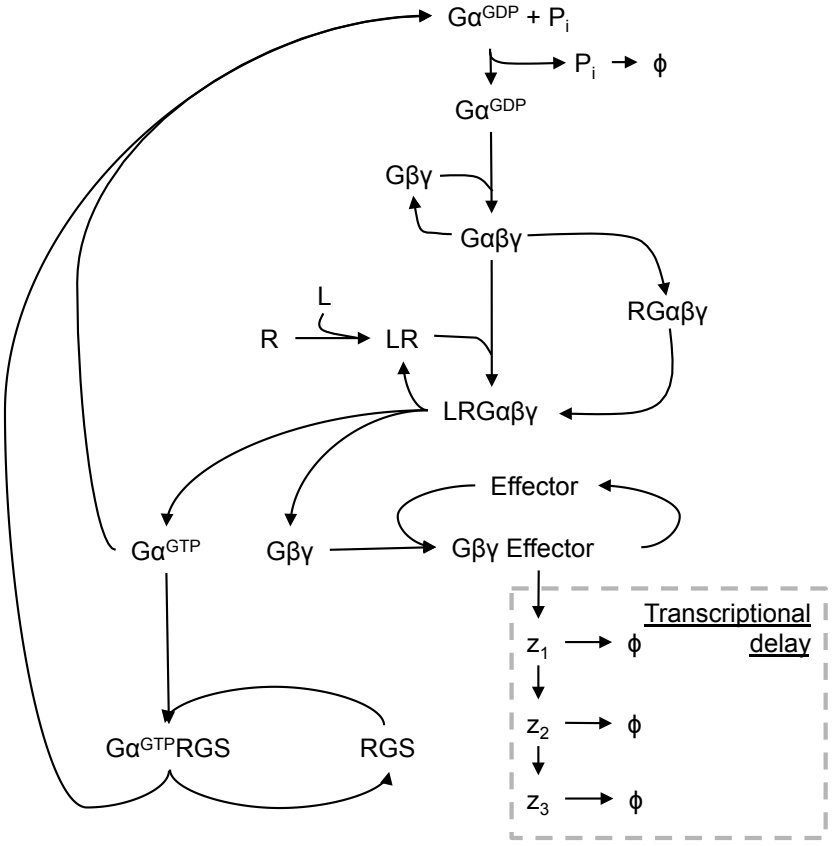

FIGURE 5.9: **The Smith model modified for the *Sc. cerevisiae* pheromone response.** This model was originally developed for the *Sz. pombe* pheromone response where $G\alpha^{GTP}$ is the effector that activates downstream signalling. Here $G\beta\gamma$ has been made the effector to approximate the equivalent *Sc. cerevisiae* system. Z_1, Z_2 and Z_3 mimic the transcriptional response. ϕ denotes a null set, or species loss from the model. Figure adapted from Smith et al. (2009).

A key component of this model is the transcriptional delay. Here G$\beta\gamma$Effector induces the formation of Z_1. This, in turn, catalyses the production of Z_2. The results in the generation of Z_3. Each of these steps has an associated activation and degradation parameter, α. Together, Z_1, Z_2 and Z_3 serve to delay and amplify the transcriptional response to active G protein, summarising the MAPK cascade of the *Sz. pombe* phermone response (Smith et al., 2009; Croft et al., 2013)

This system of ODEs, (equation arrays (5.1) and (5.16)), was implemented in Matlab and solved using the ODE23s solver to assess its suitability as a model template. Simulations were performed for 14 hours before application of ligand for a further 16 hours, consistent with the experimental and computational data described by Smith et al. (2009). A ΔRGS phenotype was replicated by setting the initial RGS concentration to 0nM (Figure 5.10). Transcriptional responses were mimicked using the species Z_1, Z_2 and Z_3 to delay and modulate the G$\beta\gamma$Effector appropriately. Consistent with Smith et al. (2009) and Croft et al. (2013), α was set as 1.5. Concentration-response curves were constructed by [Z_3] after 16 hours simulation with ligand (Figure 5.10).

$$\nu_1 = [L]\cdot[R]\cdot K_1, K_1 = 0.0025nM^{-1}h^{-1} \tag{5.1}$$

$$\nu_2 = [R]\cdot[G\alpha\beta\gamma]\cdot K_2, K_2 = 0.005nM^{-1}h^{-1} \tag{5.2}$$

$$\nu_3 = [LR]\cdot[G\alpha\beta\gamma]\cdot K_3, K_3 = 0.02nM^{-1}h^{-1} \tag{5.3}$$

$$\nu_4 = [L]\cdot[G\alpha\beta\gamma]\cdot K_4, K_4 = 0.005nM^{-1}h^{-1} \tag{5.4}$$

$$\nu_5 = [LRG\alpha\beta\gamma]\cdot K_5, K_5 = 50h^{-1} \tag{5.5}$$

$$\nu_6 = [G\alpha\beta\gamma]\cdot K_6, K_6 = 0.2h^{-1} \tag{5.6}$$

$$\nu_7 = [G\alpha^{GTP}]\cdot K_7, K_7 = 0.05h^{-1} \tag{5.7}$$

$$\nu_8 = [G\beta\gamma]\cdot[Effector]\cdot K_8, K_8 = 10nM^{-1}h^{-1} \tag{5.8}$$

$$\nu_9 = [G\beta\gamma Effector]\cdot K_9\, K_9 = 1h^{-1} \tag{5.9}$$

$$\nu_{10} = [G\alpha^{GDPP}]\cdot K_{10}, K_{10} = 1000h^{-1} \tag{5.10}$$

$$\nu_{11} = [G\beta\gamma]\cdot[G\alpha^{GDP}]\cdot K_{11}, K_{11} = 1000nM^{-1}h^{-1} \tag{5.11}$$

$$\nu_{12} = [P_i]\cdot K_{12}, K_{12} = 10h^{-1} \tag{5.12}$$

$$\nu_{13} = [G\alpha^{GTP}]\cdot[RGS]\cdot K_{13}, K_{13} = 500nM^{-1}h^{-1} \tag{5.13}$$

$$\nu_{14} = [G\alpha^{GTP}RGS]\cdot K_{14}, K_{14} = 2.5h^{-1} \tag{5.14}$$

$$\tag{5.15}$$

$$\frac{d[L]}{dt} = -\nu_1 - \nu_4 \tag{5.16}$$

$$\frac{d[R]}{dt} = \nu_1 - \nu_2 \tag{5.17}$$

$$\frac{d[LR]}{dt} = \nu_1 - \nu_3 + \nu_5 \tag{5.18}$$

$$\frac{d[RG\alpha\beta\gamma]}{dt} = \nu_2 - \nu_4 \tag{5.19}$$

$$\frac{d[LRG\alpha\beta\gamma]}{dt} = \nu_3 + \nu_4 - \nu_5 \tag{5.20}$$

$$\frac{d[G\alpha\beta\gamma]}{dt} = \nu_1 1 - \nu_2 - \nu_3 - \nu_6 \tag{5.21}$$

$$\frac{[G\alpha^{GTP}]}{dt} = \nu_5 + \nu_6 - \nu_7 - \nu_{13} \tag{5.22}$$

$$\frac{[G\alpha^{GDPP}]}{dt} = \nu_7 - \nu_{10} + \nu_{14} \tag{5.23}$$

$$\frac{[G\alpha^{GDP}]}{dt} = \nu_{10} - \nu_{11} \tag{5.24}$$

$$\frac{[P_i]}{dt} = \nu_{10} - \nu_{12} \tag{5.25}$$

$$\frac{[G\beta\gamma]}{dt} = \nu_5 + \nu_6 - \nu_8 + \nu_9 - \nu_{11} \tag{5.26}$$

$$\frac{[G\beta\gamma Effector]}{dt} = \nu_8 - \nu_9 \tag{5.27}$$

$$\frac{[Effector]}{dt} = \nu_9 - \nu_8 \tag{5.28}$$

$$\frac{[RGS]}{dt} = \nu_{14} - \nu_{13} \tag{5.29}$$

$$\frac{[G\alpha^{GTP}RGS]}{dt} - \nu_{13} - \nu_{14} \tag{5.30}$$

$$\frac{d[Z_1]}{dt} = [G\beta\gamma Effector]\cdot\alpha - [Z_1]\cdot\alpha \tag{5.31}$$

$$\frac{d[Z_2]}{dt} = [Z_1]\cdot\alpha - [Z_2]\cdot\alpha \tag{5.32}$$

$$\frac{d[Z_3]}{dt} = [Z_2]\cdot\alpha - [Z_2]\cdot\alpha \tag{5.33}$$

$$\tag{5.34}$$

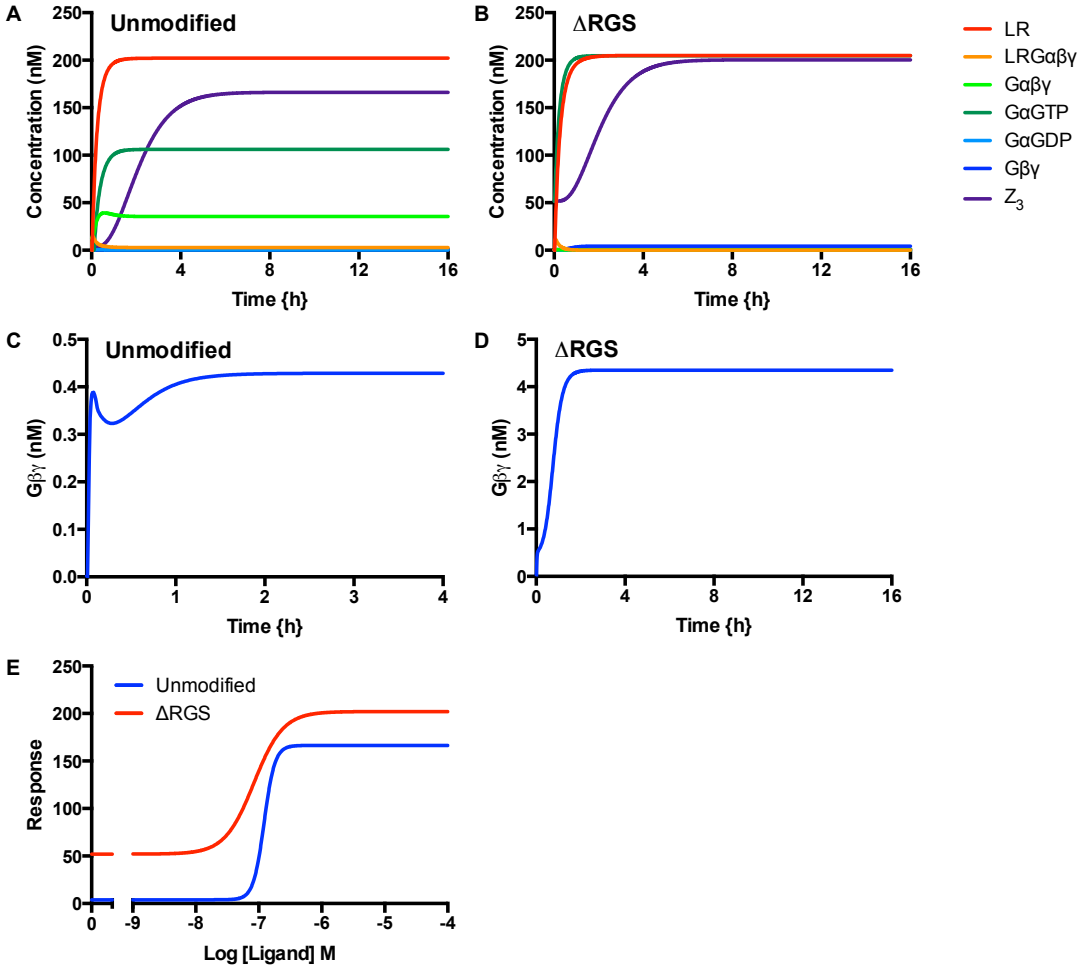

FIGURE 5.10: **Output of the Smith *Sc. cerevisiae* pheromone response model.** The Smith model was modified to make G$\beta\gamma$ the effector, as in *Sc. cerevisiae* and implemented in Matlab. The system was equilibrated for 14 hours prior to addition of ligand. Simulations were continued for 16 hours in the presence of ligand. The system was solved using the ODE23s solver. A ΔRGS phenotype was recreated by setting the initial [RGS] to 0. **A.** Time courses were performed using the unmodified model and **B.** ΔRGS variant in the presence of ligand. **C.** The G$\beta\gamma$ time courses of the modified model and **D.** ΔRGS variants. **E.** Concentration-response curves were constructed by [Z_3] after 16 hours simulation with ligand. (Figure 5.10).

The time course profiles of Figure 5.10 show different trends to the Kofahl and Klipp model output (Figure 5.7). This may not be surprising given that the original Smith model was developed to replicate end point concentration-response curves. Here, the majority of species in the model, including active G proteins, are activated quickly and persist throughout the simulation. However, the basal transcriptional activation, prior to addition of ligand, is greatly enhanced in the ΔRGS strain. Given the ability of this model to replicate ligand-independent signalling it is hardly surprising that an elevated [Z_3] is observed during equilibration in the absence of a negative regulator.

The G$\beta\gamma$ time courses contrast with that of Kofahl and Klipp (2004), and therefore experimentally determined trends (Yi et al. (2003), Figure 5.10. Here, G$\beta\gamma$ is swiftly generated within 10 minutes of ligand application, shows a slight decline before increasing and persisting at approximately 0.4nM. However, the ΔRGS variant shows an increase in free [G$\beta\gamma$] which holds at approximately 4nM (Figure 5.10D). The concentration-response curves of this model show a marginal leftwards shift in sensitivity in the ΔRGS variant ($pEC_{50} = 7.1$ compared to 6.9) and a marginal increase in E_{max} (Figure 5.10E). This is reminiscent, if not an exact match, to the equivalent experimental data where $SST2$ and $\Delta SST2$ genotypes have been reported to have potencies of 6.3 and 8.1, respectively (Hao et al., 2003).

The Smith model and the Kofahl and Klipp model also contrast in basal activity. Kofahl and Klipp (2004) assume that there is no constitutive receptor or G protein activation. Consequently, this model produces no output in absence of ligand and does not require equilibration. However, Smith et al. (2009) have produced a much more comprehensive G protein cycle containing signalling in response to spontaneous receptor and G protein activation. This requires that the model be equilibrated for 14 hours to simulate endogenous signalling processes prior to ligand application. While no detectable β-galactosidase activity was observed for the A_1R in *Sc. cerevisiae*, the $A_{2A}R$ is noted for its constitutive activity.

Though the Smith model has a far more comprehensive G protein cycle, it is far less capable of recreating the time course profiles experimentally determined by Yi et al. (2003). In contrast Kofahl and Klipp (2004) replicate the dynamic trends of the G protein cycle, at least for 1μM ligand. However, Kofahl and Klipp contains many reactions, throughout the pheromone response, that a minimal quantitative model of the G protein cycle can dispense with. The Smith model condenses an equivalent MAPK cascade to three simple equations. The strengths of these two model frameworks can be combined to greatly inform novel model development.

5.3 Model development

The aim of this study is to build and implement a minimal mathematical framework to understand the kinetics of functional selectivity of the A_1R in yeast. Through combining the strengths of Kofahl and Klipp (2004) and Smith et al. (2009), the G protein cycle and transcriptional delay respectively, we hope to create a simple representation of G protein signalling in yeast based on the law of mass action kinetics.

5.3.1 General model assumptions

A central premise of systems biology is that a model is only as good as its assumptions. Therefore assumptions represent compromises that can be the strength or Achille's heel of any given framework. The model developed here will focus on the receptor-ligand interaction and downstream G protein cycle. The majority of these assumptions will be centred on the initial conditions, particularly species concentrations. This is crucial given that ODE models are subject to mass action kinetics where the rate of reaction is a product of an intrinsic rate constant and the concentration of the reacting components.

While the receptor and G protein concentrations have already been determined for the *Sc. cerevisiae* pheromone response, all strains used in this study have been genetically modified. In particular the endogenous GPCR, STE2, has been deleted and replaced by the A_1R. Moreover, the A_1R is under the control of a constitutive promoter at the *URA3* locus. In contrast the STE2 receptor is under the control of a pheromone-responsive promoter. Consequently, A_1R expression levels could vary from that of STE2 in an unmodified strain. However, in the absence of any data regarding receptor number, we are forced to assumed an A_1R concentration of 160nM, the experimentally determined endogenous STE2 concentration.

The $G\beta\gamma$ dimer, and the relevant loci, have been unmodified in this strain. Therefore a $G\beta\gamma$ concentration of 160nM was assumed. The GPA1 gene, however, has been deleted. GPA1, and GPA1 transplants have been integrated at the *TRP1* locus under the control of the endogenous *GPA1* promoter. This leads to the assumption that GPA1 expression in the transplant system is consistent with that of unmodified strains, i.e. 160nM. Credibility is led to this assumption by the Western blots of Brown et al. (2000), who developed this system, that indicate equal GPA1 expression in all strains.

The rate parameters determined by Yi et al. (2003) will be used as initial conditions for model fitting. These parameters were determined using a FRET reporter system in which *GPA1* and *STE18* have been deleted and fluorescently-modified variants integrated into their respective loci under the control of their endogenous promoters. The fluorophores are cyan fluorescent protein (CFP) and yellow fluorescent protein (YFP), derivatives of GFP, and can interfere with protein-protein interactions thus influencing the results. Given that

these parameters have been used to build more comprehensive models, and that we will only be using these rates as initial conditions for fitting, these constants will be used to directly inform the model. However, in the absence of an RGS, G protein-mediated GTP hydrolysis is under the sole control of the RGS-fold of the Gα subunit. We will therefore assume that GTP-hydrolysis and heterotrimeric G protein reformation are not influenced by the receptor. Consequently, GTP-hydrolysis will be constrained to 14.4 nM^{-1} $hour^{-1}$, as determined by Yi et al. (2003) and implemented by Kofahl and Klipp (2004), Smith et al. (2009) and Croft et al. (2013).

A further experimental consideration of the mathematical model being developed here is is one of structural identifiability. This aspect of dynamic modelling is concerned with uniqueness of solutions. Put simply, this means a given model output, fitted to experimental data, can only be a consequence of a unique combination of initial conditions and parameters (Chis et al., 2011b). If a model structure fits this description it is termed globally and structurally identifiable (Lockley et al., 2015). However, in the absence of global identifiability, local identifiability can be achieved in which one can isolate the neighbourhood a parameter resides in. While not ideal for model fitting, local identifiability can be useful (Raue et al., 2009, 2010). While mathematically intensive, there are a number of user-friendly tools to perform structural identifiability analysis (Chis et al., 2011a; Ogungbenro and Aarons, 2011; Maiwald et al., 2012). Here, structural identifiably was performed as a the first step of model development. The GenSSI toolbox for Matlab was used due to its availability and relative ease of use (Chis et al., 2011a).

There are ways to increase the identifiability of a mathematical model. The parameters or species concentrations that can be measured directly are called observables. The more observables available to inform a mathematical model, the greater its identifiability and the more accurate its predictions (Anguelova et al., 2012). At present, the *Sc. cerevisiae* transplant strains contain two potential measures of transcription, growth and β-galactosidase activity. This study exploits the latter. But with a single observable, global and structurally identifiability can be difficult to achieve. Minimising the model to its most basic components can compensate for this. For example, no significant basal signal is produced by the A_1R in yeast. Therefore constitutive receptor and G protein activation can be sacrificed for the sake of simplicity. Further, not all parameters need to be fitted. Parameters that are unlikely to vary as a function of ligand or G protein, such as those governing downstream signalling and transcription, can be constrained to increase the likelihood of global and structural identifiability.

5.3.2 A simple model of G protein signalling in yeast

An ODE model of G protein signalling in yeast was constructed with structural identifiability as a primary concern. At present this framework has only one observable, the β-galactosidase transcriptional reporter. For this reason, the model must be minimal and consist of the basic processes that we know happen and can potentially measure. Increased complexity requires more observables for accurate model fitting. As no ligand-independent signalling of the A_1R is detectable by β-galactosidase assay, spontaneous receptor activation has been omitted. This simple model uses four processes that can eventually be experimentally validated.

- Ligand binds the receptor to promote receptor activation. Fluorescent ligands could be used to determine ligand binding rates in real time.
  $L + R -> R^*$, K_1.
- Active receptor activates a G protein that can be measured through FRET. However, the FRET studies of Yi et al. (2003) only measure the rate at which GPA1 and STE18 move within/ beyond a certain radius. Consequently, a two step G protein cycle is considered. The receptor G protein activation mechanism of Kofahl and Klipp (2004) is employed to accommodate both pre coupling and collision coupling mechanisms of receptor-dependent G protein activation.
  $G_{off} -> G_{on}$, $K_2 \cdot [R^*]$
  $G_{on} -> G_{off}$, K_3
- Active receptor is internalised. Internalisation, or lack thereof, can be elucidated using fluorescent ligand or fluorescent receptors.
  $R^* -> \phi$, K_4, where ϕ denotes a null set to which a species is lost.

Finally, G_{on} simulates a delayed transcriptional response using the delay system of Smith et al. (2009). This delay is meant to be constrained and not subject to variation between ligands or yeast strains. A schematic of these model is shown in Figure 5.11 and the equations detailed in (5.35). GenSSI confirmed that this model structure is globally and structurally identifiable.

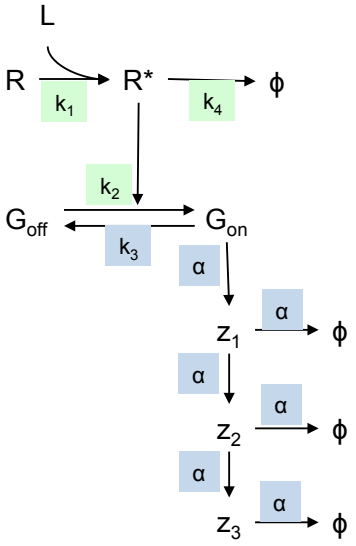

Figure 5.11: **A simple model of G protein signalling in yeast.** Here ligand activates a receptor. The active receptor catalyses the activation of a G protein. Negative regulation of this pathway is achieved through G protein deactivation or receptor internalisation. ϕ denotes a null set or loss of a species from the model. Sequential activation of Z_1, Z_2 and Z_3 is a simplification of the MAPK cascade and downstream transcription of β-galactosidase. Parameters to be fitted are shown in green. Parameters to be constrained are highlighted in blue.

$$\nu_1 = [L]\cdot[R]\cdot K_1 \tag{5.35}$$

$$\nu_2 = [R*]\cdot[G_{off}]\cdot K_2 \tag{5.36}$$

$$\nu_3 = [G_{on}]\cdot K_3 \tag{5.37}$$

$$\nu_4 = [R*]\cdot K_4 \tag{5.38}$$

$$\frac{d[L]}{dt} = -\nu_1 = -[L]\cdot[R]\cdot K_1 \tag{5.39}$$

$$\frac{d[R]}{dt} = \nu_1 = -[L]\cdot[R]\cdot K_1 \tag{5.40}$$

$$\frac{d[R*]}{dt} = \nu_1 - \nu_4 = [L]\cdot[R]\cdot K_1 - [R*]\cdot K_4 \tag{5.41}$$

$$\frac{d[G_{off}]}{dt} = \nu_3 - \nu_2 = [G_{on}]\cdot K_3 - [R*]\cdot[G_{off}]\cdot K_2 \tag{5.42}$$

$$\frac{d[G_{on}]}{dt} = \nu_2 - \nu_3 = [R*]\cdot[G_{off}]\cdot K_2 - [G_{on}]\cdot K_3 \tag{5.43}$$

$$\frac{d[Z_1]}{dt} = [G_{on}]\cdot\alpha - [Z_1]\cdot\alpha \tag{5.44}$$

$$\frac{d[Z_2]}{dt} = [Z_1]\cdot\alpha - [Z_2]\cdot\alpha \tag{5.45}$$

$$\frac{d[Z_3]}{dt} = [Z_2]\cdot\alpha \tag{5.46}$$

$$\tag{5.47}$$

This model was implemented in Matlab using receptor and inactive G protein (G_{off}) concentrations of 160nM (Figure 5.12). Rate constants were assumed from Kofahl and Klipp (2004) as shown below.

$$K_1 = 0.072nM^{-1}hour^{-1} \tag{5.48}$$

$$K_2 = 0.216nM^{-1}hour^{-1} \tag{5.49}$$

$$K_3 = 14.4hour^{-1} \tag{5.50}$$

$$K_4 = 14.4hour^{-1} \tag{5.51}$$

$$\tag{5.52}$$

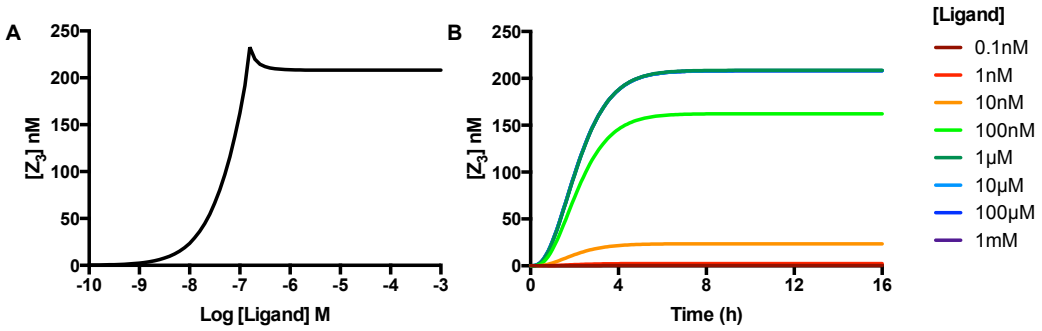

Figure 5.12: **The output of a simple model of G protein signalling.** The model described in (Figure 5.11) was implemented in Matlab and solved using the ODE23s solver. The system was simulated over 16 hours and species Z_3 used as a measure of pathway activation. At t_0 [R] = 160nM, [G_{off} = 160nM and all other species = 0. K_1 = 0.072 nM^{-1} $hr^{-}1$, K_2 = 0.216 nM^{-1} $hr^{-}1$, K_3 = 1.44 $hr^{-}1$ and K_4 = 14.4 $hr^{-}1$. α = 1.5.

Figure 5.12 show sigmoidal time course profiles that plateau after 3-4 hours simulation. However, this model also shows a maximal level of signal at 100nM ligand before a slight decrease in activity at higher concentrations. This is particularly noticeable on the concentration-response curve produced by this model (Figure 5.12B). However, this is a trend shared with Kofahl and Klipp (2004) and may be a consequence of internalisation acting as the sole receptor-level negative regulator of signalling.

To understand the effect of each of these parameters on model output a parameter sensitivity analysis was performed. Each rate constant was varied independently and simulations performed for 16 hours using the ODE23s solver (Figure 5.13). All other parameters were constrained. Time course profiles are shown for 1mM ligand so that the agonist is not the limiting factor.

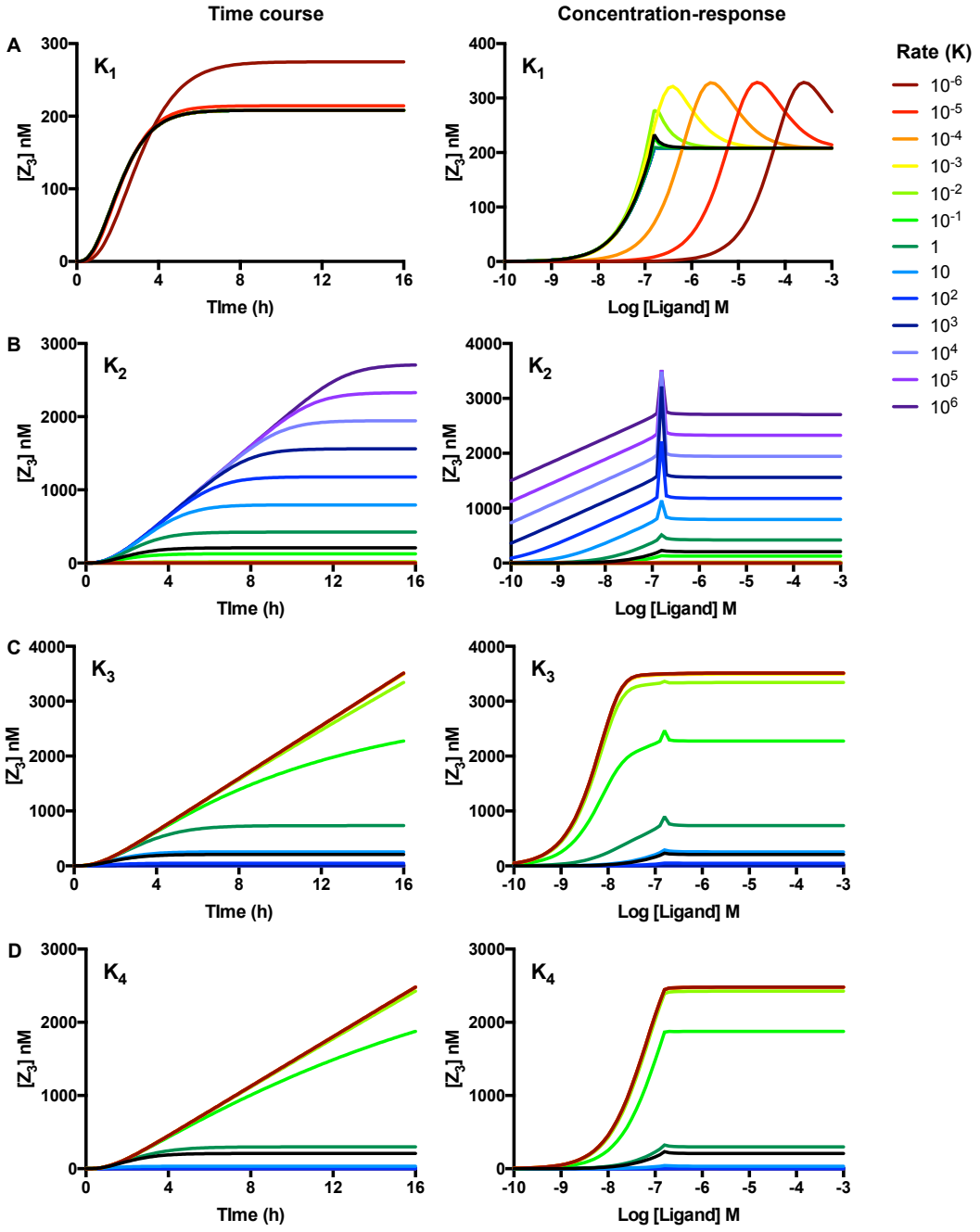

FIGURE 5.13: **Parameter sensitivity analysis of a simple model of G protein signalling.** The model described in (Figure 5.11) was implemented in Matlab and solved using the ODE23s solver. The system was simulated over 16 hours and species Z_3 used as a measure of pathway activation. At t_0 [R] = 160nM, [G_{off} = 160nM and all other species = 0. $K_1 = 0.072$ nM^{-1} hr^{-}1, $K_2 = 0.216$ nM^{-1} hr^{-}1, $K_3 = 1.44$ hr^{-}1, $K_4 = 14.4$ hr^{-}1 and $\alpha = 1.5$. These baseline simulations are shown as a black line. Each parameter was individually adjusted and outputs compared. Time course profiles shown are for 1mM ligand. Time courses profiles and concentration-response curves as a function of **A.** K_1, **B.** K_2, **C.** K_3 and **D.** K_4.

Figure 5.13 shows some particularly interesting relationships between the parameters underlying the G protein cycle and the model output. K_1, the ligand-binding rate largely influences the pEC_{50} of the concentration-response curves but cannot increase it beyond 7.3. This parameter also appears to enhance and prolong the peak in signal at an intermediate ligand concentration.

The G protein-activation constant, K_2 appears to influence the magnitude and delay of the transcriptional response. This manifests as an increase in both pEC_{50} and E_{max} on the model concentration-response curve. Unsurprisingly, the G protein-inactivation constant, K_3 has the opposite effect.

K_4, the active receptor internalisation rate, negatively influences the delay in transcription and magnitude of the response. This, in turn, decreases the E_{max} and pEC_{50} of the concentration response curve. Reducing the receptor internalisation rate to ≤ 0.1 hr^{-1} abolishes the decrease in activity as the ligand concentration increases beyond E_{max}. This confirms that this effect, also present in Kofahl and Klipp (2004), is an artefact of internalisation.

An important aspect of this model is the transcriptional delay. The intention is to use this delay to form a "black box" to estimate downstream signalling and transcription. Consequently, α will be constrained for all ligands and strains modelled. The parameter sensitivity analysis was extended to α to understand the significance of this parameter to the model output. These simulations demonstrate that α simultaneously influences both the magnitude and delay of the transcriptional response (Figure 5.14).

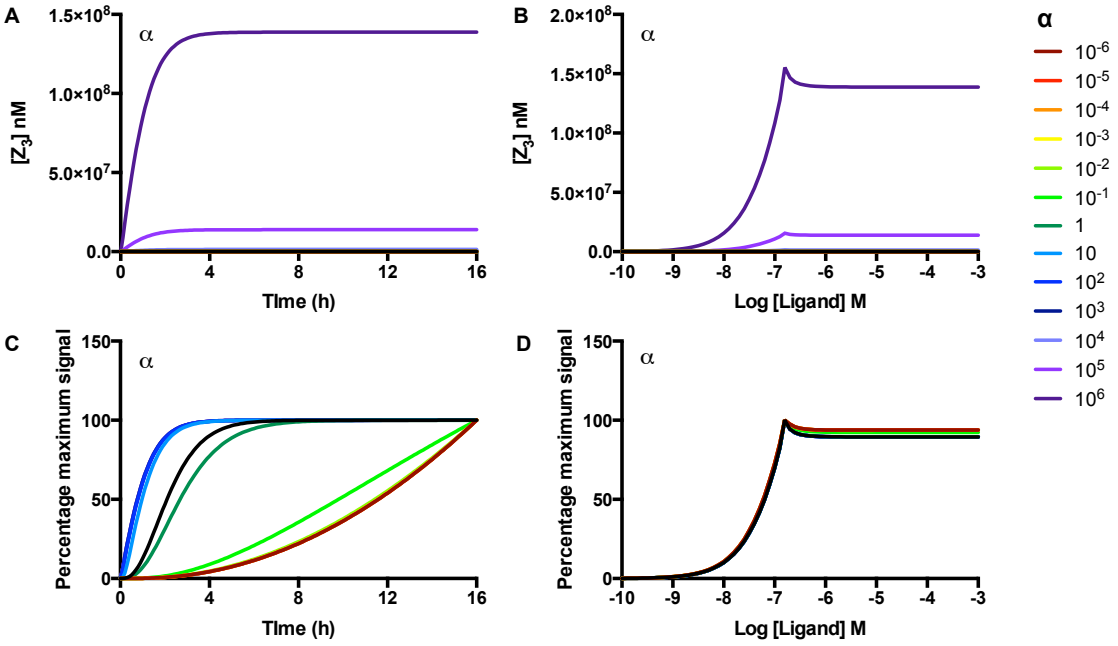

FIGURE 5.14: **Parameter sensitivity analysis of the delay equations.** The model described in (Figure 5.11) was implemented in Matlab and solved using the ODE23s solver. The system was simulated over 16 hours and species Z_3 used as a measure of pathway activation. At t_0 [R] = 160nM, [G_{off} = 160nM and all other species = 0. K_1 = 0.072 nM^{-1} $hr^{-}1$, K_2 = 0.216 nM^{-1} $hr^{-}1$, K_3 = 1.44 $hr^{-}1$, K_4 = 14.4 $hr^{-}1$ and α = 1.5. These baseline simulations are shown as a black line. α was manually adjusted and outputs compared. Time course profiles are shown for 1mM ligand. **A.** Time courses profiles and **B.** concentration-response curves as a function of α. **C.** Time courses profiles and **D.** concentration-response curves as a function of α where each curve has been expressed as a percentage of its own maximum.

The influence of α on both the magnitude and delay of the time course data presents a problem for model fitting. For a high ligand concentration, the EC_{50} occurs at approximately 4 hours. The response has also been scaled at a percentage of the maximum response. In the absence of contrary data, this has been assumed to be the A_1R::GPA1/G$\alpha_{i1/2}$ E_{max} (39.7 $\pm$ 0.7 mU). To independently manipulate the E_{max} and delay of the model time course output the parameters of the delay were split as shown:

$$\frac{d[Z_1]}{dt} = \alpha \cdot [G_{on}] - \beta \cdot [Z_1] \tag{5.53}$$

$$\frac{d[Z_2]}{dt} = \alpha_1 \cdot [Z_1] - \beta_1 \cdot [Z_2] \tag{5.54}$$

$$\frac{d[Z_3]}{dt} = \alpha_2 \cdot [Z_2] - \beta_2 \cdot [Z_3] \tag{5.55}$$

$$\tag{5.56}$$

K_1, K_2, K_3 and K_4 were constrained to 0.0072 nM^{-1} hr^{-1}, 0.216 nM^{-1} hr^{-1}, 1.44 hr^{-1} and 14.4 hr^{-1} respectively. Each α and β parameter were initially set to 1.5 and manipulated independently. Simulations were performed to assess the affect of these parameters on model output (Figure 5.15 and Figure 5.16).

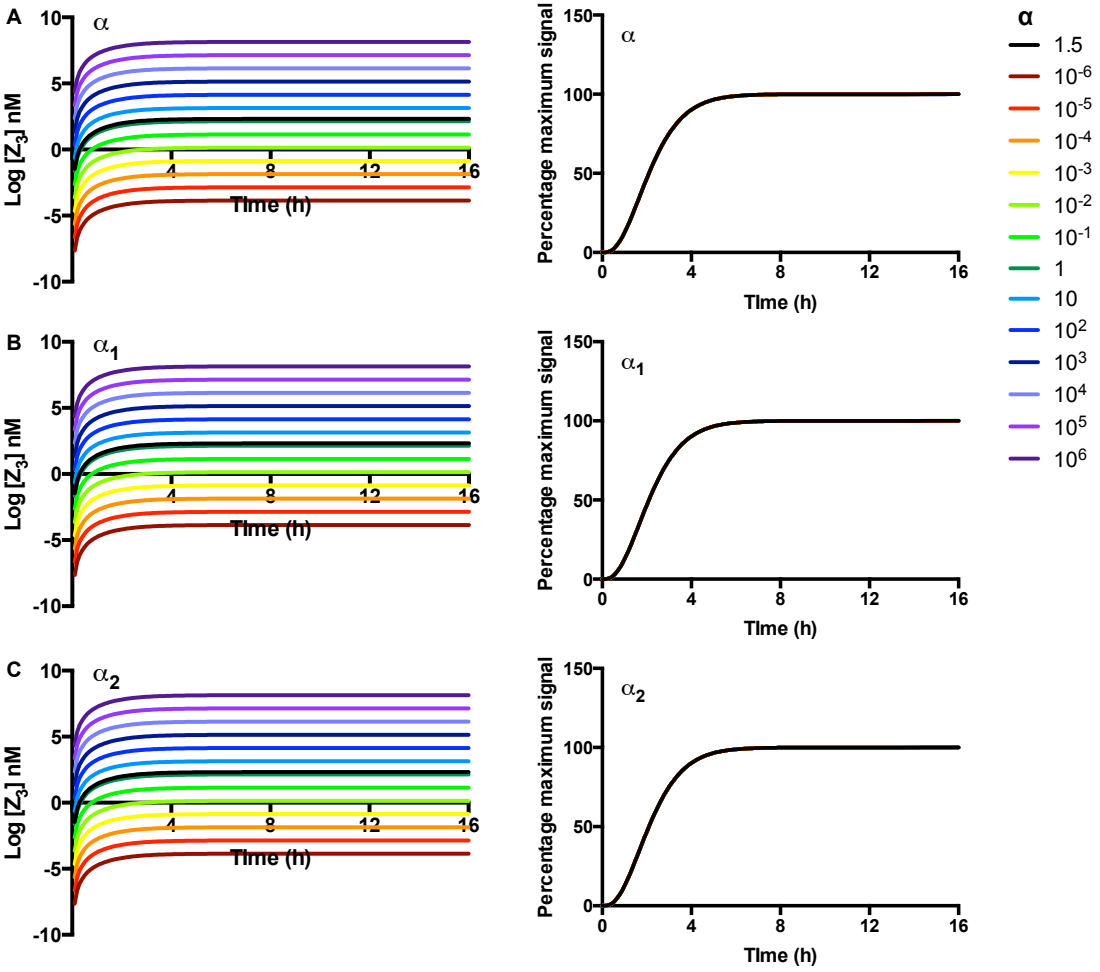

FIGURE 5.15: **Parameter sensitivity analysis of the α delay rates.** The model described in (Figure 5.11) was implemented in Matlab and solved using the ODE23s solver. The system was simulated over 16 hours and species Z_3 used as a measure of pathway activation. At t_0 [R] = 160nM, [G_{off} = 160nM and all other species = 0. K_1 = 0.072 nM^{-1} $hr^{-}1$, K_2 = 0.216 nM^{-1} $hr^{-}1$, K_3 = 1.44 $hr^{-}1$, K_4 = 14.4 $hr^{-}1$, α = 1.5, β = 1.5, α_1 = 1.5, β_1 = 1.5, α_2 = 1.5, β_2 = 0. These baseline simulations are shown as a black line. **A.** α, **B.** α_1 and **C.** α_2 were individually adjusted, with all other parameters constrained, and outputs compared. Time course profiles are shown for 1mM ligand. Also shown are the same curves expressed as a percentage of their own maximum.

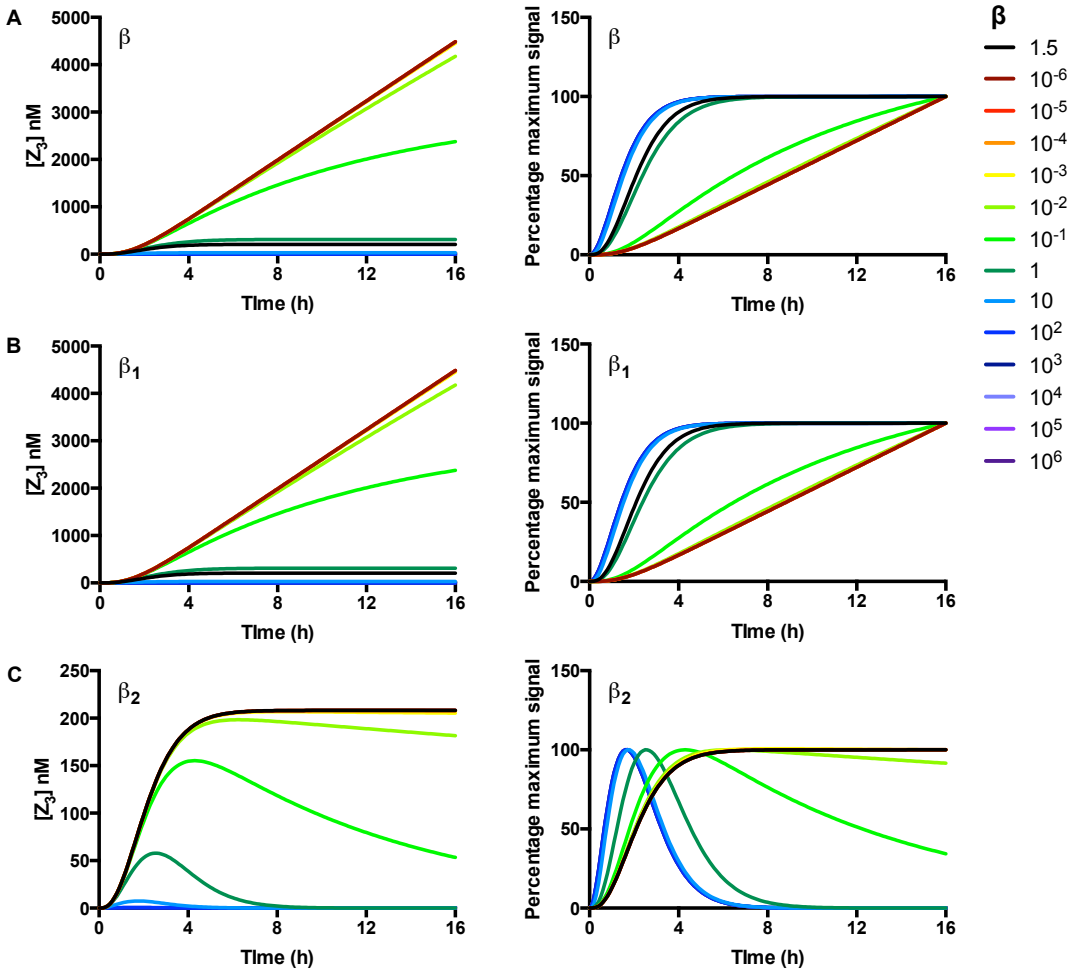

Figure 5.16: **Parameter sensitivity analysis of the β delay rates.** The model described in (Figure 5.11) was implemented in Matlab and solved using the ODE23s solver. The system was simulated over 16 hours and species Z_3 used as a measure of pathway activation. At t_0 [R] = 160nM, [G_{off} = 160nM and all other species = 0. $K_1 = 0.072$ nM^{-1} $hr^{-}1$, $K_2 = 0.216$ nM^{-1} $hr^{-}1$, $K_3 = 1.44$ $hr^{-}1$, $K_4 = 14.4$ $hr^{-}1$, $\alpha = 1.5$, $\beta = 1.5$, $\alpha_1 = 1.5$, $\beta_1 = 1.5$, $\alpha_2 = 1.5$, $\beta_2 = 0$. These baseline simulations are shown as a black line. These baseline simulations are shown as a black line. **A.** β, **B.** β_1 and **C.** β_2 were individually adjusted, with all other parameters constrained, and outputs compared. Time course profiles are shown for 1mM ligand. Also shown are the same curves expressed as a percentage of their own maximum.

α parameters influence the magnitude of the response with no appreciable effects on the delay (Figure 5.15). This is clear when then the sigmoidal time course curves are expressed as a percentage of its own maximum and overlap precisely. However, the β parameters influence both the magnitude and delay of the transcriptional response (Figure 5.16). This is encouraging as the β parameters can be used to set the delay while the α parameters can be used to scale the response. Given that this model is globally and structurally identifiable a unique combination of parameters can be determined to fit the transcriptional delay.

This model framework was implemented in the Potter's Wheel toolbox for Matlab. This software uses the Levenberg-Marquart algorithm to fit ODE models to experimental data. This uses a least squares regression approach to minimise the difference between the model output and the experimental datapoint, χ^2 (here $\chi^2 < 300$ is considered an acceptable fit). However, this approach, while incredibly powerful, has a fundamental weakness. The model will continue to fit while χ^2 is decreasing, but an increase in χ^2 forces the algorithm to assume that a best fit has been achieved. This could also be result of the a local numerical minima, and a better fit may exist that this model has not yet explored. Consequently, this algorithm is reliant on initial conditions and starting parameter values. Fortunately, the *Sc. cerevisiae* pheromone response has been very well characterised and the experimental values of STE2-G protein interaction are already known. These parameters and species concentrations were used as initial conditions for model fitting to the experimental time course data of A_1R::GPA1/Gα_{i3} (Figure 5.17).

The model was first fitted to the NECA time course data of the A_1R::GPA1/Gα_{i3} strain. The model shows good agreement with the experimental data (χ^2=366.79). However, the fit for 100nM NECA, an intermediate response, is somewhat less accurate. Regardless, this fit makes some very interesting predictions (Table 5.3). In comparison to the initial values, experimentally validated for the endogenous GPCR in this system, the ligand binding constant, K_1, is remarkably low (0.072 $^{-1}hour^{-1}$ and 1.04e^{-5} hour^{-1}, for initial and fitted values respectively). In contrast the G protein activation rate, K_2, is 213-fold higher than the initial estimate (46.17 $^{-1}hour^{-1}$ compared to 0.216 nM $^{-1}hour^{-1}$). While G protein-inactivation was constrained to 14.4 hr^{-1}, the receptor internalisation rate is substantially lower than that of the initial value (0.2 hr^{-1} and 14.4 hr^{-1}, respectively). This is encouraging given the internalisation artefacts of Figure 5.14 and the trends in model output shown through manipulation of the K_4 parameter. With the exception of 100nM ligand, the transcriptional delay shows good agreement with experimental trends ($\chi^2 = 236.3$). Consequently, the α and β parameters were constrained for fitting to the time course data of adenosine and 2CCPA.

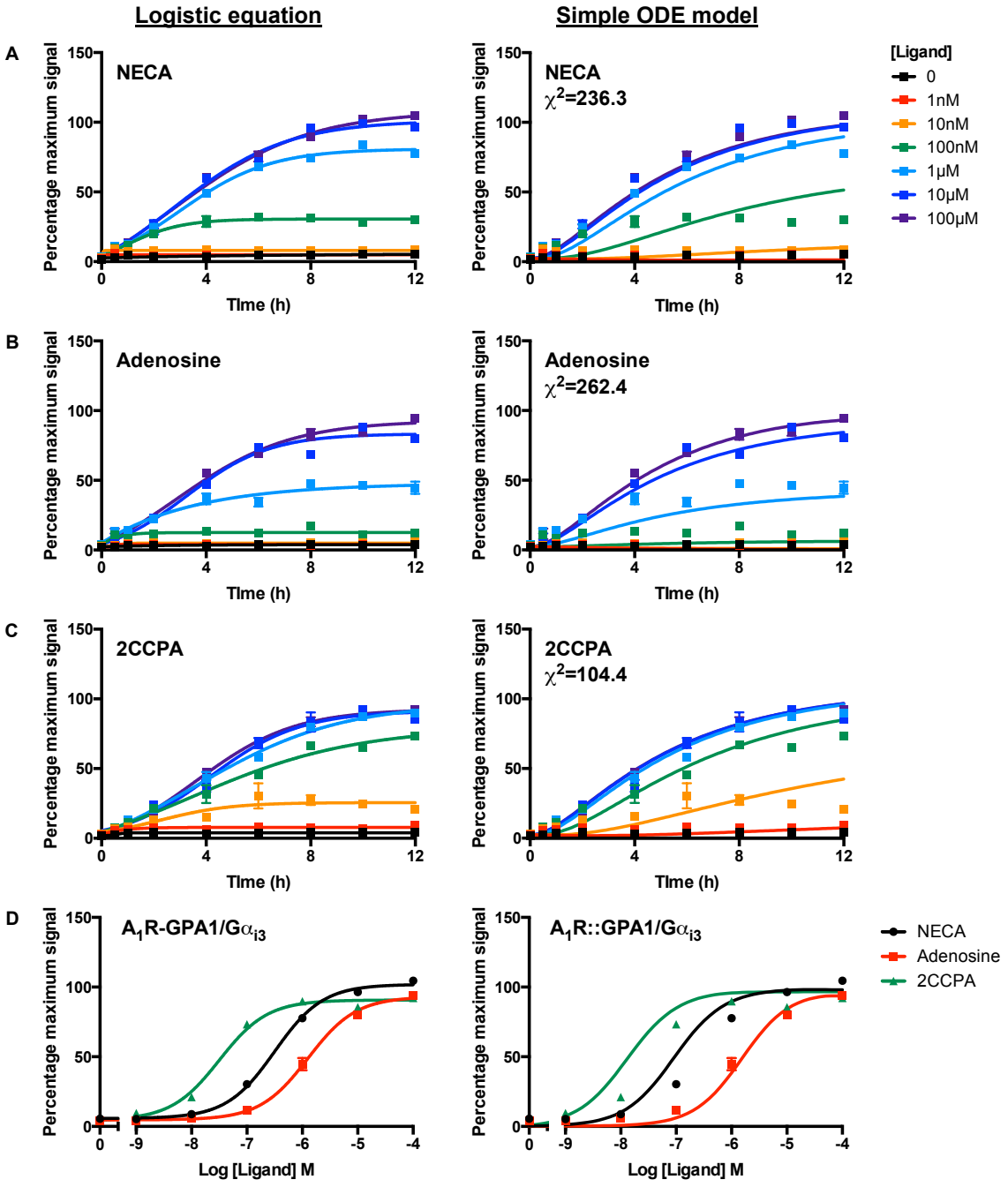

Figure 5.17: **A novel model of G protein signalling yeast fitted to the experimental time course data of the A_1R::GPA1/Gα_{i3} integrate strain.** The simple G protein model of Figure 5.11 was implemented in Potter's wheel using $K_1 = 0.072$ nM^{-1} hr^{-1}1, $K_2 = 0.216$ nM^{-1} hr^{-1}1, $K_3 = 1.44$ hr^{-1}1, $K_4 = 14.4$ hr^{-1}1. All α and β parameters were initialised as 1.5. R and G$_off$ were assumed to be 160nM, all other concentrations were set to 0nM. The model was fitted to experimental time course data using the Levenberg-Marquart algorithm. Resulting parameter sets were implemented and simulated using the ODE23s solver for 12 hours. Equivalent logistic equation fits have been included for clarity. **A.** NECA. **B.** Adenosine. **C.** 2CCPA. **D.** Concentration-response curves after 12 hours incubation with ligand.Data points represent mean ± S.E.M. of triplicate repeats. Solid lines represent model output. $\chi^2 < 300$ was considered a good git.

Table 5.3: **Parameters of a simple G protein signalling ODE model fitted to the time course data of the A_1R::GPA1/Gα_{i3} strain.** The rate constants shown were used as initial conditions for fitting to the NECA time course data of (Figure 5.17). The α and β constants were constrained and the parameter set used to estimate the parameters underlying the equivalent adenosine and 2CCPA data.

K	**Initial**	**NECA**	**Adenosine**	**2CCPA**
K_1 (nM^{-1} $hour^{-1}$)	0.072	$1.04e^{-5}$	$1.83e^{-6}$	0.0004
K_2 (nM^{-1} $hour^{-1}$)	0.216	46.17	$3.02e^{-3}$	3.28
K_3 ($hour^{-1}$)	14.4	14.4	14.4	14.4
K_4 ($hour^{-1}$)	14.4	0.2	28.6	0.008
α	1.5	11.203	11.203	11.203
β	1.5	208.27	208.27	208.27
α_1	1.5	24.362	24.362	24.362
β_1	1.5	0.909	0.909	0.909
α_2	1.5	0.100	0.100	0.100
β_2	1.5	0.207	0.207	0.207
χ^2		236.3	262.4	104.4

The model fits for adenosine, while acceptable ($\chi^2 < 300$), are less consistent with the experimental data than those of NECA, as evidenced by a higher χ^2 value (Table 5.3). However, there is a much closer alignment between model output and the time course of an intermediate adenosine concentration (1μM). The predicted rates of ligand-binding and G protein-activation ($1.83e^{-6}$ nM^{-1} $hour^{-1}$ and $3.02e^{-3}$ nM^{-1} $hour^{-1}$ respectively) are substantially lower than their NECA counterparts. However, the internalisation rate shows a two-fold increase relative to the experimentally known value for STE2 (28.6 $hour^{-1}$ compared to 14.4 $hour^{-1}$. Thus, this model suggests that receptor-level negative regulation has a greater influence on adenosine in the A_1R::GPA1/Gα_{i3} strain than NECA.

This simple model of G protein-signalling yielded a good fit to the time course data of 2CCPA in this strain (Figure 5.17, Table 5.3, $\chi^2 = 104.4$). This predicts that ligand-binding rates and G protein-activation rates are higher for 2CCPA than for NECA and adenosine. The receptor internalisation rate is substantially lower than the experimentally determined value for STE2 (Table 5.3) which may be consistent with predictions for NECA.

Taken together, this model predicts the ligand-binding, G protein-activation and receptor internalisation are influenced by the ligand consistent with functional selectivity. To further validate model output concentration-response curves were constructed from the simulated time course data at 12 hours. Non-linear regression of the logistic equation was used to compare the experimental concentration-response curves of A_1R::GPA1/Gα_{i3} and those generated using the simple model (Figure 5.17D, Table 5.3).

Table 5.4: **Pharmacological parameters of the A_1R::GPA1/Gα_{i3} endpoint concentration response curves and associated simple G protein model output.** The logistic equation was applied to the data of Figure 5.17D by non-linear regression. pEC_{50} $= -Log\ EC_{50}$ (potency), E_{max} = maximum level of signal. pEC_{50} and E_{max} of the model and experimental data were compared by Student's T-test, *P < 0.05.

Ligand	pEC_{50} **Experimental**	pEC_{50} **Model**	E_{max} **Experimental**	E_{max} **Model**
NECA	6.5±0.1	7.0±0.1*	101.9±1.2	98.3±0.1
Adenosine	5.9± 0.1	5.8±0.1	90.7±1.5	96.4±0.1*
2CCPA	7.5±0.1	7.9±0.1*	93.1±1.6	96.7±0.1

The endpoint data demonstrate significant differences between the NECA and 2CCPA model pEC_{50} and equivalent experimental data. While the model E_{max} is consistent with experimental data for these ligands it does deviate significantly for adenosine. Also, while the χ^2 values suggest that these are good fits, this model does not reproduce the plateau in signal at intermediate concentrations of NECA and adenosine (100nM and 10nM respectively). This may explain why this model does not accurately reproduce the concentration-response curve. This suggests weaknesses in the model structure. However, this model is fitted to time course data to infer dynamic processes throughout the ligand-receptor-G protein cycle. This provides an opportunity to validate this model. At present G protein activation cannot be measured directly in the yeast transplant strains. But these fitted parameter sets can be used to simulate G protein activation in the A_1R::GPA1/Gα_{i3} strain in response to NECA, adenosine and 2CCPA (Figure 5.18).

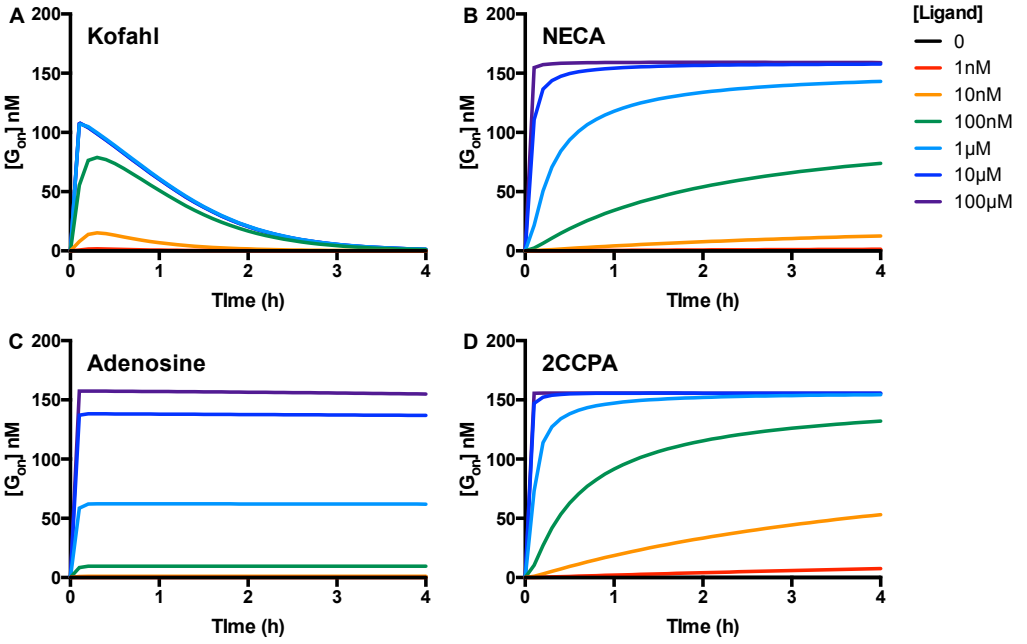

Figure 5.18: **Predicted G protein activation time course profiles for the A_1R::GPA1/G$\alpha_{i1/2}$ strain in a simple model of G protein signalling.** The parameter sets of Table 5.3 were used to simulate changes in G_{on}. **A.** Simulations using the rates of the Kofahl and Klipp model and fitted parameters of **B.** NECA, **C.** adenosine and **D.** 2CCPA.

The G protein activation profiles generated using the parameters of the Kofahl and Klipp profile show a rapid increase in free G$\beta\gamma$ followed by a steady decline. For the $\Delta SST2\Delta FAR1\Delta BAR1$ modification of the Kofahl and Klipp model the period of this trend is 30 minutes (Figure 5.7). However, in the simple model developed here, the G_{on} profile, as function of the same parameters, yields a similar trend but with a period of 4 hours for 1μM ligand (Figure 5.18A). This suggests a problem with the model structure. This is more evident for the NECA, adenosine and 2CCPA G_{on} profiles (Figure 5.18B, C and D, respectively). Here G_{on} is rapidly produced for all ligands and there is no appreciable decline in concentration. This is in complete contrast to the experimental FRET data generated by Yi et al. (2003), and recreated by Kofahl and Klipp (2004), where active G protein persists for less than 30 minutes. While this may indeed be correct for the A_1R, a non-native GPCR, in the yeast system, this profile is counterintuitive as it implies constant signalling through the pheromone-response pathway. Continuous signalling has been associated with toxicity. Also the discrepancies between the the endpoint predictions and experimental data for NECA, adenosine and 2CCPA shed doubt on the validity of this model structure (Figure 5.4). Consequently this framework may need to be modified or extended.

5.3.3 Development of an extended model of G protein signalling

The extended period of the G_{on} time course using the Kofahl and Klipp parameters in the simple model of G protein signalling may provide a means to improve this model structure. This minimal model was intended to include the most basic and essential features of G protein signalling in yeast for ease of fitting and structural identifiability concerns. However, the models of Kofahl and Klipp (2004) and Smith et al. (2009) have the G$\beta\gamma$ interacting with an effector to promote downstream signalling. Indeed, G$\beta\gamma$ is known to directly interact with the MAPK cascade of the *Sc. cerevisiae* pheromone response. Consequently, this scaffold will compete for free G$\beta\gamma$. This may explain the observed difference in G protein activation between the simple G protein model described here and the Kofahl and Klipp STE4 STE18 time course output. To explore this further the minimal model was extended to include a G_{on}-Effector interaction, as in Smith et al. (2009) and Croft et al. (2013) (Figure 5.19). The resulting G_{on}Effector complex then promotes downstream signalling via Z_1, Z_2 and Z_3. This new model will be referred to as the extended model.

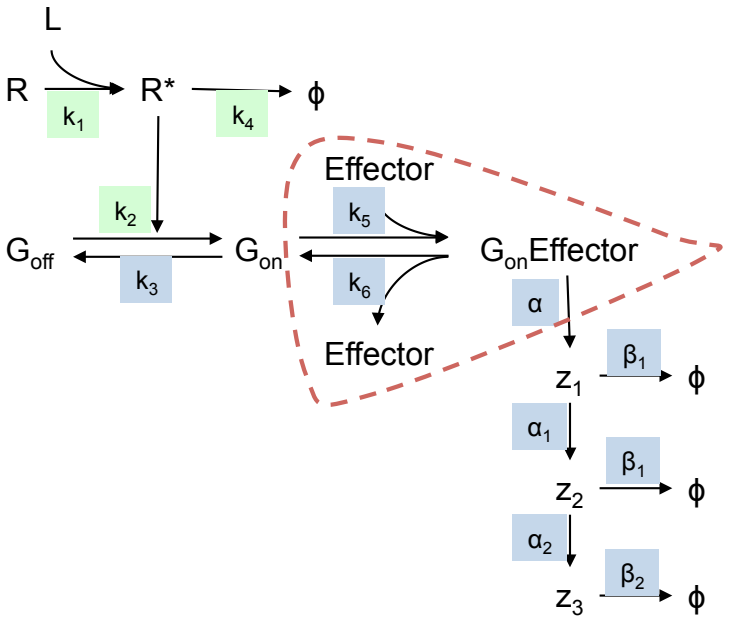

Figure 5.19: **A novel model of G protein signalling yeast including a G$\beta\gamma$ Effector interactions.** Here ligand binds an inactive receptor to form the active R* conformation. This can activate a G protein (G_{off} -> Gon) to trigger downstream signalling via an interaction with an Effector. Negative regulation in this model can be achieved through internalisation of R*, spontaneous G protein-inactivation or dissociation of G_{on} from the G_{on}Effector complex. Parameters to be fitted are highlighted in green. Parameters to be constrained are highlight in blue. The extension to the previous model iteration, the simple model, is highlighted with a red dotted line.

$$\nu_1 = [L]\cdot[R]\cdot K_1 \tag{5.57}$$

$$\nu_2 = [R*]\cdot[G_{off}]\cdot K_2 \ \nu_3 = [G_{on}]\cdot K_3 \tag{5.58}$$

$$\nu_4 = [R*]\cdot K_4 \tag{5.59}$$

$$\nu_5 = [G_{on}]\cdot[Effector]\cdot K_5 \tag{5.60}$$

$$\nu_6 = [G_{on}Effector]\cdot K_6 \tag{5.61}$$

$$\frac{d[L]}{dt} = -\nu_1 \tag{5.62}$$

$$\frac{d[R]}{dt} = -\nu_1 \tag{5.63}$$

$$\frac{d[R*]}{dt} = \nu_1 - \nu_4 \tag{5.64}$$

$$\frac{d[G_{off}]}{dt} = \nu_3 - \nu_2 \tag{5.65}$$

$$\frac{d[G_{on}]}{dt} = \nu_2 + \nu_6 - \nu_3 - \nu_7 \tag{5.66}$$

$$\frac{d[Effector]}{dt} = \nu_6 - \nu_5 \tag{5.67}$$

$$\frac{d[G_{on}]Effector}{dt} = \nu_5 - \nu_6 \tag{5.68}$$

$$\frac{d[Z_1]}{dt} = [G_{on}Effector]\cdot\alpha - [Z_1]\cdot\beta \tag{5.69}$$

$$\frac{d[Z_2]}{dt} = [Z_1]\cdot\alpha_1 - [Z_2]\cdot\beta_1 \tag{5.70}$$

$$\frac{d[Z_3]}{dt} = [Z_2]\cdot\alpha_2 - [Z_2]\cdot\beta_2 \tag{5.71}$$

$$\tag{5.72}$$

This model was implemented in GenSSI and structural identifiability analysis performed. This demonstrated that this framework is globally and structurally identifiable, an essential prerequisite of model development here. The parameters of Kofahl and Klipp (2004), experimentally determined by Yi et al. (2003), were assumed and simulations performed for 12 hours, consistent with the time course data generated here (Figure 5.20). The delay parameters, α, β, α_1, β_1, α_2 and β_2, were assumed to be the rates determined using the simple model of G protein signalling (Table 5.3).

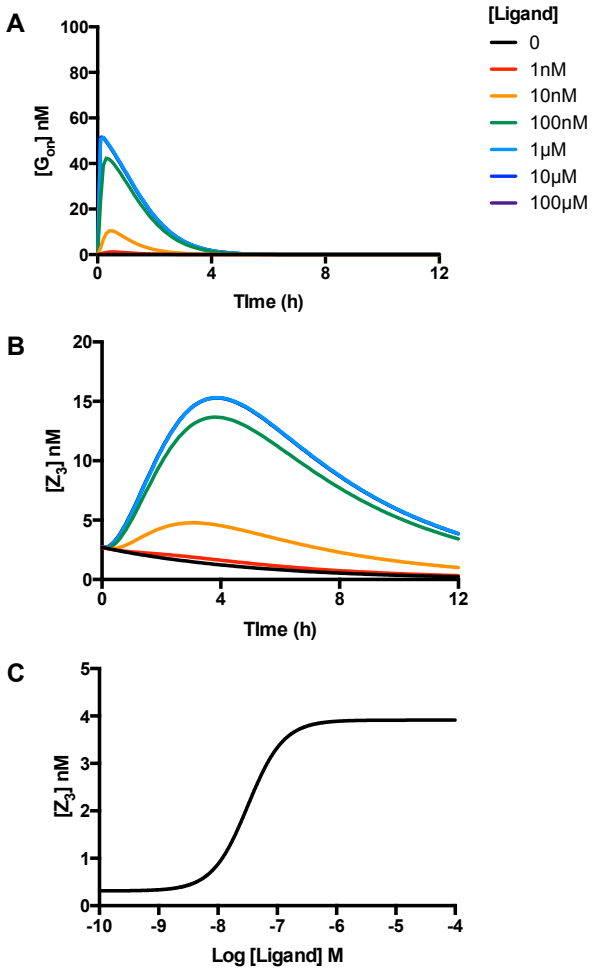

Figure 5.20: **Output of the extended model of G protein signalling using the parameters of the endogenous *Sc. cerevisiae* pheromone response.** The parameters of Kofahl and Klipp (2004), experimentally determined by Yi et al. (2003), were implemented in the model of Figure 5.19 and simulated in Matlab using the ODE23s solver. **A.** G_{on} time course data as a function of ligand. **B.** Simulated transcriptional response, $[Z_3]$. **C.** Z_3 concentration-response curves determined at 12 hours simulation.

Once again a biphasic simulated G_{on} response was observed with a peak in activity within 6 minutes and a decline in free active G protein over 4 hours (Figure 5.20). However, the transcriptional response shows a marked change. Here, $[Z_3]$ peaks at 15 nM within four hours with a steady decline to 4 nM over 12 hours. The resulting end-point curve yields a pEC_{50} of 7.5 nM but with a low E_{max} of 3.9 nM. Clearly, the delay parameters of the simple model are inappropriate for this extended variant. The experimental time course data provides a means to remedy this. Experimental studies have shown that the pEC_{50} for the *Sc. cerevisiae* pheromone response, under a ΔSST2 phenotype, is 8.1M. In A_1R::GPA1/Gα_{i3} 2CCPA is a full agonist with a pEC_{50} of 8.3±0.1 M. If we assume that α-factor is a full agonist of the *Sc. cerevisiae* pheromone response, and that 2CCPA is eliciting the maximum response possible through this strain, an E_{max} concentration of this agonist can be used to determine more appropriate delay parameters.

The time course data for A_1R::GPA1/Gα_{i3} incubated with 100μM 2CCPA was used to fit the α, β, α_1, β_1, α_2 and β_2 parameters. K_1, K_2, K_3 and K_4 were constrained to 0.072, 0.216, 14.4 and 14.4 respectively, consistent with Yi et al. (2003). However, K_5 and K_6, which govern the G_{on} Effector association and G_{on}Effector complex dissociation respectively, have not been experimentally determined. These parameters were estimated by Kofahl and Klipp (2004). Consequently, these parameters were also fitted using Potter's Wheel, as shown in Table 5.5. For time course data a single ligand concentration $\chi^2 < 10$ was considered an acceptable fit.

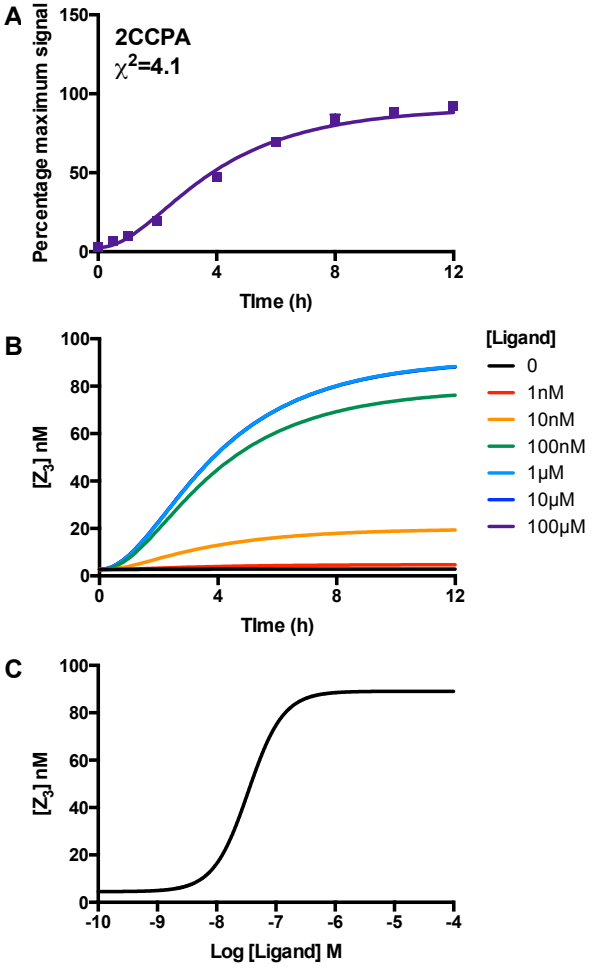

Figure 5.21: **Fitting the delay parameters of the extended model of G protein signalling.** The parameters of Kofahl and Klipp (2004), experimentally determined by Yi et al. (2003), were implemented and constrained in the Potter's Wheel toolbox for Matlab. Initial α and β parameters were determined by fitting the simple model of G protein signalling to experimental data. **A.** These parameters were then fitted to the experimental time course data of A_1R::GPA1/Gα_{i3} incubated with 100μM 2CCPA using the Levenberg-Marquardt least squares regression algorithm. Here, $\chi^2 < 10$ was considered an good fit. The resulting parameters were used to simulate **B.** time course and **C.** end-point data for a range of ligand concentrations.

The new fitted delay parameters of Table 5.5 show excellent agreement with the 2CCPA time course data of A_1R-GPA1/Gα_{i3} ($\chi^2 = 4.1$). This yielded a sigmoidal response that plateaus at 8-12 hours (Figure 5.21A). To confirm that the profile of this response is consistent between ligand concentrations, simulations were extended to generate multiple time course profiles and concentration-response curves (Figure 5.21). At all ligand concentrations tested this model produced a sigmoidal temporal response (Figure 5.21B). Consistent with the $\Delta SST2$ Kofahl and Klipp model variant, the pEC_{50} of the concentration-response curve was 7.5±0.1 (Figure 5.21B). Taken together, this suggests that the parameters underlying the delay equations are appropriate for this model structure and were constrained at these respective values.

TABLE 5.5: **Parameters of the extended model delay fitted to the time course data of the A_1R::GPA1/Gα_{i3} integrate strain incubated with 100μM 2CCPA.** The rate constants shown were used as initial conditions for fitting to the 2CCPA time course data of (Figure 5.17). K_1, K_2, K_3 and K_4 were constrained. This parameter set used to estimate an appropriate delay for this model structure.

K	Initial	Fitted
K_1 (nM^{-1} $hour^{-1}$)	0.072	0.072
K_2 (nM^{-1} $hour^{-1}$)	0.216	0.216
K_3 ($hour^{-1}$)	14.4	14.4
K_4 ($hour^{-1}$)	14.4	14.4
K_5 (nM^{-1} $hour^{-1}$)	6	3.76
K_6 ($hour^{-1}$)	300	339.27
α	11.20	12.71
β	208.27	1929.14
α_1	24.36	0.31
β_1	0.91	0.31
α_2	0.10	1.91
β_2	0.21	0.001

The effect of each parameter on this new model structure were assessed by individually manipulating constants and comparing model output (Figure 5.22). Consistent with Kofahl and Klipp (2004) and the simple model generated here, the ligand-binding constant, K_1, causes a rightward shift in the concentration-response curve and potentiation of signal at intermediate ligand concentrations, an artefact of internalisation. The G protein activation and inactivation constants, K_2 and K_3 respectively, have diametrically opposed effects. Increasing K_2 prolongs the time course response and increases the level of activity in time course data. This manifests in a leftward shift in the concentration-response curves and increased E_{max}. In contrast, K_3 reduces maximal activity. The internalisation rate, K_4, shows a similar trend to K_3 in that time course and endpoint responses decrease as this constant increases. This is unsurprising given that these are negative regulators of this pathway. While the aim is to constrain K_5 and K_6 in this extended model structure, the parameter sensitivity analysis was extended to include these rates. Here K_5 serves to increase both the delay and the maximal response, while promoting leftward shifts in the concentration-response curves, K_6 has the opposite effect.

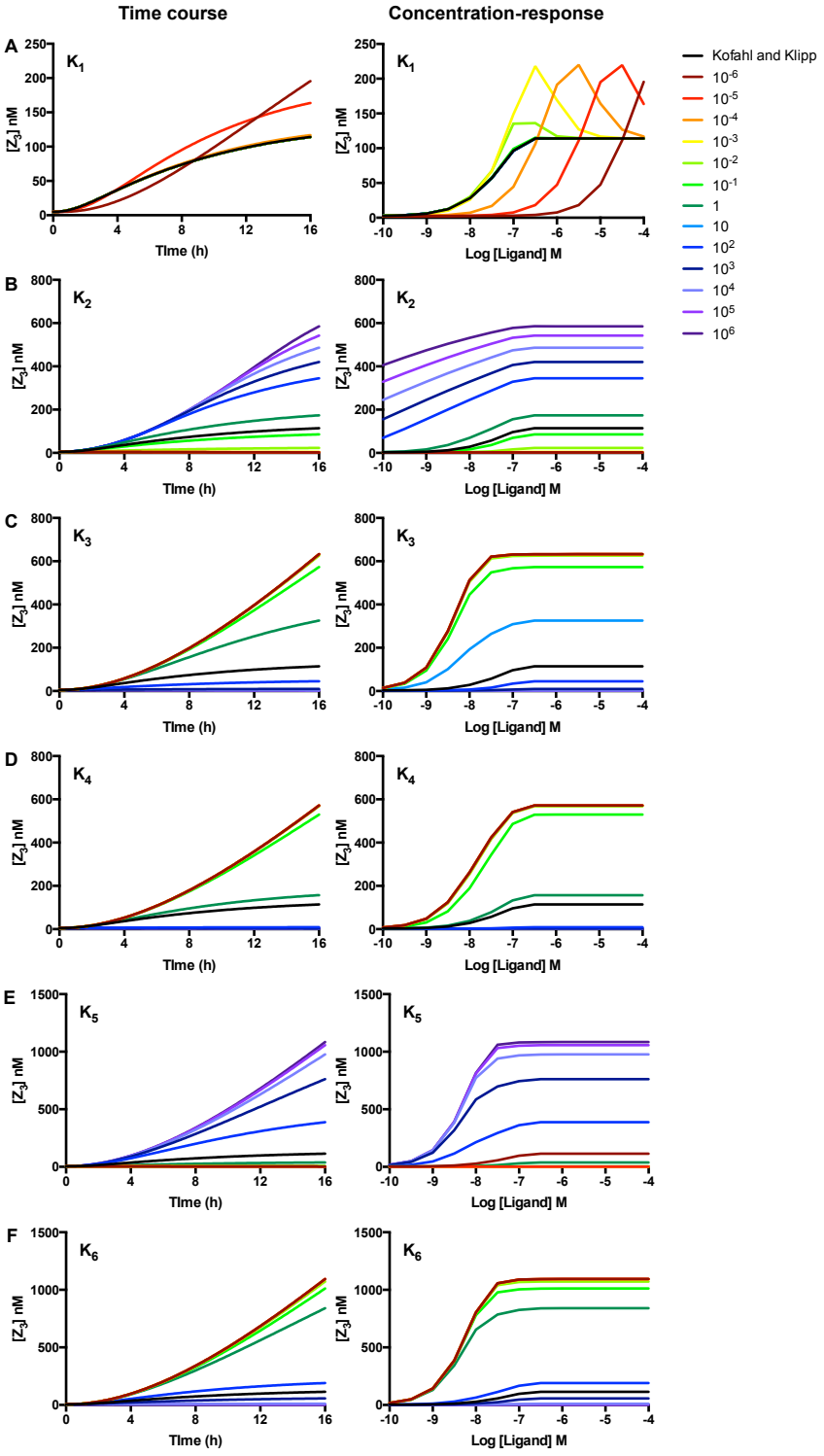

Figure 5.22: **Parameter sensitivity of the extended model of G protein signalling.** The parameters of Kofahl and Klipp (2004), and delay parameters of Figure 5.21 were implemented in Matlab. Each parameter was individually manipulated and simulations performed for 12 hours using the ODE23s solver. Timecourse and concentration-response curves as a function of **A.** K_1, **B.** K_2,**C.** K_3, **D.** K_4, **E.** K_5 and **F.** K_6.

Given that 2CCPA was the ligand used to fit the delay, these time course data were fitted with the extended model using the initial conditions of Table 5.5. Once again this fit showed good agreement with experimental data ($\chi^2 = 37.3$, Figure 5.23B). This predicted a high ligand binding rate (20.74 nM^{-1} $hour^{-1}$ compared to the 0.072 nM^{-1} $hour^{-1}$ initial value) and a two-fold increase in G protein activation ($K_2 = 0.52$ nM^{-1} $hour^{-1}$). Interestingly, a low internalisation rate in response to 2CCPA has also been predicted by this model (Table 5.6C).

Encouraged by this result, the extended model was fitted to the time course profiles of NECA in the same strain. However, this yielded a far less satisfactory fit ($\chi^2 > 300$, Figure 5.23A). As this is a regression based approach it is possible that the algorithm is becoming trapped in a numerical minima. To circumvent this multiple initial conditions were considered and all fits converged on the same parameters. These suggest a low ligand binding affinity ($K_1 = 0.001$ nM^{-1} $hour^{-1}$) and 3.6-fold decrease in G protein activation relative to the experimentally determined values for this pathway. Once again receptor internalisation is low ($K_4 = 0.77$ $hour^{-1}$, Table 5.6).

Applying this model to the adenosine time course data yielded a poor fit with similar trends to that of NECA ($\chi^2 = 419.6$, Figure 5.23B). Here, low receptor and G protein activation rates are predicted (K_1 and $K_2 = 0.0001$ and 0.03 nM^{-1} $hour^{-1}$ respectively. Interestingly, the fitted internalisation rate is half that of NECA ($K_4 = 0.384$). However, despite this lower value, adenosine shows the same artefact of internalisation simulated for NECA.

The model concentration-response curves yielded pEC_{50} values of 7.1±0.1, 6.1±0.1 and 7.6±0.1 compared to 6.5±0.1, 5.9±0.1 and 7.5±0.1 for NECA, adenosine and 2CCPA respectively (Figure 5.23D). This may suggest that this model cannot replicate the time course and endpoint data simultaneously for lower-affinity ligands. This study aims to develop and ODE model to describe functional selectivity of the A_1R in yeast. Thus, it is essential this model fits data for all ligands in this system. Consequently, the model structure was revisited.

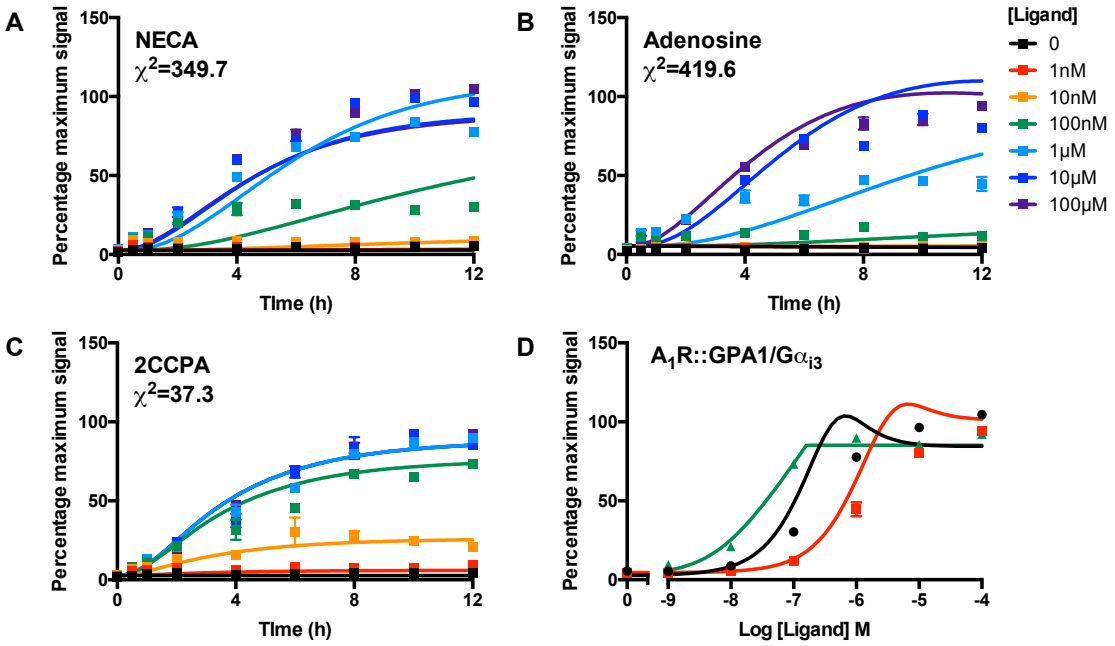

FIGURE 5.23: **Fitting the extended model to the time course data of the A_1R::GPA1/Gα_{i3} strain.** The parameters of Table 5.6 were used as initial conditions for fitting the time course data of **A.** NECA, **B.** adenosine and **C.** 2CCPA using Potter's Wheel. **D.** The resulting parameters were used to simulate the concentration-response of these compounds after 12 hours incubation. Points represent experimental data and the solid line represents fitted model output. $\chi^2 < 300$ was considered a good fit.

TABLE 5.6: **Parameters of an extended GPCR model fitted to the time course data of the A_1R::GPA1/Gα_{i3} integrate strain incubated with 2CCPA or NECA.** The rate constants shown were used as initial conditions for fitting to the 2CCPA time course data of Figure 5.17. K_4, K_5, K_6 and the delay α and β parameters were constrained.

K	Initial	NECA	Adenosine	2CCPA
K_1 (nM^{-1} $hour^{-1}$)	0.072	0.001	$1e^{-4}$	20.74
K_2 (nM^{-1} $hour^{-1}$)	0.216	0.06	0.03	0.52
K_3 ($hour^{-1}$)	14.4	14.4	14.4	14.4
K_4 ($hour^{-1}$)	14.4	0.77	0.38	2.06
K_5 (nM^{-1} $hour^{-1}$)	3.76	3.76	3.76	3.76
K_6 ($hour^{-1}$)	339.27	339.27	339.27	339.27
α	12.71	12.71	12.71	12.71
β	1929.14	1929.14	1929.14	1929.14
α_1	0.31	0.31	0.31	0.31
β_1	0.311	0.31	0.31	0.31
α_2	01.91	1.91	1.91	1.91
β_2	0.001	0.001	0.001	0.001
χ^2		349.7	419.6	37.3

5.3.4 Refining the model to include ligand dissociation

The extended model contains the basic components of G protein activation and signalling. Ligand binds a receptor to form the active R* state. The R* then activates a G protein in a simple two-stage mechanism. The active G protein interacts with an Effector to influence downstream signalling. However, negative regulation of this pathway contains far fewer steps. At the G protein-level negative regulation is achieved through G protein inactivation or dissociation of the G_{on}Effector complex. Termination of signalling at the receptor level is controlled solely by R* internalisation. This may be responsible for the lack of flexibility preventing accurate fitting to NECA time course data. The Kofahl and Klipp (2004) model has a term for conversion of R* to the inactive R state. Ligand is not regenerated by this reaction in this framework and is consequently lost. However, ligand can dissociate from bound targets. This is exploited by *in vitro* radioligand binding assays that rely on the ability of one ligand to displace another (Bylund and Toews, 2011). Consequently, the extended model was developed further to allow a reversion from the R* to the R state with regeneration of ligand, R* -> R + L, K_7 (Figure 5.24). This model will be referred to as the refined model. In *Sc. cerevisiae* the rate of receptor inactivation is 36 hour^{-1} (Yi et al., 2003). Consequently, this value was used as the initial parameter for model validation and fitting.

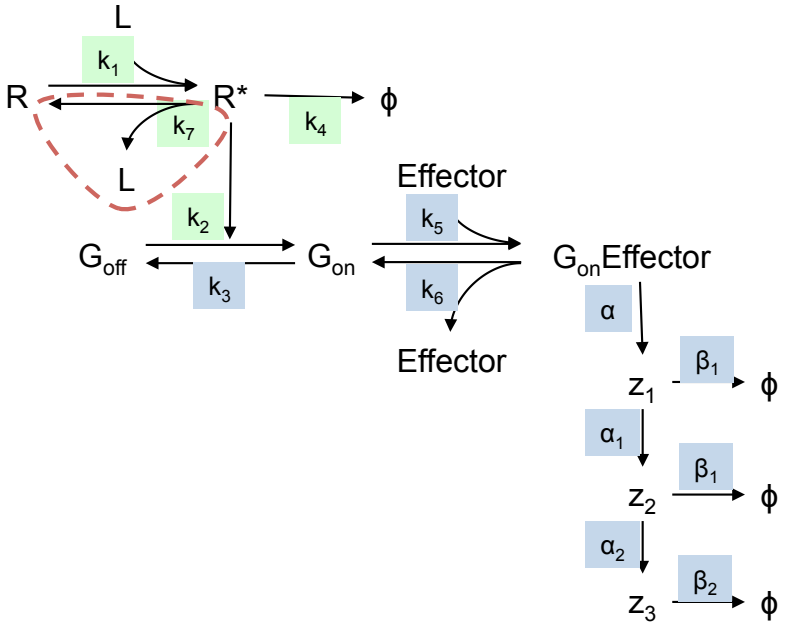

Figure 5.24: **A refined model of G protein signalling yeast including a G$\beta\gamma$ Effector interactions.** Here ligand binds an inactive receptor to form the active R* conformation in a reversible reaction. R* can activate a G protein (G_{off} -> Gon) to trigger downstream signalling via an interaction with an Effector. Negative regulation in this model can be achieved through internalisation of R*, spontaneous G protein-inactivation or dissociation of G_{on} from the G_{on}Effector complex. Parameters to be fitted are highlighted in green. Parameters to be constrained are highlight in blue. The extension to the previous model iteration, the extended model, is highlighted with a red dotted line.

$$\nu_1 = [L]\cdot[R]\cdot K_1 \tag{5.73}$$

$$\nu_2 = [R*]\cdot[G_{off}]\cdot K_2 \tag{5.74}$$

$$\nu_3 = [G_{on}]\cdot K_3 \tag{5.75}$$

$$\nu_4 = [R*]\cdot K_4 \tag{5.76}$$

$$\nu_5 = [G_{on}]\cdot[Effector]\cdot K_5 \tag{5.77}$$

$$\nu_6 = [G_{on}Effector]\cdot K_6 \tag{5.78}$$

$$\nu_7 = [R*]\cdot K_7 \tag{5.79}$$

$$\frac{d[L]}{dt} = \nu_7 - \nu_1 \tag{5.80}$$

$$\frac{d[R]}{dt} = \nu_7 - \nu_1 \tag{5.81}$$

$$\frac{d[R*]}{dt} = \nu_1 - \nu_4 - \nu_7 \tag{5.82}$$

$$\frac{d[G_{off}]}{dt} = \nu_3 - \nu_2 \tag{5.83}$$

$$\frac{d[G_{on}]}{dt} = \nu_2 + \nu_6 - \nu_3 - \nu_5 \tag{5.84}$$

$$\frac{d[Effector]}{dt} = \nu_6 - \nu_5 \tag{5.85}$$

$$\frac{d[G_{on}]Effector}{dt} = \nu_5 - \nu_6 \tag{5.86}$$

$$\frac{d[Z_1]}{dt} = [G_{on}Effector]\cdot\alpha - [Z_1]\cdot\beta \tag{5.87}$$

$$\frac{d[Z_2]}{dt} = [Z_1]\cdot\alpha_1 - [Z_2]\cdot\beta_1 \tag{5.88}$$

$$\frac{d[Z_3]}{dt} = [Z_2]\cdot\alpha_2 - [Z_2]\cdot\beta_2 \tag{5.89}$$

$$\tag{5.90}$$

This refined model was implemented in GenSSI, using the equations described above, and found to be globally and structurally identifiable. The parameters of Kofahl and Klipp (2004), and the delay fitted here as described in Table 5.6, were used to simulate this system in Matlab with the ODE23s solver (Figure 5.25).

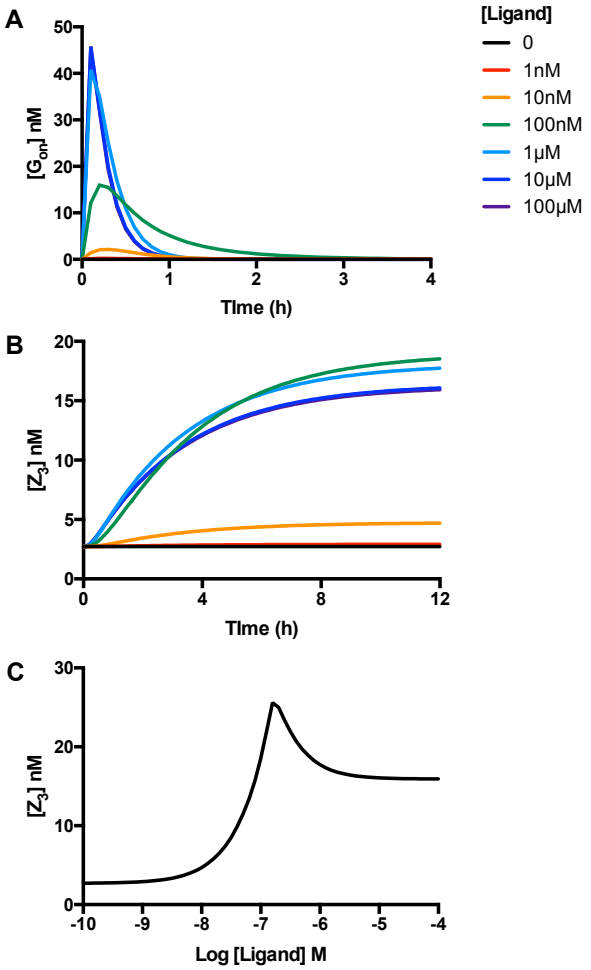

Figure 5.25: **Output of the refined model of G protein signalling including ligand dissociation.** The model schematic of (Figure 5.24) was implemented in Matlab. R, G_{on} and Effector were initialised as 160nM. Z_3 was set to 2.7nM. All other species were initialised to 0. $K_1 = 0.072\ nM^{-1}hour^{-1}$, $K_2 = 0.216\ nM^{-1}hour^{-1}$, $K_3 = 14.4\ hour^{-1}$, $K_4 = 14.4\ hour^{-1}$, $K_5 = 3.76\ nM^{-1}hour^{-1}$, $K_6 = 339.27\ hour^{-1}$. $K_7 = 36\ hour^{-1}$. α =12.71, $\beta = 1929.14$. α_1 =0.31, $\beta_1 = 0.31$. α_2 =1.91, $\beta_2 = 0.001$. Simulations were performed for 12 hours using the ODE23s solver. **A.** G_{on} and **B.** Z_3 time course profiles as a function of ligand. **C.** Z_3 concentration-response curve determined at 12 hours simulation.

Figure 5.25 shows a rapid peak in $[G_{on}]$ within 6 minutes and a steady decline in activity over the next hour in response to 1μM ligand. This shorter period is much closer to experimental data of Yi et al. (2003) than the previous model iterations and indicates a positive step in model development. However, the transcriptional responses of this framework show a greatly reduced E_{max} of 18.52nM for 100nM ligand for this parameter set. This is also observed in the concentration response curves where activity peaks at 100nM and decreases with increasing ligand concentration.

While the improved G protein activation profile is encouraging, these simulations suggest that the delay parameters are inappropriate for this extended model variant. Therefore new α, β, α_1, β_1, α_2 and β_2 values were determined by constraining all other parameters and fitting to the experimental time course data of A_1R:GPA1/Gα_{i3} incubated with 100μM 2CCPA. This yielded a reasonable fit to the experimental data (Figure 5.26, $\chi^2 = 6.5$) and the parameters are shown in Table 5.7.

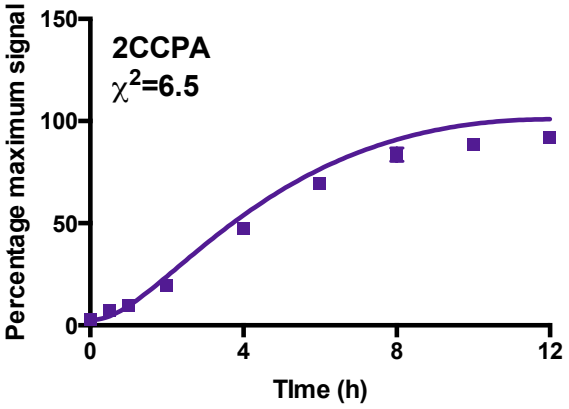

FIGURE 5.26: **Fitting new delay parameters to the refined model extended to include ligand dissociation.** K_1, K_2, K_3, K_4, K_4, K_6 and K_7 were constrained. All other parameters were fitted to the experimental time course data of A_1R::GPA1/Gα_{i3}, incubated with 100μM 2CCPA, using the Levenberg-Marquardt least squares regression algorithm. The resulting parameters were used to simulate time course data for this ligand concentration. Points represent experimental data and the solid line represents fitted model output. For a single ligand concentration $\chi^2 > 10$ was considered a good fit.

TABLE 5.7: **Parameters of the refined model delay fitted to the time course data of the A_1R::GPA1/Gα_{i3} integrate strain incubated with 100μM 2CCPA.** The rate constants shown were used as initial conditions for fitting to the 2CCPA time course data of (Figure 5.17). K_1, K_2, K_3, K_4, K_5, K_6 and K_7 were constrained. This parameter set used to estimate an appropriate delay for this model structure.

K	Initial	Fitted
K_1 (nM^{-1} hour^{-1})	0.072	0.072
K_2 (nM^{-1} hour^{-1})	0.216	0.216
K_3 (hour^{-1})	14.4	14.4
K_4 (hour^{-1})	14.4	14.4
K_5 (nM^{-1} hour^{-1})	3.76	3.76
K_6 (hour^{-1})	339.27	339.27
K_7 (hour^{-1}	36	36
α	11.20	17.75
β	208.27	1859.57
α_1	24.36	42.41
β_1	0.91	0.93
α_2	0.10	0.93
β_2	0.21	0.12

This delay was constrained and the remaining parameters fitted to the experimental time course data of A_1R::GPA1/Gα_{i3} in response to multiple concentrations of NECA, adenosine and 2CCPA (Figure 5.27, Table 5.8).

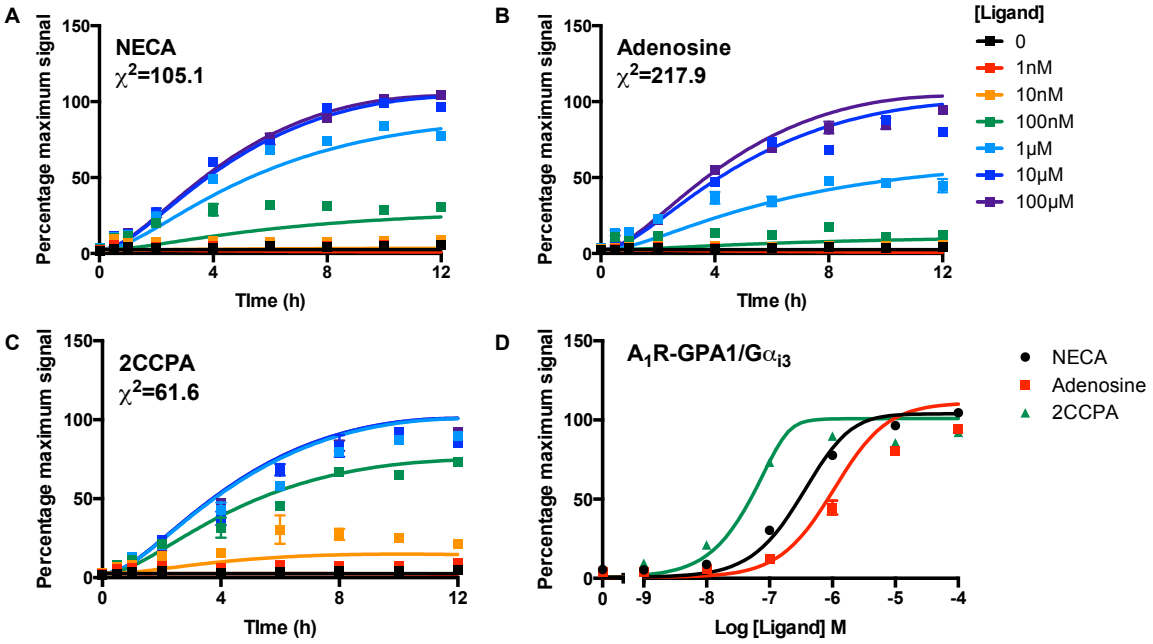

Figure 5.27: **The refined model of G protein signalling fitted to the time course data of the A_1R::GPA1/Gα_{i3} in response to NECA, adenosine and 2CCPA.** The refined model was implemented in Potter's Wheel using the rates of Table 5.8. K_1, K_2, K_4 and K_7 were fitted to the experimental data of Figure 5.4. All other parameters were constrained. The fitted parameters were assumed by the ODE and simulated for 12 hours using the ODE23s solver. Points represent experimental data and solid lines represent equivalent simulations with fitted parameters for **A.** NECA **B.** adenosine and **C** 2CCPA. **D.** Concentration-response curves as determined by model output after 12 hours.

Table 5.8: **Parameters of the refined model of G protein signal fitted to the time course data of the A_1R::GPA1/Gα_{i3} in response to NECA, adenosine and 2CCPA.** The rate constants shown were used as initial conditions for fitting K_1, K_2, K_4 and K_7 to the NECA, adenosine and time course data of (Figure 5.4). All other parameters were constrained.

K	Initial	NECA	Adenosine	2CCPA
K_1 (nM^{-1} $hour^{-1}$)	0.072	0.15	0.07	4.39
K_2 (nM^{-1} $hour^{-1}$)	0.216	0.09	0.07	0.09
K_3 ($hour^{-1}$)	14.4	14.4	14.4	14.4
K_4 ($hour^{-1}$)	14.4	0.14	0.07	0.14
K_5 (nM^{-1} $hour^{-1}$)	3.76	3.76	3.76	3.76
K_6 ($hour^{-1}$)	339.27	339.27	339.27	339.27
K_7 ($hour^{-1}$)	36	310	310	310
χ^2		105.1	217.9	61.6

Developing the model to include ligand dissociation has enabled a reasonable fit to the NECA time course data (Figure 5.27A, $\chi^2 = 105.1$). The ligand binding rate, K_1 is higher than that of α-factor for STE2 (0.15 $nM^{-1}hour^{-1}$ and $0.072nM^{-1}hour^{-1}$ respectively). Interestingly, this model predicts the G protein activation rate, K_2, in response to the NECA-bound A_1R in this strain is lower than the endogenous reaction of this system (0.09 $nM^{-1}hour^{-1}$ compared to 0.216 $nM^{-1}hour^{-1}$ respectively). This prediction is realistic given that this is a non-native GPCR coupled to a modified cell-signalling system. Also the R* internalisation rate, K_4, is 100-fold lower than the experimental value for STE2 (Yi et al., 2003). Again this could be expected as the A_1R internalises through β-arrestins in mammalian cells (Baker and Hill, 2006). Consequently, it may not couple as efficiently to the yeast GPCR internalisation machinery as the endogenous STE2 and STE3 receptors. Interestingly, the NECA dissociation rate (K_7) is 8.6-fold higher than the initial value.

A good fit was achieved for the adenosine time course data generated in A_1R::GPA1/Gα_{i3} (Figure 5.27B, $\chi^2 = 217.9$). This model predicts that the ligand binding rate of adenosine is less than half that of NECA (0.07 nM^{-1} $hour^{-1}$), but G protein activation is only marginally reduced ($K_2 = 0.7$ $hour^{-1}$). Ligand dissociation rates are conserved for NECA and adenosine. However, there is a two-fold decrease in adenosine induced R* internalisation compared to NECA (Table 5.8).

This model also fitted the 2CCPA time course data of this strain remarkably well and predicts that only a single parameter differentiates the pharmacology of this ligand from NECA in this strain, the ligand binding rate (Figure 5.27C, $\chi^2 = 61.6$). Here, $K_1 = 4.39$ $nM^{-1}hour^{-1}$, a 29-fold increase on the equivalent value for NECA. Given that NECA, adenosine and 2CCPA all appear to be full agonists of the A_1R integrated into this strain it is encouraging that this model predicts largely conserved G protein activation rates between agonists but differences in ligand-binding.

Thus far, this model is capable of fitting the time course data of A_1R::GPA1/Gα_{i3} for multiple ligands. Here, ligand binding, G protein activation have been predicted to vary as a function of ligand. To date, these parameters have not been experimentally determined or computation inferred for the A_1R in yeast and validation of these predictions is required. However, this study aims to model functional selectivity of the A_1R using yeast as an experimental system. Consequently, this model must be able to fit the time course data of multiple ligands in multiple strains. A_1R::GPA1/Gα_z only elicits a fraction of the response of the equivalent GPA1/Gα_i strains in response to NECA, adenosine and 2CCPA Figure 5.5. This difference in pharmacology presents an opportunity to test the flexibility of this model.

The rates obtained by fitting of A_1R-GPA1/Gα_{i3} strain (Table 5.8) were used as initial conditions for fitting the respective time course profiles of A_1R-GPA1/Gα_z (Figure 5.28). The delay parameters and rate of G protein hydrolysis (K_3) were constrained. For fitting multiple ligand concentrations $\chi^2 < 300$ was considered a good fit (Table 5.9).

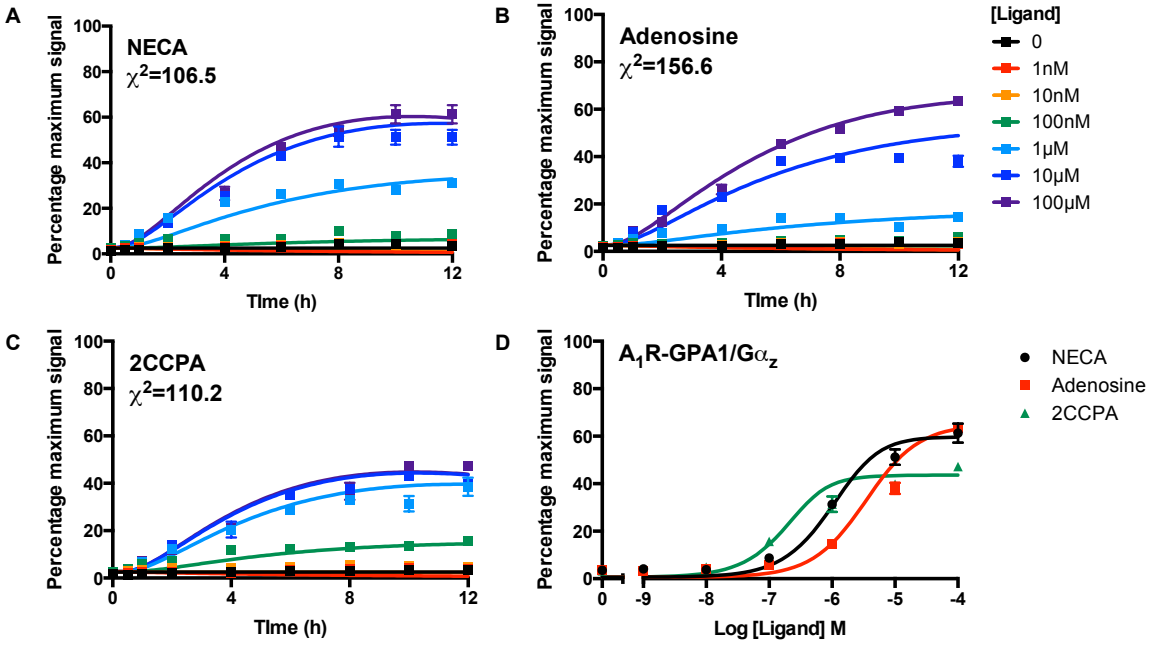

Figure 5.28: **The refined model of G protein signalling fitted to the time course data of the A_1R::GPA1/Gα_z in response to NECA, adenosine and 2CCPA.** This model was implemented in Potter's Wheel using the rates of Table 5.8. K_1, K_2, K_4 and K_7 were fitted to the experimental data of Figure 5.5. All other parameters were constrained. The fitted parameters were assumed by the ODE and simulated for 12 hours using the ODE23s solver. Points represent experimental data and solid lines represent equivalent simulations with fitted parameters for **A.** NECA **B.** adenosine and **C** 2CCPA. **D.** Concentration-response curves as determined by model output after 12 hours.

Table 5.9: **Parameters of the refined model of G protein signal fitted to the time course data of the A_1R::GPA1/Gα_z strain in response to NECA, adenosine and 2CCPA.** The rate constants of Table 5.8 initial conditions for fitting K_1, K_2, K_4 and K_7 to the NECA, adenosine and time course data of (Figure 5.5). All other parameters were constrained.

K	NECA	Adenosine	2CCPA
K_1 (nM^{-1} $hour^{-1}$)	0.08	0.04	0.63
K_2 (nM^{-1} $hour^{-1}$)	0.03	0.02	0.02
K_3 ($hour^{-1}$)	14.4	14.4	14.4
K_4 ($hour^{-1}$)	0.14	0.07	0.14
K_5 (nM^{-1} $hour^{-1}$)	3.76	3.76	3.76
K_6 ($hour^{-1}$)	339.27	339.27	339.27
K_7 ($hour^{-1}$)	310	310	310
χ^2	106.5	156.6	110.2

This model yielded excellent fits to the time course data of NECA, adenosine and 2CCPA in this strain ($\chi^2 = 106.5$, 156.6 and 110.2 respectively). Interestingly, it predicts that only the ligand binding and G protein activation parameters (K_1 and K_2 respectively) vary between NECA, adenosine and 2CCPA between A_1R::-GPA1/Gα_{i3} and A_1R::GPA1/Gα_z. However, K_2 is remarkably well conserved for all ligands in this strain (0.03 0.02 and 0.02 nM^{-1} $hour^{-1}$ for NECA, adenosine and 2CCPA respectively). Similarly, this parameter is consistent for NECA, adenosine and 2CCPA in A_1R::GPA1/Gα_{i3}. This mirrors and reinforces differences in signal transduction efficiency suggested by the operational model for the A_1R in the GPA1/Gα_i and GPA1/Gα_z strains. In A_1R::GPA1/Gα_z ligand binding rates are estimated to be 0.08, 0.04 and 0.063 $nM^{-1}hour^{-1}$ for NECA, adenosine and 2CCPA respectively. This is consistently lower than the equivalent rates for A_1R::GPA1/Gα_{i3}. Thus this model suggests that the G protein influences the ligand binding rates of NECA, adenosine and 2CCPA, demonstrating functional selectivity of the A_1R. Interestingly, receptor internalisation rates are conserved between yeast strains for all ligands. This would predict that the G protein does not affect A_1R internalisation in yeast. This model also predicts that neither G protein transplant or ligand affect dissociation of the agonist-receptor complex in yeast.

Thus far, this model has made some interesting predictions of A_1R pharmacology in yeast. Here, G protein activation is reduced in A_1R::GPA1/Gα_z relative to A_1R/GPA1/Gα_{i3} (Table 5.8 and Table 5.9). Indeed, the operational model predicts similar trends in signal transduction efficiency from end point data but suggests that ligand binding affinities of the A_1R are not affected by the G protein in yeast. However, the refined model predicts that the ligand binding rate is a function of G protein in yeast but ligand dissociation is conserved for all ligands and strains. The changes in ligand binding rates suggest that this model can be used to study functional selectivity. However, the dynamic predictions of this model have to be experimentally validated and there is currently no dynamic data of A_1R pharmacology available. In the absence of a means to do so directly, opportunities to challenge this framework further were sought.

A C-terminal A_1R^{GFP} fusion construct has remarkably different pharmacology from the unmodified A_1R in yeast. When expressed from a plasmid the A_1R^{GFP} shows a pEC_{50} consistent with its untagged counterpart but with an increased E_{max}. Experimental data suggests that this may be a consequence of reduced internalisation (Figure 3.11, Niebauer et al. (2004)). This model can be used to explore differences between the pharmacology of the A_1R and A_1R^{GFP} variants described here. Reproduction of such trends by model fitting would lend credibility to its predictions of functional selectivity in the A_1R. However, like the A_1R, A_1R^{GFP} requires chromosomal expression to be effectively modelled.

5.4 Characterisation of chromosomal A_1R^{GFP} yeast strains

The C-terminal A_1R^{GFP} fusion construct was cloned into the pRS306GPD vector under the control of the constitutive GAPDH promoter. This was linearised by restriction digest and chromosomally integrated at the *URA3* locus of the GPA1/Gα_o, GPA1/G$\alpha_{i1/2}$, GPA1/Gα_{i3} and GPA1/Gα_z strains. 8-16 colonies were selected and incubated with 100μM NECA for 16 hours. Cells were lysed and β-galactosidase activity determined (Figure 5.29). The equivalent strains expressing the A_1R^{GFP} from the p426GPD plasmid, using the same promoter, were included for comparison. For convenience, and to distinguish them from their plasmid counterparts, the integrate strains will be referred to A_1R^{GFP}::GPA1/Gα_o, A_1R^{GFP}::GPA1/G$\alpha_{i1/2}$, A_1R^{GFP}::GPA1/Gα_{i3} and A_1R^{GFP}::GPA1/Gα_z.

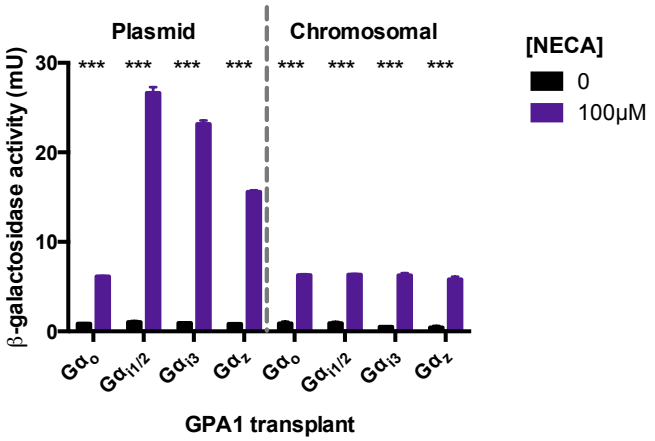

FIGURE 5.29: **Screening A_1R^{GFP} integrates for β-galactosidase activity in response to NECA.** The A_1R^{GFP} was placed under the control of the constitutive *GAPDH* promoter and integrated into the *URA3* locus of the GPA1/Gα_o, GPA1/G$\alpha_{i1/2}$, GPA1/Gα_{i3} and GPA1/Gα_z transplant strains. 8-16 colonies were selected and incubated with 100μM NECA for 16 hours. Cells were lysed and β-galactosidase activity determined. The equivalent strains expressing the A_1R^{GFP} from the p426GPD expression plasmid were included for comparison. *** $P < 0.0005$, Student's T-test compared to vehicle alone control.

In contrast to the A_1R, A_1R^{GFP} shows no significant difference in signal in response to NECA between any G protein transplant strain (6.3±0.1, 6.3±0.2, 6.3±0.3 and 5.8±0.3 mU for GPA1/Gα_o, GPA1/G$\alpha_{i1/2}$, GPA1/Gα_{i3}, and GPA1/Gα_z respectively). While this is consistent with the level of signal in the A_1R^{GFP}-GPA1/Gα_o plasmid strain, this is significantly lower then the equivalent A_1R and A_1R^{GFP} chromosomally-integrated and plasmid strains respectively. Concentration-response curves demonstrate reduced E_{max} for NECA, adenosine and 2CCPA in all A_1R^{GFP} chromosomal expression strains relative to plasmid counterparts, but shared pEC_{50} (Figure 5.29). The operational model suggests this is the result of reduced signal transduction efficiency in these strains and not necessarily sensitivity to ligand (Table 5.10).

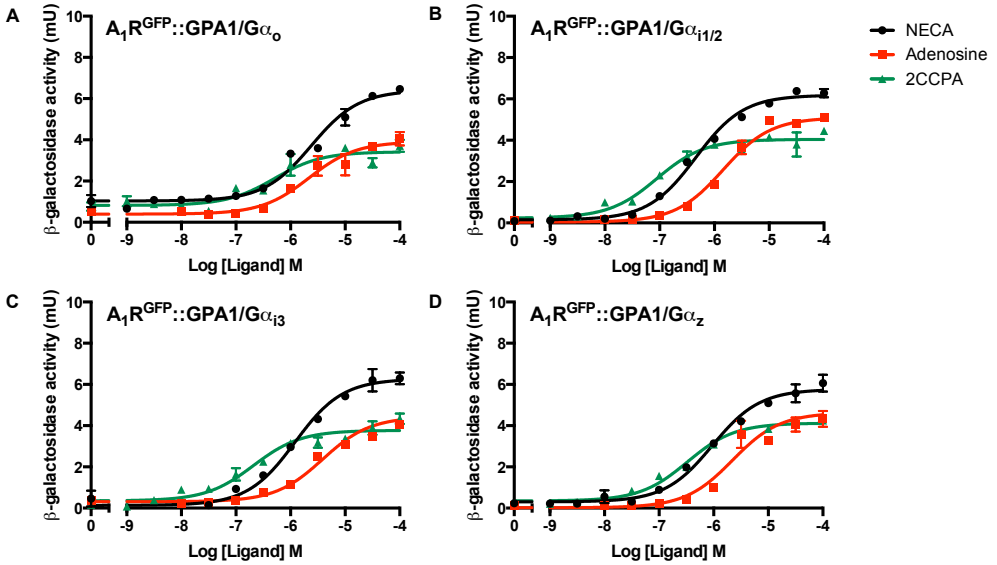

FIGURE 5.30: **A_1R^{GFP} integrate pharmacology in yeast.** The integrate strains were incubated with NECA, adenosine or 2CCPA for 16 hours. Cells were lysed and β-galactosidase activity determined. **A.** A_1R^{GFP}::GPA1/Gα_o. **B.** A_1R^{GFP}::GPA1/G$\alpha_{i1/2}$. **C.** A_1R^{GFP}::GPA1/Gα_{i3}. **D.** A_1R^{GFP}::GPA1/Gα_z. Data represents the mean of triplicate repeats ± S.E.M fitted with the logistic equation.

TABLE 5.10: **Pharmacological parameters of the integrated A_1R^{GFP}.** The logistic equation and the operational model were applied to the data of Figure 5.30 by non-linear regression. $pEC_{50} = -Log\ EC_{50}$ (potency), E_{max} = maximum level of signal, $pK_A = -\text{Log}\ K_A$ (ligand binding affinity) and τ = efficacy. Equivalent plasmid parameters have been included for comparison. * P < 0.05, ** P < 0.005, *** P < 0.0005, Student's T-test comparing parameter for chromosomal-expression to plasmid counterpart.

Strain	**Ligand**	pEC_{50}	E_{max}	pK_A	$log\tau$
A_1R^{GFP}::GPA1/Gα_o (Chromosomal)	NECA	5.6±0.1	6.4±0.2	4.1±0.1	1.5±0.1
	Adenosine	5.7±0.1	3.9±0.1	4.8±0.2	0.1±0.1
	2CCPA	6.3±0.2	3.4±0.2	5.8±0.2	−0.1±0.1
A_1R^{GFP}-GPA1/Gα_o (Plasmid)	NECA	5.9±0.1	5.8±0.1	4.1±0.1	1.8±0.1
	Adenosine	5.8±0.2	3.9±0.2	5.3±0.1	0.3±0.1
	2CCPA	6.6±0.1	3.4±0.1	6.2±0.1	0.1±0.1
A_1R^{GFP}::GPA1/G$\alpha_{i1/2}$ (Chromosomal)	NECA	6.3±0.1*	6.2±0.1***	4.8±0.1*	1.5±0.1
	Adenosine	5.8±0.1**	5.1±0.1***	5.0±0.1***	0.7±0.1
	2CCPA	7.1±0.1*	4.0±0.1***	6.6±0.1***	0.3±0.1
A_1R^{GFP}-GPA1/G$\alpha_{i1/2}$ (Plasmid)	NECA	5.8±0.1	26.1±0.5	4.4±0.1	1.4±0.1
	Adenosine	4.8±0.1	23.5±0.7	3.8±0.2	0.9±0.1
	2CCPA	6.6±0.1	17.2±0.4	6.2±0.1	0.3±0.1
A_1R^{GFP}::GPA1/Gα_{i3} (Chromosomal)	NECA	5.9±0.1	6.3±0.2***	3.1±0.1***	2.7±0.4***
	Adenosine	5.4±0.1	5.4±0.1***	4.7±0.1*	0.4±0.1*
	2CCPA	6.7±0.1	6.7±0.1***	6.2±0.1	0.1±0.1*
GA_1R^{GFP}-PA1/Gα_{i3} (Plasmid)	NECA	5.7±0.1	23.4±0.2	5.1±0.0	1.0±0.1
	Adenosine	5.3±0.1	20.1±0.5	4.2±0.1	1.0±0.1
	2CCPA	6.8±0.1	17.8±0.3	6.1±0.1	0.5±0.1
A_1R^{GFP}::GPA1/Gα_z (Chromosomal)	NECA	6.0±0.1	5.8±0.1***	4.4±0.1	1.6±0.1
	Adenosine	5.7±0.1	4.6±0.2***	4.6±0.2	0.7±0.1
	2CCPA	6.5±0.1	4.1±0.1**	5.8±0.1*	0.4±0.1*
A_1R^{GFP}-GPA1/Gα_z (Plasmid)	NECA	5.7±0.1	16.0±0.4	4.4±0.1	1.5±0.1
	Adenosine	5.5±0.1	11.8±0.6	5.0±0.1	0.4±0.1
	2CCPA	6.5±0.2	7.4±0.4	6.2±0.2	−0.1±0.1

β-galactosidase assays are a measure of a population level response. As we have observed, A_1R^{GFP} expression varies considerably across a population when expressed from a plasmid. Flow cytometry was used to measure single cell fluorescence to ensure ubiquitous and consistent expression of the chromosomally-expressed A_1R^{GFP} receptor between the strains (Figure 5.31).

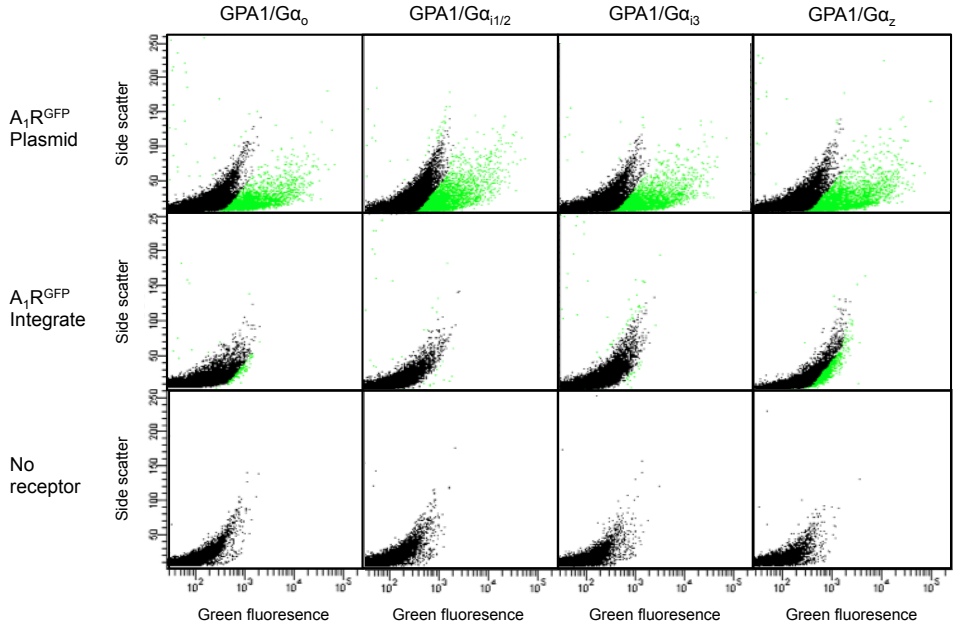

FIGURE 5.31: **Flow cytometry of A_1R^{GFP} yeast chromosomal integrates** A_1R^{GFP} integrate strains underwent single-cell analysis using a LSRII flow cytometer. 3x10^4 cells were analysed and fluorescence intensity in the GFP channel quantified for each cell. The graphs show fluorescence intensity vs. side scatter (a measure of cell width). Thresholds were set using the equivalent A_1R expressing strains. Cells with fluorescence below the threshold are shown in black. Cells with GFP fluorescence above the threshold are shown in green.

The data of Figure 5.31 suggests a contrast between the A_1R^{GFP} chromosomal and plasmid expression strains. While plasmid expressed receptor is clearly observed, only a marginal increase in fluorescence was detected in A_1R^{GFP}::GPA1/Gα_z with no significant signal present in the A_1R^{GFP}::GPA1/Gα_o, A_1R^{GFP}::GPA1/G$\alpha_{i1/2}$ and A_1R^{GFP}::GPA1/Gα_{i3} strains. Clearly the strains express the receptor, as evidenced by their response to NECA, but the ability of this modified receptor to transduce signal may be reduced. This is in contrast to the plasmid expression system where A_1R^{GFP} typically yields a higher E_{max} than the A_1R. The operational model suggests that this is due to a higher signal transduction efficiency across the population. This may be due in part to the high fluorescence values of a proportion of the population. It is possible that the high expression level in these cells overcomes the limited signal transduction efficiency. Further study is required to confirm this.

The difference between the A_1R and A_1R^{GFP} chromosomal-expression strains present an attractive contrast to probe through mathematical modelling. By fitting the model to time course data of the A_1R^{GFP}, it may be possible to estimate why the pharmacology of this receptor differs from the A_1R when chromosomally-expressed in yeast.

5.4.1 Modelling A_1R^{GFP} pharmacology in yeast

Confocal microscopy studies in Chapter 3 suggest that A_1R^{GFP} is not internalised in response to ligand when when expressed from a plasmid. Thus, it can be assumed that the chromosomally-expressed receptor is not internalised in response to ligand in 16 hours in yeast. Consequently, this rate can be initialised as 0. This would eliminate receptor internalisation in the model but allow for very slow receptor loss to be accommodated. To explore this further time course data were generated for the A_1R^{GFP} integrated and expressed in the GPA1/Gα_{i3} and GPA1/Gα_z strains. The refined model of G protein signalling developed here was fitted to this data using Potter's Wheel. The fitted parameters of A_1R described in Table 5.8 and Table 5.9 were used as initial estimates for fitting the time course data of A_1R^{GFP}::GPA1/Gα_{i3} and A_1R^{GFP}::GPA1/Gα_z, respectively.

Consistent with its unmodified counterpart, A_1R^{GFP}::GPA1/Gα_{i3} shows a sigmoidal response to NECA, adenosine and 2CCPA that plateaus at 6-8 hours. However, signal is reduced for all ligands against the A_1R compared to A_1R^{GFP} in this strain. This is consistent with the concentration-response curves of Figure 5.2 and Figure 5.30. To explore these differences the refined model was fitted to the time course data of Figure 5.32. Initial parameters were assumed from the fitting of the model to the A_1R::GPA1/Gα_{i3} strain. However, confocal microscopy studies suggested no appreciable internalisation of A_1R^{GFP} in response to ligand. Studies of C-terminally modified $A_{2A}R^{GFP}$ suggested internalisation takes 48 hours in yeast the presence of ligand (Niebauer et al., 2004; Niebauer and Robinson, 2006). It is therefore possible that A_1R^{GFP} internalises, albeit slowly. To allow for this, the relevant rate, K_4, was initially set to 0 but not constrained (Table 5.11).

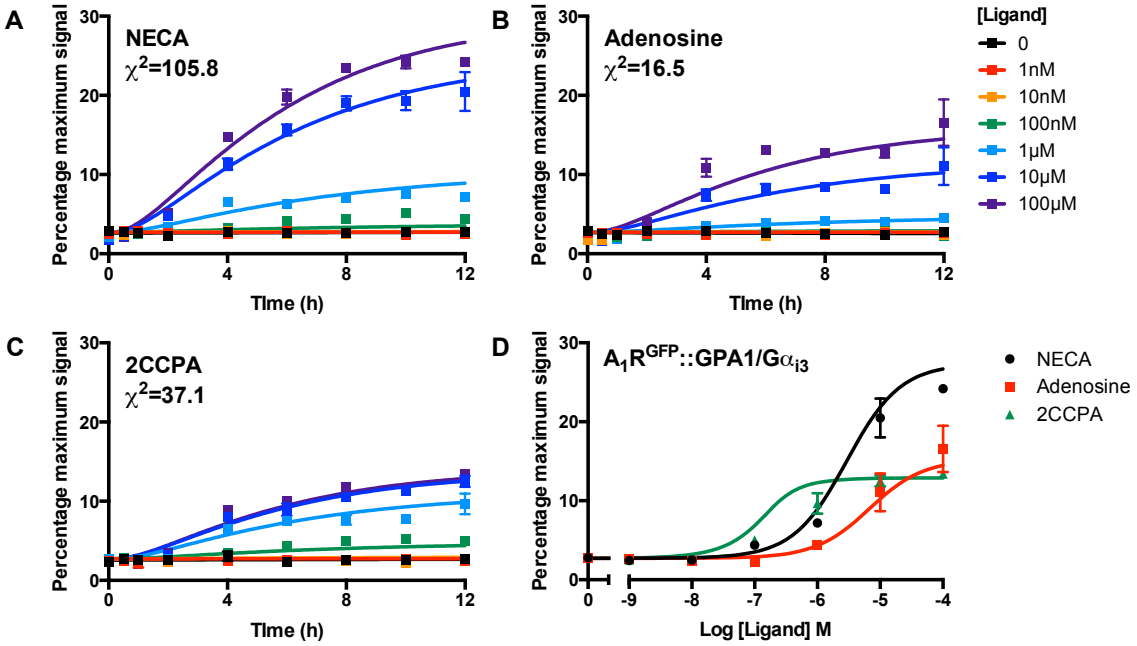

Figure 5.32: **The refined model of G protein signalling fitted to the time course data of the A_1R^{GFP}::GPA1/Gα_{i3} in response to NECA, adenosine and 2CCPA.** Time course data were generated by incubating cells in ligand for 0, 0.5,1, 2, 4, 6, 8 ,10 and 12 hours before lysis and determination of β-galactosidase activity. A_1R::GPA1/G$\alpha_{i1/2}$ was incubated with 100μM NECA as a positive control and assumed to represent the maximal response of this system. This model was implemented in Potter's Wheel using the rates of Table 5.11. K_1, K_2, K_4 and K_7 were fitted to the experimental data. All other parameters were constrained. The fitted parameters were implemented in the ODE model and simulated for 12 hours. Points represent experimental data and solid lines represent equivalent simulations with fitted parameters for **A.** NECA **B.** adenosine and **C** 2CCPA where $\chi^2 < 300$ was considered a good fit. **D.** Concentration-response curves as determined by model output after 12 hours.

Table 5.11: **Parameters of the refined model of G protein signal fitted to the time course data of the A_1R^{GFP}::GPA1/Gα_{i3} in response to NECA, adenosine and 2CCPA.** The rate constants shown were used as initial conditions for fitting K_1, K_2, K_4 and K_7 to the NECA, adenosine and time course data of (Figure 5.32). All other parameters were constrained.

K	NECA Initial	NECA Fitted	Adenosine Initial	Adenosine Fitted	2CCPA Initial	2CCPA Fitted
K_1 (nM^{-1} $hour^{-1}$)	0.150	0.075	0.071	0.029	4.390	4.390
K_2 (nM^{-1} $hour^{-1}$)	0.094	0.005	0.066	0.002	0.086	0.002
K_4 ($hour^{-1}$)	0	0.029	0	0.029	0	0.029
K_7 ($hour^{-1}$)	310	310	310	310	310	310
χ^2		105.8		16.51		37.12

The refined model shows a good fit to the experimental time course data of Figure 5.32 (χ^2 = 105.8, 16.5 and 37.1 for NECA, adenosine and 2CCPA respectively). Interestingly, there is a two-fold reduction in the predicted NECA and adenosine ligand-binding rate, K_1, compared to the A_1R in this strain (Table 5.11). However, K_1 has not changed between the A_1R and A_1R^{GFP} in the presence of GPA1/Gα_{i3}. Interestingly, ligand dissociation, does not change between ligands or receptor variant in this strain ($K_7 = 310\ hour^{-1}$). However, the G protein activation rate, K_2, is substantially lower in this model for the tagged-receptor compared to its unmodified counterpart for NECA, adenosine and 2CCPA. This further suggests that the C-terminal fluorophore interferes with the interaction of the integrated receptor with the G protein. This is unsurprisingly given the extensive interactions between the C-termini of GPCRs and the cell-signalling machinery. However, this region is also responsible for recruiting the receptor-internalisation machinery of *Sc. cerevisiae*. This model predicts that internalisation of A_1R^{GFP} does occur in response to these ligands with a rate of 0.029 $hour^{-1}$. This is much lower than the predicted rates for the A_1R in this strain (0.14 $hour^{-1}$ for NECA and 2CCPA, 0.07 $hour^{-1}$ for adenosine). This would suggest that the C-terminal modification of the A_1R hinders, but does not necessarily abolish, the internalisation of this receptor.

These model predictions were explored by repeating this study in the A_1R^{GFP}::GPA1/Gα_z strain. Time course data were generated in the presence of NECA, adenosine or 2CCPA. Cells were incubated with ligand, lysed and β-galactosidase activity determined. Once again, the A_1R::GPA1/G$\alpha_{i1/2}$ integrate strain was used a positive control and to calculate percentage maximal signal (Figure 5.33).

The time course data of Figure 5.33 shows a sigmoidal response to NECA, adenosine and 2CCPA that plateaus at 6-8 hours, consistent with all other strains tested. Similarly, the maximum level of response is lower for A_1R^{GFP} than for the unmodified counterpart integrated into the GPA1/Gα_z strain. The refined model was applied to these data using Potter's Wheel using the parameter set determined by fitting to the time course data of the A_1R-GPA1/Gα_z strain (Table 5.12). Once again K_4 was initially implemented as, but not constrained to, 0. Ligand-binding, G protein activation and ligand-dissociation (K_1, K_2 and K_3 respectively) were fitted to the experimental data while all other parameters were constrained.

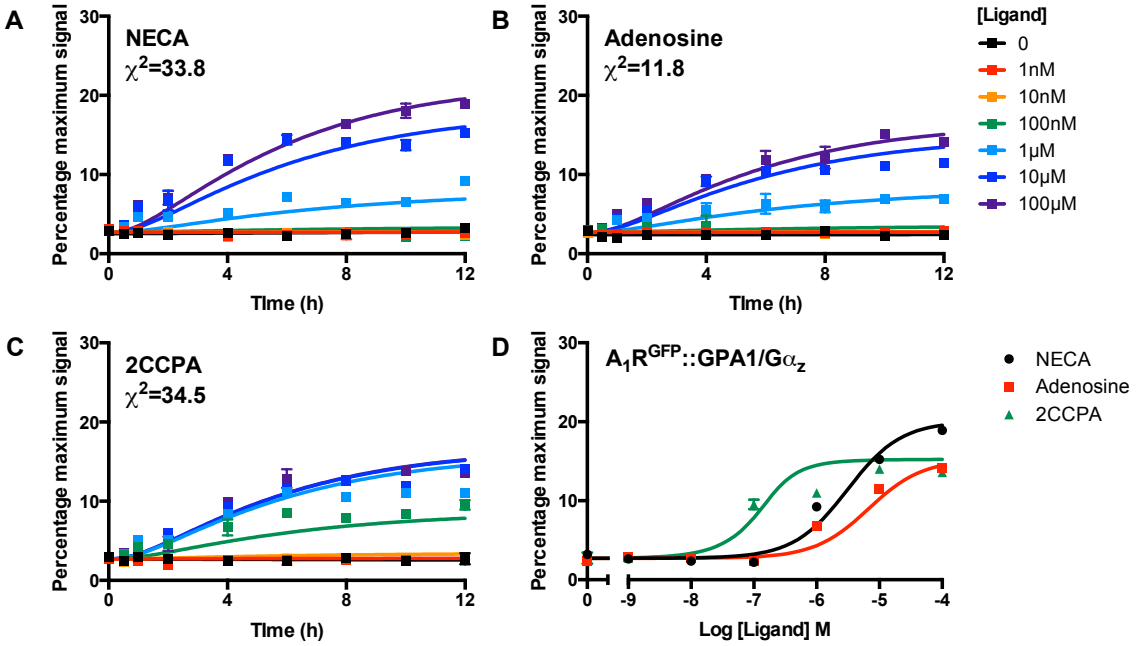

Figure 5.33: **The refined model of G protein signalling fitted to the time course data of the A_1R^{GFP}::GPA1/Gα_z in response to NECA, adenosine and 2CCPA.** Time course data were generated by incubating cells in ligand for 0, 0.5,1, 2, 4, 6, 8 ,10 and 12 hours before lysis and determination of β-galactosidase activity. A_1R::GPA1/Gα_{i12} was incubated with 100μM NECA as a positive control and assumed to represent the maximal response of this system. This model was implemented in Potter's Wheel using the rates of Table 5.12. K_1, K_2, K_4 and K_7 were fitted to the experimental data. All other parameters were constrained. The fitted parameters were implemented in the ODE model and simulated for 12 hours using the ODE23s solver. Points represent experimental data and solid lines represent equivalent simulations with fitted parameters for **A.** NECA **B.** adenosine and **C** 2CCPA. **D.** Concentration-response curves as determined by model output after 12 hours.

Table 5.12: **Parameters of the refined model of G protein signal fitted to the time course data of the A_1R^{GFP}::GPA1/Gα_z in response to NECA, adenosine and 2CCPA.** The rate constants shown were used as initial conditions for fitting K_1, K_2, K_4 and K_7 to the NECA, adenosine and time course data of (Figure 5.33). All other parameters were constrained.

K	NECA Initial	NECA Fitted	Adenosine Initial	Adenosine Fitted	2CCPA Initial	2CCPA Fitted
K_1 (nM^{-1} $hour^{-1}$)	0.075	0.075	0.035	0.035	0.627	4.390
K_2 (nM^{-1} $hour^{-1}$)	0.029	0.003	0.022	0.002	0.020	0.002
K_4 ($hour^{-1}$)	0	0.029	0	0.029	0	0.029
K_7 ($hour^{-1}$)	310	310	310	310	310	310
χ^2		33.84		11.82		34.53

Once again, the refined model achieves a good fit to the experimental time course data of all ligands tested (Figure 5.33). Here, the model predicts that the binding of NECA and adenosine is unaffected by the C-terminal modification of this receptor in this strain. However, there is a 7-fold increase in the simulated 2CCPA-binding rate. But ligand dissociation does not vary between ligands, or indeed strains, in this model ($K_7 = 310$ hour^{-1}). Similarly, the A_1R^{GFP} internalisation rate is remarkably consistent between ligands and strains ($K_4 = 0.029$ hour^{-1} for NECA, adenosine and 2CCPA in both GPA1/Gα_{i3} and GPA1/Gα_z). Once again this predicts that receptor loss is hindered by the C-terminal GFP.

This model predicts that G protein activation is 10-fold lower in this model in response to NECA, adenosine and 2CCPA for the A_1R^{GFP} compared to the A_1R (Table 5.12). This once again predicts that C-terminal modification of the A_1R interferes with G protein activation in yeast. However, these predicted values are consistent with equivalent parameters for A_1R^{GFP}::GPA1/Gα_{i3}. This may imply that the GFP-tag also hinders selective G protein activation, and therefore functional selectivity, of the A_1R in yeast. However, without further data this is speculation but is worthy of future study.

The minimal mathematical model described here is capable of fitting the time course data of the A_1R, and A_1R^{GFP} in yeast in response to multiple ligands. Here, the C-terminal modification is predicted to interfere with G protein activation and receptor internalisation in both A_1R::GPA1/Gα_{i3} and A_1R::GPA1/Gα_z. Indeed, the latter prediction is consistent with experimental studies of an $A_{2A}R^{GFP}$ variant. G protein-coupling is known to occur through extensive contacts on the intracellular face of the GPCR. Thus, the reduced G protein activation predicted here is reasonable. To date, adenosine receptor pharmacology has never been modelled using ODEs in yeast. Thus, the predictions of this model require validation but lend credibility to its use as a tool to study functional selectivity of the A_1R in yeast.

5.5 Summary

The aim of this study is to understand the contribution of the ligand, the receptor and the G protein to functional selectivity of the A_1R by applying mathematical models to experimental data. Limitations in the operational model and a need to predict the biochemical rate constants underlying functional selectivity required the use of ODE models. However, these models are governed by mass action kinetics and uniform expression of the receptor across the population is essential for meaningful model fitting. Consequently, the receptor expression was changed from a variable, plasmid-based system to one of chromosomal integration. However, integration increased the maximum amount of signal relative to plasmid counterparts.

A model framework was iteratively developed with structural identifiability as a key concern. A structurally identifiable model ensures that a given fit to experimental data can only be the result of a unique set of initial conditions and parameters. This demands a minimal model with as many measurable processes as possible that fits specifically to time course data. Here, a minimal model of the yeast pheromone response, guided by the studies Kofahl and Klipp (2004) and Smith et al. (2009), was developed. This model was extended to include a G protein-Effector interaction and ligand interaction to enhance its ability to fit to time course data generated in yeast. Fitting this model to A_1R::GPA1/Gα_{i3} and A_1R::GPA1/Gα_z suggests that ligand binding, G protein activation and receptor internalisation of the A_1R are indeed influence by the G protein in yeast. Thus, the model developed here can describe functional selectivity in yeast. However, to date, no dynamic experimental or computations studies of the A_1R in yeast have been reported. Consequently, these predictions require validation. However, a C-terminal A_1R^{GFP} fusion construct provided the means to further challenge the flexibility and credibility of the model.

Here, A_1R^{GFP} was chromosomally integrated in the yeast transplant strains. However, this reduced E_{max} significantly relative to their plasmid counterparts. Further, the pharmacology of the A_1R^{GFP} was remarkably consistent between strains in contrast to the A_1R. The mathematical model described here was fitted to time course data generated in A_1R^{GFP}::GPA1/Gα_{i3} and A_1R^{GFP}::GPA1/Gα_z to try to understand the differences between A_1R and A_1R^{GFP} while challenging this framework. These fits suggests that the C-terminal fluorophore hinders both G protein activation and receptor internalisation. This is consistent with our current understanding GPCRs and reinforces the usefulness of the model developed here for understanding the contribution of the ligand, receptor and G protein to functional selectivity

Chapter 6

Discussion

6.1 Overview

This ultimate goal of this study was to understand the contribution of the ligand, the receptor and the G protein to functional selectivity through modelling mammalian GPCRs in yeast. To do so this study aimed to:

- Establish and validate adenosine receptor pharmacology in yeast
- Use yeast as a screening platform to aid novel fluorescent compound development
- Develop a quantitative mathematical model of A_1R signalling in yeast

The simple yeast system is an incredibly powerful tool to study mammalian GPCRs in different G protein backgrounds. While the functionality of the A_1R, $A_{2A}R$ and $A_{2B}R$ in yeast has been previously reported (Brown et al., 2000; Stewart et al., 2009; Peeters et al., 2011, 2012; Bertheleme et al., 2013, 2014), a crucial first step of the work presented here was to establish the pharmacology of yeast in our hands.

Previously, the A_1R has been shown to couple to, and signal through, G proteins containing the C-terminal amino acids of $G\alpha_o$, $G\alpha_{i1/2}$ and $G\alpha_{i3}$ in yeast (Stewart et al., 2009). Here similar coupling-profiles were observed when the A_1R was expressed from a plasmid. Interestingly, we observed a previously unreported interaction between GPA1/$G\alpha_z$ and the A_1R. While this is an artificial interaction, given the nature of the transplant G protein, this may have relevance for mammalian systems. $G\alpha_z$ is a cerebrally and pancreatically-distributed member of the $G\alpha_i$ family (Kimple et al., 2005; Wettschureck, 2005; Hinton et al., 1990). Similarly, the A_1R has a wide tissue distribution but prevalent inhibitory effects on adenylate cyclase in the brain. Consequently, this interaction could potentially occur in mammalian systems.

Concentration-response curves were constructed for the A_1R in the strains expressed GPA1/Gα_o, GPA1/G$\alpha_{i1/2}$, GPA1/Gα_{i3} and GPA1/Gα_z. Both β-galactosidase and growth in histidine-deficient media were used as transcriptional reporters of pathway activation. Clear differences were observed between the transcriptional reporters for all ligands. β-galactosidase activity showed significant differences in maximal activity between strains but a 15-fold reduction in sensitivity to ligand relative to equivalent mammalian systems. In contrast, growth showed greater sensitivity to ligands. However, all strains reached comparable maximal levels of signal in response to all ligands tested. Therefore, all ligands were full agonists by this assay and strain differences were difficult to assess. Consequently, β-galactosidase activity was used as the primary measure of pathway activation.

The $A_{2A}R$, $A_{2B}R$ and A_3R were expressed in the yeast system. Significant activity was observed in the GPA1/G$\alpha_{i1/2}$ and GPA1/Gα_s strains in response to both A_2 receptors. Interesting, the latter coupling is consistent with mammalian data but has never been reported in yeast. While significant activity was observed for the A_3R in yeast, the response was too limited to be of any pharmacological use.

Here, the G protein background influenced receptor pharmacology. The preferential activation of different cell-signalling pathways by ligands through a shared drug target is termed bias and is of significant interest to the pharmaceutical industry (reviewed by Shonberg et al. (2014)). For the first time ligand bias was directly quantified for adenosine receptors in yeast. Given that strains only differ in their receptor and 5 C-terminal amino acids of GPA1, this method was applied to as a single quantitative measure of receptor selectivity. To our knowledge, this use of bias has never been reported.

Dr. Jennifer Hemmings and Prof. Martin Lochner of the University of Bern (Switzerland) were seeking to develop novel fluorescent, A_1R-selective agonists. Indeed, fluorescent agonists would greatly inform novel model development. Establishment of the experimental system as a platform to quantify receptor pharmacology, G protein bias and receptor selectivity naturally led to a collaboration where novel agonists were screened and developed. Traditional fluorescent compounds consistent of a ligand domain covalently attached to a fluorescent group through a linker. The group used for attachment was explored as a means of controlling adenosine receptor selectivity. Consequently, Dr. Hemmings synthesised a range of precursor ligands containing these groups prior to fluorophore attachment. N^6-cyclopentyl regions appeared to enhance A_1R pharmacology while showing reduced activity in the A_2R in yeast. However, the N^6-adamantyl compounds demonstrated A_1R/A_2R selectivity, albeit with a reduced potency to the A_1R relative to their precursor ligands.

As N^6-cyclopentyl modifications enhance A_1R potency and receptor selectivity, these compounds were further modified to contain fluorescent BODIPY moieties. However, the N^6-cyclopentyl fluorescent agonist showed a marked reduction in potency against the A_1R relative to its non-fluorescent precursor. Fluorescent N^6-adamantyl agonists yielded no response against the A_1R. Low A_1R potency was shared by CAS200623, a commercially available fluorescent agonist that was used as a comparator. However, fluorescent studies of this compound suggested non-specific binding of A_1R and non-A_1R expressing strains alike.

Pharmacological characterisation of the A_1R was extended to include antagonism. Typically competitive antagonists induce rightward shifts in the concentration-response curves with a conserved maximal activity. Here, A_1R antagonists increase the maximum signal while shifting the concentration-response curve. This effect has been documented in mammalian cells, albeit through β-arrestin dependent assays (Gracia et al., 2013). The presence of biphasic antagonism in yeast, that do not signal through β-arrestins, suggest this is a receptor-level effect. While the underlying mechanism is unknown, it was interesting to note that it does not extend to the novel N^6-adamantyl agonists screened characterised here.

Validation of adenosine receptor pharmacology in yeast, and compound screening, used a plasmid expression-system. Studies of an in frame C-terminal A_1R^{GFP} fusion construct suggested significant variation in receptor expression across the population. However, a significant objective here is to develop a quantitative mathematical framework to understand functional selectivity in yeast. ODE models of biochemical pathways assume the laws of mass action kinetics where the rate of reaction is a product of an intrinsic rate constant and the concentrations of the reacting components. Therefore, uniform receptor expression across the population is desirable. To this end, the A_1R was chromosomally expressed in the GPA1/Gα_o, GPA1/G$\alpha_{i1/2}$, GPA1/Gα_{i3} and GPA1/Gα_z strains. Interestingly, the maximal level of signal in these strains was increased relative to their plasmid counterparts.

The kinetic information gained from ODE model fitting is limited by structural identifiability, or the guarantee that a given model output can only be the result of a unique combination of parameters and initial conditions. Consequently, structural identifiability is an essential prerequisite of any mathematical framework developed here. The model must be fitted to time course data to satisfy this criteria. Also, in the presence of a single quantitative measure, the transcriptional reporter, the model must be as minimal as possible to ensure accuracy of fitting. Several increasingly complex iterations were developed to achieve satisfactory model fits for all ligands. The final model variant required that the G protein signalled via an effector and ligand dissociated from the receptor. Fitting this model to A_1R::GPA1/Gα_{i3} and A_1R::GPA1/Gα_z strains predicted largely consistent ligand binding and receptor activation rates as a function of G protein, but that differences

in pharmacology are driven by G protein-activation efficiency.

When chromosomally-expressed in yeast, the A_1R^{GFP} shows a marked decreased in maximum level of activity relative to plasmid counterparts, a direct contrast to the A_1R. The difference in pharmacology between these receptor variants presented an interesting challenge through which to validate the model developed here. This framework was fitted to the time course data of A_1R^{GFP}::GPA1/Gα_{i3} and A_1R^{GFP}::GPA1/Gα_z. This predicted that, while ligand binding is consistent between the A_1R and A_1R^{GFP}, the C-terminal fluorophore may hinder G protein-activation and receptor internalisation in yeast. This prediction is biologically valid given the known structures of, and interactions between, GPCRs and G proteins.

6.2 Adenosine receptor pharmacology in yeast

The yeast strains here represent an incredibly powerful platform for drug screening. Their fast growth, genetic amenability and experimental robustness lend themselves particularly well to high-throughput screening processes in the drug discovery process. Indeed, this is their primary function in the pharmaceutical industry in which they were developed.

However, this system, like all experimental tools have some significant flaws. Most notably, the lack of β-arrestins. Typically, functional selectivity in GPCR signalling is described with regard to activation of G protein or β-arrestin-dependent pathways. Indeed, this form of functional selectivity is more intensively investigated (reviewed by Shonberg et al. (2014)). This is due in part to the experimental assay system. For example, the A_1R, has been shown to signal through Gα_i or activate ERK1/2 in a β-arrestin-dependent manner. This has been shown through cAMP accumulation and ERK phosphorylation assays respectively (Stewart et al., 2009; Gracia et al., 2013). Consequently, there are clearly distinct experimental readouts of pathway activation. The vast differences between these measures are also reflected in their downstream effects. For instance the μ-opioid receptor induces analgesia through G protein signalling but also promotes osteochondritis through β-arrestins (Raehal, 2005; Pradhan et al., 2010, 2012). This off-target effect is relatively easy for the pharmaceutical industry to investigate. However, functional selectivity on a G protein level is far more difficult to elucidate in a mammalian setting.

Here, the A_1R signals through G protein transplants representing $G\alpha_o$, $G\alpha_{i1/2}$, $G\alpha_{i3}$ and $G\alpha_z$ in yeast. These are all $G\alpha_i$ family members that primarily inhibit adenylate cyclase. Thus, they are nearly impossible to differentiate in mammalian signalling systems. This represents a strength of the yeast system as differences between these families can be approximated. However, the argument is frequently made that yeast are not mammalian systems, the GPCR G protein interactions are still largely artificial and the amount of information available is limited. Here some potentially artificial couplings of the A_2R and A_3R subtypes were observed, through GPA1/$G\alpha_{i3}$ and GPA1/$G\alpha_{12}$ respectively, with no equivalent data in mammalian systems. It is also possible that, due to restrictions in tissue distribution, that the GPCR will never have the opportunity to signal through that subunit. Thus, while structurally feasible, these interactions have no physiological basis. However, the A_1R has a sufficiently wide tissue distribution that this is not a particular issue for this receptor.

However, the argument persists that the A_1R in yeast is still a non-native GPCR and downstream measures may not representative of a true mammalian system. Most cell-signalling assays exploit cell lines. These lines are typically oncogenic and by definition exhibit aberrant cellular behaviour. Consequently, one can counter that yeast are no more or less valid than mammalian cell lines as an experimental system. However, we accept that the yeast strains used here may be regarded as a predictive system of selective G protein activation and mammalian validation is needed. Indeed, this approach was used by Weston et al. (2014) whose studies of GLP-1 in yeast was conducted alongside the studies described here. The A_1R is known to signal through $G\alpha_o$, $G\alpha_{i1}$ and $G\alpha_{i3}$ *in vivo*. The potential for $G\alpha_z$ signalling in response to this receptor is unique to this study and requires mammalian validation. Difficulties in distinguishing between mammalian $G\alpha_i$ subtypes may be overcome using the experimental tools commonly associated with measuring cAMP. Cholera toxin ADP-ribosylates $G\alpha_s$, rendering it permanently GTP-bound thus promoting adenylate cyclase activity (Ribeiro-Neto et al., 1985). Similarly forskolin, directly interacts with and activates adenylate cyclase (Sadana and Dessauer, 2009). The elevated intracellular cAMP concentrations allow for measurements of $G\alpha_i$-mediated inihibition of adenylate cyclase. However, $G\alpha_i$ family members are ADP-ribosylated by pertussis toxin, uncoupling it from the receptor and preventing downstream effects on adenylate cyclase (Ribeiro-Neto et al., 1985; Gancedo, 2013). $G\alpha_z$ is an exception to this rule. This G protein lacks the ADP-ribosylation site and is considered to be pertussis-toxin insensitive (Hinton et al., 1990). Thus, it may be possible to use pertussis toxin to confirm A_1R-$G\alpha_z$ interactions *in vivo*.

Despite experimental limitations, the validation of the yeast system presented here represents some interesting trends that may bear significance. Here, at least with regard to β-galactosidase activity, the G protein subtype influences A_1R pharmacology in yeast. This is most notable in maximal activity where E_{max} is progressively lower for GPA1/G$\alpha_{i1/2}$ >GPA1/Gα_{i3} >GPA1/Gα_z >GPA1/Gα_o >. The differences in the maximal level of signal also extends to the pharmacology of individual ligands. NECA is a full agonist of the A_1R in all strains tested. However, while 2CCPA is a full agonist against A_1R-GPA1/Gα_{i3}, it appears to be a high-affinity partial agonist in the other strains, when expressing the A_1R from a plasmid. 2CCPA has been established a full agonist in mammalian systems where the A_1R can be potentially interacting with multiple G proteins. Thus, this study in yeast would predict that 2CCPA is a G protein subtype-specific partial agonist. This could be therapeutically relevant. Clinical trials of A_1R-selective antagonists have been largely unsuccessful. This has lead to the use of high-affinity partial agonists to outcompete endogenous adenosine to reduce E_{max}. This study would predict that 2CCPA, an A_1R-selective partial agonist could be used reduce A_1R-mediated activity in a receptor subtype specific manner. This would be an interesting prediction to test *in vivo*.

6.3 Do adenosine receptors truly show functional selectivity?

This study represents the first attempt to directly quantify bias for adenosine receptors. The ability of the yeast system to predict differences between members of the Gα_i family has particular advantages for the A_1R. Indeed, differences in β-galactosidase activity were observed between strains expressing this receptor. However, the potencies of the novel and commercially available ligands characterised here are conserved between strains. This may suggest that the differences in pharmacology are largely a consequence of G protein-coupling efficiency in yeast. However, bias plots are constructed relative to NECA, that would be subject to the same signalling-efficiency constraints as other ligands in each strain. These plots suggest the commercially available and novel ligands characterised here show little bias between G$\alpha_{i1/2}$ and Gα_{i3}, but significant bias between these G protein subtypes and GPA1/Gα_z. Thus, the A_1R is subject to functional selectivity, but whether any Gα_z-mediated signalling has physiological relevance remains to be determined.

Similarly, the A_2R receptor subtypes signalled though GPA1/Gα_{i3} in yeast, an interaction with no documented equivalent in more complex systems. No previous $A_{2A}R$ Gα_s interaction has been reported in yeast. Interestingly, Bertheleme et al. (2013, 2014) have used GPA1/Gα_{i3} to elucidate receptor level effects of $A_{2A}R$ mutants. A study based on GPA1/Gα_s would be much more physiologically relevant. However, there is a key difference between that study and the data presented here. Bertheleme et al. (2013, 2014) used growth in histidine-deficient media as a transcriptional reporter. Here, the $A_{2A}R$-GPA1/Gα_s interaction yielded significant responses to ligand by β-galactosidase assay only. The difference in pathway measurement may explain why this physiologically-relevant interaction was overlooked.

However, here we demonstrate that the the effect of G protein subtype on $A_{2A}R$ pharmacology is far more pronounced than for the A_1R. Here we show a marked reduction in the potency of NECA in the $A_{2A}R$-GPA1/Gα_s strain relative to its GPA1/Gα_{i3} counterpart. Adenosine and 2CCPA yielded no response in $A_{2A}R$-GPA1/G$\alpha_{i1/2}$. However, the CGS21680 pharmacology is preserved between the two strains. This suggests that functional selectivity does occur for this receptor. However, bias could not be directly quantified. If the $A_{2A}R$-Gα_i interaction is preserved in a mammalian setting this does raise some interesting questions. Could the $A_{2A}R$-Gα_i interaction be insensitive to the endogenous agonist adenosine? Do non-native ligands such as NECA promote $A_{2A}R$-Gα_i signalling *in vivo*? Could this effect be exploited for therapeutic benefit? However, these questions, while interesting, are speculative and substantial research into the physiological significance of this predicted coupling is required.

A similar G protein-coupling profile was observed for the $A_{2B}R$ as for the $A_{2A}R$. The existence of identical coupling profiles for both A_2R receptor subtypes is encouraging and may, to a small extent, validate the $A_{2A}R$-GPA1/G$\alpha_{i1/2}$ interaction described here. Encouragingly, the $A_{2B}R$ was shown to signal via GPA1/Gα_s in yeast by Brown et al. (2000) when these strains were first developed and characterised. However, to our knowledge, this is the first and last time this physiologically-significant interaction has been explored. Further studies of this receptor in yeast relied on the GPA1/Gα_{i3} strain ((Peeters et al., 2011; Liu et al., 2014)). Why the authors focussed on this strain is a mystery as no explanation is provided in their publications. However, the data presented here suggests that, despite a higher E_{max} for $A_{2B}R$-GPA1/G$\alpha_{i1/2}$, the G protein subtype does little to influence pharmacology or bias.

Unfortunately, this study was not successfully extended to include the A_3R and any bias it may exhibit. As an emerging target for immunomodulatory disease it would have been interesting to compare the pharmacology of this receptor to the similarly-coupled A_1R. Indeed, this would have greatly helped to elucidate whether the novel compounds described here, particularly the N^6-adamantyl agonists, are truly A_1R-selective.

6.4 N^6-substituents and biphasic pharmacology

The yeast transplant strains used here were originally developed, and continue to be used, as a high-throughput drug screening platform. Consequently, this study used this tool to elucidate the A_1R/A_2R-selectivity of N^6-substituted and fluorescent adenosine receptor agonists. This is summarised in Figure 6.1.

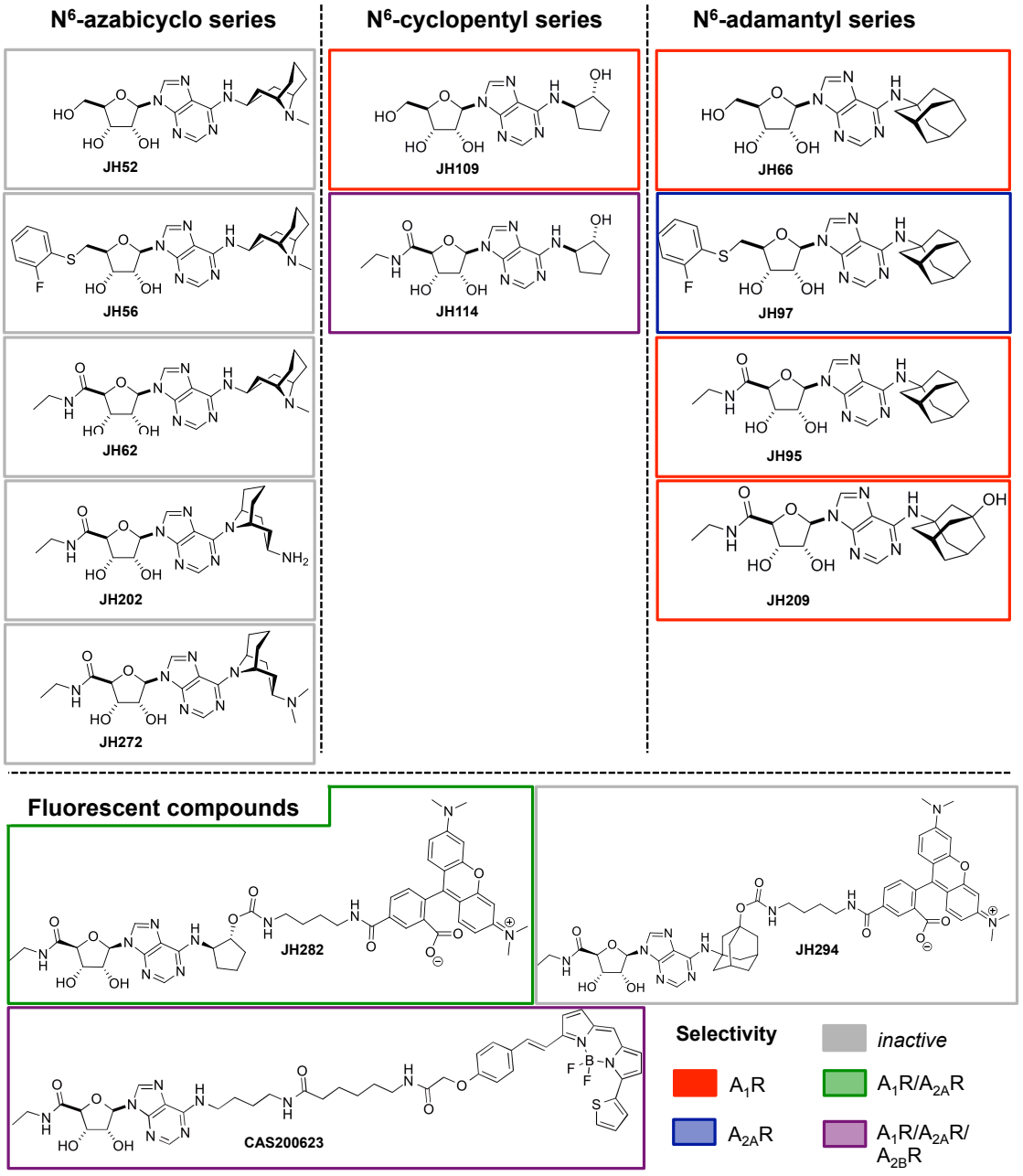

FIGURE 6.1: **Adenosine receptor selectivity of N^6-substituents and fluorescent agonists.** Compounds that promoted no response in any strain are highlighted in grey. Agonists that are A_1R or $A_{2A}R$ selective in yeast are highlighted in red and blue respectively. Compounds highlighted in green are A_1R and $A_{2A}R$ selective while those highlighted in purple activated all strains tested.

N^6-substituted agonists we chosen as candidates for fluorescent compound development due to their established role in adenosine receptor selectivity (Shearer et al., 2009; Colca, 2012). Indeed, N^6-cyclopentyl modifications appear to increase A_1R sensitivity while decreasing potency against the A_2R subtypes in yeast, relative to their precursors. However, this moiety is relatively two-dimensional. Larger three-dimensional adamantyl groups show total A_1R/ A_2R selectivity at the expense of A_1R potency. A_1R sensitivity is further reduced by the addition of a hydroxyl group to the adamantyl region. This may imply steric hindrance at the A_1R. Docking and simulation studies of an A_1R homology model are currently underway to explore this further (Knight *et al., in preparation*).

However, the effect of N^6-adamantyl agonists on A_1R antagonism warrants further investigation. Here, antagonists such as DPCPX and SLV-320 increase the E_{max} of NECA, adenosine and 2CCPA while promoting rightward shifts in the concentration-response curve. Schild analyses suggest that these ligands are not solely competitive. Studies on the $A_{2B}R$ receptor suggest that this is not a yeast-specific effect. This effect has also been reported in mammalian cells by G protein and β-arrestin-dependent assays, suggesting that this non-competitive interaction is a receptor-level effect. To date, only Gracia et al. (2013) has tried to find the structure-activity relationship underlying this effect. They report that dimerisation of the A_1R forms homodimers and claim that biphasic antagonism is a consequence of agonist and antagonist binding separate promoters. However, without supporting data this is more speculation than hypothesis. Without an A_1R crystal structure, or knowledge of the dimerisation interface, monomer and dimer antagonism cannot be experimentally or theoretically compared. However, N^6-adamantyl agonists show no increase in E_{max} while shifting the concentration-response curve. Thus they may provide a tool to explore the mechanisms of biphasic antagonism.

Schild analyses support the idea of multiple binding sites as a cause of biphasic antagonism. Indeed, this could be down to interactions between two occupied orthosteric sites across a dimer. However, this study favours allosteric antagonism as explanation for this behaviour. PD81723 is commonly accepted to be an allosteric antagonist, capable of binding both allosteric and orthosteric sites on the A_1R to positively or negative regulate signal, respectively, depending on ligand concentration. This study suggests that DPCPX, SLV-320 and caffeine may also be allosteric antagonists. The behaviour of N^6-adamantyl agonists would support this theory. The interaction between ECL2 and TM3 of the A_1R has been shown to be essential to allosterism of the A_1R (Peeters et al., 2012). This interaction is in close proximity to the proposed A_1R orthosteric site. The reduced potency of N^6-adamantyl-substituents may be due to steric hindrance around the orthosteric site. If so, it may be possible that the bulky N^6 group could deny antagonists access to the allosteric site. However, without further information this is also speculation, not hypothesis. But given the use of partial A_1R agonists as negative regulators of signalling due to

antagonist trial failure, the novel compounds characterised here may be able to directly compete with antagonists *in vivo* and have therapeutic potential.

6.5 Yeast for screening fluorescent ligands

The N^6-agonists described here were explored as precursors for fluorescent compound development. NECA-based compounds were found to have higher potency against the A_1R in yeast that was increased by N^6-cyclopentyl modifications. However, N^6-adamantyl attachments decrease A_1R potency while promoting total A_1R/A_2R selectivity in yeast. Similarly, the commercially available CAS200623 shows a reduced potency against the A_1R relative to its NECA precursor in yeast. Thus, the A_1R-selective JH95 and the high potency JH114, both based on NECA, were ideal candidates for fluorescent compound development. This resulted in JH294 and JH282 respectively. JH282 was shown to be a weak full-agonist of the A_1R and $A_{2A}R$, while JH294 showed no response in any strain tested. Given that extended N^6-modifications reduce potency against the A_1R, and that JH95 is a weak full agonist, a lack of response is unsurprising. The ability to perform these analyses with a limited stock of agonist highlights a strength of the yeast system for compound screening, experimental robustness and reproducibility.

However, these experiments highlight a weakness of yeast as a compound screening system. CAS200623 was found to bind A_1R-expressing and non-expressing cells alike. This raises several questions. Is non-specific binding of this compound unique to yeast? Or is non-specific binding a problem for this specific compound? The studies of Middleton et al. (2007) and May et al. (2010) of similar fluorescent compounds on the A_1R would suggest that this is a yeast-specific effect. This is feasible given that yeast have a cell wall that mammalian cells lack. This may non-specifically bind the fluorescent compound. This can be elucidated through removing the yeast cell wall and repeating the binding experiments. This could be complemented by flow cytometry of mammalian cells. Unfortunately, limited compound stocks and supplier difficulties prevented these studies here. Regardless, non-specific binding limited the usefulness of CAS200623 in modelling A_1R pharmacology in yeast.

However, it is possible that the fluorophore is responsible for non-specific binding of yeast. The presence of a BODIPY region on CAS200623 guided the decision to include a TAMRA group on the fluorescent compounds developed here. Binding studies of the active and inactive JH282 and JH294, respectively, could help explain the contribution of fluorophore to non-specific binding, if any. These studies are ongoing in both yeast and mammalian cells. Further, this continuing collaboration is being extended to include a range of ligand and fluorophore domains and their implications for specificity of adenosine receptor binding and activation.

6.6 Quantitative mathematical modelling

The ultimate aim of this study is to develop a quantitative mathematical model to describe GPCR pharmacology in yeast. The A_1R was intended to be a testbed upon which this framework could be built. This was due to the proven functionality in yeast and the vast array of tools to probe the pharmacological characteristics of this receptor. This model was then to be extended to include other mammalian GPCRs. Here models were constructed from biological reaction schemes and ODEs derived. The structural identifiability of the model was confirmed, before implementation, as an essential requisite followed by parameter sensitivity analyses. Fitting the model to experimental time course data yielded parameters underlying G protein signalling that have to be experimentally validated (Figure 6.2).

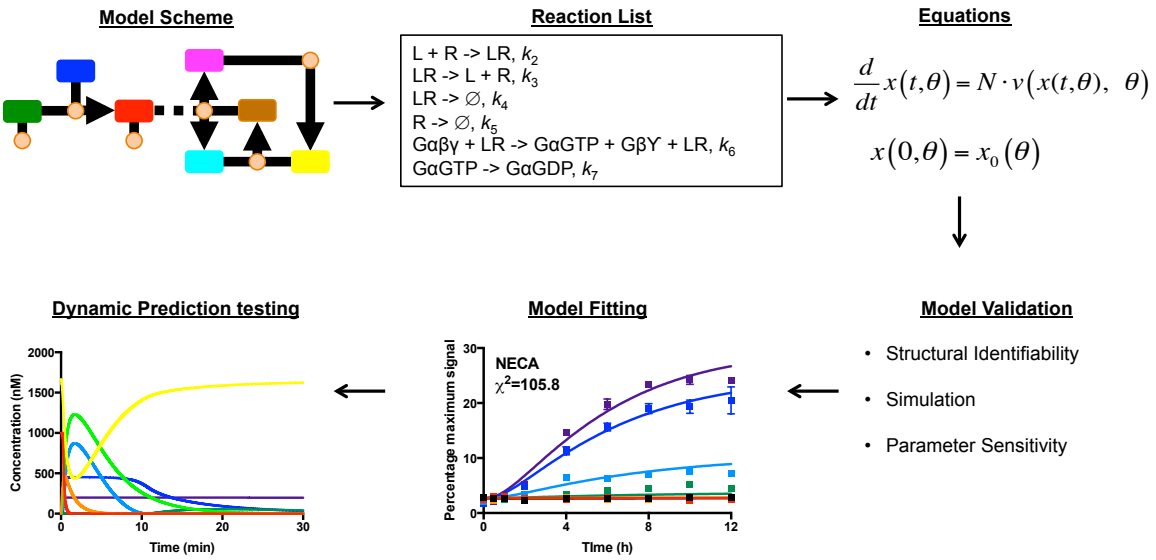

FIGURE 6.2: **Schematic representation of quantitative model development.** Biochemical reaction schemes are converted to ODE equations by assuming the laws of mass action kinetics. The suitable of this model framework for model fitting is ascertained through implementation and parameter sensitivity analysis. Structural identifiability is an essential prerequisite of model fitting. Once this criteria is satisfied the model can be fitted to experimental time course data. The resulting predictions can than be experimentally verified.

ODE models are subject to the laws of mass action kinetics. While the models presented here are globally and structurally identifiable, the reliability of their predictions are intrinsically linked to the accuracy of their initial species concentrations. The yeast strains presented here are a modified experimental system and the concentrations of receptor and G protein are unknown. For example, the A_1R is under the control of the constitutive *GAPDH* promoter. The data used to generate this model, and those upon which it is based, were derived from studies the the native GPCR, STE2, under the control of its endogenous pheromone-responsive promoter. Consequently, receptor concentrations in the models presented here may not be the 160nM that is used in the model. Similarly, the GPA1 G protein has been deleted and transplant variants chromosomally-expressed from the *TRP1* locus. While this is under the control of the endogenous *GPA1* promoter, epigenetic influences may affect GPA1 expression. Thus, the initial species concentrations underlying this model need to be confirmed. Until these conditions are elucidated, the predictions presented here are semi-quantitative at best. Quantitative Western blotting and mass spectrometry studies are currently underway to elucidate the concentrations of receptor and G protein in the yeast strains used here.

Despite this, a great deal has been learned from the model developed here. While not necessarily quantitative without known initial species concentrations, the resulting predictions are useful. The relative ratios of parameters estimated should be conserved. The successive model iterations suggest that ligand dissociation, receptor internalisation and G protein-effector interactions are essential to model fitting to yeast data. This led to the development of the refined model fitted here. Fitting this model to experimental time course data of A_1R::GPA1/Gα_{i3} and A_1R::GPA1/Gα_z suggested that G protein subtype does indeed influence ligand-binding, receptor activation and downstream G protein signalling. In particular, ligand binding and G protein activation were reduced in a GPA1/Gα_z background relative to GPA1/Gα_{i3}. However, this model suggested that ligand dissociation and receptor internalisation are not affected by G protein. Knowledge of initial conditions can translate these predictions to quantitative intrinsic parameters through more accurate model fitting.

Once quantitative, the model predictions could be applied to mammalian systems. For example, here we model A_1R agonist pharmacology in GPA1/Gα_{i3} and GPA1/Gα_z backgrounds. Therefore these models can be merged to include both Gα_{i3} and Gα_z signalling (Figure 6.3). However, both these effectors result in inhibition of adenylate cyclase *in vivo*. The yeast system has demonstrated that the GLP-1R can both positively and negative regulate adenylate cyclase activity through Gα_s and Gα_i respectively (Weston et al., 2014). Thus, this model could be applied to a variety of mammalian GPCRs functional in yeast with multiple G protein signalling outcomes (Figure 6.3).

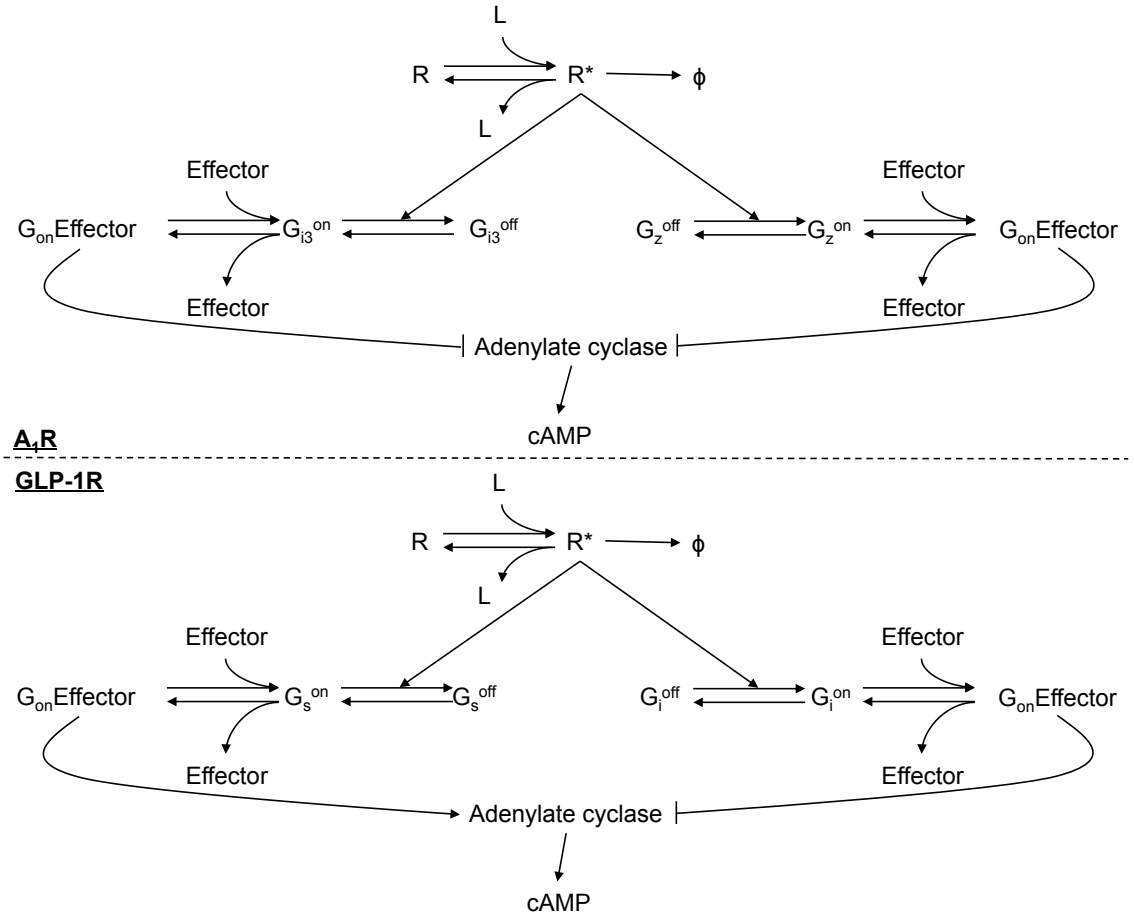

FIGURE 6.3: **Merging multiple yeast models to approximate mammalian G protein signalling.** Individual ligand-GPCR-G protein interactions can be isolated and modelled using the yeast system. These predictions can be merged to approximate multiple signalling processes in mammalian systems. GPCRs that signal through multiple G protein families in yeast and mammalian systems could also be vulnerable to this approach **A.** Combining A_1R models of GPA1/Gα_i signalling in yeast to describe inhibition of adenylate cyclase in a mammalian setting. **B.** Combining GLP-1R models of GPA1/Gα_i and GPA1/Gα_s signalling in yeast to describe inhibition and stimulation of adenylate cyclase in a mammalian setting, respectively.

6.7 Future work

6.7.1 Modelling the $A_{2A}R$ receptor

The A_1R was selected as a tool for validation and development of a G protein signalling model in yeast. On reflection, the $A_{2A}R$ may have represented a better choice. The $A_{2A}R$ has also been extensively characterised and is vulnerable to the same pharmacological tools as the A_1R, including fluorescent ligands. At present, the framework presented here cannot reproduce signal in the absence of ligand. The presence of significant basal signalling, through constitutive receptor activation, could have increased the versatility of the model. Also, the differences in $A_{2A}R$ pharmacology in the presence of GPA1/Gα_s and GPA1/Gα_i may warrant further investigation. A A_{2A}-Gα_i interaction has yet to be demonstrated in mammalian cells but, in yeast the $A_{2A}R$::GPA1/G$\alpha_{i1/2}$ strain did not respond to the endogenous ligand adenosine. However, NECA and CGS21680 did elicit a response in this strain. This demonstrates functional selectivity of the $A_{2A}R$. Thus, a natural extension of this study is to model $A_{2A}R$-mediated signalling in yeast and further validation in mammalian systems.

6.7.2 Dynamic studies in yeast

A model is only as good as the predictions it makes. One obvious way to improve the predictions presented here is clarification of initial conditions throughout the modified yeast pathway. Structural identifiability ensures accuracy of model fitting through the use of dynamic data. This study exploits a single transcriptional reporter as an observable measure of pathway activation. Validation of model predictions, and structural identifiability, can be further addressed by taking multiple dynamic measurements throughout the yeast pathway. Fluorescent ligands, such as JH282, can be used to generated dynamic receptor-level data such as binding and internalisation. This is assuming that this compound does not non-specifically bind the yeast cell surface. A non-invasive method of measuring receptor loss is key due to the effects of C-terminal GFP modifications on A_1R pharmacology. Further modification of the yeast pheromone-response can be used to generate dynamic data throughout the pathway to validate and inform model predictions (Figure 6.4).

FRET studies exploit the interaction between fluorescent regions to quantify protein-protein interactions. Here the emission wavelength of one fluorophore is the excitation wavelength of its FRET partner. If the proteins are within a certain radius, one fluorophore can be excited but the other detected. Consequently, the rate that these fluorophores separate can be quantified. Intra- and intermolecular FRET can be used as dynamic reporters of protein state.

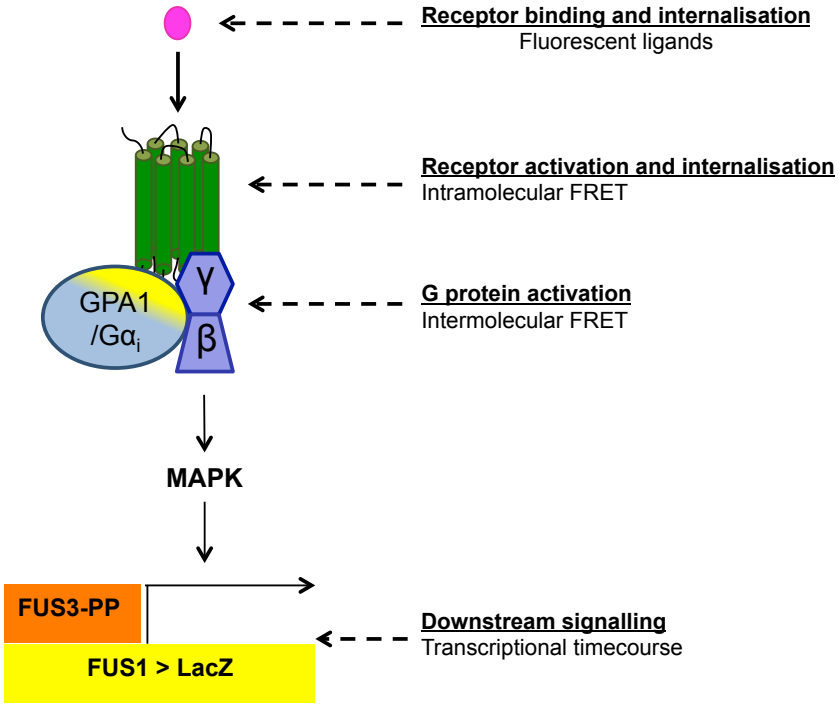

FIGURE 6.4: **Multiple dynamic measurements of G protein signalling in yeast.** Fluorescent ligands can be used to quantify ligand-binding and receptor internalisation. Receptor and G protein-activation can be measured by intra- and intermolecular FRET respectively.

Receptor activation states are determined by the orientation of the TM helices. Small fluorescent regions, such as FlAsh, can used to label individual domains. This approach has been used to measure receptor activation of the A_1R and $A_{2A}R$ through rearrangement of the α-helical domains (Hoffmann et al., 2005). These intramolecular FRET reporter constructs have been obtained and are currently being investigated in yeast (Ladds *et al.*, unpublished data).

Previously, G protein activation has been measured in yeast through intermolecular FRET between YFP and CFP-modified GPA1 and STE18 ($G\gamma$). Yi et al. (2003) have kindly provided the G protein constructs used to develop these strains. Efforts to modify and express these fluorescent G protein subunits in the yeast transplant system are underway. In time, these strains will be able to generate receptor, G protein and transcriptional-level dynamic data. Thus, the yeast transplant strains would be a more versatile tool for applying a systems pharmacology approach to a range of GPCRs.

6.8 Concluding remarks

For the first time, an ODE model has been used to describe functional selectivity of the A_1R in yeast. This model predicts that the rates of ligand binding, G protein activation and receptor internalisation are indeed a function of the G protein. However, further experimental refinements are required to produce a truly quantitative model. For instance, the concentrations of receptor and G protein need to be elucidated and the dynamic model predictions can be tested through functional selectivity. Once this has been achieved, the theoretical framework developed here could be used to investigate functional selectivity in a range of GPCRs.

Bibliography

Agoram, B. M. and Demin, O. (2011). Integration not isolation: arguing the case for quantitative and systems pharmacology in drug discovery and development. *Drug Discovery Today* **16**, 1031–1036.

Alexander, S. P., Curtis, A. R., Kendall, D. A. and Hill, S. J. (2006). A1 adenosine receptor inhibition of cyclic AMP formation and radioligand binding in the guinea-pig cerebral cortex. *British Journal of Pharmacology* **113**, 1501–1507.

Anguelova, M., Karlsson, J. and Jirstrand, M. (2012). Minimal output sets for identifiability. *Mathematical Biosciences* **239**, 139–153.

Antonioli, L., Csóka, B., Fornai, M., Colucci, R., Kókai, E., Blandizzi, C. and Haskó, G. (2014). Adenosine and inflammation: what's new on the horizon? *Drug Discovery Today* **19**, 1051–1068.

Attwood, T. K. and Findlay, J. B. C. (1994). Fingerprinting G-protein-coupled receptors. *Protein Engineering, Design and Selection* **7**, 195–203.

Avlani, V. A., Gregory, K. J., Morton, C. J., Parker, M. W., Sexton, P. M. and Christopoulos, A. (2007). Critical role for the second extracellular loop in the binding of both orthosteric and allosteric G protein-coupled receptor ligands. *The Journal of Biological Chemistry* **282**, 25677–25686.

Avruch, J. (1998). Insulin signal transduction through protein kinase cascades. *Molecular and Cellular Biochemistry* **182**, 31–48.

Bai, J. P. F., Fontana, R. J., Price, N. D. and Sangar, V. (2014). Systems pharmacology modeling: an approach to improving drug safety. *Biopharmaceutics and Drug Disposition* **35**, 1–14.

Bai, M., Trivedi, S. and Brown, E. M. (1998). Dimerization of the extracellular calcium-sensing receptor (CaR) on the cell surface of CaR-transfected HEK293 cells. *The Journal of Biological Chemistry* **273**, 23605–23610.

Baker, J. G. and Hill, S. J. (2006). A comparison of the antagonist affinities for the Gi- and Gs-coupled states of the human adenosine A1-receptor. *Journal of Pharmacology and Experimental Therapeutics* **320**, 218–228.

Baker, J. G., Middleton, R., Adams, L., May, L. T., Briddon, S. J., Kellam, B. and Hill, S. J. (2010). Influence of fluorophore and linker composition on the pharmacology of fluorescent adenosine A1 receptor ligands. *British Journal of Pharmacology* **159**, 772–786.

Ballesteros, J. A., Jensen, A. D., Liapakis, G., Rasmussen, S. G., Shi, L., Gether, U. and Javitch, J. A. (2001). Activation of the beta 2-adrenergic receptor involves disruption of an ionic lock between the cytoplasmic ends of transmembrane segments 3 and 6. *The Journal of Biological Chemistry* **276**, 29171–29177.

Bardwell, L., Cook, J. G., Chang, E. C., Cairns, B. R. and Thorner, J. (1996). Signaling in the yeast pheromone response pathway: specific and high-affinity interaction of the mitogen-activated protein (MAP) kinases Kss1 and Fus3 with the upstream MAP kinase kinase Ste7. *Molecular and cellular biology* **16**, 3637–3650.

Bardwell, L. and Thorner, J. (1996). A conserved motif at the amino termini of MEKs might mediate high-affinity interaction with the cognate MAPKs. *Trends in Biochemical Sciences* **21**, 373–374.

Berger, S. I. and Iyengar, R. (2011). Role of systems pharmacology in understanding drug adverse events. *Wiley Interdisciplinary Reviews. Systems Biology and Medicine* **3**, 129–135.

Berridge, M. J. (1993). Inositol trisphosphate and calcium signalling. *Nature* **361**, 315–325.

Berridge, M. J. (2009). Inositol trisphosphate and calcium signalling mechanisms. *Biochimica et Biophysica Acta* **1793**, 933–940.

Bertheleme, N., Singh, S., Dowell, S. J., Hubbard, J. and Byrne, B. (2013). Loss of constitutive activity is correlated with increased thermostability of the human adenosine A2A receptor. *British Journal of Pharmacology* **169**, 988–998.

Bertheleme, N., Strege, A., Bunting, S. E., Dowell, S. J. and Byrne, B. (2014). Arginine 199 and leucine 208 have key roles in the control of adenosine A2A receptor signalling function. *PLoS ONE* **9**, e89613.

Bevan, N., Palmer, T., Drmota, T., Wise, A. and Coote, J. (1999). Functional analysis of a human A1 adenosine receptor/green fluorescent protein/Gi1α fusion protein following stable expression in CHO cells. *FEBS Letters* **462**, 61–65.

Bjarnadóttir, T. K., Geirardsdóttir, K., Ingemansson, M., Mirza, M. A. I., Fredriksson, R. and Schiöth, H. B. (2007). Identification of novel splice variants of adhesion G protein-coupled receptors. *Gene* **387**, 38–48.

Black, J. W. and Leff, P. (1983). Operational models of pharmacological agonism. *Proceedings of the Royal Society of London. Series B, Royal Society (Great Britain)* **220**, 141–162.

Blumer, K. J., Reneke, J. E. and Thorner, J. (1988). The STE2 gene product is the ligand-binding component of the alpha-factor receptor of *Saccharomyces cerevisiae*. *The Journal of Biological Chemistry* **263**, 10836–10842.

Bockaert, J. and Pin, J. P. (1999). Molecular tinkering of G protein-coupled receptors: an evolutionary success. *The EMBO Journal* **18**, 1723–1729.

Bos, J. L., Rehmann, H. and Wittinghofer, A. (2007). GEFs and GAPs: critical elements in the control of small G proteins. *Cell* **129**, 865–877.

Briddon, S. J., Middleton, R. J., Cordeaux, Y., Flavin, F. M., Weinstein, J. A., George, M. W., Kellam, B. and Hill, S. J. (2004). Quantitative analysis of the formation and diffusion of A1-adenosine receptor-antagonist complexes in single living cells. *Proceedings of the National Academy of Sciences of the United States of America* **101**, 4673–4678.

Brinkerhoff, C. J., Traynor, J. R. and Linderman, J. J. (2008). Collision coupling, crosstalk, and compartmentalization in G-protein coupled receptor systems: can a single model explain disparate results? *Journal of Theoretical Biology* **255**, 278–286.

Brown, A. J. (2002). The orphan G protein-coupled receptors GPR41 and GPR43 are activated by propionate and other short chain carboxylic acids. *Journal of Biological Chemistry* **278**, 11312–11319.

Brown, A. J., Daniels, D. A., Kassim, M., Brown, S., Haslam, C. P., Terrell, V. R., Brown, J., Nichols, P. L., Staton, P. C., Wise, A. and Dowell, S. J. (2011). Pharmacology of GPR55 in yeast and identification of GSK494581A as a mixed-activity glycine transporter subtype 1 inhibitor and GPR55 agonist. *Journal of Pharmacology and Experimental Therapeutics* **337**, 236–246.

Brown, A. J., Dyos, S. L., Whiteway, M. S., White, J. H., Watson, M. A., Marzioch, M., Clare, J. J., Cousens, D. J., Paddon, C., Plumpton, C., Romanos, M. A. and Dowell, S. J. (2000). Functional coupling of mammalian receptors to the yeast mating pathway using novel yeast/mammalian G protein alpha-subunit chimeras. *Yeast* **16**, 11–22.

Bruns, R. F. and Fergus, J. H. (1990). Allosteric enhancement of adenosine A1 receptor binding and function by 2-amino-3-benzoylthiophenes. *Molecular Pharmacology* **38**, 939–949.

Butz, J. A., Niebauer, R. T. and Robinson, A. S. (2003). Co-expression of molecular chaperones does not improve the heterologous expression of mammalian G-protein coupled receptor expression in yeast. *Biotechnology and Bioengineering* **84**, 292–304.

Bylund, D. B. and Toews, M. L. (2011). Radioligand binding methods for membrane preparations and intact cells. *Methods in Molecular Biology* **746**, 135–164.

Casadó, V., Barrondo, S., Spasic, M., Callado, L. F., Mallol, J., Canela, E., Lluís, C., Meana, J., Cortés, A., Sallés, J. and Franco, R. (2010). Gi protein coupling to adenosine A1-A2A receptor heteromers in human brain caudate nucleus. *Journal of Neurochemistry* **114**, 972–980.

Chalmers, D. T. and Behan, D. P. (2002). The use of constitutively active GPCRs in drug discovery and functional genomics. *Nature Reviews Drug Discovery* **1**, 599–608.

Chan, R. K. and Otte, C. A. (1982a). Isolation and genetic analysis of *Saccharomyces cerevisiae* mutants supersensitive to G1 arrest by a factor and alpha factor pheromones. *Molecular and Cellular Biology* **2**, 11–20.

Chan, R. K. and Otte, C. A. (1982b). Physiological characterization of *Saccharomyces cerevisiae* mutants supersensitive to G1 arrest by a factor and alpha factor pheromones. *Molecular and Cellular Biology* **2**, 21–29.

Charest, P. G., Terrillon, S. and Bouvier, M. (2005). Monitoring agonist-promoted conformational changes of beta-arrestin in living cells by intramolecular BRET. *EMBO Reports* **6**, 334–340.

Chattoo, B. B., Sherman, F., Azubalis, D. A., Fjellstedt, T. A., Mehnert, D. and Ogur, M. (1979). Selection of lys2 Mutants of the yeast *Saccharomyces cerevisiae* by the utilization of alpha-aminoadipate. *Genetics* **93**, 51–65.

Chen, R. E. and Thorner, J. (2007). Function and regulation in MAPK signaling pathways: lessons learned from the yeast *Saccharomyces cerevisiae*. *Biochimica et Biophysica Acta* **1773**, 1311–1340.

Chen, X.-T., Pitis, P., Liu, G., Yuan, C., Gotchev, D., Cowan, C. L., Rominger, D. H., Koblish, M., Dewire, S. M., Crombie, A. L., Violin, J. D. and Yamashita, D. S. (2013). Structure-activity relationships and discovery of a G protein biased μ opioid receptor ligand, [(3-methoxythiophen-2-yl)methyl](2-[(9 R)-9-(pyridin-2-yl)-6-oxaspiro-[4.5]decan-9-yl]ethyl)amine (TRV130), for the treatment of acute severe pain. *Journal of Medicinal Chemistry* **56**, 8019–8031.

Cheong, S. L., Federico, S., Venkatesan, G., Mandel, A. L., Shao, Y.-M., Moro, S., Spalluto, G. and Pastorin, G. (2013). The A3 adenosine receptor as multi-faceted therapeutic target: pharmacology, medicinal chemistry, and in silico approaches. *Medicinal Research Reviews* **33**, 235–335.

Chien, E. Y. T., Liu, W., Zhao, Q., Katritch, V., Han, G. W., Hanson, M. A., Shi, L., Newman, A. H., Javitch, J. A., Cherezov, V. and Stevens, R. C. (2010). Structure of the human dopamine D3 receptor in complex with a D2/D3 selective antagonist. *Science* **330**, 1091–1095.

Chinault, S. L. and Blumer, K. J. (2003). The C-terminal tail preceding the CAAX box of a yeast G protein gamma subunit is dispensable for receptor-mediated G protein activation in vivo. *The Journal of Biological Chemistry* **278**, 20638–20644.

Chis, O., Banga, J. R. and Balsa-Canto, E. (2011a). GenSSI: a software toolbox for structural identifiability analysis of biological models. *Bioinformatics* **27**, 2610–2611.

Chis, O.-T., Banga, J. R. and Balsa-Canto, E. (2011b). Structural identifiability of systems biology models: a critical comparison of methods. *PLoS ONE* **6**, e27755.

Christopoulos, A. (2014). Advances in G protein-coupled receptor allostery: from function to structure. *Molecular Pharmacology* **86**, 463–478.

Christopoulos, A. and Kenakin, T. (2002). G protein-coupled receptor allosterism and complexing. *Pharmacological Reviews* **54**, 323–374.

Colca, J. R. (2012). Discontinued drugs 2011: endocrine and metabolic. *Expert Opinion on Investigational Drugs* **21**, 1619–1624.

Córdova-Sintjago, T., Sakhuja, R., Kondabolu, K., Canal, C. E. and Booth, R. G. (2012). Molecular determinants for ligand binding at serotonin 5-HT2A and 5-HT2C GPCRs: experimental affinity results analyzed by molecular modeling and ligand docking studies. *International Journal of Quantum Chemistry* **112**, 3807–3814.

Correll, C. C. and McKittrick, B. A. (2014). Biased ligand modulation of seven transmembrane receptors (7TMRs): functional implications for drug discovery. *Journal of Medicinal Chemistry* **57**, 6887–6896.

Costanzi, S. (2012). Homology modeling of class A G protein-coupled receptors. *Methods in Molecular Biology* **857**, 259–279.

Costanzi, S. (2013). Modeling G protein-coupled receptors and their interactions with ligands. *Current Opinion in Structural Biology* **23**, 185–190.

Croft, W., Hill, C., McCann, E., Bond, M., Esparza-Franco, M., Bennett, J., Rand, D., Davey, J. and Ladds, G. (2013). A physiologically required G protein-coupled receptor (GPCR)-regulator of G protein signaling (RGS) interaction that compartmentalizes RGS activity. *The Journal of Biological Chemistry* **288**, 27327–27342.

Dajas-Bailador, F. and Wonnacott, S. (2004). Nicotinic acetylcholine receptors and the regulation of neuronal signalling. *Trends in Pharmacological Sciences* **25**, 317–324.

Dale, C. L., Hill, S. J. and Kellam, B. (2012). New potent, short-linker BODIPY-630/650™ labelled fluorescent adenosine receptor agonists. *Medicinal Chemistry Communications* **3**, 333.

Daly, J. W., Padgett, W., Thompson, R. D., Kusachi, S., Bugni, W. J. and Olsson, R. A. (1986). Structure-activity relationships for N6-substituted adenosines at a brain A1-adenosine receptor with a comparison to an A2-adenosine receptor regulating coronary blood flow. *Biochemical Pharmacology* **35**, 2467–2481.

Davey, J. (1998). Fusion of a fission yeast. *Yeast* **14**, 1529–1566.

De Smet, F., Christopoulos, A. and Carmeliet, P. (2014). Allosteric targeting of receptor tyrosine kinases. *Nature Biotechnology* **32**, 1113–1120.

DeFea, K. A. (2011). Beta-arrestins as regulators of signal termination and transduction: How do they determine what to scaffold? *Cellular Signalling* **23**, 621–629.

DeWire, S. M., Yamashita, D. S., Rominger, D. H., Liu, G., Cowan, C. L., Graczyk, T. M., Chen, X. T., Pitis, P. M., Gotchev, D., Yuan, C., Koblish, M., Lark, M. W. and Violin, J. D. (2013). A G protein-biased ligand at the μ-opioid receptor Is potently analgesic with reduced gastrointestinal and respiratory dysfunction compared with morphine. *Journal of Pharmacology and Experimental Therapeutics* **344**, 708–717.

Dirnberger, D. and Seuwen, K. (2007). Signaling of human frizzled receptors to the mating pathway in yeast. *PLoS ONE* **2**, e954.

Dohlman, H. G., Apaniesk, D., Chen, Y., Song, J. and Nusskern, D. (1995). Inhibition of G-protein signaling by dominant gain-of-function mutations in Sst2p, a pheromone desensitization factor in *Saccharomyces cerevisiae*. *Molecular and Cellular Biology* **15**, 3635–3643.

Dowell, S. J. and Brown, A. J. (2009). Yeast assays for G protein-coupled receptors. *Methods in Molecular Biology* **552**, 213–229.

Edwards, H. V., Christian, F. and Baillie, G. S. (2012). cAMP: novel concepts in compartmentalised signalling. *Seminars in Cell and Developmental Biology* **23**, 181–190.

Erlenbach, I., Kostenis, E., Schmidt, C., Hamdan, F. F., Pausch, M. H. and Wess, J. (2001a). Functional expression of M(1), M(3) and M(5) muscarinic acetylcholine receptors in yeast. *Journal of Neurochemistry* **77**, 1327–1337.

Erlenbach, I., Kostenis, E., Schmidt, C., Serradeil-Le Gal, C., Raufaste, D., Dumont, M. E., Pausch, M. H. and Wess, J. (2001b). Single amino acid substitutions and deletions that alter the G protein coupling properties of the V2 vasopressin receptor identified in yeast by receptor random mutagenesis. *The Journal of Biological Chemistry* **276**, 29382–29392.

Falkenstein, E., Tillmann, H. C., Christ, M., Feuring, M. and Wehling, M. (2000). Multiple actions of steroid hormones–a focus on rapid, nongenomic effects. *Pharmacological Reviews* **52**, 513–556.

Ferrell, J. E. and Bhatt, R. R. (1997). Mechanistic studies of the dual phosphorylation of mitogen-activated protein kinase. *The Journal of Biological Chemistry* **272**, 19008–19016.

Fredriksson, R., Lagerström, M. C., Lundin, L.-G. and Schiöth, H. B. (2003). The G-protein-coupled receptors in the human genome form five main families. Phylogenetic analysis, paralogon groups, and fingerprints. *Molecular Pharmacology* **63**, 1256–1272.

Gabrielsson, J., Green, A. R. and Van der Graaf, P. H. (2010). Optimising in vivo pharmacology studies - practical PKPD considerations. *Journal of Pharmacological and Toxicological Methods* **61**, 146–156.

Galés, C., Rebois, R. V., Hogue, M., Trieu, P., Breit, A., Hébert, T. E. and Bouvier, M. (2005). Real-time monitoring of receptor and G-protein interactions in living cells. *Nature Methods* **2**, 177–184.

Gancedo, J. M. (2013). Biological roles of cAMP: variations on a theme in the different kingdoms of life. *Biological Reviews of the Cambridge Philosophical Society* **88**, 645–668.

Gao, Z.-G., Blaustein, J. B., Gross, A. S., Melman, N. and Jacobson, K. A. (2003). N6-substituted adenosine derivatives: selectivity, efficacy, and species differences at A3 adenosine receptors. *Biochemical Pharmacology* **65**, 1675–1684.

Gautam, N., Downes, G. B., Yan, K. and Kisselev, O. (1998). The G-protein $\beta\gamma$ complex. *Cellular Signalling* **10**, 447–455.

Gietz, R. D. and Schiestl, R. H. (2007). High-efficiency yeast transformation using the LiAc/SS carrier DNA/PEG method. *Nature Protocols* **2**, 31–34.

Goutelle, S., Maurin, M., Rougier, F., Barbaut, X., Bourguignon, L., Ducher, M. and Maire, P. (2008). The Hill equation: a review of its capabilities in pharmacological modelling. *Fundamental and Clinical Pharmacology* **22**, 633–648.

Gracia, E., Moreno, E., Cortés, A., Lluís, C., Mallol, J., McCormick, P. J., Canela, E. I. and Casadó, V. (2013). Homodimerization of adenosine A1 receptors in brain cortex explains the biphasic effects of caffeine. *Neuropharmacology* **71**, 56–69.

Hao, N., Yildirim, N., Wang, Y., Elston, T. C. and Dohlman, H. G. (2003). Regulators of G protein signaling and transient activation of signaling: experimental and computational analysis reveals negative and positive feedback controls on G protein activity. *The Journal of Biological Chemistry* **278**, 46506–46515.

Hawley, T. S., Herbert, D. J., Eaker, S. S. and Hawley, R. G. (2004). Multiparameter flow cytometry of fluorescent protein reporters. *Methods in Molecular Biology* **263**, 219–238.

Hicke, L., Zanolari, B. and Riezman, H. (1998). Cytoplasmic tail phosphorylation of the alpha-factor receptor is required for its ubiquitination and internalization. *The Journal of Cell Biology* **141**, 349–358.

Hill, S. J., May, L. T., Kellam, B. and Woolard, J. (2014). Allosteric interactions at adenosine A(1) and A(3) receptors: new insights into the role of small molecules and receptor dimerization. *British Journal of Pharmacology* **171**, 1102–1113.

Hinton, D. R., Blanks, J. C., Fong, H. K., Casey, P. J., Hildebrandt, E. and Simons, M. I. (1990). Novel localization of a G protein, Gz-alpha, in neurons of brain and retina. *The Journal of Neuroscience* **10**, 2763–2770.

Hirsch, J. A., Schubert, C., Gurevich, V. V. and Sigler, P. B. (1999). The 2.8 A crystal structure of visual arrestin: a model for arrestin's regulation. *Cell* **97**, 257–269.

Hocher, B. (2010). Adenosine A1 receptor antagonists in clinical research and development. *Kidney International* **78**, 438–445.

Hoffman, C. S. (2005). Except in every detail: comparing and contrasting G-protein signaling in *Saccharomyces cerevisiae* and *Schizosaccharomyces pombe*. *Eukaryotic Cell* **4**, 495–503.

Hoffmann, C., Gaietta, G., Bünemann, M., Adams, S. R., Oberdorff-Maass, S., Behr, B., Vilardaga, J.-P., Tsien, R. Y., Ellisman, M. H. and Lohse, M. J. (2005). A FlAsH-based FRET approach to determine G protein-coupled receptor activation in living cells. *Nature Methods* **2**, 171–176.

Hwa, J., Garriga, P., Liu, X. and Khorana, H. G. (1997). Structure and function in rhodopsin: packing of the helices in the transmembrane domain and folding to a tertiary structure in the intradiscal domain are coupled. *Proceedings of the National Academy of Sciences of the United States of America* **94**, 10571–10576.

IJzerman, A. P., Fredholm, B. B., Jacobson, K. A., Linden, J. and Mueller, C. E. (2014a). IUPHAR/ BPS guide to pharmacology. Adenosine receptors: A_1 receptor. `http://www.guidetopharmacology.org/GRAC/ObjectDisplayForward?objectId=18`. Accessed: 17-06-2015.

IJzerman, A. P., Fredholm, B. B., Jacobson, K. A., Linden, J. and Mueller, C. E. (2014b). IUPHAR/ BPS guide to pharmacology. Adenosine receptors: A_{2B} receptor. `http://www.guidetopharmacology.org/GRAC/ObjectDisplayForward?objectId=20`. Accessed: 17-06-2015.

Jacobson, K. A. (2009). Introduction to adenosine receptors as therapeutic targets. *Handbook of Experimental Pharmacology* **193**, 1–24.

Jacobson, K. A. and Gao, Z.-G. (2006). Adenosine receptors as therapeutic targets. *Nature Reviews Drug Discovery* **5**, 247–264.

Jacobson, K. A., Ukena, D., Padgett, W., Kirk, K. L. and Daly, J. W. (1987). Molecular probes for extracellular adenosine receptors. *Biochemical Pharmacology* **36**, 1697–1707.

Jarvis, M. F., Gessner, G., Shapiro, G., Merkel, L., Myers, M., Cox, B. F. and Martin, G. E. (1999). Differential effects of the adenosine A1 receptor allosteric enhancer PD 81,723 on agonist binding to brain and adipocyte membranes. *Brain Research* **840**, 75–83.

Kenakin, T. (2004). Principles: receptor theory in pharmacology. *Trends in Pharmacological Sciences* **25**, 186–192.

Kenakin, T., Jenkinson, S. and Watson, C. (2006). Determining the potency and molecular mechanism of action of insurmountable antagonists. *Journal of Pharmacology and Experimental Therapeutics* **319**, 710–723.

Kenakin, T., Watson, C., Muniz-Medina, V., Christopoulos, A. and Novick, S. (2012). A simple method for quantifying functional selectivity and agonist bias. *ACS Chemical Neuroscience* **3**, 193–203.

Kimple, M. E., Nixon, A. B., Kelly, P., Bailey, C. L., Young, K. H., Fields, T. A. and Casey, P. J. (2005). A role for Gz in pancreatic islet β-cell biology. *Journal of Biological Chemistry* **280**, 31708–31713.

King, K., Dohlman, H. G., Thorner, J., Caron, M. G. and Lefkowitz, R. J. (1990). Control of yeast mating signal transduction by a mammalian beta 2-adrenergic receptor and Gs alpha subunit. *Science* **250**, 121–123.

Klco, J. M., Wiegand, C. B., Narzinski, K. and Baranski, T. J. (2005). Essential role for the second extracellular loop in C5a receptor activation. *Nature Structural and Molecular Biology* **12**, 320–326.

Knudsen, L. B., Kiel, D., Teng, M., Behrens, C., Bhumralkar, D., Kodra, J. T., Holst, J. J., Jeppesen, C. B., Johnson, M. D., de Jong, J. C., Jorgensen, A. S., Kercher, T., Kostrowicki, J., Madsen, P., Olesen, P. H., Petersen, J. S., Poulsen, F., Sidelmann, U. G., Sturis, J., Truesdale, L., May, J. and Lau, J. (2007). Small-molecule agonists for the glucagon-like peptide 1 receptor. *Proceedings of the National Academy of Sciences of the United States of America* **104**, 937–942.

Kobilka, B. K. and Deupi, X. (2007). Conformational complexity of G-protein-coupled receptors. *Trends in Pharmacological Sciences* **28**, 397–406.

Kofahl, B. and Klipp, E. (2004). Modelling the dynamics of the yeast pheromone pathway. *Yeast* **21**, 831–850.

Kozma, E., Jayasekara, P. S., Squarcialupi, L., Paoletta, S., Moro, S., Federico, S., Spalluto, G. and Jacobson, K. A. (2013). Fluorescent ligands for adenosine receptors. *Bioorganic and Medicinal Chemistry Letters* **23**, 26–36.

Kroeze, W. K., Sheffler, D. J. and Roth, B. L. (2003). G-protein-coupled receptors at a glance. *Journal of Cell Science* **116**, 4867–4869.

Kukovetz, W. R., Holzmann, S. and Romanin, C. (1987). Mechanism of vasodilation by nitrates: role of cyclic GMP. *Cardiology* **74**, 12–19.

Kumar, T. S., Mishra, S., Deflorian, F., Yoo, L. S., Phan, K., Kecskés, M., Szabo, A., Shinkre, B., Gao, Z.-G., Trenkle, W. and Jacobson, K. A. (2011). Molecular probes for the A2A adenosine receptor based on a pyrazolo[4,3-e][1,2,4]triazolo[1,5-c]pyrimidin-5-amine scaffold. *Bioorganic Medicinal Chemistry Letters* **21**, 2740–2745.

Laburthe, M., Couvineau, A., Gaudin, P., Maoret, J.-J., Rouyer-Fessard, C. and Nicole, P. (2006). Receptors for VIP, PACAP, secretin, GRF, glucagon, GLP-1, and other members of their new family of G protein-linked receptors: structure-function relationship with special reference to the human VIP-1 receptor. *Annals of the New York Academy of Sciences* **805**, 94–109.

Ladds, G., Davis, K., Das, A. and Davey, J. (2005a). A constitutively active GPCR retains its G protein specificity and the ability to form dimers. *Molecular Microbiology* **55**, 482–497.

Ladds, G., Davis, K., Hillhouse, E. W. and Davey, J. (2003). Modified yeast cells to investigate the coupling of G protein-coupled receptors to specific G proteins. *Molecular Microbiology* **47**, 781–792.

Ladds, G., Goddard, A. and Davey, J. (2005b). Functional analysis of heterologous GPCR signalling pathways in yeast. *Trends in Biotechnology* **23**, 367–373.

Lagane, B., Gaibelet, G., Meilhoc, E., Masson, J. M., Cézanne, L. and Lopez, A. (2000). Role of sterols in modulating the human mu-opioid receptor function in *Saccharomyces cerevisiae*. *The Journal of Biological Chemistry* **275**, 33197–33200.

Lambright, D. G., Sondek, J., Bohm, A., Skiba, N. P., Hamm, H. E. and Sigler, P. B. (1996). The 2.0 A crystal structure of a heterotrimeric G protein. *Nature* **379**, 311–319.

Lebon, G., Warne, T., Edwards, P. C., Bennett, K., Langmead, C. J., Leslie, A. G. W. and Tate, C. G. (2011). Agonist-bound adenosine A2A receptor structures reveal common features of GPCR activation. *Nature* **474**, 521–525.

Lefkowitz, R. J. (2005). Transduction of receptor signals by β-arrestins. *Science* **308**, 512–517.

Lei, Q., Jones, M. B., Talley, E. M., Garrison, J. C. and Bayliss, D. A. (2003). Molecular mechanisms mediating inhibition of G protein-coupled inwardly-rectifying K+ channels. *Molecules and Cells* **15**, 1–9.

Leonard, S. and Bertrand, D. (2001). Neuronal nicotinic receptors: from structure to function. *Nicotine and Tobacco Research* **3**, 203–223.

Leplatois, P., Josse, A., Guillemot, M., Febvre, M., Vita, N., Ferrara, P. and Loison, G. (2001). Neurotensin induces mating in *Saccharomyces cerevisiae* cells that express human neurotensin receptor type 1 in place of the endogenous pheromone receptor. *European Journal of Biochemistry* **268**, 4860–4867.

Leslie, F. M., Mojica, C. Y. and Reynaga, D. D. (2013). Nicotinic receptors in addiction pathways. *Molecular Pharmacology* **83**, 753–758.

Linderman, J. J. (2009). Modeling of G-protein-coupled receptor signaling pathways. *Journal of Biological Chemistry* **284**, 5427–5431.

Liu, R., Groenewoud, N. J. A., Peeters, M. C., Lenselink, E. B. and IJzerman, A. P. (2014). A yeast screening method to decipher the interaction between the adenosine A2B receptor and the C-terminus of different G protein α-subunits. *Purinergic Signalling* **10**, 441–453.

Lockley, R., Ladds, G. and Bretschneider, T. (2015). Image based validation of dynamical models for cell reorientation. *Cytometry. Part A : the Journal of the International Society for Analytical Cytology* **87**, 471–480.

Logothetis, D. E., Kurachi, Y., Galper, J., Neer, E. J. and Clapham, D. E. (1987). The $\beta\gamma$ subunits of GTP-binding proteins activate the muscarinic K+ channel in heart. *Nature* **325**, 321–326.

Lohse, M. J. (2010). Dimerization in GPCR mobility and signaling. *Current Opinion in Pharmacology* **10**, 53–58.

Lohse, M. J., Nuber, S. and Hoffmann, C. (2012). Fluorescence/bioluminescence resonance energy transfer techniques to study G-protein-coupled receptor activation and signaling. *Pharmacological Reviews* **64**, 299–336.

Lüscher, C. and Slesinger, P. A. (2010). Emerging roles for G protein-gated inwardly rectifying potassium (GIRK) channels in health and disease. *Nature Reviews Neuroscience* **11**, 301–315.

Lynge and Hellsten (2000). Distribution of adenosine A1, A2A and A2B receptors in human skeletal muscle. *Acta Physiologica Scandinavica* **169**, 283–290.

Macchia, M., Bertini, S., Di Bussolo, V., Manera, C., Martini, C., Minutolo, F., Mori, C., Saccomanni, G., Tuscano, D. and Ferrarini, P. L. (2002). 4-[6-(Dansylamino)hexylamino]-7-methyl-2-phenyl-1,8-naphthyridine as a new potential fluorescent probe for studying A1-adenosine receptor. *Il Farmaco* **57**, 783–786.

Macchia, M., Salvetti, F., Barontini, S., Calvani, F., Gesi, M., Hamdan, M., Lucacchini, A., Pellegrini, A., Soldani, P. and Martini, C. (1998). Fluorescent probes for adenosine receptors: synthesis and biology of N6-dansylaminoalkyl-substituted NECA derivatives. *Bioorganic and Medicinal Chemistry Letters* **8**, 3223–3228.

MacKay, V. L., Welch, S. K., Insley, M. Y., Manney, T. R., Holly, J., Saari, G. C. and Parker, M. L. (1988). The *Saccharomyces cerevisiae* BAR1 gene encodes an exported protein with homology to pepsin. *Proceedings of the National Academy of Sciences of the United States of America* **85**, 55–59.

Maiwald, T., Eberhardt, O. and Blumberg, J. (2012). Mathematical modeling of biochemical systems with PottersWheel. *Methods in Molecular Biology* **880**, 119–138.

Maiwald, T. and Timmer, J. (2008). Dynamical modeling and multi-experiment fitting with PottersWheel. *Bioinformatics* **24**, 2037–2043.

Marchese, A., Paing, M. M., Temple, B. R. S. and Trejo, J. (2008). G protein-coupled receptor sorting to endosomes and lysosomes. *Annual Review of Pharmacology and Toxicology* **48**, 601–629.

May, L. T., Bridge, L. J., Stoddart, L. A., Briddon, S. J. and Hill, S. J. (2011). Allosteric interactions across native adenosine-A3 receptor homodimers: quantification using single-cell ligand-binding kinetics. *The FASEB Journal* **25**, 3465–3476.

May, L. T., Self, T. J., Briddon, S. J. and Hill, S. J. (2010). The effect of allosteric modulators on the kinetics of agonist-G protein-coupled receptor interactions in single living cells. *Molecular Pharmacology* **78**, 511–523.

McCudden, C. R., Hains, M. D., Kimple, R. J., Siderovski, D. P. and Willard, F. S. (2005). G-protein signaling: back to the future. *Cellular and Molecular Life Sciences* **62**, 551–577.

Merlini, L., Dudin, O. and Martin, S. G. (2013). Mate and fuse: how yeast cells do it. *Open Biology* **3**, 130008–130008.

Middleton, R. J., Briddon, S. J., Cordeaux, Y., Yates, A. S., Dale, C. L., George, M. W., Baker, J. G., Hill, S. J. and Kellam, B. (2007). New fluorescent adenosine A1 receptor agonists that allow quantification of ligand-receptor interactions in microdomains of single living cells. *Journal of Medicinal Chemistry* **50**, 782–793.

Milligan, G. (2009). G protein-coupled receptor hetero-dimerization: contribution to pharmacology and function. *British Journal of Pharmacology* **158**, 5–14.

Milligan, G., Canals, M., Pediani, J. D., Ellis, J. and Lopez-Gimenez, J. F. (2007). The role of GPCR dimerisation/oligomerisation in receptor signalling. *Ernst Schering Foundation Symposium Proceedings* **2**, 145–162.

Mos, M., Esparza-Franco, M. A., Godfrey, E. L., Richardson, K., Davey, J. and Ladds, G. (2013). The role of the RACK1 ortholog Cpc2p in modulating pheromone-induced cell cycle arrest in fission yeast. *PLoS ONE* **8**, e65927.

Motulsky, H. and Christopoulos, A. (2004). *Fitting models to biological data using linear and nonlinear regression: a practical guide to curve fitting.*. San Diego CA: GraphPad Software Inc.

Mustain, W. C., Rychahou, P. G. and Evers, B. M. (2011). The role of neurotensin in physiologic and pathologic processes. *Current Opinion in Endocrinology, Diabetes and Obesity* **18**, 75–82.

Narlawar, R., Lane, J. R., Doddareddy, M., Lin, J., Brussee, J. and IJzerman, A. P. (2010). Hybrid ortho/allosteric ligands for the adenosine A1 receptor. *Journal of Medicinal Chemistry* **53**, 3028–3037.

Neildez-Nguyen, T. M. A., Parisot, A., Vignal, C., Rameau, P., Stockholm, D., Picot, J., Allo, V., Le Bec, C., Laplace, C. and Paldi, A. (2007). Epigenetic gene expression noise and phenotypic diversification of clonal cell populations. *Differentiation* **76**, 33–40.

Nichols, A. S., Floyd, D. H., Bruinsma, S. P., Narzinski, K. and Baranski, T. J. (2013). Frizzled receptors signal through G proteins. *Cellular Signalling* **25**, 1468–1475.

Niebauer, R. T. and Robinson, A. S. (2006). Exceptional total and functional yields of the human adenosine (A2A) receptor expressed in the yeast *Saccharomyces cerevisiae*. *Protein Expression and Purification* **46**, 204–211.

Niebauer, R. T., Wedekind, A. and Robinson, A. S. (2004). Decreases in yeast expression yields of the human adenosine A2A receptor are a result of translational or post-translational events. *Protein expression and Purification* **37**, 134–143.

Nobles, M., Benians, A. and Tinker, A. (2005). Heterotrimeric G proteins precouple with G protein-coupled receptors in living cells. *Proceedings of the National Academy of Sciences of the United States of America* **102**, 18706–18711.

Ogungbenro, K. and Aarons, L. (2011). Structural identifiability analysis of pharmacokinetic models using DAISY: semi-mechanistic gastric emptying models for 13C-octanoic acid. *Journal of Pharmacokinetics and Pharmacodynamics* **38**, 279–292.

O'Hara, P. J., Sheppard, P. O., Thógersen, H. and Venezia, D. (1993). The ligand-binding domain in metabotropic glutamate receptors is related to bacterial periplasmic binding proteins. *Neuron* **11**, 41–52.

Okamoto, T., Sekiyama, N., Otsu, M., Shimada, Y., Sato, A., Nakanishi, S. and Jingami, H. (1998). Expression and purification of the extracellular ligand binding region of metabotropic glutamate receptor subtype 1. *The Journal of Biological Chemistry* **273**, 13089–13096.

Olah, M. E., Jacobson, K. A. and Stiles, G. L. (1994). Role of the second extracellular loop of adenosine receptors in agonist and antagonist binding. Analysis of chimeric A1/A3 adenosine receptors. *The Journal of Biological Chemistry* **269**, 24692–24698.

Olesnicky, N. S., Brown, A. J., Dowell, S. J. and Casselton, L. A. (1999). A constitutively active G-protein-coupled receptor causes mating self-compatibility in the mushroom *Coprinus*. *The EMBO journal* **18**, 2756–2763.

Paing, M. M., Temple, B. R. S. and Trejo, J. (2004). A tyrosine-based sorting signal regulates intracellular trafficking of protease-activated receptor-1: multiple regulatory mechanisms for agonist-induced G protein-coupled receptor internalization. *The Journal of Biological Chemistry* **279**, 21938–21947.

Palczewski, K., Kumasaka, T., Hori, T., Behnke, C. A., Motoshima, H., Fox, B. A., Le Trong, I., Teller, D. C., Okada, T., Stenkamp, R. E., Yamamoto, M. and Miyano, M. (2000). Crystal structure of rhodopsin: a G protein-coupled receptor. *Science* **289**, 739–745.

Papadaki, P., Pizon, V., Onken, B. and Chang, E. C. (2002). Two ras pathways in fission yeast are differentially regulated by two ras guanine nucleotide exchange factors. *Molecular and Cellular Biology* **22**, 4598–4606.

Park, J. H., Scheerer, P., Hofmann, K. P., Choe, H.-W. and Ernst, O. P. (2008). Crystal structure of the ligand-free G-protein-coupled receptor opsin. *Nature* **454**, 183–187.

Peeters, M. C., van Westen, G. J. P., Guo, D., Wisse, L. E., Muller, C. E., Beukers, M. W. and IJzerman, A. P. (2011). GPCR structure and activation: an essential role for the first extracellular loop in activating the adenosine A2B receptor. *The FASEB Journal* **25**, 632–643.

Peeters, M. C., Wisse, L. E., Dinaj, A., Vroling, B., Vriend, G. and IJzerman, A. P. (2012). The role of the second and third extracellular loops of the adenosine A1 receptor in activation and allosteric modulation. *Biochemical Pharmacology* **84**, 1–12.

Peleg, S., Varon, D., Ivanina, T., Dessauer, C. W. and Dascal, N. (2002). G(alpha)(i) controls the gating of the G protein-activated K(+) channel, GIRK. *Neuron* **33**, 87–99.

Perez, P. and Rincón, S. A. (2010). Rho GTPases: regulation of cell polarity and growth in yeasts. *Biochemical Journal* **426**, 243–253.

Pradhan, A. A., Smith, M. L., Kieffer, B. L. and Evans, C. J. (2012). Ligand-directed signalling within the opioid receptor family. *British Journal of Pharmacology* **167**, 960–969.

Pradhan, A. A. A., Walwyn, W., Nozaki, C., Filliol, D., Erbs, E., Matifas, A., Evans, C. and Kieffer, B. L. (2010). Ligand-directed trafficking of the μ-opioid receptor in vivo: two paths toward analgesic tolerance. *Journal of Neuroscience* **30**, 16459–16468.

Price, L. A., Strnad, J., Pausch, M. H. and Hadcock, J. R. (1996). Pharmacological characterization of the rat A2A adenosine receptor functionally coupled to the yeast pheromone response pathway. *Molecular Pharmacology* **50**, 829–837.

Raehal, K. M. (2005). Morphine side effects in β-arrestin 2 knockout mice. *Journal of Pharmacology and Experimental Therapeutics* **314**, 1195–1201.

Rajagopal, S., Ahn, S., Rominger, D. H., Gowen-MacDonald, W., Lam, C. M., Dewire, S. M., Violin, J. D. and Lefkowitz, R. J. (2011). Quantifying ligand bias at seven-transmembrane receptors. *Molecular Pharmacology* **80**, 367–377.

Randazzo, P. A. and Kahn, R. A. (1994). GTP hydrolysis by ADP-ribosylation factor is dependent on both an ADP-ribosylation factor GTPase-activating protein and acid phospholipids. *The Journal of Biological Chemistry* **269**, 10758–10763.

Rasmussen, S. G. F., DeVree, B. T., Zou, Y., Kruse, A. C., Chung, K. Y., Kobilka, T. S., Thian, F. S., Chae, P. S., Pardon, E., Calinski, D., Mathiesen, J. M., Shah, S. T. A., Lyons, J. A., Caffrey, M., Gellman, S. H., Steyaert, J., Skiniotis, G., Weis, W. I., Sunahara, R. K. and Kobilka, B. K. (2011). Crystal structure of the β2 adrenergic receptor-Gs protein complex. *Nature* **477**, 549–555.

Raue, A., Kreutz, C., Maiwald, T., Bachmann, J., Schilling, M., Klingmüller, U. and Timmer, J. (2009). Structural and practical identifiability analysis of partially observed dynamical models by exploiting the profile likelihood. *Bioinformatics* **25**, 1923–1929.

Raue, A., Kreutz, C., Maiwald, T., Klingmüller, U. and Timmer, J. (2010). Addressing parameter identifiability by model-based experimentation. *IET Systems Biology* **5**, 120–130.

Ribeiro, J. A. and Sebastiao, A. M. (2010). Caffeine and adenosine. *Journal of Alzheimer's Disease* **20**, S3–S15.

Ribeiro-Neto, F. A., Mattera, R., Hildebrandt, J. D., Codina, J., Field, J. B., Birnbaumer, L. and Sekura, R. D. (1985). ADP-ribosylation of membrane components by pertussis and cholera toxin. *Methods in Enzymology* **109**, 566–572.

Rivero-Müller, A., Jonas, K. C., Hanyaloglu, A. C. and Huhtaniemi, I. (2013). Di/oligomerization of GPCRs-mechanisms and functional significance. *Progress in Molecular Biology and Translational Science* **117**, 163–185.

Robinson, D. R., Wu, Y. M. and Lin, S. F. (2000). The protein tyrosine kinase family of the human genome. *Oncogene* **19**, 5548–5557.

Romano, C., Yang, W. L. and O'Malley, K. L. (1996). Metabotropic glutamate receptor 5 is a disulfide-linked dimer. *The Journal of Biological Chemistry* **271**, 28612–28616.

Ross, E. M. and Wilkie, T. M. (2000). GTPase-activating proteins for heterotrimeric G proteins: regulators of G protein signaling (RGS) and RGS-like proteins. *Annual Review of Biochemistry* **69**, 795–827.

Roth, A. F. and Davis, N. G. (1996). Ubiquitination of the yeast a-factor receptor. *The Journal of Cell Biology* **134**, 661–674.

Rozenfeld, R. and Devi, L. A. (2010). Exploring a role for heteromerization in GPCR signalling specificity. *Biochemical Journal* **433**, 11–18.

Sachdeva, S. and Gupta, M. (2013). Adenosine and its receptors as therapeutic targets: an overview. *Saudi Pharmaceutical Journal* **21**, 245–253.

Sadana, R. and Dessauer, C. W. (2009). Physiological roles for G protein-regulated adenylyl cyclase isoforms: insights from knockout and overexpression studies. *Neuro-Signals* **17**, 5–22.

Sambrook, J., Fritsch, E. F. and Maniatis, T. (1989). Molecular Cloning. Cold Spring Harbor Laboratory Press, Cold Spring Harbor, New York.

Scarselli, M. and Donaldson, J. G. (2009). Constitutive internalization of G protein-coupled receptors and G proteins via clathrin-independent endocytosis. *The Journal of biological chemistry* **284**, 3577–3585.

Schild, H. O. (1947). pA, a new scale for the measurement of drug antagonism. *British Journal of Pharmacology and Chemotherapy* **2**, 189–206.

Schild, H. O. (1949). pAx and competitive drug antagonism. *British Journal of Pharmacology and Chemotherapy* **4**, 277–280.

Schrattenholz, A. and Soskić, V. (2008). What does systems biology mean for drug development? *Current Medicinal Chemistry* **15**, 1520–1528.

Shao, D., Zheng, W., Qiu, W., Ouyang, Q. and Tang, C. (2006). Dynamic studies of scaffold-dependent mating pathway in yeast. *Biophysical Journal* **91**, 3986–4001.

Sharman, J. L., Mpamhanga, C. P., Spedding, M., Germain, P., Staels, B., Dacquet, C., Laudet, V. and Harmar, A. J. (2011). IUPHAR-DB: new receptors and tools for easy searching and visualization of pharmacological data. *Nucleic acids Research* **39**, D534–D538.

Shea, L. D., Neubig, R. R. and Linderman, J. J. (2000). Timing is everything the role of kinetics in G protein activation. *Life Sciences* **68**, 647–658.

Shearer, J., Severson, D. L., Su, L., Belardinelli, L. and Dhalla, A. K. (2009). Partial A1 adenosine receptor agonist regulates cardiac substrate utilization in insulin-resistant rats in vivo. *Journal of Pharmacology and Experimental Therapeutics* **328**, 306–311.

Shenoy, S. K., Drake, M. T., Nelson, C. D., Houtz, D. A., Xiao, K., Madabushi, S., Reiter, E., Premont, R. T., Lichtarge, O. and Lefkowitz, R. J. (2006). β-arrestin-dependent, G protein-independent ERK1/2 activation by the β2 adrenergic receptor. *The Journal of Biological Chemistry* **281**, 1261–1273.

Shenoy, S. K. and Lefkowitz, R. J. (2011). β-arrestin-mediated receptor trafficking and signal transduction. *Trends in Pharmacological Sciences* **32**, 521–533.

Sheth, S., Brito, R., Mukherjea, D., Rybak, L. P. and Ramkumar, V. (2014). Adenosine receptors: expression, function and regulation. *International Journal of Molecular Sciences* **15**, 2024–2052.

Shonberg, J., Lopez, L., Scammells, P. J., Christopoulos, A., Capuano, B. and Lane, J. R. (2014). Biased agonism at G protein-coupled receptors: the promise and the challenges - a medicinal chemistry perspective. *Medicinal Research Reviews* **34**, 1286–1330.

Sitaraman, S. V., Wang, L., Wong, M., Bruewer, M., Hobert, M., Yun, C.-H., Merlin, D. and Madara, J. L. (2002). The adenosine 2B receptor is recruited to the plasma membrane and associates with E3KARP and Ezrin upon agonist stimulation. *The Journal of Biological Chemistry* **277**, 33188–33195.

Smith, B., Hill, C., Godfrey, E. L., Rand, D., van den Berg, H., Thornton, S., Hodgkin, M., Davey, J. and Ladds, G. (2009). Dual positive and negative regulation of GPCR signaling by GTP hydrolysis. *Cellular Signalling* **21**, 1151–1160.

Sokal, I., Alekseev, A. and Palczewski, K. (2003). Photoreceptor guanylate cyclase variants: cGMP production under control. *Acta Biochimica Polonica* **50**, 1075–1095.

Sorger, P. K., Allerheiligen, S. and Abernethy, D. R. (2011). Quantitative and systems pharmacology in the post-genomic era: new approaches to discovering drugs and understanding therapeutic mechanisms. *An NIH white paper by the QSP Workshop Group* .

Sprang, S. R. (1997). G protein mechanisms: insights from structural analysis. *Annual Review of Biochemistry* **66**, 639–678.

Stewart, G. D., Sexton, P. M. and Christopoulos, A. (2010). Detection of novel functional selectivity at M3 muscarinic acetylcholine receptors using a *Saccharomyces cerevisiae platform. American Chemical Society Chemical Biology* **5**, 365–375.

Stewart, G. D., Valant, C., Dowell, S. J., Mijaljica, D., Devenish, R. J., Scammells, P. J., Sexton, P. M. and Christopoulos, A. (2009). Determination of adenosine A1 receptor agonist and antagonist pharmacology using *Saccharomyces cerevisiae*: implications for ligand screening and functional selectivity. *Journal of Pharmacology and Experimental Therapeutics* **331**, 277–286.

Sunahara, R. K., Inada, Y., Ono, T., Kuroda, S., Yasuda-Kamatani, Y., Ishiguro, M., Tanaka, T., Misaka, T., Abe, K. and Ueda, M. (2012). Chimeric yeast G-protein α subunit harboring a 37-residue C-Terminal gustducin-specific sequence is functional in *Saccharomyces cerevisiae*. *Bioscience, Biotechnology, and Biochemistry* **76**, 512–516.

Taussig, R. and Zimmermann, G. (1998). Type-specific regulation of mammalian adenylyl cyclases by G protein pathways. *Advances in Second Messenger and Phosphoprotein Research* **32**, 81–98.

Thatcher, G. R. J., Nicolescu, A. C., Bennett, B. M. and Toader, V. (2004). Nitrates and NO release: contemporary aspects in biological and medicinal chemistry. *Free Radical Biology and Medicine* **37**, 1122–1143.

Thomson, T. M., Benjamin, K. R., Bush, A., Love, T., Pincus, D., Resnekov, O., Yu, R. C., Gordon, A., Colman-Lerner, A., Endy, D. and Brent, R. (2011). Scaffold number in yeast signaling system sets tradeoff between system output and dynamic range. *Proceedings of the National Academy of Sciences of the United States of America* **108**, 20265–20270.

Tolkovsky, A. M. and Levitzki, A. (1978). Mode of coupling between the beta-adrenergic receptor and adenylate cyclase in turkey erythrocytes. *Biochemistry* **17**, 3795.

Tsuchiya, D., Kunishima, N., Kamiya, N., Jingami, H. and Morikawa, K. (2002). Structural views of the ligand-binding cores of a metabotropic glutamate receptor complexed with an antagonist and both glutamate and Gd3+. *Proceedings of the National Academy of Sciences of the United States of America* **99**, 2660–2665.

Tuccinardi, T., Ortore, G., Manera, C., Saccomanni, G. and Martinelli, A. (2006). Adenosine receptor modelling. A1/A2A selectivity. *European Journal of Medicinal Chemistry* **41**, 321–329.

Tyers, M. and Futcher, B. (1993). Far1 and Fus3 link the mating pheromone signal transduction pathway to three G1-phase Cdc28 kinase complexes. *Molecular and Cellular Biology* **13**, 5659–5669.

Valant, C., Lane, J. R., Sexton, P. M. and Christopoulos, A. (2012). The best of both worlds? Bitopic orthosteric/allosteric ligands of G protein-coupled receptors. *Annual Review of Pharmacology and Toxicology* **52**, 153–178.

Valant, C., May, L. T., Aurelio, L., Chuo, C. H., White, P. J., Baltos, J.-A., Sexton, P. M., Scammells, P. J. and Christopoulos, A. (2014). Separation of on-target efficacy from adverse effects through rational design of a bitopic adenosine receptor agonist. *Proceedings of the National Academy of Sciences of the United States of America* **111**, 4614–4619.

van Drogen, F., Stucke, V. M., Jorritsma, G. and Peter, M. (2001). MAP kinase dynamics in response to pheromones in budding yeast. *Nature Cell Biology* **3**, 1051–1059.

Verzijl, D. and IJzerman, A. P. (2011). Functional selectivity of adenosine receptor ligands. *Purinergic Signalling* **7**, 171–192.

Vicini, P. and van der Graaf, P. H. (2013). Systems pharmacology for drug discovery and development: paradigm shift or flash in the pan? *Clinical Pharmacology and Therapeutics* **93**, 379–381.

Wagner, R., Ngamsri, K. C., Stark, S., Vollmer, I. and Reutershan, J. (2010). Adenosine receptor A3 is a critical mediator in LPS-induced pulmonary inflammation. *American Journal of Physciology: Lung Cellular and Molecular Physiology* **299**, L502–L512.

Wedlock, N., Furmaniak, J., Fowler, S., Kiso, Y., Bednarek, J., Baumann-Antczak, A., Morteo, C., Sudbery, P., Hinchcliff, A. and Smith, B. R. (1993). Expression of human thyroid peroxidase in the yeasts *Saccharomyces cerevisiae* and *Hansenula polymorpha*. *Journal of Molecular Endocrinology* **10**, 325–336.

Weiss, J. M., Morgan, P. H., Lutz, M. W. and Kenakin, T. P. (1996). The cubic ternary complex receptor-occupancy model. III. Resurrecting efficacy. *Journal of Theoretical Biology* **181**, 381–397.

Weston, C., Poyner, D., Patel, V., Dowell, S. J. and Ladds, G. (2014). Investigating G protein signaling bias at the glucagon-like peptide-1 receptor in yeast. *British Journal of Pharmacology* **171**, –3665.

Wettschureck, N. (2005). Mammalian G proteins and their cell type specific functions. *Physiological Reviews* **85**, 1159–1204.

Whelan, W. L., Gocke, E. and Manney, T. R. (1979). The CAN1 locus of *Saccharomyces cerevisiae*: fine-structure analysis and forward mutation rates. *Genetics* **91**, 35–51.

Willars, G. B. (2006). Mammalian RGS proteins: multifunctional regulators of cellular signalling. *Seminars in Cell and Developmental Biology* **17**, 363–376.

Wise, A., Foord, S. M., Fraser, N. J., Barnes, A. A., Elshourbagy, N., Eilert, M., Ignar, D. M., Murdock, P. R., Steplewski, K., Green, A., Brown, A. J., Dowell, S. J., Szekeres, P. G., Hassall, D. G., Marshall, F. H., Wilson, S. and Pike, N. B. (2003). Molecular identification of high and low affinity receptors for nicotinic acid. *The Journal of Biological Chemistry* **278**, 9869–9874.

Wolfe, B. L. and Trejo, J. (2007). Clathrin-dependent mechanisms of G protein-coupled receptor endocytosis. *Traffic* **8**, 462–470.

Wolfe, J. T., Wang, H., Howard, J., Garrison, J. C. and Barrett, P. Q. (2003). T-type calcium channel regulation by specific G-protein $\beta\gamma$ subunits. *Nature* **424**, 209–213.

Wootten, D., Christopoulos, A. and Sexton, P. M. (2013). Emerging paradigms in GPCR allostery: implications for drug discovery. *Nature Reviews Drug Discovery* **12**, 630–644.

Xu, F., Wu, H., Katritch, V., Han, G. W., Jacobson, K. A., Gao, Z.-G., Cherezov, V. and Stevens, R. C. (2011). Structure of an agonist-bound human A2A adenosine receptor. *Science* **332**, 322–327.

Yi, T.-M., Kitano, H. and Simon, M. I. (2003). A quantitative characterization of the yeast heterotrimeric G protein cycle. *Proceedings of the National Academy of Sciences of the United States of America* **100**, 10764–10769.

Yildirim, N., Hao, N., Dohlman, H. G. and Elston, T. C. (2004). Mathematical modeling of RGS and G-protein regulation in yeast. *Methods in Enzymology* **389**, 383–398.

Zhang, X. C., Liu, J. and Jiang, D. (2014). Why is dimerization essential for class-C GPCR function? New insights from mGluR1 crystal structure analysis. *Protein Cell* **5**, 492–495.

Zhang, Z., Qian, W. and Zhang, J. (2009). Positive selection for elevated gene expression noise in yeast. *Molecular Systems Biology* **5**, 1–12.

Zou, J., Zheng, M.-W., Li, G. and Su, Z.-G. (2013). Advanced systems biology methods in drug discovery and translational biomedicine. *BioMed Research International* **2013**. Article ID 742835.